UNIVERSITÉ DU QUÉBEC À MONTRÉAL

DYNAMIQUE DE LA COMPOSITION ET DES EXPORTS DE MATIÈRE ORGANIQUE DISSOUTE AU SEIN D'UN BASSIN VERSANT BORÉAL DOMINÉ PAR UNE TOURBIÈRE OMBROTROPHE, MINGANIE, QUÉBEC, CANADA

THÈSE

PRÉSENTÉE

COMME EXIGENCE PARTIELLE DU

DOCTORAT EN SCIENCES DE L'ENVIRONNEMENT

PAR

ANTONIN PRIJAC

JUILLET 2023

REMERCIEMENTS

Michelle et Laure, mes directrices, je me sens extrêmement privilégié d'avoir été dirigé par vous deux. Je serai éternellement reconnaissant d'avoir pu bénéficier de vos expériences et expertises au cours de mon doctorat. Les mots me manquent tant vous aurez été importantes dans ma construction en tant que scientifique, mais aussi en tant qu'adulte. Vous m'avez appris à me dépasser, à raisonner et surtout, à être fier de mon travail. C'est certain qu'un doctorat en temps de pandémie sort du cadre normal, cependant, contre vents et marées, nous avons réussi à nous adapter et nous arrivons au bout du chemin ! Merci pour cela, merci pour votre humanité et votre patience. Merci de m'avoir poussé à toujours persévérer pour donner le meilleur.

Merci à toi Pierre d'avoir été un exemple sur qui m'appuyer. J'ai énormément appris à tes côtés et ta détermination m'a souvent inspiré. Je garde des souvenirs impérissables de nos années passées ensemble, sur le terrain comme au labo. Merci à toi Khawla pour ta collaboration et ton partage. On l'aura parcouru dans les moindres méandres ce ruisseau ! Je suis très fier de l'équipe que nous avons formée ensemble et d'avoir participé à ce projet à vos côtés. C'est une belle amitié qui est née sur la tourbière Bouleau. Merci d'avoir continué de contribuer à mon travail jusqu'aux derniers moments. J'ai également une pensée pour toi Guillaume qui fut le premier à travailler à Bouleau ! Je tiens à vous remercier Laurent et Marc-André. Votre collaboration fut riche et précieuse. Vous avez apporté une expertise complémentaire qui a permis de rendre ce travail encore meilleur. Vos idées et votre positivisme ont été un bel ajout à notre équipe. Vous partagez une bonne humeur, une sympathie et une ouverture qui rend le travail à vos côtés très facile et surtout très enrichissant !

Merci à Alain et François pour votre précieux support pour nous avoir donné les meilleures conditions possibles pour réaliser notre travail et pour nous avoir permis de maintenir nos activités durant la pandémie. Un grand merci aux professeurs Paul del Giorgio et André Saint-Hilaire pour votre implication dans le comité de suivi de mon doctorat. Vous avez apporté un regard éclairant sur mon travail. Merci aux équipes du GRIL et du GEOTOP à Montréal, du Laboratoire Écologie Fonctionnelle et Environnement à Toulouse, de Géosciences à Rennes et du Jan Veizer Laboratory à Ottawa pour votre contribution aux analyses de laboratoire.

Un grand merci aux personnes ayant accepté d'évaluer ma thèse, Yves Prairie, Isabelle Laurion et François Guillemette. J'ai énormément apprécié échanger avec vous. Merci aussi à Dolors Planas d'avoir accepté de représenter le doyen.

Je tiens aussi à remercier les étudiants et étudiantes qui ont participé à ce projet. Léonie, merci pour toutes les responsabilités prises les premiers mois de l'été 2018. Tu as une part importante dans la réalisation de ce projet. Bravo. Merci à toi Charles d'avoir accepté de passer un été à mes côtés sur la tourbière et merci pour ton aide durant ces campagnes. Merci, Alex pour ta collaboration. Malgré la pandémie, ton travail a été important pour Pierre et moi. Merci aussi à toutes les personnes qui ont participé aux campagnes sur la tourbière Bouleau : Camille, Charles-Élie, Éloise, Karelle, Louis-Martin, Nicole, Pénélope et Roman. Merci aux tourbeux et aux tourbeuses de former un groupe de recherche aussi soudé et bienveillant. Un grand merci à toutes les belles personnes que j'ai rencontrées au GEOTOP. Un merci particulier à ma précieuse amie Rivellie, je te souhaite le meilleur pour la fin de ton doctorat ! Une pensée chaleureuse pour toutes celles et ceux qui ont suivi le même cheminement de programme de doctorat que moi et avec qui nous

avons partagé de nombreux cours, du Mont-Saint-Hilaire aux Laurentides, en passant par le complexe des sciences de l'UQAM.

Merci à tous mes amis. Merci, Marc-Antoine et Nicholas de m'avoir accueilli au Québec et de m'avoir appris à devenir québécois. Merci à Fabrice, Coralie, Sacha et Lucile. Votre amitié m'est précieuse et vous avez toujours été là pour m'aider à décrocher et partager de bons moments ! Sacha, il ne faut pas juste lire le résumé. Charles-Élie, je pourrais écrire une thèse rien que sur notre amitié qui est née et a grandi avec ce doctorat. Ce serait principalement constitué de mêmes et de réflexions politiques, mais je suis certain que ça vaudrait la peine d'être publié. Plus sérieusement, tu es comme un ami d'enfance que j'ai rencontré il y a quelques années. Merci d'avoir été présent durant ces années ! Merci à tous mes amis « d'avant », d'Angers, de Saintes, de Paris ou de Clermont-Ferrand, la distance nous a éloignés, mais je pense à vous tous.

Merci à m'a famille qui a vécu tout cela à distance. Je sais néanmoins que vous êtes fiers et que vous avez toujours été derrière moi. J'ai beaucoup pensé à vous de l'autre côté de l'Atlantique et il y a bien des moments où j'aurais aimé être en Anjou le temps d'un week-end pour me ressourcer à vos côtés. Merci à mes parents, mon frère et ma sœur. Ce n'est pas un choix facile d'immigrer et encore moins pour un doctorat, mais vous m'avez soutenu et épaulé malgré la distance. J'aurai passé deux belles vacances d'été avec vous et je suis tellement content d'avoir sillonné et découvert le Québec avec vous. Ça a bien rempli ma boite à souvenirs et il y en aura plein d'autres à venir. Merci à Jean-Claude, France, William et Maude de m'avoir accueilli dans votre famille et de m'avoir encouragé et soutenu durant ces dernières années.

Marie-Philippe. Quoique j'écrive, on va pleurer ensemble. Le doctorat est plein de surprises, mais la plus grande est de t'avoir rencontrée. Je sais que tu sais déjà tout ce que je pourrais écrire sur nous ou pour te remercier. Tu m'as supporté, tu m'as accompagné, tu m'as obligé à affronter mes démons et tu m'aides constamment à devenir meilleur et plus grand. Grâce à toi ces dernières années ont été plus douces. Je t'aime.

Merci Pixel pour les quelques mots que tu as écrits (accidentellement) dans cette thèse et merci d'avoir été un si bon animal de soutien pendant ces derniers mois.

Je terminerai avec cette citation de Pierre Perrault (*Toutes isles*) : « La chicouté est une mûre blanche, fruit de la ronce petit mûrier, qui fréquente les pays de mousses et de lichens et d'épais silences, les prairies spongieuses qu'ils appellent mollière. »

AVANT-PROPOS

Cette thèse s'inscrit dans le cadre du projet d'aménagement hydro-électrique de la rivière Romaine (Minganie, Québec, Canada) et dont la compagnie Hydro-Québec s'est donné le mandat d'établir l'impact de cet aménagement sur le bilan de carbone des écosystèmes du bassin versant. Ce projet a fait l'objet d'une subvention de recherche et développement coopérative du Conseil de Recherche en Sciences Naturelles et en Génie du Canada (CRSNG-RDC), porté par la professeure Michelle Garneau, en collaboration avec Hydro-Québec, et dont les fonds ont permis de financer les travaux de recherche présentés dans cette thèse.

La présente thèse est composée de trois articles scientifiques rédigés en anglais. Les autres parties de la thèse sont rédigées en français, selon les exigences de l'UQAM. J'ai agi pour l'ensemble des trois articles comme premier auteur, ce qui signifie que j'ai été le principal responsable de la collecte des données, des analyses de laboratoire, de l'interprétation des résultats et de la rédaction des documents. Les co-auteurs ont individuellement contribué à une ou plusieurs des tâches mentionnées précédemment.

Le premier article est intitulé « *Hydrological connectivity controls dissolved organic carbon exports in a peatland-dominated boreal catchment stream* » et a été soumis en décembre 2022 au journal *Hydrology and Earth System Science* et la pré-impression a été publiée le 21 mars 2023. Les co-auteurs sont ma codirectrice Laure Gandois (CNRS), Pierre Taillardat (National University of Singapore), Marc-André Bourgault (Université Laval), Khawla Riahi (INRS-ETE), Alex Ponçot (UQAM), Alain Tremblay (Hydro-Québec) et ma directrice Michelle Garneau (UQAM). L'article est en processus de révision par les pairs.

Le second article intitulé « *Hydrological conditions control dissolved organic matter dynamics along a peatland drainage boreal headwater stream* » et sera soumis à la revue *Journal of Geophysical Research : Biogeosciences*. Les coauteurs de cet article sont ma codirectrice Laure Gandois (CNRS), Pierre Taillardat (National University of Singapore) et ma directrice Michelle Garneau (UQAM).

Le troisième article est intitulé « *Dissolved organic matter concentration and composition discontinuity at the peat-pool interface in a boreal peatland* » et a été publié le 22 septembre 2022 dans la revue *Biogeosciences*. Les coauteurs sont ma codirectrice Laure Gandois (CNRS), Laurent Jeanneau (CNRS), Pierre Taillardat (National University of Singapore) et ma directrice Michelle Garneau (UQAM).

Ces travaux ont fait l'objet de trois communications scientifiques orales. La première, « *Dissolved organic matter as an indicator of processes at the interface between terrestrial and aquatic ecosystems in a boreal peatland* » a été présentée en mars 2021 dans le cadre du congrès du GEOTOP (Montréal, Canada). La seconde, « *Dissolved organic matter as an indicator of processes at the terrestrial and aquatic interface of a boreal peatland* » a été présentée en juin 2021 dans le cadre du symposium du GRIL (Montréal, Canada). La troisième a été présentée en mars 2023 dans le cadre du congrès du GEOTOP (Montréal, Canada), et intitulée « Hydrological controls on dissolved organic carbon exports and composition in a peatland-dominated boreal catchment, Minganie, Quebec, Canada ». Par ailleurs, le projet de recherche dans lequel s'inscrit ma thèse a fait d'objet d'un autre article, intitulé « *Carbon dioxyde and methane dynamics in a peatland headwater stream: origins, processes and implications* », dont Pierre Taillardat a été le premier auteur et auquel j'ai agi en tant que coauteur. Cet article a été publié en juillet 2022 dans la revue *Journal of Geophysical Research : Biogeosciences*.

TABLE DES MATIÈRES

LISTE DES FIGURES

LISTE DES TABLEAUX

LISTE DES ABRÉVIATIONS, DES SIGLES ET DES ACRONYMES

β : α : indice de fraicheur / freshness index

BNCE ou NECB : balance nette de carbone de l'écosystème / net ecosystem carbon balance

Cal BP : calibrated years before present (AD 1950)

%CAR : carbohydrates proportion

%CAR_MIC : microbial-derived carbohydrates proportion

CH_4 : methane

CID ou DIC : carbon inorganique dissous / dissolved inorganic carbon

CO_2 : dioxyde de carbon / carbon dioxyde

COD ou DOC : carbone organique dissous / dissolved organic carbon

COP ou POC : carbone organique particulaire / particulate organic carbon

COT ou TOC : carbone organique total / total organic carbon

C / *V* ratio : sum of coumaric and ferulic acids divided by the sum of vanillic acid, vanillaldehyde, and acetovanillone

$\delta^{13}C$: isotope stable du carbone 13 / stable 13 carbon isotope

^{14}C : isotope radiogénique du carbone 14 / radiogenic isotope 14 carbon

deoxyC6 : *C*5 : mixing model based on the proportion of deoxyC6 carbohydrates and the proportion of C5 carbohydrates

ENE ou NEE : échange net de l'écosystème / net ecosystem exchange

*f*DOC : flux of dissolved organic carbon

*f*MIC : proportion of microbial molecular marker

FT-ICR-MS : spectrométrie de masse à résonnance cyclonique ionique / Fourrier-transform ions cyclotron resonance-mass spectrometry

FI : indice de fluorescence / fluorescence index

*f*VEG : proportion of vegetation molecular markers

GES ou GHG : gaz à effet de serre / greenhouse gases

HDPE : high-density polyethylene

HI : indice d'hystérèse / hysteresis index

HMM : hidden Markov model

%HMW_FA : proportion of high molecular weight fatty acids

HPLC : chromatographie en phase liquide à haute performance / high performance liquid chromatography

%LMW_FA : proportion of low molecular weight fatty acid

MIC : VEG : sum of microbial molecular markers divided by the sum of vegetation molecular makers ratio

MOD ou DOM : matière organique dissoute / dissolved organic matter

MODc ou cDOM : matière organique dissoute chromophorique / chromophoric dissolved organic matter

MODf ou fDOM : matière organique dissoute fluorescente / fluorescent organic matter

MSF : mass spectra factor

NN ou WTD : niveau de la nappe / water table detph

NOD ou DON : azote organique dissous / dissolved organic nitrogen

NT ou TN : azote total / total nitrogen

PCA : principal component analysis

%Phenols : phenol markers proportion

PNE ou NEP : production nette de l'écosystème / net ecosystem production

PPB ou GP : production primaire brute / gross primary production

Py-GC-MS : pyrolyse-chromatographie en phase gazeuse-spectrométrie de masse / pyrolysis-gas chromatography-mass spectrometry

Q : débit / discharge

RDOC : removal rate of dissolved organic carbon

Rt : retention time

%SOA : proportion of small organic acids

S_R : ratio des pentes spectrales / spectral slope ratio

SS-NDIR : solid-state non-dispersive infrared

$SUVA_{254}$: absorbance spécifique de la matière organique dissoute à 254 nm / specific absorbance of dissolved organic matter at 254 nm

THM-GC-MS : chimiolyse thermique et méthylation-chromatographie en phase gazeuse-spectrométrie de masse / thermally assisted methylation-gas chromatography-mass spectrometry

RÉSUMÉ

Les tourbières représentent l'un des plus importants puits de carbone terrestre dans le biome boréal. L'établissement du bilan de carbone des tourbières est donc important afin de quantifier la capacité des tourbières à accumuler du carbone. Cependant, une part importante du carbone capté par les tourbières peut être perdue par les transferts latéraux vers les milieux aquatiques dont la majorité est constituée de carbone organique dissous (COD). Le COD est d'autant plus important dans le cycle du carbone des tourbières que cette forme réactive est sensible à différents processus, notamment la minéralisation pouvant maintenir la sursaturation des ruisseaux de tête de bassin versant en dioxyde de carbone (CO_2). Les flux de COD sont particulièrement sensibles aux variations des conditions hydroclimatiques (p. ex., température, précipitation) et varient en fonction des saisons et du débit. Ainsi, la majorité des exports ont lieu durant de courts évènements de crues. Aussi, le calcul des exports spécifiques de COD provenant des tourbières (normalisé par la surface contribuant aux exports) peut être complexe étant donné les différentes sources (p. ex., les écosystèmes forestiers) pouvant contribuer aux flux de COD dans les bassins versants.

L'étude de la composition de la matière organique dissoute (MOD) permet d'identifier sa nature, ses sources et comment elle peut être affectée par les différents processus biogéochimiques tels que les processus de minéralisation. Cependant, la composition de la MOD au sein du continuum hydrologique tourbière-ruisseau et sous différentes conditions hydrologiques reste mal connue bien qu'il ait été établi qu'elle puisse varier entre ces conditions. Les mares font partie, au même titre que les platières, les buttes et les dépressions, des microformes des tourbières, pouvant couvrir plus de la moitié de la surface de ces écosystèmes. Les mares peuvent représenter un compartiment important dans le cycle du carbone des tourbières en émettant des quantités substantielles de gaz à effet de serre. La dynamique de la MOD en termes de concentration et de composition n'a été que peu décrite dans les tourbières boréales. Ainsi, il n'existe que très peu d'étude sur l'évolution de la MOD durant la saison de croissance, que ce soit dans l'eau interstitielle des tourbières ou dans les mares.

Les objectifs de cette thèse sont de i. quantifier les exports de COD depuis une tourbière boréale ombrotrophe et de caractériser les mécanismes de transfert du COD durant les épisodes de crues (chapitre 2), ii. expliquer l'effet des conditions hydrologiques du bassin versant sur les changements de composition et les processus de transformation de la MOD au cours de son export dans le ruisseau de drainage (chapitre 3), et iii. préciser le rôle des mares dans la production et la transformation de la MOD de la tourbière (chapitre 4).

De juin 2018 à mai 2020, une tourbière boréale ombrotrophe du nord-est du Québec (Canada) (tourbière Bouleau, nom non officiel) a été instrumentée et échantillonnée. La mesure de la concentration en COD (par l'intermédiaire d'un proxy ; la MOD fluorescente) et du débit ont permis de quantifier le flux en COD à l'exutoire du ruisseau de drainage de la tourbière. L'étude des séries temporelles de concentration de COD et de niveau de la nappe, les hydrogrammes de crue et les indices qui en ont été extraits ont permis d'étudier les mécanismes de transfert de la MOD. Des échantillonnages ponctuels ont été effectués dans le ruisseau, les mares et l'eau interstitielle de la tourbière étudiée. À partir de ces échantillons, une combinaison de méthodes élémentaires, isotopiques, optiques et moléculaires et des expériences de biodégradation et de photodégradation ont été utilisées afin de décrire la composition de la MOD.

Afin de calculer les flux spécifiques de COD, une nouvelle approche a été proposée dans le chapitre 2 pour calculer les flux de COD en distinguant les périodes de hautes eaux et de basses eaux. Durant les périodes de hautes eaux, l'augmentation du niveau de la nappe de la tourbière favorise la connectivité hydrologique entre la tourbière et le ruisseau. On peut ainsi émettre l'hypothèse que la tourbière est la principale contributrice au flux de COD et considérer la surface de la tourbière dans le calcul du flux spécifique de COD. À l'inverse, en période de basses eaux, dû au bas niveau de la nappe de la tourbière, la connectivité hydrologique entre la tourbière et le ruisseau est moins importante. La contribution de la tourbière pendant ces périodes étant limité par la plus faible connectivité hydrologique, on considèrera la surface du bassin versant dans le calcul du flux spécifique du COD. Ainsi, 93-94 % du COD est exporté durant les périodes de hautes eaux, qui constituent 44-59 % de la série temporelle, mettent en évidence que les crues sont à l'origine de la majorité des exports de COD. L'étude des mécanismes de transfert du COD lors des évènements de crue durant la saison de croissance a aussi mis en évidence l'importance du niveau initial de la nappe et de l'augmentation du niveau de la nappe au cours de l'évènement sur la quantité de COD exportée. Cependant, des évènements exceptionnels de crues représentant de 3 à 8% de la période de mesures peuvent exporter 25% des exports totaux de COD pendant la saison de croissance.

Dans le chapitre 3, l'étude de la MOD dans le ruisseau a permis de mettre en évidence des liens entre la composition de la MOD, le débit, le temps de résidence de la MOD dans le ruisseau et le flux de minéralisation. La composition de la MOD dans le ruisseau est variable en fonction des conditions hydrologiques. En période de hautes eaux, une MOD semblable à l'eau interstitielle de la tourbière a été observée en termes de rapport COD:NOD et d'aromaticité, tout en présentant un poids moléculaire moyen plus faible que dans l'eau interstitielle et en période de basses eaux. Durant ces périodes de débit élevé et de faible temps de résidence, la MOD est rapidement transférée vers l'aval de la tourbière sans être affectée par les processus de minéralisation. À l'inverse, un changement de composition de la MOD est observé pendant les périodes de basses eaux, marquées par une augmentation de l'aromaticité et du poids moléculaire de la MOD. Ces changements sont associés à une plus grande contribution de la minéralisation de la MOD au flux de COD lorsque les temps de résidence dans le ruisseau sont les plus longs.

Le chapitre 4 présente la dynamique de la MOD au sein du complexe tourbière-mare. La contribution de la tourbière à la MOD des mares a été mise en évidence par la dominance des marqueurs moléculaires dérivée de la végétation au sein de la tourbière et le rapport COD:NOD élevé. Cependant, des concentrations de COD deux fois plus faibles sont mesurées dans les mares et ces concentrations augmentent de 2.5 fois pendant la saison de croissance dans l'eau interstitielle contre seulement 1.7 fois dans les mares alors qu'il se produit un changement de composition entre l'eau interstitielle et les mares et une dynamique différente au cours de la saison de croissance. Dans l'eau interstitielle, la MOD est marquée par une aromaticité et un poids moléculaire importants et peu variables. Dans les mares, l'aromaticité et le poids moléculaire augmentent au cours de la saison de croissance, mais restent plus faibles que dans l'eau interstitielle. Ces différences sont expliquées par une combinaison de facteurs biologiques, chimiques et physiques.

Cette thèse met en avant la sensibilité des exports de COD et de la composition de la MOD aux facteurs hydroclimatiques à différentes échelles spatio-temporelles dans un bassin versant boréal dominé par une tourbière ombrotrophe. Dans un contexte de changements climatiques, l'augmentation des températures moyennes annuelles, le changement du régime des précipitations et l'augmentation de la période sans glace pourraient impacter la production, la minéralisation et les exports de COD. Ces perturbations du cycle du COD pourraient ultimement affecter le bilan de carbone des tourbières boréales.

Mots clés : tourbière ombrotrophe, carbone organique dissous, matière organique dissoute, mares, exutoire, biogéochimie, hydrologie, bassin versant, biome boréal, Minganie

ABSTRACT

Peatlands represent one of the most important terrestrial carbon sink within the boreal biome. The calculation of peatland net carbon balance is important in order to quantify the peatland capacity to accumulate carbon. However, an important proportion of carbon is lost through lateral exports to aquatic environments and mainly under the form of dissolved organic carbon (DOC). DOC is important in the peatland carbon cycle and this reactive form of carbon is sensitive to mineralization processes which sustain the carbon dioxide (CO_2) supersaturation of headwater streams. DOC fluxes are particularly sensitive to hydroclimatic conditions variations (e.g., temperature, precipitation) and vary according to seasons and stream discharge. More, the majority of DOC exports can occur during short flood events. The calculation of specific DOC exports from a peatland surface area in a watershed is challenging as different sources (e.g., adjacent upland forests) can also contribute to DOC exports in the catchment.

The study of dissolved organic matter (DOM) composition allows to identify the nature of DOM, its source and how it is affected by biogeochemical processes such as mineralization processes. However, the DOM composition within the peatland-stream aquatic continuum and under different hydroclimatic conditions are poorly documented while it was hypothesized that DOM composition could vary between those conditions. Peatland pools, as lawns, hummocks, and depressions, constitute the microforms that can cover more than half of the peatland areas. Pools can represent an important compartment of the peatland carbon cycle as being a source of important greenhouse gas emissions. DOM dynamics, in terms of concentration and composition, was poorly documented in boreal peatlands and only few studies documented the evolution of DOM composition during the growing season in peatland porewater or peatland pools.

The objectives of this thesis are to i. quantify DOC exports and to characterize the mechanisms of these exports during flood events in an ombrotrophic boreal peatland (chapter 2), ii. explain the impact of hydrological conditions in DOM composition and transformation processes during its exports to the drainage stream (chapter 3), and iii. specify the role of pools in the production and transformation of DOM in the studied peatland (chapter 4).

From June 2018 to May 2020, an ombrotrophic boreal peatland (Bouleau peatland, unofficial name) from northeastern Quebec (Canada) was instrumented and sampled. The DOC concentration (through the measurement of the fluorescent DOM as a proxy) and stream discharge monitoring allowed to calculate the DOC exports at the outlet of the peatland drainage stream. The study of DOC, water table depth (WTD) time series, discharge and extracted indices from them allowed to study DOC transfer mechanisms. Punctual sampling was performed in the stream, pools and in the peatland. From those samples, elemental, isotopic, optical, molecular and incubation experiments were conducted in order to define the DOM composition.

A new approach was proposed in chapter 2 to calculate the specific DOC exports by distinguishing high-flow and low-flow periods. During high-flow periods, WTD increase had promoted the hydrological connectivity between the peatland and the stream. We hypothesized that the peatland was the main contributor to DOC exports and considered the peatland surface area in the specific DOC export calculation. Conversely, during low-flow periods, the hydrological connectivity between the peat and the stream was less important due to the low WTD. As the peat contribution to DOC export was limited by lower

hydrological connectivity during these periods, the catchment area was considered in the specific DOC export calculation. Hence, 93-94 % of DOC was exported during high-flow periods which accounted for 44-59 % of the complete time series, highlighting the importance of flood events on DOC exports. The study of DOC exports mechanisms during high-flow periods showed that the initial WTD and its increase during events were the main drivers of the amount of exported DOC. However, short exceptional flood events (3-8% of the time series) have represented up to 25% of the total exports during the growing seasons.

In chapter 3, the study of DOM in the stream allowed to highlight the links between DOM composition, stream discharge, residence time in the stream and the contribution of the mineralization to DOC exports. DOM composition in the stream varied according to hydrological conditions. During high-flow, DOM was similar between the stream and peat porewater in terms of DOC : DON ratio and aromaticity but presented a lower molecular weight. During those periods of high-flow and short residence time, DOM was rapidly flushed downstream without being affected by mineralization processes. Conversely, change in DOM composition was observed during low-flow periods with an increase of DOM aromaticity and molecular weight. Those changes are correlated with the higher contribution of DOC mineralization fluxes during longer residence time in the stream.

The chapter 4 studied the DOM dynamics in the peatland-pool complex. The contribution of the peatland to DOM in pools was highlighted by the dominance of molecular markers derived from peatland vegetation and by high DOC:DON ratios. DOC concentration was twice higher in peat porewater compared to pools and those concentrations increased 2.5 times in peat porewater and 1.7 times in pools during the growing season. More, a change in DOM composition was observed between peat porewater and pools with contrasted dynamics during the growing seasons. In peat porewater, DOM was characterized by high DOM aromaticity and molecular weight that poorly fluctuate during the growing season. In pools, DOM aromaticity and molecular weight increased during the growing season but were still low compared to peat porewater. Those differences can be explained by a combination of biological, chemical and physical drivers.

This thesis highlights the sensitivity of DOC exports and DOM composition to hydroclimatic factors at different spatiotemporal scales within a boreal catchment dominated by an ombrotrophic peatland. In the context of climate change, increasing temperature, changes in precipitation regime and longer ice-free season could affect DOC production, mineralization and exports. Those perturbations could then affect the overall peatland carbon balance.

Keywords : ombrotrophic peatland, dissolved organic carbon, dissolved organic matter, pool, stream outlet, biogeochemistry, hydrology, catchment, boreal biome, Minganie

INTRODUCTION

1.1 Le cycle du carbone à l'interface entre les écosystèmes terrestres et aquatiques dans le biome boréal

1.1.1 Définition du bilan de carbone de l'écosystème

Le bilan de carbone d'un écosystème est une approche méthodologique permettant, *in fine*, de calculer la valeur nette du carbone qui est emmagasiné par l'écosystème en intégrant celui qui est perdu par différentes voies (Chapin et al., 2006). Si le bilan est négatif et que l'écosystème emmagasine plus de carbone qu'il n'en perd, il pourra être qualifié de puits de carbone. À l'inverse, un bilan positif indique que l'écosystème représente une source de carbone. Puisque ces flux entrants et sortants sont quantifiables, il est possible de déterminer à grande échelle si un paysage est un puits ou une source de carbone. Le bilan de carbone des écosystèmes terrestres a été introduit par Woodwell and Whittaker (1968) en tant que production nette de l'écosystème (PNE ou NEP : *net ecosystem production*), permettant de calculer le bilan entre la production primaire brute (PPB ou GP : *gross production*) de l'écosystème et la respiration (autotrophe et hétérotrophe). Une approche plus exhaustive a été développée par Randerson et al. (2002) pour calculer la PNE en s'appuyant sur l'ensemble des flux qui régulent le cycle du carbone. Ainsi, la PNE est équivalente à la somme des flux entrants et sortants de l'écosystème. En plus des flux relatifs à l'activité photosynthétique et à la respiration, Randerson et al. (2002) incluent des flux contrôlés par des facteurs abiotiques tels que le lessivage qui correspond au transfert latéral de carbone organique dissous (COD), de carbone inorganique dissous (CID) et de méthane (CH_4) en dehors des limites de l'écosystème.

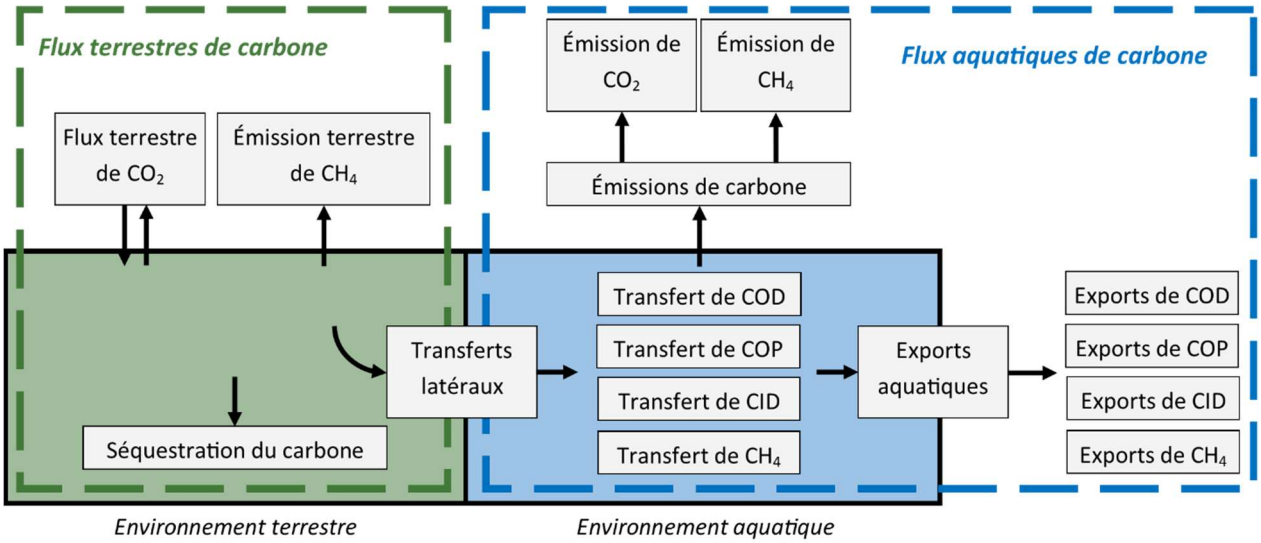

Figure 1.1 Schéma conceptuel des composantes du bilan net de carbone de l'écosystème incluant à la fois les flux terrestres de carbone (en vert) et les flux aquatiques de carbone (en bleu). D'après Chapin et al. (2006) et Webb et al. (2019).

Cette approche a été formalisée par Chapin et al. (2006) sous le terme de bilan écosystémique net de carbone (BNCE ou NECB : *net ecosystem carbon balance*, Fig. 1.1). Elle propose une méthode basée sur la mesure des flux des différentes catégories de carbone plutôt que des différents processus (Fig. 1.1). L'application de cette approche conceptuelle permet de mesurer les flux en se focalisant sur les formes chimiques du carbone plutôt que sur les procédés, ce qui évite de faire des approximations ou de négliger les flux issus de processus moins documentés (Chapin et al., 2006; Randerson et al., 2002), comme notamment le transfert des formes dissoutes du carbone (Cole et al., 2007; Webb et al., 2019).

1.1.2 Le bilan de carbone en contexte boréal

Le biome boréal contient la plus grande forêt contiguë de la planète en couvrant 11.7 % des terres émergées, soit un total de $15x10^6$ km^2 (Dinerstein et al., 2017). On considère que 1095 Pg de C (sol + biomasse aérienne) sont stockés dans le biome boréal (Bradshaw & Warkentin, 2015) ce qui en fait le biome où la densité en C est la plus importante sur la planète. L'échange net de l'écosystème (ENE ou NEE : *net ecosystem exchange*, correspondant à la quantité nette de CO_2 captée ou émise par un écosystème) à l'échelle du biome boréal est compris entre -36 et -17 g C m^{-2} an^{-1} (Virkkala et al., 2021) ce qui en fait un important puits naturel de dioxyde de carbone (CO_2). Cependant, à l'échelle locale, la capacité de séquestration du CO_2 par les forêts est sensible à des facteurs tels que la productivité végétale (Järveoja et al., 2018; Schulze et al., 1999), la composition végétale (Laganière et al., 2015), les conditions

climatiques (p. ex., température, humidité et durée de la saison de croissance) (Lund, et al., 2009; Nobrega & Grogan, 2008), le type de sol et de ses propriétés (p. ex., disponibilité de l'azote et du phosphore, épaisseur de l'horizon organique) (Hyvönen et al., 2007; Lund, et al., 2009; Palmroth et al., 2006). L'ensemble de ces facteurs peut affecter positivement ou négativement la capacité des écosystèmes à séquestrer le carbone.

Le biome boréal est aussi composé d'une mosaïque d'autres écosystèmes qui, comme les forêts, jouent un rôle clé dans le cycle du carbone. La majorité du carbone est stocké dans les sols forestiers et les tourbières (Bradshaw & Warkentin, 2015). Le stock de carbone dans les sols minéraux des forêts varie entre 208 et 373 Pg (Bradshaw & Warkentin, 2015) alors qu'il atteint 415 ± 147 Pg dans les tourbières (Hugelius et al., 2020). Le reste du carbone stocké dans le biome boréal se trouve dans la végétation de surface, dans la végétation au pourtour des lacs, ainsi que le carbone contenu dans les sédiments des écosystèmes lentiques et lotiques (Bradshaw & Warkentin, 2015).

1.1.3 L'importance des milieux aquatiques dans l'élaboration d'un bilan de carbone

Les compartiments aquatiques connectés aux milieux terrestres ont souvent été négligés dans le calcul des bilans de carbone des écosystèmes (Webb et al., 2019). Pourtant, il a été établi que les milieux aquatiques peuvent jouer un rôle majeur dans le cycle du carbone des écosystèmes (Aufdenkampe et al., 2011; Cole et al., 2007). Les exports latéraux depuis les milieux terrestres peuvent contribuer significativement aux émissions de CO_2 et de CH_4 des milieux aquatiques (Rasilo et al., 2017). Ce changement de paradigme, considérant les écosystèmes aquatiques tels que les ruisseaux et les rivières comme un milieu dynamique soutenant de nombreux processus du cycle du carbone (Cole et al., 2007) plutôt que comme des « tuyaux passifs » (passive pipes), a permis d'intégrer progressivement les milieux aquatiques au bilan de carbone des écosystèmes.

L'intégration du continuum entre les milieux terrestres et aquatiques a permis de réévaluer les bilans de carbone des écosystèmes en plus de reconnaitre à quel point ces flux peuvent représenter une source significative de carbone pour les écosystèmes terrestres. Les flux représentent entre 3.8 g C m^{-2} an^{-1} et 18.1 g C m^{-2} an^{-1} (Chi et al., 2020; de Wit et al., 2015; Dyson et al., 2011; Huotari et al., 2013; Jonsson et al., 2007; Juutinen et al., 2013; Leach et al., 2016; Nilsson et al., 2008; Rantakari et al., 2010). Ces études montrent l'importance du COD qui est la forme dominante des flux aquatiques de carbone, constituant

entre 67.5 % (Rantakari et al., 2010) et 97.4% du flux total (Juutinen et al., 2013) et particulièrement dans les cours d'eau de tête de bassin (Dyson et al., 2011; Laudon et al., 2011; Rantakari et al., 2010).

1.2 La matière organique dissoute : un outil de compréhension de la dynamique du carbone entre les compartiments terrestres et aquatiques

La dominance du COD dans les flux depuis le milieu terrestre vers le milieu aquatique a incité des recherches pour identifier les molécules qui composent la matière organique dissoute (MOD ; Aitkenhead et al., 2003). Cela a permis d'identifier l'origine de la MOD au sein de bassins versants, mais également l'âge et les différents processus physiques, chimiques et biologiques subis depuis sa production vers son export vers les milieux aquatiques. Ainsi, l'étude de la composition de la MOD est complémentaire à la quantification des flux afin de comprendre les mécanismes sous-jacents à son export, mais également la composition et la réactivité du carbone exporté.

1.2.1 L'origine de la matière organique dissoute

L'origine de la MOD correspond au processus biologique relié à la production des molécules qui la composent. On distingue deux sources de MOD présente dans les milieux aquatiques : autochtone et allochtone. Les sources autochtones de MOD indiquent que la MOD est issue du métabolisme au sein du milieu aquatique. La MOD autochtone peut provenir de la production primaire issue du métabolisme photosynthétique des microalgues et des macrophytes (Bertilsson & Jones, 2003). Les sources allochtones quant à elles proviennent du métabolisme externe aux milieux aquatiques et elles ont subi des processus menant à leur export vers ces milieux (Kaplan & Cory, 2016). Les sources allochtones sont souvent celles considérées comme dominant la MOD des milieux aquatiques (Aitkenhead et al., 1999; Billett et al., 2012; Kaplan & Cory, 2016; Raymond et al., 2016; Tank et al., 2018). La MOD allochtone est ainsi composée de molécules issues du métabolisme végétal lessivé dans le sol et de molécules issues du métabolisme microbien, utilisant les molécules végétales comme substrat (Aitkenhead et al., 2003).

1.2.2 La composition de la matière organique dissoute

La matière organique dissoute constitue la matière organique en solution, dans la tourbe ou dans les eaux de surface. Le seuil de la matière organique sous sa forme dissoute est composé des molécules passant au travers de membranes filtrantes de 0.2 à 0.7 µm (Denis et al., 2017) avec une masse moléculaire comprise entre 100 et 100 000 Da (Aitkenhead et al., 2003). Au-delà de ces valeurs, la matière organique est considérée comme de la matière organique particulaire.

Comme la MOD peut provenir de différentes sources et être issue de différents processus biologiques et chimiques, elle constitue un mélange complexe et hétérogène de molécules (Kaplan & Cory, 2016). On peut cependant classer ces molécules dans différents groupes. Parmi les molécules constituant la MOD, on trouve les phénols, qui groupent des molécules telles que les lignines et les tannins et qui dominent le mélange de MOD des eaux interstitielle de tourbières (Page et al., 2002). Le reste de la MOD est composé de terpénoïdes de la famille des hydrocarbures, de polysaccharides, d'acides aminés et d'acides organiques et d'acides gras (Leenheer, 2009).

1.2.3 Les outils de quantification et de caractérisation de la MOD

Différentes méthodes ont été développées pour quantifier la MOD, caractériser les molécules la composant et déterminer certaines propriétés moléculaires par l'intermédiaire d'indicateurs (p. ex. l'aromaticité ou le poids moléculaire) ou composition isotopique (Chasar et al., 2000; Cory et al., 2007; Helms et al., 2008; Jeanneau et al., 2014; Lamb et al., 2006; Weishaar et al., 2003). Ces indicateurs peuvent fournir des informations sur l'origine de la MOD (autochtone ou allochtone) et sa transformation par des processus de biodégradation ou de photodégradation. Il est important de combiner différentes méthodes analytiques pour décrire la MOD. En effet, l'interprétation des résultats et des méthodes décrites ci-dessous découle d'une utilisation croisée entre les méthodes, renforçant les connaissances sur les sources de la MOD et les processus biogéochimiques auxquels ils sont exposés (Dean et al., 2019; Hansen et al., 2016; Helms et al., 2008; Hutchins et al., 2017; Tfaily et al., 2015, 2018).

Les méthodes quantitatives permettent de déterminer les concentrations en COD, ainsi qu'en azote organique dissous (NOD ; Kaplan, 1992; Aiken et al., 2002; Aitkenhead et al., 2003). Cela permet de déterminer le rapport COD:NOD qui est notamment un indicateur de l'origine de la MOD (Lamb et al., 2006) ou de l'étendue de la dégradation microbienne de la MOD (Autio et al., 2016; McKnight et al., 2001). Dans l'eau interstitielle de tourbières, on constate une large gamme de concentrations en COD, allant de 20 à 250 mg L^{-1} (Birkel et al., 2017; Broder & Biester, 2015). Tfaily et al. (2015) ont montré que la gamme de concentrations pouvait varier de 56 à 185 mg L^{-1} en fonction de la profondeur à un même point d'échantillonnage. Comme pour l'eau interstitielle, la gamme de concentrations moyennes mesurées dans des ruisseaux de drainage de tourbières est très large et peut varier en moyenne entre 2.7 mg L^{-1} (Huotari et al., 2013) et 36.2 mg L^{-1} (Köhler et al., 2008). Cette variabilité des concentrations peut être expliquée par la proportion de tourbières dans l'ensemble de la superficie du bassin versant. Ainsi, Huotari et al. (2013), qui ont étudié 14 bassins versants boréaux, ont identifié une corrélation positive entre la

concentration en COD dans les cours d'eau et la proportion de tourbières dans les bassins versants (r = 0.87; p-value < 0.001). Au cours d'une année, les concentrations en COD peuvent également être très variables. On peut observer des concentrations augmentant d'un facteur 1.5 à 10 au sein d'un même ruisseau (Huotari et al., 2013). Des études ont également observé d'importantes variations interannuelles de concentrations en COD allant d'un facteur de 1.6 à 2.9 entre les années (Koehler et al., 2008; Leach et al., 2016). Ces variations peuvent être expliquées par les quantités de précipitation qui influencent les concentrations de COD (Sarkkola et al., 2009).

Outre les méthodes quantitatives, l'analyse de la MOD se base également sur l'utilisation de méthodes d'analyse qualitative. Ces analyses incluent les méthodes moléculaires, telles que la spectrométrie de masse à résonnance cyclonique ionique (FT-ICR-MS) (Kim et al., 2003), les méthodes telles que la pyrolyse combinée à une chromatographie en phase gazeuse et une spectrométrie de masse (Py-GC-MS) et la chemiolyse thermique et méthylation combinée à une chromatographie en phase gazeuse et une spectrométrie de masse (THM-GC-MS ; van Heemst et al., 2000; Page et al., 2002) qui sera spécifiquement utilisée dans les chapitres suivant.

À l'aide de ces méthodes, Tfaily et al. (2018, 2013) ont montré que la composition de la MOD présente dans l'eau interstitielle d'une tourbière ombrotrophe était variable en fonction de la profondeur. En surface, bien que la composition soit dominée par les lignines et les tannins, les auteurs ont également observé une proportion importante de lipides, de protéines et d'aminosucres dérivés de l'activité de la végétation de surface et leur proportion diminue avec la profondeur. En revanche, conjointement à l'augmentation de la proportion de lignines et de tannins en profondeur, les auteurs ont aussi observé une augmentation de la proportion des composés aromatiques condensés et des composés aliphatiques, dérivés des processus de biodégradation plus importants à l'interface entre le catotleme et l'acrotelme (Tfaily et al., 2014). Cependant, les auteurs observent une composition relativement similaire entre la surface et la profondeur et expliquent cette similarité par la résistance de ces composés aux processus de biodégradation qui persistent lors de l'advection verticale vers les horizons de tourbe les plus profonds (Tfaily et al., 2013).

Kaal et al. (2020) ont étudié la composition moléculaire de la MOD (constituée de polyphénols, d'acides gras, de carbohydrates, de protéines, de macromolécules aliphatiques) dans un ruisseau drainant une tourbière ainsi que dans une zone boisée et ils ont comparé les résultats aux potentielles sources de

végétation présentes dans le bassin versant (provenant d'échantillons végétaux de matière organique et de la matière organique soluble dans l'eau). Ils ont observé qu'en amont, la tourbière diffusait dans le ruisseau une grande proportion de tannins, des molécules aromatiques du groupe des cynnamyles et des lignines riches en lignols de types S et H contribuant majoritairement à la composition de la MOD. En revanche, cette composition changeait radicalement lorsque le ruisseau traversait la section forestière du bassin versant où ils ont alors observé une importante contribution de lignine riche en lignols de type G, mettant en évidence la contribution majoritaire des molécules dérivées des conifères au mélange de MOD.

Les méthodes isotopiques de la MOD qui correspondent à la détermination des isotopes stables du carbone (δ^{13}C-COD) et des isotopes radiogéniques (^{14}C-COD) sont également utilisées. Le δ^{13}C-COD combiné aux mesures de COD : NOD est un indicateur de l'état de décomposition et de l'origine de la matière organique dissoute. La MOD dans les eaux a un δ^{13}C-COD compris entre ≈ -25‰ et ≈ -32‰ et des ratios COD : NOD supérieurs à ≈12 (Lamb et al., 2006). Ainsi, le δ^{13}C-COD est un traceur robuste de la MOD et a permis, par exemple, à Buzek et al. (2019) d'identifier quels horizons soutenaient les exports de carbone depuis une tourbière vers un ruisseau en considérant aussi les conditions de crue et d'étiage. Le ^{14}C-COD renseigne quant à lui sur l'âge de la MOD et a montré une augmentation de l'âge de la MOD de l'eau interstitielle de la tourbe avec la profondeur (Clymo & Bryant, 2008). Cette méthode a permis à Catalán et al. (2016) de mettre en évidence une proportion importante de MOD récente et un renouvellement rapide de la MOD dans les eaux de surface. Le ^{14}C-COD a également permis d'observer une proportion significative de MOD ancienne exportée depuis les milieux terrestres vers les eaux de surface dans le cas de tourbières dégradées ou exploitées (Dean et al., 2019).

Les méthodes optiques ont permis de développer différents indicateurs de dégradation de la matière organique. On distingue les méthodes de spectrométrie d'absorbance et les méthodes de spectrofluorimétrie. La spectrométrie d'absorbance mesure la fraction de MOD chromophorique absorbant la lumière (MODc). La spectrofluorométrie mesure la MOD fluorescente (MODf) en mesurant l'émission de lumière d'un échantillon soumis à une gamme de longueurs d'onde (λ) d'excitation (des ultra-violets aux infrarouges). Parmi ces indices, l'absorbance spécifique des ultra-violets à 254 nm normalisé par la concentration en COD ($SUVA_{254}$) est un des indices les plus largement utilisés et dont les valeurs les plus élevées reflètent une matière organique plus aromatique et de plus haut poids moléculaire (Cory et al., 2011; Weishaar et al., 2003). Parmi les autres indices optiques communs, le ratio $E2 : E3$ et le ratio des pentes spectrales (S_R) sont utilisés comme des indicateurs du poids moléculaire moyen de la

MODc auxquels ils sont négativement corrélés (Haan & Boer, 1987; Helms et al., 2008). Ainsi, le $SUVA_{254}$ étant positivement corrélé au poids moléculaire, il est négativement corrélé au $E2 : E3$ et au S_R (Broder et al., 2017; Huotari et al., 2013). Parmi les indices permettant de caractériser la MODf, l'indice de fluorescence (FI) est largement utilisé et permet de discriminer les sources terrestres de MOD (FI ≈ 1.4) par opposition aux sources microbiennes (FI ≈ 1.9 ; Cory et al., 2010). L'indice de fraicheur ($\beta:\alpha$) qui renseigne sur la proportion de MOD récemment produite et dérivée de l'activité microbienne est également utilisé (Parlanti, 2000; Wilson & Xenopoulos, 2009). Les valeurs de $SUVA_{254}$ mesurées dans les ruisseaux drainant des bassins versants dominés par des tourbières sont généralement comprises entre 3.0 L mg^{-1} m^{-1} et 5.4 L mg^{-1} m^{-1} (Austnes et al., 2010; Broder et al., 2017; Hulatt et al., 2014; Huotari et al., 2013; Leach et al., 2016) alors que dans l'eau interstitielle, les mesures de $SUVA_{254}$ sont comprises entre 1.35 L mg^{-1} m^{-1} et 4.76 L mg^{-1} m^{-1} (Arsenault et al., 2019; Burd et al., 2020; Frey et al., 2016; Tfaily et al., 2015). Par ailleurs, il a été montré que, comme pour la concentration en COD, le $SUVA_{254}$ était significativement corrélé à la proportion de surfaces couvertes par des tourbières dans un bassin versant (Huotari et al., 2013; Olefeldt et al., 2013).

L'ensemble de ces indices sont sensibles aux processus de biodégradation et de photodégradation et peuvent être ainsi utilisés pour caractériser l'altération de la composition de la MOD sous l'influence de ces processus (Hansen et al., 2016). Par exemple, Mann et al. (2012) ont exploré les changements du $SUVA_{254}$, du S_R et du FI d'échantillons d'eaux prélevés dans la rivière Kolyma en Sibérie après 14 jours d'exposition à l'ensoleillement naturel. Ils ont observé que la photodégradation entrainait une augmentation du S_R de valeurs initiales allant de 0.78 à 0.82 à des valeurs de 1.02 à 1.1, ce qui représente une augmentation de 24 à 38% de cet indice. En revanche, ils ont observé pour des $SUVA_{254}$ initiaux allant de 3.91 à 4.07, une variation de +1% à -42% avec généralement une diminution de l'aromaticité. Ils ont également observé des variations du FI qui diminuait de 5 à 11% au cours des expériences de photodégradation, pour des valeurs initiales comprises entre 1.38 et 1.51 et donc qui conservait une signature proche de la MOD d'origine terrestre (Cory et al., 2010). À l'inverse, durant des expériences de biodégradation, des augmentations du $SUVA_{254}$ de 12% à 58% pour de l'eau provenant de ruisseau et de 14% à 28% pour de l'eau interstitielle de tourbières ont été mesurées (Payandi-Rolland et al., 2020). Comme pour l'exposition aux processus de photodégradation, Payandi-Rolland et al. (2020) ont noté une diminution du FI au cours des expériences de biodégradation, de -15% pour des échantillons d'eau interstitielle et de -12 à -32% pour des échantillons de ruisseau. Alors qu'une augmentation des valeurs de FI seraient attendues à la suite des processus de biodégradation, les auteurs expliquent la diminution du

FI par la persistance de molécules peu dégradables à la fin des incubations, suggérant une tendance vers des signatures proches de celle de la MOD d'origine terrestre (FI ≈ 1.4 ; Cory et al., 2010).

1.3 Les tourbières : un élément important cycle du carbone dans les bassins versants

À l'échelle des bassins versants, plusieurs facteurs peuvent influencer la quantité et la composition du carbone et particulièrement du COD exporté dont la topographie, la composition des sols et de la végétation (Kortelainen et al., 2006; Rantakari et al., 2010). En contexte boréal, plusieurs études ont mis de l'avant l'importance des surfaces occupées par les tourbières comme prédicteurs de la quantité de COD exportée et de la composition de la MOD (Aitkenhead et al., 1999; Kortelainen et al., 2006; Laudon et al., 2011; Rantakari et al., 2010).

L'augmentation du degré de décomposition de la tourbe avec la profondeur induit une diminution de la porosité de la tourbe (Quinton et al., 2008; Surridge et al., 2005) et de la conductivité hydraulique (Hoag & Price, 1995). Les tourbières sont caractérisées par deux horizons organiques principaux appelés acrotelme et catotelme (Ingram, 1983; Ivanov, 1981). L'acrotelme correspond à la couche de surface, peu dégradée et constituée de fragments végétaux peu décomposés. C'est dans l'acrotelme que le niveau de la nappe varie et donc où ont lieu les processus de décomposition. Le catotelme est la couche de tourbe située en dessous de la surface de la nappe. Il est constitué de matière organique plus ou moins décomposée selon les horizons et il est toujours saturé en eau. Du fait de la saturation en eau, la dégradation de la matière organique se fait uniquement par des processus anaérobiques.

La structure de la tourbe, caractérisée par sa porosité importante en surface (Rezanezhad et al., 2016), va favoriser la solubilisation du COD dans l'eau interstitielle de l'acrotelme (Tfaily et al., 2018). La production de COD augmente avec la température de l'air et par le niveau de la nappe qui favorise des conditions aérobiques (Clark et al., 2009; Grand-Clement et al., 2014; Zhu et al., 2022). Ainsi, des expériences menées en conditions contrôlées par Clark et al. (2009) ont montré que l'augmentation de la température de 10°C à 20°C entrainait une augmentation de la production de COD d'un facteur 1.84 en condition anaérobique et d'un facteur 3.84 en condition aérobique. Cependant, Laudon et al. (2012) ont montré que l'amplification de la production de COD avec l'augmentation des températures est limitée. En effet, au-delà d'un certain seuil de température, la minéralisation par le métabolisme oxique (Clark et al., 2009; Grand-Clement et al., 2014) augmente de façon disproportionnelle par rapport à la production de COD qui devient limitante.

L'eau qui circule dans la tourbe par les écoulements de subsurface va pouvoir se charger en COD, consécutivement à l'augmentation du niveau de la nappe (Evans et al., 1999). La connectivité hydrologique entre les tourbières et le reste du bassin versant, notamment les ruisseaux, va entrainer le transfert latéral de COD vers les milieux en aval de la tourbière (Billett et al., 2006). Ces transferts de COD sont favorisés par les faibles processus d'adsorption, liés à l'absence de phase minérale. De ce fait, de plus grandes proportions de COD sont exportées depuis les bassins versants où d'importantes superficies sont couvertes par des tourbières (Fig. 1.2, Laudon et al., 2004, 2011; Rantakari et al., 2010; Olefeldt et al., 2013).

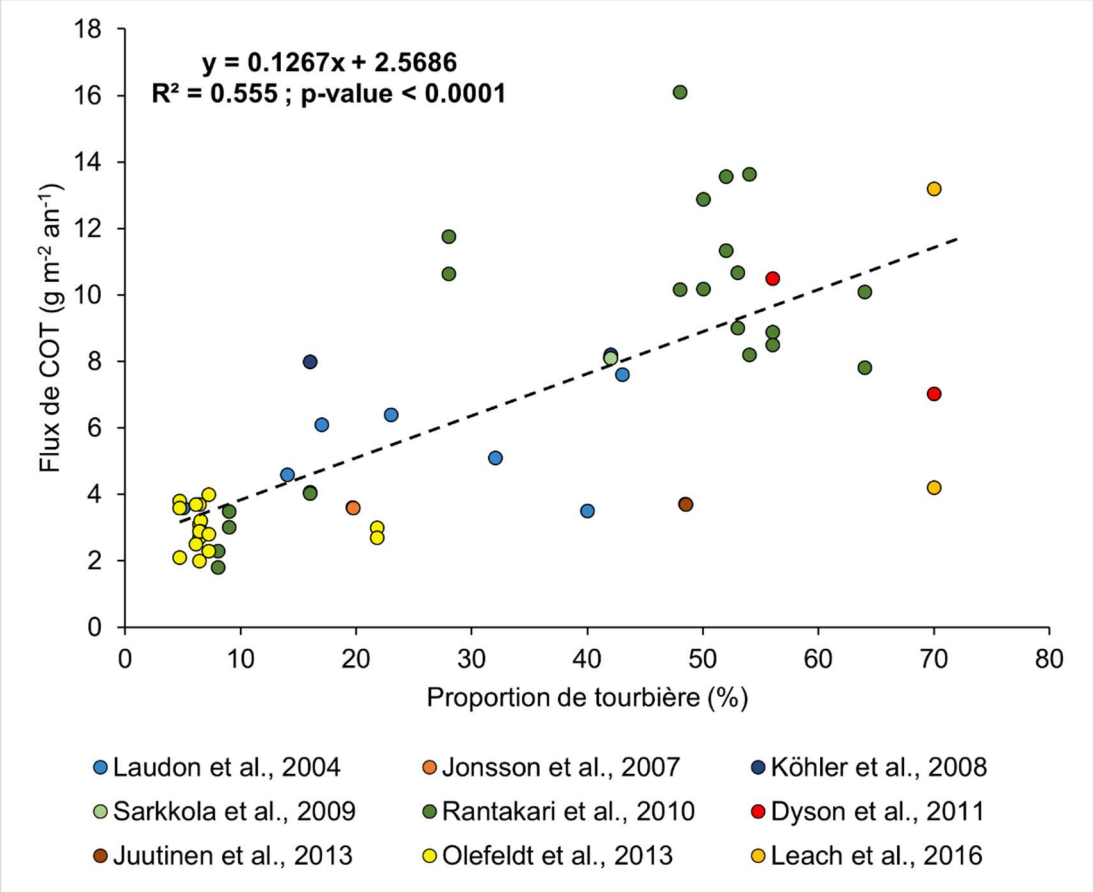

Figure 1.2 Flux de carbone organique total (COT) en fonction de la proportion du bassin versant couverte par des tourbières dans différents bassins versants boréaux (données tirées de Laudon et al., 2004; Jonsson et al., 2007; Köhler et al., 2008; Sarkkola et al., 2009; Rantakari et al., 2010; Dyson et al., 2011; Juutinen et al., 2013; Olefeldt et al., 2013; Leach et al., 2016).

Les tourbières boréales semblent transférer moins de COD (13.7 g m^{-2} an^{-1} en moyenne ; Rosset et al., 2022) comparativement aux tourbières situées en milieu tempéré ou tropical qui exportent en moyenne 24.2 g m^{-2} an^{-1} et 57.9 g m^{-2} an^{-1} respectivement (Evans et al., 2016; Rosset et al., 2022). Cependant leur importante densité dans certaines régions nordiques (Yu et al., 2010) où se trouve 85% de la surface globale de tourbières, souligne l'importance de mesurer adéquatement leurs flux. En effet, 58% du COD exporté par les tourbières vers les eaux de surface proviendrait des tourbières boréales (Rosset et al., 2022). Bien que les flux de carbone peuvent être sous différentes formes (COP, CO_2 ou CH_4), le COD constitue la forme principale d'exports, représentant de 57 à 91 % des flux totaux de carbone aquatique exporté par les tourbières (Dinsmore et al., 2013; Holden et al., 2012; Leach et al., 2016; Roulet et al., 2007; Worrall et al., 2009). Ces flux peuvent représenter entre 14% et 132% du ENE (Roulet et al., 2007; Nilsson et al., 2008; Worrall et al., 2008; Dinsmore et al., 2010) et ainsi excéder le ENE certaines années de mesures, favorisées par d'importantes précipitations annuelles et des températures moyennes annuelles plus élevées (Koehler et al., 2011; Roulet et al., 2007).

1.4 Les mécanismes de transfert de la matière organique dissoute et le devenir de la MOD exportée

1.4.1 Les mécanismes de transfert de la MOD

La MOD exportée depuis les tourbières vers les eaux de surface des bassins versants (par ex., les ruisseaux, les mares ou les lacs) provient principalement de la MOD produite et diffusée dans l'acrotelme (Billett et al., 2006; Worrall et al., 2008; Buzek et al., 2019). Ainsi, la MOD peut être transférée par des écoulements de subsurface (Freeman et al., 2001; Laudon et al., 2011; Tunaley et al., 2016) et des infiltrations de l'eau interstitielle provenant du catotelme vers les eaux de surface (Tunaley et al., 2017). L'étude des transferts de COD est importante à étudier, considérant que sa dégradation une fois transférée peut contribuer jusqu'à 75 % du flux de CO_2 des milieux aquatiques (Rasilo et al., 2017) , sous l'effet des processus de biogédradation et de photodégradation (Lapierre & del Giorgio, 2014; Vonk et al., 2015).

L'étude des relations entre le débit (*Q*) et le COD et entre le niveau de la nappe (NN) et le COD a fait ressortir des relations non linéaires telles que des relations hystérétiques ou logarithmiques (Birkel et al., 2017; Blaurock et al., 2021; Gómez-Gener et al., 2021; Laudon et al., 2011; Tunaley et al., 2016, 2017). Bien que quelques études aient présenté un processus de dilution du COD lors d'épisodes de crues (Broder et al., 2017; Clark et al., 2008) et particulièrement lors des crues de printemps (Dyson et al., 2011; Leach et al., 2016), plusieurs autres études ont mis de l'avant une augmentation de la concentration en COD durant ces évènements (Austnes et al., 2010; Birkel et al., 2017; Blaurock et al., 2021; Dick et al., 2015;

Rosset et al., 2020; Sharma et al., 2022; Tunaley et al., 2016; Zhu et al., 2022). Cela suggère que les évènements de crues sont des moments importants pour l'export de COD (Birkel et al., 2017; Broder & Biester, 2015; Clark et al., 2007; Dick et al., 2015; Rosset et al., 2019; Tunaley et al., 2017)

1.4.2 L'étude des évènements de crues pour mieux comprendre les mécanismes de transfert de la matière organique dissoute

Des indices ont été développés à partir de l'analyse des relations entre le débit et les concentrations en COD durant les évènements de crues. Le développement de ces indices a permis de quantifier la réponse du COD à une augmentation du débit durant les différentes phases de l'hydrogramme de crue. Ils ont également permis d'identifier les mécanismes de transfert du COD au sein d'un bassin versant (Godsey et al., 2009, 2019; Langlois et al., 2005; Lawler et al., 2006; Lloyd et al., 2016; Zarnetske et al., 2018).

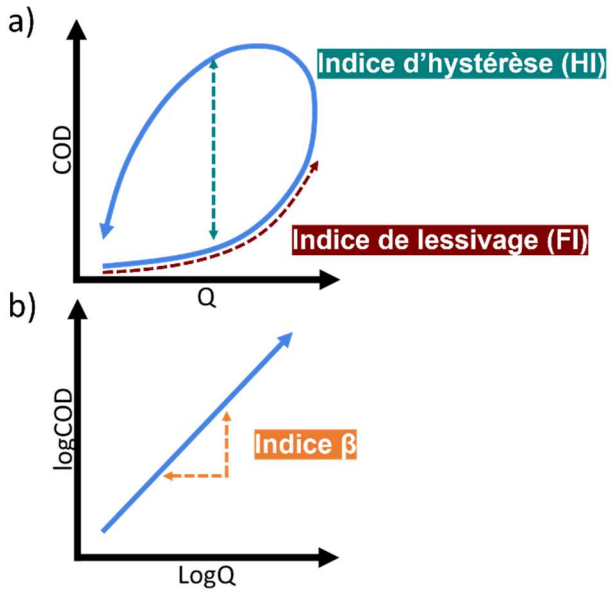

Figure 1.3 Représentation a) des indices HI et FI basée sur la relation entre la concentration de COD et le débit, présentée ici dans le cas d'une relation hystérétique anti-horaire positive, et b) de l'indice β déterminé par la relation entre la concentration en COD et le débit après une transformation logarithmique.

Parmi ces indices, les indices d'hystérèses (HI) ont été développés afin d'identifier la présence de relation hystérétique et les caractéristiques des hystérèses (Fig. 1.3.a ; Langlois et al., 2005; Lawler et al., 2006; Lloyd et al., 2016; Zuecco et al., 2016). Une hystérèse est la réponse non linéaire d'une variable dépendante, telle que la concentration en COD, à une variable indépendante, telle que le débit (Phillips,

2003). Les boucles hystérétiques apparaissent avec un décalage temporel entre la réponse de la variable dépendante aux fluctuations de la variable indépendante (Prowse, 1984). L'étude de ces relations et le développement d'indices hystérétiques permettent de rendre compte des processus hydrologiques sous-jacents aux fluctuations de la variable dépendante (Zuecco et al., 2016). Par exemple, l'étude des relations hystérétiques entre la concentration en COD et le Q a permis d'émettre des hypothèses sur la distance entre les origines de COD au sein d'un bassin versant et le cours d'eau où étaient mesurées les concentrations en fonction de l'amplitude de la boucle hystérétique (Tunaley et al., 2017). L'observation d'hystérèses antihoraires peut également suggérer un décalage entre les concentrations en COD et le débit, à la suite de l'augmentation progressive du niveau de la nappe dans le bassin versant, illustrant la progression de l'augmentation de la connectivité hydrologique entre le bassin versant et le cours d'eau (Blaurock et al., 2021). L'étude des relations hystérétiques lors de la fonte de la neige au printemps a également permis de différencier les origines de COD entre les écoulements de subsurface et ceux provenant du manteau neigeux (Ågren et al., 2010).

En plus des indices relatifs aux hystérèses, d'autres indices peuvent être utilisés pour décrire la relation entre le COD et le Q durant les évènements de crues. L'utilisation de l'indice FI (*flushing index*) rend compte de la réaction de la concentration en COD durant la phase de croissance de la crue (Fig. 1.3.a ; Vaughan et al., 2017). Le calcul de cet indice se base sur la différence entre la concentration initiale en COD et la concentration lorsque le pic de crue est atteint. Il permet ainsi d'identifier un effet de dilution ou une augmentation de la concentration en COD à la suite de l'augmentation du débit. L'indice β correspond à la pente de la relation logarithmique entre le débit et la concentration en COD (Fig. 1.3.b ; Godsey et al., 2009). Son utilisation permet de renseigner sur le facteur limitant des exports de COD. Les exports peuvent être limités par le transport, les sources ou être chemostatiques (Godsey et al., 2009, 2019; Zarnetske et al., 2018).

À ce jour, les études portant sur les exports de COD durant des évènements de crues dans des ruisseaux de drainage de tourbières boréales se sont concentrées sur l'étude des crues de printemps (Ågren et al., 2010; Dyson et al., 2011; Laudon et al., 2004; Tiwari et al., 2018). L'étude des évènements de crues est importante pour comprendre les mécanismes qui contrôlent la quantité de COD exportée. Par exemple, l'étude des crues printanières a permis de montrer qu'une majorité des exports annuels de COD pouvaient avoir lieu pendant cet évènement consécutif au dégel du bassin versant (Ågren et al., 2010; Dyson et al., 2011; Leach et al., 2016) et malgré la dilution des concentrations en COD engendrée par la fonte de la

neige (Ågren et al., 2010; Leach et al., 2016). Cependant, Laudon et al. (2004) ont montré que la proportion du COD exporté durant les crues de printemps était négativement corrélée à la proportion de tourbières dans un bassin versant du fait du ruissellement de l'eau de fonte, peu chargée en COD, sur des tourbières encore gelées. En revanche, la relation inverse était observée lorsqu'on mesurait les exports de COD sur une année complète (Laudon et al., 2011). Ce constat renforce la nécessité de documenter les mécanismes du transfert de COD des tourbières boréales en étudiant des évènements isolés.

Durant la saison de croissance, les exports de COD vers les ruisseaux de drainage semblent être favorisés par les précipitations (Birkel et al., 2017) qui entrainent une augmentation du niveau de la nappe (Broder & Biester, 2015; Clark et al., 2007; Inamdar et al., 2004). Cette augmentation du niveau de la nappe dans l'acrotelme renforce la connectivité hydraulique entre la tourbe et les eaux de surface et crée des conditions favorables aux exports de COD (Bishop et al., 2004; Frei et al., 2010; Birkel et al., 2017 ; Fig. 1.3). Dans l'ensemble, la température de l'air (Dinsmore et al., 2013; Koehler et al., 2009), les fluctuations du niveau de la nappe (Broder & Biester, 2015; Clark et al., 2007; Inamdar et al., 2004), les sécheresses précédant un évènement de crue (Birkel et al., 2017; Tunaley et al., 2016) créent des conditions favorables à la production de COD dans l'acrotelme qui sera par la suite disponible pour l'export vers les eaux de surface. En revanche, des évènements de crues rapprochés dans le temps peuvent entrainer une diminution des exports de COD due aux réserves de COD qui ne sont pas totalement restaurées à la suite des évènements successifs (van Verseveld et al., 2009). L'étude des relations COD-Q lors des évènements de crues, en dehors de la crue de printemps, permettrait de mieux comprendre les mécanismes et les facteurs favorisant les exports de COD durant ces périodes.

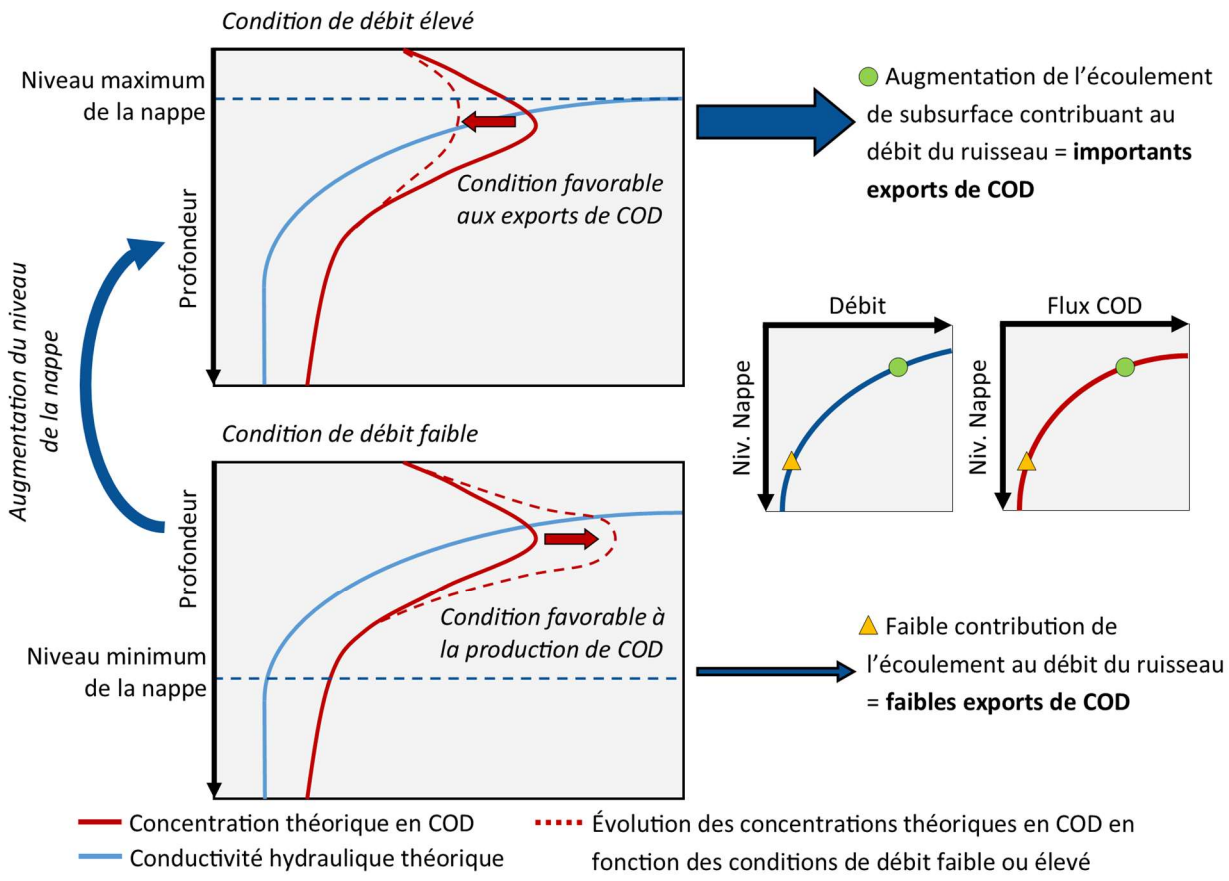

Figure 1.4 Modèle conceptuel des exports de carbone organique dissous depuis une tourbière vers un ruisseau de drainage en fonction des conditions hydrologiques de débits élevés ou de débits faibles (selon Bishop et al., 2004 ; Holden, 2005 ; Clark et al., 2008, 2009 ; Ågren et al., 2010 ; Tunaley et al., 2016, 2017 ; Birkel et al., 2017)

Tout comme les concentrations de COD varient en fonction du débit ou du niveau de la nappe, des études ont également montré des variations dans la composition de la MOD en fonction des conditions hydrologiques (Austnes et al., 2010; Buzek et al., 2019) et des saisons (Broder et al., 2017). Des travaux ont également montré que la composition de la MOD variait en fonction de la température de l'air (Birkel et al., 2017; Fenner et al., 2005; Moore et al., 2008; Worrall et al., 2008), des variations du niveau de la nappe (Clark et al., 2009; Grand-Clement et al., 2014) et des processus de biodégradation et de photodégradation (Autio et al., 2016; Cory et al., 2007, 2013; Hulatt et al., 2014; Payandi-Rolland et al., 2020; Saadi et al., 2006).

Cependant, la variabilité spatio-temporelle de la composition de la MOD exportée depuis les tourbières vers les eaux de surface n'a été que peu documentée à ce jour (Austnes et al., 2010; Broder et al., 2017; Buzek et al., 2019). Grand-Clement et al. (2014) ont montré que la composition de la MOD exportée vers les cours d'eau pouvait refléter l'action des processus de dégradation (Payandi-Rolland et al., 2020). Buzek et al. (2019), en comparant la signature isotopique de la MOD dans une tourbière et dans un ruisseau sous différentes conditions de débit, ont montré que la MOD exportée provenait d'une profondeur de tourbe spécifique où l'eau circule. Broder et al. (2017) ont observé des changements de composition de la MOD, dépendamment des écosystèmes contribuant aux exports de COD au sein d'un bassin versant. Par exemple, ils ont souligné que bien le S_R soit en moyenne similaire entre un ruisseau drainant une zone tourbeuse (S_R = 1.80 ± 0.9) et un autre drainant une zone forestière (S_R = 1.84 ± 0.08), des valeurs plus importantes ont été mesurées dans la zone forestière durant la fonte de la neige (S_R = 2.2) ou durant des évènements de pluie (S_R = 2.0) révélant un plus faible poids moléculaire de la MOD. Ils ont également montré que malgré une faible variabilité du FI au cours de l'année, cet indice était significativement plus élevé dans le ruisseau de la zone forestière (FI = 1.63 ± 0.05) que dans la zone tourbeuse (FI = 1.58 ± 0.04), permettant de distinguer ces deux sources.

Austnes et al. (2010), qui ont étudié des évènements de crues dans un ruisseau de drainage d'une tourbière du Pays de Galles, ont aussi montré que durant les épisodes de crues, le COD : NOD pouvait augmenter de 57 à 103% par rapport aux valeurs en période de basses eaux. Ils ont également montré que le $SUVA_{254}$ pouvait diminuer de 16 à 28%, tandis que le ratio $E2 : E3$ pouvait augmenter de 3 à 27% durant les épisodes de crues. Ils ont expliqué ce changement de composition, vers une MOD moins aromatique et de plus faible poids moléculaire, par le basculement d'une source d'eau dans le ruisseau provenant majoritairement des eaux souterraines pendant les périodes de basses eaux à source d'eau provenant du ruissellement de subsurface dans la tourbe pendant les périodes de hautes eaux, entrainant la MOD récemment produite dans l'acrotelme.

1.4.3 Le cas des mares de tourbières dans le cycle du carbone

Bien que les exports de COD depuis les tourbières vers les milieux aquatiques (Birkel et al., 2017; Dick et al., 2015; Juutinen et al., 2013; Koehler et al., 2009; Leach et al., 2016; Rantakari et al., 2010; Roulet et al., 2007) et la composition de la MOD exportée (Austnes et al., 2010; Broder et al., 2017; Buzek et al., 2019; Grand-Clement et al., 2014) aient été documentés, très peu d'études portent sur la connectivité entre les mares de tourbières et les implications sur la composition de la MOD (Arsenault et al., 2019; Banaś, 2013;

Schindler et al., 1997). Les mares de tourbières de hautes latitudes font partie des microformes typiques de ces écosystèmes avec les buttes, les platières et les dépressions (Charman, 2002). Elles sont importantes, car elles peuvent représenter une proportion de 5 % à 50 % de la surface des tourbières (Pelletier et al., 2014, 2015; White, 2011) et elles constituent des sources nettes de CO_2 et de CH_4 vers l'atmosphère (Pelletier et al., 2014). Cependant, les sources de la MOD, ainsi que les processus de production et de dégradation au sein de mares ont été très peu documentés. La contribution de MOD dérivée de la tourbière a déjà été mise en évidence (Banaś, 2013) et des études ont présenté des différences dans la composition de la MOD entre l'eau interstitielle des tourbières et celle des mares (Payandi-Rolland et al., 2020; Schindler et al., 1997). Ces différences pourraient être associées à des processus de biodégradation et de photodégradation dans les mares (Arsenault et al., 2019; Laurion et al., 2021; Laurion & Mladenov, 2013) contribuant ainsi aux émissions de carbone mesurées à leur surface (Pelletier et al., 2015). L'approfondissement de l'étude de la MOD dans les mares est donc crucial afin de mieux comprendre le rôle qu'elles jouent dans le cycle du carbone des tourbières.

1.5 Méthodes et enjeux de la mesure des flux de carbone organique dissous

1.5.1 Les méthodes de suivis à haute fréquence

Un des enjeux de la quantification de la concentration en COD est la variabilité temporelle (Downing et al., 2009). Il est aujourd'hui largement admis que dans les eaux de surface, la concentration en COD peut varier rapidement de plusieurs ordres de grandeur en fonction du débit (Birkel et al., 2017; Clark et al., 2007; Dick et al., 2015; Rosset et al., 2019; Tunaley et al., 2017). Depuis la fin des années 2000, le développement de nouveaux outils a permis de faire des suivis à haute fréquence des concentrations en COD par une mesure de la MODf (Downing et al., 2009). Malgré que les mesures réalisées par ces capteurs soient sensibles à certains facteurs environnementaux (par ex., la température, la turbidité ou l'effet de filtre interne), des méthodes de correction du signal de la MODf ont été développées (de Oliveira et al., 2018). Ainsi, les méthode de mesure à haute fréquence ont permis des avancées majeures dans la précision de la quantification des flux comme dans la compréhension des mécanismes d'export de COD, basées sur les relations non linéaires entre les concentrations COD et le débit (Blaurock et al., 2021; Tunaley et al., 2016, 2017) et entre les concentrations en COD et le niveau de la nappe (Rosset et al., 2020) que ne permettraient pas des échantillonnages ponctuels.

1.5.2 Les limites de la quantification des flux de carbone organique dissous

Bien que les tourbières représentent une source majeure du COD au sein d'un bassin versant (Billett et al., 2006; Laudon et al., 2011; Rantakari et al., 2010; Tipping et al., 2010), la contribution des autres sources (p. ex., forêts, milieux humides, prairies ou agroécosystèmes) au flux de carbone mesuré dans les milieux aquatiques ne doit pas être négligée (Webb et al., 2019). La capacité de calculer un flux spécifique de COD, soit une quantité de COD exportée par année et normalisée par la surface contributrice au flux, dans l'établissement d'un bilan de carbone est cruciale pour ne pas sous-estimer le flux de DOC provenant d'une tourbière et par conséquent surestimer l'accumulation de carbone (Billett et al., 2006, 2012; Rosset et al., 2019; Tipping et al., 2010). Ceci aurait pour conséquence, par soustraction à la PNE, de sous-estimer l'accumulation de carbone dans la tourbière. Des méthodes ont dû être définies afin de calculer des flux spécifiques. Cependant, la difficulté d'obtention de flux spécifiques a conduit certaines études à envisager une approche conservatrice. Ces études s'appuient sur l'hypothèse que le flux est composé de sources d'origines variées au sein de l'écosystème sans pouvoir les discriminer et elles utilisent la surface du bassin versant pour normaliser le flux de COD (Dick et al., 2015; Dinsmore et al., 2013; Koehler et al., 2009; Köhler et al., 2008; Worrall et al., 2009). La limite de cette approche est de sous-estimer le flux de COD provenant de tourbières, et ce, particulièrement pendant les épisodes de crues durant lesquels elles seraient les principales contributrices (Birkel et al., 2017; Buzek et al., 2019; Rosset et al., 2019). Une autre méthode, basée sur la configuration physiographique du bassin versant, consiste à soustraire les flux entrants dans une tourbière aux flux de COD sortants en émettant l'hypothèse que la différence entre les deux correspond à la contribution de la tourbière (Rosset et al., 2019). Cependant, cette méthode n'est applicable que dans le cas où l'ensemble des sources sont identifiables et peuvent être instrumentées.

Une approche intermédiaire doit être trouvée, présentant les avantages i. d'être conservatrice sans mésestimer le flux spécifique de COD dans les tourbières et ii. d'être applicable à différentes configurations de bassins versants. L'exploration des relations COD-Q issues du suivi à haute fréquence du débit et des concentrations en COD peut alors devenir une voie intéressante à exploiter afin de répondre aux avantages mentionnés précédemment. Les travaux basés sur ces relations et les indices qui ont été développés sont autant d'outils qui permettent à la fois d'explorer les sources et les mécanismes de transfert du carbone vers les milieux aquatiques (voir section 1.4.1).

1.6 Objectifs généraux

À la lumière de cet état des connaissances, les travaux menés durant cette thèse ont eu pour objectif principal de quantifier la dynamique spatio-temporelle de la composition de la MOD et les exports de COD issus d'une tourbière ombrotrophe au sein d'un bassin versant boréal de l'est du Québec (Canada). Les travaux reposent sur la mesure à haute fréquence du COD et du débit à l'exutoire du ruisseau en tête de bassin versant, sur des échantillonnages ponctuels d'eau ayant permis d'analyser la composition de la MOD ainsi que sur les variations de la nappe au cours de la saison de croissance. Ces travaux constituent la première contribution des exports de COD dans une tourbière boréale de l'est du Québec. L'originalité des travaux repose également sur l'utilisation d'une combinaison de méthodes analytiques (élémentaires, moléculaires, isotopiques et optiques) permettant de décrire la composition de la MOD dans l'eau interstitielle de la tourbière, des mares et du ruisseau durant neuf missions de terrain ayant eu lieu entre juin 2018 et octobre 2019. Les échantillonnages ont eu lieu au cours de différentes saisons et sous différentes conditions hydroclimatiques. Ils offrent ainsi un portrait complet de la composition de la MOD et des variations saisonnières de celle-ci.

Plus précisément, les objectifs spécifiques de cette thèse sont :

i) De quantifier les exports spécifiques de COD et de caractériser les mécanismes de transfert du COD durant les épisodes de crues.
ii) D'évaluer l'effet des conditions hydrologiques dans le bassin versant sur les changements de composition et les processus de transformation de la MOD au cours de son export dans le ruisseau de drainage.
iii) D'approfondir les connaissances sur le rôle des mares dans la production et la transformation du COD à travers l'étude de sa composition et de sa dégradabilité dans l'eau interstitielle et dans les mares.

Le premier chapitre porte sur les relations entre les exports de COD à l'exutoire de la tourbière et les variables hydrologiques (niveau de la nappe et débit). L'étude des données à haute fréquence a permis de mettre en évidence les liens entre les exports de COD et les données hydrologiques du ruisseau et de la tourbière. Cela a permis de calculer efficacement les flux spécifiques de COD provenant de la tourbière en décomposant la série temporelle des débits du ruisseau entre des périodes de hautes eaux et de basses eaux. Par ailleurs, l'étude des évènements de crues isolés de la série temporelle et le calcul d'indices

spécifiques à ce type d'évènements ont aussi permis de caractériser les mécanismes d'exports de COD depuis la tourbière vers le ruisseau. Le chapitre a été soumis pour publication à la revue *Hydrology and Earth System Science* en décembre 2022 (pré-impression publiée en mars 2023).

Le second chapitre visait à étudier la variabilité de la composition de la MOD au sein du ruisseau en lien avec les exports de COD provenant de la tourbière. Ce travail a permis de se concentrer sur la variabilité de la composition de la MOD entre les périodes de basses eaux et de hautes eaux qui ont été décrites dans le premier chapitre. Il a aussi permis de souligner la variabilité spatiale de la composition de la MOD du ruisseau et de la croiser avec les apports de COD obtenus par des bilans de masse ponctuels réalisés durant les quatre campagnes de terrain de l'année 2019. Ce chapitre sera prochainement soumis pour publication à la revue Journal of Geophysical Research : Biogeosciences.

Le troisième et dernier chapitre vise à apporter de nouvelles connaissances sur le rôle des mares de tourbière dans le cycle du carbone à travers l'étude de l'origine, de la composition et de la dégradabilité de la MOD dans les mares et l'eau interstitielle de la tourbière étudiée. Ce chapitre présente également l'évolution de la composition de la MOD dans l'eau interstitielle et les mares au cours de la saison de croissance. Finalement, il permet d'identifier la contribution des mares au bilan de carbone de la tourbière. Ce chapitre qui a été soumis à la revue *Biogeosciences* a été publié en septembre 2022.

CHAPITRE 2

Hydrological connectivity controls dissolved organic carbon exports in a peatland-dominated boreal catchment stream

Antonin Prijac[1,2,3], Laure Gandois[4], Pierre Taillardat[1,2,5], Marc-André Bourgault[6], Khawla Riahi[7], Alex Ponçot[1], Alain Tremblay[8] and Michelle Garneau[1,2,3,9]

[1]Centre de Recherche sur la Dynamique du Système Terre (GÉOTOP), Université du Québec à Montréal, Montréal, Canada
[2]Groupe de Recherche Inter-universitaire en limnologie (GRIL), Université du Québec à Montréal, Montréal, Canada
[3]Institut des Sciences de l'Environnement (ISE), Université du Québec à Montréal, Montréal, Canada
[4]Laboratoire Écologie Fonctionnelle et Environnement, UMR 5245, CNRS-UPS-INPT, Toulouse, France
[5]NUS Environmental Research Institute, National University of Singapore, Singapore
[6] Département de Géographie, Université Laval, Québec, Canada
[7]Centre Eau, Terre et Environnement, Institut National de la Recherche Scientifique, Québec, Canada
[8]Programme Gaz à Effet de Serre, Hydro-Québec, Montréal, Canada
[9]Département de Géographie, Université du Québec à Montréal, Montréal, Canada

Pré-impression publiée en mars 2023 dans la revue Hydrology and Earth System Science

Résumé

Les exports de carbone organique dissous (COD) provenant des tourbières boréales sont variables pendant la saison sans glace, en fonction du niveau de la nappe de la tourbière et de l'alternance des périodes de hautes eaux et de basses eaux dans le ruisseau drainant la tourbe. Cependant, le calcul des flux spécifiques de COD provenant d'une tourbière peut-être difficile considérant les multiples sources potentielles de COD au sein du bassin versant. Une approche de calcul basée sur la connectivité hydrologique entre la tourbe et le ruisseau pourrait aider à résoudre ce problème, cette approche est utilisée dans cette étude. L'étude s'est étendue entre juin 2018 et juin 2020 dans un bassin versant boréal du nord-est du Canada, couvert à 76.7% par une tourbière ombrotrophe. Les objectifs sont (1) d'établir les relations entre les exports de COD depuis le ruisseau de tête de bassin versant et l'hydrologie de la tourbière, (2) de quantifier, à l'échelle du bassin versant, la quantité de COD exportée vers le ruisseau de drainage et (3) de définir les types de mobilisation du COD pendant les évènements de hautes eaux. À l'exutoire du ruisseau de drainage, les concentrations en COD ont été mesurées à la fréquence horaire à l'aide d'un capteur de mesure de la matière organique fluorescente, un proxy du COD. Les variables hydrologiques, incluant le débit du ruisseau à l'exutoire et le niveau de la nappe (NN) de la tourbière, ont été mesurées en continu pendant les deux années. Nos résultats montrent le contrôle direct et décalé des écoulements de subsurface depuis la tourbière vers le ruisseau, auxquels sont associés les exports de COD. Les évènements de pluie entrainent une augmentation du NN de la tourbière qui augmente la connectivité hydrologique entre la tourbière et le ruisseau. Cela entraine une augmentation du débit et un décalage dans l'augmentation des concentrations en COD, typique des écoulements de subsurface. L'intensité de l'augmentation du NN joue un rôle crucial, influençant la quantité de COD exportée. À partir de l'hypothèse que la tourbière est le principal contributeur du COD exporté et que les autres sources sont négligeables pendant les hautes eaux, nous proposons une nouvelle approche pour calculer les flux spécifiques de COD attribuables à la tourbière, en distinguant la surface utilisée pour calculer le flux entre les périodes de basses et hautes eaux. En 2018-2019, 92.6% du COD a été exporté pendant les périodes de crue, alors que ces périodes comptent pour 59.1% de la période de mesure. En 2019-2020, 93.8% du COD a été exporté pendant les périodes de crue, alors que ces périodes comptent pour 44.1% de la période de mesure. Notre analyse des évènements individuels de crue montre trois types d'évènements et de mobilisation du COD. Le premier type est caractérisé par des précipitations importantes qui entrainent une importante augmentation du NN, favorisant la connexion entre la tourbière et le ruisseau et entrainant d'importants flux de COD. Le second est caractérisé par une importante augmentation du NN succédant à un précédent évènement qui a diminué la quantité de COD disponible à l'export dans le ruisseau et entraine de plus faibles exports. Le troisième type correspond à de faibles évènements de précipitation qui amènent à une augmentation insuffisante du NN pour amener à une importante reconnexion entre la tourbière et le ruisseau et conduisent à de faibles exports. Ainsi, les exports de COD sont sensibles aux conditions hydroclimatiques. Cependant les évènements de crues, le changement des régimes de précipitations, la durée de la période sans glace et la température de la tourbe pourraient affecter la quantité de COD exportée et de ce fait, partiellement, contrebalancer la capacité de séquestration du carbone des tourbières.

Abstract

Peatland-derived dissolved organic carbon (DOC) exports from boreal peatlands are variable during the ice-free season, depending on the peatland water table and the alternation of low and high flow in peat-draining streams. However, calculation of the specific DOC exports from a peatland can be challenging considering the multiple potential DOC sources within the catchment. A calculation approach based on the hydrological connectivity between the peat and the stream could help to solve this issue, an approach used in the present study. This study took place from June 2018 to October 2019 in a boreal catchment in north-eastern Canada, with 76.7% of the catchment covered by ombrotrophic peatland. The objectives were (1) to establish relationships between DOC exports from a headwater stream and the peatland hydrology; (2) to quantify, at the catchment scale, the amount of DOC laterally exported to the draining stream; and (3) to define the patterns of DOC mobilization during high river flow events. At the peatland headwater stream outlet, the DOC concentrations were monitored at a high frequency (hourly) using a fluorescent dissolved organic matter (fDOM) sensor, a proxy for DOC concentrations. Hydrological variables, such as stream outlet discharge and the peatland water table depth (WTD), were continuously monitored at 1h intervals for 2 years. Our results highlight the direct and delayed control of subsurface flow from peat to the stream and associated DOC exports. Rain events raised the peatland WTD, which increased the hydrological connectivity between the peatland and the stream. This led to increased stream discharge (*Q*) and a delayed DOC concentration increase, typical of lateral subsurface flow. The magnitude of the WTD increase played a crucial role in influencing the quantity of exported DOC. Based on the assumption that the peatland is the major contributor to DOC exports and other DOC sources were negligible during high-flow periods, we propose a new approach to calculate the specific DOC exports attributable to the peatland by distinguishing the surface used to the calculation between high-flow and low-flow periods. In 2018–2019, 92.6% of DOC was exported during flood events, despite accounting for 59.1% of the period. In 2019–2020, 93.8% of DOC was exported during flood events, which represented 44.1% of the period. Our analysis of individual flood events revealed three types of events and DOC mobilization patterns. The first type is characterized by high rainfall leading to an important WTD increase favouring the connection between the peatland and the stream, leading to high DOC exports. The second is characterized by a large WTD increase succeeding a previous event that had depleted DOC available to be transferred to the stream, leading to lower DOC exports. The third type corresponds to low rainfall events with an insufficient WTD increase to reconnect the peatland and the stream, leading to low DOC exports. Hence, DOC exports are sensitive to hydroclimatic conditions. Moreover, flood events, changes in rainfall regimes, the ice-free season duration and porewater temperatures may affect the exported DOC and, consequently, partially offset the carbon sequestration capacity of peatlands.

2.1 Introduction

At the global scale, boreal peatlands are the main contributors of dissolved organic carbon (DOC) exported to the aquatic continuum, accounting for 58% of the global exports (Rosset et al., 2022). In the context of a net ecosystem carbon budget, quantifying DOC exports, as well as particulate organic carbon (POC) and dissolved inorganic carbon (DIC) exports, it is crucial to evaluate how much carbon is lost through this pathway (Webb et al., 2019). Ignoring those carbon losses may, in some cases, overestimate annual peatland carbon accumulation by 40%–80% (Roulet et al., 2007). DOC is the main form of exported carbon and accounts for 54.3%–91% of the total aquatic carbon exported (Dinsmore et al., 2013; Holden et al., 2012; Leach et al., 2016; Roulet et al., 2007; Worrall et al., 2009). Moreover, DOC can be mineralized along the aquatic continuum and get converted into dissolved CO_2 (Aho & Raymond, 2019). Hence, lateral DOC exports from peatland headwater streams are important to quantify considering it can lead to greenhouse gas (GHG) emissions to the atmosphere (Billett et al., 2012; Rasilo et al., 2017; Wallin et al., 2013b).

One challenge related to net ecosystem carbon budget assessment is that, within a catchment, DOC export to stream(s) comes from the different ecosystems (i.e., forest, wetlands, etc.) in the landscape (Webb et al., 2019). Thus, it is methodologically challenging to differentiate the respective contributions of each ecosystem (Billett et al., 2006a, 2012; Rosset et al., 2019; Tipping et al., 2010). However, peatlands are recognized as hotspots for production and transfer of DOC through lateral discharge (including subsurface runoff and porewater seepage) to stream networks (Freeman et al., 2001; Laudon et al., 2011; Rosset et al., 2019; Zhu et al., 2022). Strong positive relationships have already been established between the surface of a catchment covered by peat and the exported DOC to surface waters (Billett et al., 2006a; Laudon et al., 2011; Olefeldt, Roulet, et al., 2013).

To obtain a precise estimate of the peatland contribution in DOC exports, a specific DOC export (i.e., a flux normalized to a surface) that includes the peatland surface area within the catchment must be determined. Most of the previous studies have presented DOC exports normalized to the total surface of peatland-dominated catchments rather than normalized to the peatland surface area within the catchment (Köhler et al., 2008, 2009; Worrall et al., 2009; Dinsmore et al., 2013; Dick et al., 2015), possibly leading to underestimation of DOC exports. Leach et al. (2016) proposed calculating the specific exports using both total catchment area and peatland surfaces in the catchment as a way to report minimum and maximum values of DOC exports. The minimum value of the specific exports uses the catchment area as a reference, based on the hypothesis that DOC exported from the peatland is equivalent to DOC exported from the

non-peatland areas. The maximum value of the specific exports is calculated by using the peatland area and considered that the DOC contribution from non-peatland ecosystems can be negligible. Another approach to obtain peatland-specific DOC exports is by subtracting the sum of DOC entering the peatland to DOC exports at the peatland outlet (Rosset et al. 2019). Unfortunately, this approach is not scalable to all peatlands given the variability in catchment configurations.

Recent advances in high-frequency measurements of fluorescence of dissolved organic matter (fDOM), a quantitative proxy of DOC, has allowed researchers to accurately measure DOC exported at high temporal frequency (Blaurock et al., 2021; Rosset et al., 2019; Tunaley et al., 2016). This high-frequency monitoring is essential to catch DOC export variations during flood events, which are believed to be crucial moments of DOC transfers (Raymond et al., 2016; Tipping et al., 2010). Pulses of DOC during flood events can be understood as a succession of hydrological connection and disconnection between the peatland and the stream, causing changes in DOC concentrations in the stream (Billett et al., 2006a; Jutebring Sterte et al., 2022; Laudon et al., 2011). The runoff generation into the peat is controlled by the water table depth (WTD; Holden and Burt, 2003; Frei et al., 2010), where a large WTD increase during flood events leads to hydrological reconnection between DOC sources (Inamdar et al., 2004; Rosset et al., 2020; Tunaley et al., 2016) and greater DOC exports (Blaurock et al., 2021).

Advances in high-frequency monitoring and better effort directed towards flood events have confirmed that the majority of DOC is exported from peatlands during flood periods rather than during recession periods (Birkel et al., 2017; Blaurock et al., 2021; Dick et al., 2015). During flood events, DOC exports in the catchment dominated by peatlands are mainly composed of recently produced carbon derived from peat (Tipping et al., 2010; Billett et al., 2012; Holden et al., 2012; Juutinen et al., 2013; Dean et al., 2019). Recent studies have pointed out the importance of characterizing DOC export variability rather than identifying their sources to understand the processes underlying DOC mobilization (Birkel et al., 2017; Blaurock et al., 2021; Zhu et al., 2022).

DOC exports during flood events may vary depending on many parameters: the magnitude of the rainfall events, the season and the porewater temperature, the recurrence of high-flow events, the presence of a free-rainfall period, and the antecedent wetness of the catchment (Blaurock et al., 2021; Leach et al., 2016; Rosset et al., 2020; Tiwari et al., 2018). Previous studies have highlighted that these long periods between rainfall events favour DOC production (Clark et al., 2007; Glatzel et al., 2006; Grand-Clement et al., 2014).

Greater DOC exports are measured once the hydrological connection is restored, given the large amounts of DOC recently produced in the peatland and which could be mobilized through lateral discharge (Buzek et al., 2019; Clark et al., 2009; Grand-Clement et al., 2014; Worrall et al., 2008). Others have shown that great WTD before a rain event favour rapid DOC mobilization and lead to greater exports, independently of the recurrence between events in a peatland (Birkel et al., 2017; Blaurock et al., 2021). The amount of exported DOC is also controlled by production processes, stimulated by the temperature (Clark et al., 2007, 2009; Grand-Clement et al., 2014; Zhu et al., 2022) because DOC concentrations in the peat pore water increase with the temperature (Buzek et al., 2019; Freeman et al., 2001).

Among the studies that have used an event-based approach in peatland streams, most of them have been performed in temperate (Austnes et al., 2010; Grand-Clement et al., 2014; Tunaley et al., 2016; Worrall et al., 2008) and alpine (Birkel et al., 2017; Rosset et al., 2020) catchments, and none have been realized in boreal environments. Boreal catchments are constrained by seasonal freezing and pronounced snowmelt (Ågren et al., 2010; Leach et al., 2016; Tiwari et al., 2018) that potentially affect and delay DOC exports (Laudon et al., 2012). The seasonal and interannual variability also influence DOC production.

Considering the particular climatic context of boreal peatlands and the importance of hydrological processes on DOC exports, this study aimed to characterize patterns of DOC exports from a boreal peatland headwater stream over two consecutive years. Based on high-frequency DOC concentrations and different hydrological parameters including rainfall, stream discharge and WTD, we used an event-based approach to document the mechanisms driving DOC mobilization and exports during flood events. Individual flood events were compared in order to understand how hydrological and meteorological variables control the amount of exported DOC. This study comprises three research objectives: (1) to establish relationships between DOC exports from a headwater stream and the peatland hydrology; (2) to quantify, at the catchment scale, the amount of DOC laterally exported to the draining stream; and (3) to define the patterns of DOC mobilization during high river flow events.

2.2 Study site

The study site, located in north-eastern Canada within the Romaine River catchment (14 500 km^2), adjacent to the Labrador border, was previously described in Prijac et al. (2022). It is located in the eastern spruce–moss bioclimatic domain of the closed boreal forest (Payette, 2001) at the limit of the coastal plain and the Highlands of the Laurentian Plateau of the Precambrian Shield (Dubois, 1980). The Bouleau

peatland study site (50°31'N, 63°12'W; altitude 108 ± 5 m) is an ombrotrophic, slightly dome-shaped bog positioned at the head of a catchment (Fig. 2.1). Peat accumulation was initiated ca. 9260 calibrated years before present, and the maximum peat depth reaches 440 cm (Primeau and Garneau, 2021). The surface microtopography of the peatland shows a clear patterned surface of alternating dry hummocks, lawns, hollows and pools. The surface vegetation varies according to the microtopography, with *Sphagnum fuscum*, *S. capillifoium* and *Cladonia rangiferina* on the hummocks; *S. magellanicum*, *S. rubellum*, *S. cuspidatum* and *Trichophorum cespitosum* on the lawns; and *Sphagnum majus* and *S. pulchrum* on the hollows (Primeau and Garneau, 2021).

The study focused on the outlet of the peatland drained by a headwater stream of about 3 km in length, which flows north to south across the peatland from the western side. The catchment and peatland areas were determined through ArcGIS Pro 2.8.0 based on Lidar data covering the study site and provided by Hydro-Québec. The surface of the catchment drained by the stream is 2.22 km^2 and the area of the catchment covered by peat is 1.70 km^2.

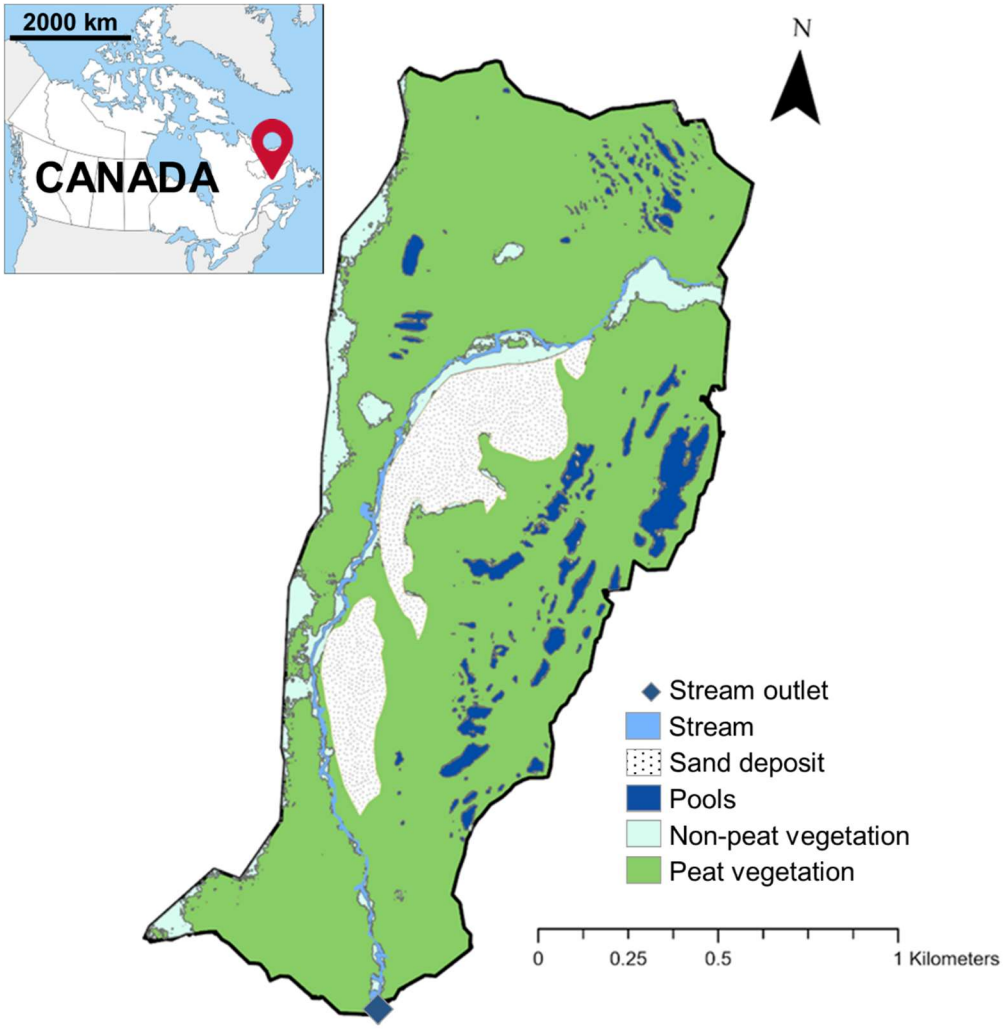

Figure 2.1 Map of the land cover of the Bouleau catchment with distinguishing areas covered by the drainage stream, sand deposits, pools, non-peat vegetation and peat vegetation.

As described in Prijac et al. (2022), based on the regional climate data, the mean annual temperature is 1.5°C and the total annual precipitation is 1011 mm, of which 590 mm falls as snow. An average monthly positive temperature occurs from May to October with 191.5 growing degree days above zero (Havre-Saint-Pierre meteorological station, mean 1990–2019, Environment of Canada). During the growing season, the average air temperature was 13.2 ± 6.9°C, with a minimum of -7.9°C in early October 2018 and a maximum of 30.8°C in late July 2018. The warmest month was July 2018, with an average monthly temperature of 17.9 ± 5.6°C, and the coldest month was October 2018, with an average monthly temperature of 3.52 ± 5.29°C. Average rainfall events were 7 mm day^{-1} and maximum daily rainfall was in

July 2018, with 41 mm day^{-1}. The wettest month was August 2019, with total rainfall of 129 mm, while the driest month was July 2019, with total rainfall of 27 mm.

The measurement period started in June 2018. Consequently, meteorological, hydrological and physicochemical variables are presented for the growing season defined from June to October, as described by Prijac et al. (2022). Annual DOC exports are presented for two complete periods of 12 months ranging from June 2018 to May 2019 for the first year and from June 2019 to May 2020 for the second year.

2.3 Methods

2.3.1 Water sampling

Manual water sampling along the studied headwater stream was performed during the same sampling periods as described in Prijac et al. (2022): five times during the 2018 growing season (14 June, 12 July, 8 August, 1 September and 10 October) and four times in 2019 (8 June, 3 August, 5 September and 10 October).

Stream surface water was collected at 11 sampling stations along the headwater stream (Fig annexe A.1). Samples were also collected from three tributaries at about 10 m before the confluence (Fig. annexe A.1). Because the stream was intermittent in the upstream section during the growing season, stations R01 and R02 were not sampled during each campaign.

The physicochemical parameters (temperature, pH, specific conductivity and dissolved oxygen saturation) were measured from a multi-parameter portable meter (Multiline Multi-3620 IDS, WTW, Germany) at each sampling site. All water samples were collected in polypropylene bottles previously cleaned with ultra-pure water and rinsed with sample water. The samples were filtered on GF/F filters (Whatman) that had been pre-combusted for 4 h at 450°C.

2.3.2 Analyses of DOC concentrations

Filtered water was prepared for DOC analysis, following the method described in Prijac et al. (2022), by acidification to pH 2 with 1 M HCl and stored in 40 mL glass vials. DOC and total nitrogen (TN) concentrations were analyzed using the catalytic oxidation method followed by non-dispersive infrared

(NDIR) detection of produced CO_2 (TOC analyser TOC-L, Shimadzu, Japan) with a limit of quantification of 0.1 mg C L^{-1}.

2.3.3 *In situ* high frequency monitoring

2.3.3.1 Fluorescence of DOM and physicochemical parameters

An EXO2 multi-parameter probe (YSI, USA) was placed at the stream outlet, at the same station where discharge was monitored and approximately 40 cm above the stream bed. The physicochemical parameters (water temperature, pH, specific conductivity and dissolved oxygen concentration and saturation) were recorded hourly from June 2018 to May 2020 and calibrated about once a month during the growing season.

The parameters monitored included the fluorescence of DOM (fDOM) measurements ($\lambda_{excitation}$ = 365 ± 5 nm / $\lambda_{emission}$ = 480 ± 40 nm) and turbidity. The time series includes the removal of some fDOM measurements when the probe was found in the stream sediments from mid-July to mid-August 2018 and in July and late August 2019. fDOM measurements were removed when turbidity exceeded a threshold of 50 FNU as it might alter the values (de Oliveira et al., 2018). Except for the periods when the probe was found in the sediments, there was no important turbidity peak, so the study focused on DOC.

A total of 826 individual measurements were removed in 2018, corresponding to 26.2% of data recorded during the growing season. In 2019, 1168 measurements were removed, corresponding to 37.1% of the growing season period. The correction of fDOM signal to the temperature was performed at reference temperature (20°C), as proposed by de Oliveira et al. (2018).

During the 2018 and 2019 growing seasons, punctual water samplings were taken in the stream (n = 69). At each sampling station, water samples were analyzed for the DOC concentration and fDOM measurements taken with the EXO2 multi-parameter probe along the stream. The fDOM measurements were used to determine DOC, considering the relationship *f*(fDOM) = [DOC], where fDOM is the corrected signal fluorescence of DOM measured in quinine sulfate units (QSU) and [DOC] is the dissolved organic carbon concentration in mg C L^{-1} (Table SI.1).

The first EXO2 multi-parameter probe that had been installed in June 2018 (calibration model I) was replaced with a new EXO2 multi-parameter probe in August 2018 which was used to the end of the data

monitoring in May 2020 (calibration model II; Table SI.1). Each EXO2 multi-parameter probe was calibrated independently. Due to fouling (development of a biofilm on the surface of the sensor) of the fDOM sensor leading to a deviation of the calibration model, the calibration model was adjusted during the 2019 growing season and two more calibration models were developed to correct the fDOM deviation. The models are presented in Table SI.1.

2.3.3.2 Stream hydrology

At the outlet of the stream, a 'V-shaped' weir was installed perpendicularly to the stream. The discharge was derived from the water level in the stream measured by an ultrasonic distance sensor (SR50A, Campbell, USA) during the 2018 growing season. The calculation method for the discharge was described by Taillardat et al. (2022). The distance between the surface water and the ultrasonic distance sensor gives the flooded vertical area in the 'V-shaped' weir and the Thomson's triangular-notch equation allow calculating the discharge from water-level measurements (Shein, 1979).

Starting from June 2019, a water-level logger (U201-04, Hobo, Onset, USA) was installed at the stream outlet to replace the ultrasonic distance sensor, damaged during the spring freshet. Water-level-discharge rating curves were calculated following the method described by (Taillardat et al., 2022). Discharge was measured at the stream outlet using a portable flow velocity probe (Flo-mate model 2000, Marsh-McBirney Inc., USA) measuring water velocity in a stream cross-section at subsections of 20 cm with intervals. The cumulative discharge (Q; in $m^3\ s^{-1}$) was measured by summing the discharge obtain for each subsection by Equation (1) where V is the water velocity measured by portable flow velocity probe (in m s^{-1}) and A is the flooded vertical area (in m^2) and obtain by multiplied depth (in m) to the width of the section (in m).

Discharge monitored data during the spring thaw was not available due to the absence of monitored data from the ultrasonic distance sensor SR-50A during 2019 spring freshet, because the sensor was damaged during the flood and because of measurements during 2020 spring thaws cannot be measured as the flooded section exceed the stream bed and the Thomson's triangular notch equation cannot be applied. Consequently, daily water discharge was modelled during the whole studied period, using the Peatland Hydrologic Impact Model (PHIM) developed by Guertin et al. (1987) and detailed by Riahi (2021).

2.3.3.3 Peatland hydrology

Water table depth (WTD) was recorded hourly at the six wells (Fig. annexe A.1) inserted at about two meters depth into the peat and equipped with a water-level data logger (HOBO, Onset, USA) for continuous hourly measurement of WTD and temperature, from June to October 2018 and from June to October 2019 as described in Prijac et al. (2022). In 2018, the water level loggers were U20-001-04 models (Hobo, Onset, USA) and replaced in 2019 with U20l-04 models (Hobo, Onset, USA). Those are slightly less precise (± 0.2% against ± 0.1% for the 2018 sensors) but better adapted to the meteorological conditions of the study site because of the battery durability for periods when temperatures are below 0°C. The sensors were placed into wells, suspended with a measured metal wire and kept submerged (i.e., about -0.6 m below the peat surface). Another sensor was installed next to a rain gauge to record atmospheric pressure variability and to correct piezometer pressure.

2.3.3.4 Rainfall

Rainfall was measured from July 2018 to May 2020 using a tilting bucket rain gauge (Onset, 0.2 mm). The bucket was connected to a sealed reed switch that produced a contact closure for every 0.2 mm of rainfall. Hourly measurements of rainfall consisted of the number of contacts resulting from 0.2 mm of rainfall.

2.3.4 Calculation of DOC exports

2.3.4.1 DOC concentration gap filling

Considering the percentage of removed fDOM signals (31.7% of the total measurements), a gap-filling method was performed on hourly DOC concentrations. The gap filling was conducted with a random forest model using a training data set containing the stream discharge record, water temperature, pH, dissolved oxygen saturation and specific conductivity (54.6% of the time series). The prediction of the data used by the random forest method (from the 'randomForest' package in R) was based on an unsupervised and nonparametric method of modelling. Models based on the validation dataset (13.7% of the time series) presented a good fit between the observed and predicted DOC concentrations, with a correlation of 0.99 (p-value < 0.0001); the mean squared residuals was 0.28 and the percentage of variance explained by the model was 98.7% (p-value < 0.0001; Fig. annexe A.2a). Modelled concentrations were included in the calculation of DOC exports. The importance of variables included in the random forest model is presented in Table annexe A.2. They were obtained using the argument 'importance' of the RandomForest function in R.

Gap filling of the DOC concentration was also performed during the rest of the time series (i.e., non-growing season). The same method was applied on the daily-interval data set to model the missing DOC concentrations (51.3% of the data set).The data set contained the PHIM simulated discharge, water temperature, pH, dissolved oxygen saturation and specific conductivity. The training data set corresponded to 26% of the data set and validation data set corresponded to 22.7% of the data set. The validation test of the random forest model gave a relatively good fit with a strong positive correlation between observed and modelled DOC concentration (cor = 0.84; p-value < 0.0001), the mean root-square residuals was 2.15 and the percentage of variance explained by the model was 71% (p-value < 0.0001; Fig. annexe A.2b).

2.3.4.2 Calculation of stream DOC exports

The DOC load at the outlet of the catchment (g C m^{-2} $year^{-1}$) was calculated as in equation (1).

$$DOC_f = \frac{\sum_{i=1}^{n}[DOC]_i \times Q_i \times dt}{S} \quad (1)$$

In the above equation, $[DOC]_i$ correspond to the DOC concentration in g m^{-3} at step measurement *i*, Q_i corresponds to the stream discharge in m^3 h^{-1} at step measurement *i*, the variable d*t* corresponds to the time step between high-frequency measurements and *S* corresponds to the surface drained by the stream. d*t* corresponds to 1h intervals during the growing season (i.e., from June to October) and 1 day for the remaining part of the time series.

2.3.4.3 DOC exports standar deviation calculation

Uncertainties associated with DOC exports calculation was obtained using a Monte Carlo simulation approach and applied on Eq. (1) (Cook et al., 2018; Rosset et al., 2019). The Monte Carlo simulation randomly calculate for each interval a DOC concentration and discharge obtained from a normal distribution of the observed values. Mean of the normal distribution corresponds to the mean of observed values. The standard deviation for DOC calculation corresponds to the mean square error of the random forest models and are ±0.28 mg C L^{-1} for the 1h-interval period (from June to October 2018 and from June to October 2019) and ±2.15 mg C L^{-1} for the rest of the time series at daily intervals. An arbitrary and conservative standard deviation was settled at 50% during high flow periods (determined by Hidden Markov Model in the next section) and 10% during low flow periods. After 5000 iterations, the mean was

obtained by the best estimate value and the standard error estimation was assumed to represent the standard deviation of DOC exports.

2.3.5 Analyses of flood events

2.3.5.1 Classification of time series in high- and low-flow periods to determine flood events

During the growing season, the hidden Markov model (HMM) was used to classify the time series into two states corresponding to the high- and low-flow periods (Guilpart et al., 2021; Kehagias, 2004) using the R packages 'depmixS4' (Visser & Speekenbrink, 2010) and 'HiddenMarkov' (Harte, 2021). The HMM was applied on both 1h-interval discharge data and on PHIM modelized daily-interval discharge data. The distribution of probability to go from one state to another was calibrated manually. After the HMM classification, the high-flow periods were manually adjusted to get a better integration of their beginnings. They were determined as the inflection of Q before a persistent increase in this variable within a 12 h interval of a high-flow period determined by the HMM (or within a day for the daily-interval dataset).

In addition, 12 individual flood events were manually isolated, six in 2018 and six in 2019 (Table annexe A.3) among the time series including DOC measurements of a satisfying quality (e.g., gap-filled DOC export values from the random forest were excluded). Flood events were a subset of the total time series for individual analyses. They were identified by a two-letter code, the first letter corresponding to the year of the flood event (*A* for 2018 and *B* for 2019) and the second to the rank of the flood events each year, from *a* and following the alphabetical order.

2.3.5.2 Flood events characteristics

For each of the 12 flood events, several descriptive and quantitative indicators were calculated; they are described in Table 2.1. During the event, rainfall was summed up under the variable PP event. Rainfall was also summed up 2 days before the beginning of the event (AP2) and 14 days before the beginning of the event (AP14). The PP event and AP14 were added to obtain the variable PP total.

Table 2.1 List of the variables with their acronyms and units

Acronyms	Variable	Units
AP14	Antecedent precipitation 14 days before the beginning of an event	mm
AP2	Antecedent precipitation two days before the beginning of an event	mm
β	Index corresponding to the slope of the log-log DOC-Q relation during flood events (Godsey et al., 2009, 2019)	
DO mgL	Concentration of dissolved oxygen	mg L^{-1}
DO sat	Saturation of dissolved oxygen	% saturation
DOC	Dissolved organic carbon	mg C L^{-1}
DOC lag time	Duration between the Q peak and the DOC peak during a flood event	h
DOC_{90}	Duration when 90% of maximum DOC concentrations were exceeded during a flood event	h
DOC_{LOAD}	Cumulative quantities of DOC exported to the stream per square meter during a defined time period	kg DOC-C m^{-2} *time unit*
ΔDOC	Difference between initial DOC concentration at the beginning of the event and the peak of DOC concentration	mg C L^{-1}
Δ*Q*	Difference between initial discharge at the beginning of the event and the peak of discharge	m^3 s^{-1}
ΔWTD	Difference between initial WTD at the beginning of the event and the peak of WTD	mm
FI	Flushing index which corresponds to the difference between DOC concentration at the peak of discharge and DOC concentration at the beginning of the event (Vaughan et al., 2017)	
HI	Hysteresis index which corresponds to the differences between the normalized DOC concentration during the falling limb to an event and the rising limb to an event at an interval of 0.05 normalized Q (Lloyd et al., 2016)	
PP event	Cumulative precipitation during a storm event	mm
P-Q lag time	Duration between the beginning of a precipitation event and the Q increase at the beginning of a flood event	h
SPC	Specific conductivity	µS cm^{-1}
Q	Stream discharge	m^3 s^{-1}
Q lag time	Time elapsed between the beginning of Q increase and its reached peak	h
Total PP	Total catchment wetness corresponding to the sum of AP14 and PP event	mm
WTD	Water table depth	m

The P–Q lag time (in minutes) corresponds to the duration between the start of the rainfall and the *Q* increase at the beginning of the event. The *Q* lag time corresponds to the duration between the beginning

of the event and the reaching of the peak of Q (Q_{max}). The DOC lag time corresponds to the duration between Q_{max} and the peak of DOC (DOC_{max}). The DOC_{90} corresponds to the period when 90% of DOC_{max} was exceeded and can be summarized as the duration of the DOC plateau before the DOC concentrations decreased. The DOC load (DOC_{load}) was calculated as the DOC exports shown in equation (1) and corresponds to the quantity of DOC exported during the flood event. DOC_{load} was divided by the event duration (in h) to provide a better comparison between events ($DOC_{load\ kgh}$).

The hysteresis index (HI), the flushing index (FI) and the β index were determined from the relation between Q and the DOC concentration. The HI was used to identify the hysteretic relation between DOC and Q and corresponds to the difference in the integrals during the rising limb (i.e., the increasing phase of Q during a high-flow event) and the falling limb (i.e., the decreasing phase of Q during a high-flow event) of a high-flow event (Lloyd et al., 2016). HI values range from -1 for strong anticlockwise hysteretic relations to 1 for strong clockwise hysteretic relations; 0 indicates the absence of a hysteretic relation. The FI was calculated to describe the response of the DOC concentration during the rising limb of the flood (Vaughan et al., 2017). The FI ranges from -1 to 1; a value < 0 indicates that DOC is diluted during the rising limb while a value > 0 indicates accretion of DOC during the rising limb. The β index corresponds to the slope of the logarithmic relation between Q and the DOC concentration and provide information regarding the limiting factor of the DOC exports (Godsey et al., 2009). A β index value < 0 indicates a source limitation of the DOC exports, a β index value > 0 reveals that the DOC exports are transport-limited and β = 0 indicates the DOC exports are chemostatic (Godsey et al., 2009, 2019; Zarnetske et al., 2018).

2.3.6 Statistical analyses

The data analyses were performed in R (CRAN-Project) and RStudio interface (RStudio Inc., USA). The figures were produced using the package 'ggplot2' (Wickham, 2016). Correlations between DOC and explanatory variables (porewater, air and stream temperature, Q, conductivity, pH, saturation of dissolved oxygen and dissolved oxygen concentrations) were evaluated using a multiple linear regression model. The p-values and Spearman correlation factors of individual variable effects on DOC concentrations were used as an indicator of model quality.

Prior to clustering the flood events, correlation and collinearity between variables were evaluated by measuring the variance inflation factor (VIF) function using the R package 'car'. Variables were removed when the correlation with another variable exceeded 0.8 and the VIF exceeded 5. The variables retained

to perform clustering were the event duration, the minimum temperature, the average *Q*, the minimum WTD, the ΔDOC, the HI index, the *β* index, the FI, the initial WTD, the Q_{max} and the DOC_{load}. As precipitation data were not available for all events (i.e., Aa and Ab), precipitation-related variables were excluded from the clustering to keep the maximum number of events. Hierarchical clustering was performed based on principal component analysis (PCA) to classify each individual event into clusters. The number of clusters was determined according to the 'elbow method' as the optimal number of clusters corresponds to values when the inertia (i.e., the information given by additional clusters) decreases. The R package 'FactoMineR' was used for the PCA and hierarchical clustering.

The low- and high-flow periods were determined by using the HMM with the R package 'HiddenMarkov', which is designed for time series data. The HMM on log-transformed *Q* (log*Q*) was performed based on hourly data.

2.4 Results

2.4.1 High frequency monitoring of hydrological variables and temperature

The maximum daily rainfall was 41 mm day^{-1} in September 2018 (for the 2018–2019 period) and 39 mm day^{-1} in August 2019 (for the 2019–2020 period). During the summer of 2018, the wettest month was July with total rainfall of 98 mm, while the wettest month during the summer of 2019 was August with 129 mm. The average WTD was -0.26 m and ranged from -0.09 to -0.43 m. The lowest WTD was in July and August 2019 with a monthly average of -0.30 ± 0.06 and -0.30 ± 0.07 m, respectively. The average annual *Q* was 0.020 m^3 s^{-1} in 2018–2019 and 0.017 m^3 s^{-1} in 2019–2020. During the growing season, the lowest monthly average discharge occurred in July of each year, with 0.010 m^3 s^{-1} in 2018–2018 and 0.007 m^3 s^{-1} in 2019–2020. In 2018–2019, the highest discharge was 0.068 m^3 s^{-1} measured in June 2018 and in 2019–2020 it was 0.100 m^3 s^{-1} measured in September 2019.

There was a strong positive exponential relationship between WTD and *Q* (*rho* = 0.82, $p < 0.0001$; Fig. 2.2a). This nonlinear relationship suggests a threshold of WTD on lateral discharge generation. When low, WTD variations do not influence *Q,* which remains low. An increase in WTD above a threshold observed between -0.33 and -0.19 m leads to lateral discharge generation and an increase in *Q* (Fig. 2.2a).

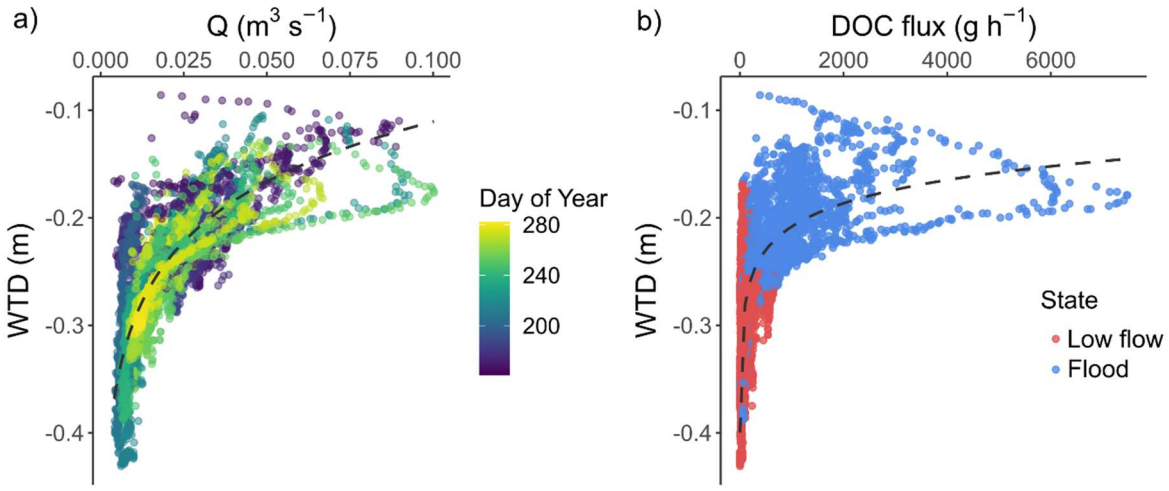

Figure 2.2 a) Relation between hourly measurements of the water table depth (WTD, in m) and stream discharge (*Q*, in m^3 s^{-1}). The colour represents the day of the year and the dashed line corresponds to the logarithmic relation between WTD and *Q*. b) Relation between the hourly measurements of WTD (m) and hourly DOC flux in the stream (g DOC-C h^{-1}). The colour represents the hydrological state according to the hidden Markov model and the dashed line corresponds to the logarithmic relation between WTD and DOC flux.

The average peat porewater temperature was 11.5 ± 2.4°C and was very similar in 2018 (11.4 ± 2.6°C) and 2019 (11.7 ± 2.3°C). The warmest peat porewater temperature was 15.1°C measured in August 2019 and the coldest was 5.6°C measured in June 2018. During the summer, the average monthly temperature in June increased from 7.1 ± 1.0°C in 2018 and 8.3 ± 0.8°C in 2019 to reach a maximum of slightly above 14°C in August. The temperature decreased in autumn, to a similar average October temperature (8.6 ± 0.4°C in 2018 and 8.7 ± 0.5°C 2019). The average water temperature recorded at the stream outlet was 13.2 ± 6.7°C. The average water temperature in 2018 was warmer, 13.9 ± 7.0°C compared with 12.7 ± 6.2°C in 2019. As for the air temperature, the water temperature increased from about 11°C in June to 15.6°C and 16.9°C in July and August, respectively. The water temperature subsequently decreased in September, with similar values in both years (10.6 ± 3.5°C in 2018 and 10.2 ± 2.7°C in 2019).

2.4.2 Dissolved organic carbon concentrations and exports from the peatland stream outlet

The average DOC concentration recorded at the peatland stream outlet was 6.3 ± 4.6 mg C L^{-1} and the median was 4.9 mg C L^{-1}. The maximum DOC concentration was 24.2 mg C L^{-1} in early August 2019 and the minimum was 0.9 mg C L^{-1} in September 2018 (Fig. 2.3d). Correlations between the DOC concentration and hydrological and physicochemical variables are presented in Table annex A.2. The DOC concentration was significantly positively correlated with *Q* and WTD (Table annex A.2). DOC was positively correlated

with water temperature but only when considering the complete period of measurements. The random forest model applied during the growing season data set highlighted the important contribution of hydrological variables (WTD and *Q*; Table annexe A.2). During the growing season, the log-transformed hourly DOC exports were significantly correlated with *Q* (cor = 0.79, p < 0.0001) and with WTD (cor = 0.75, p < 0.0001; Fig. 2.2b).

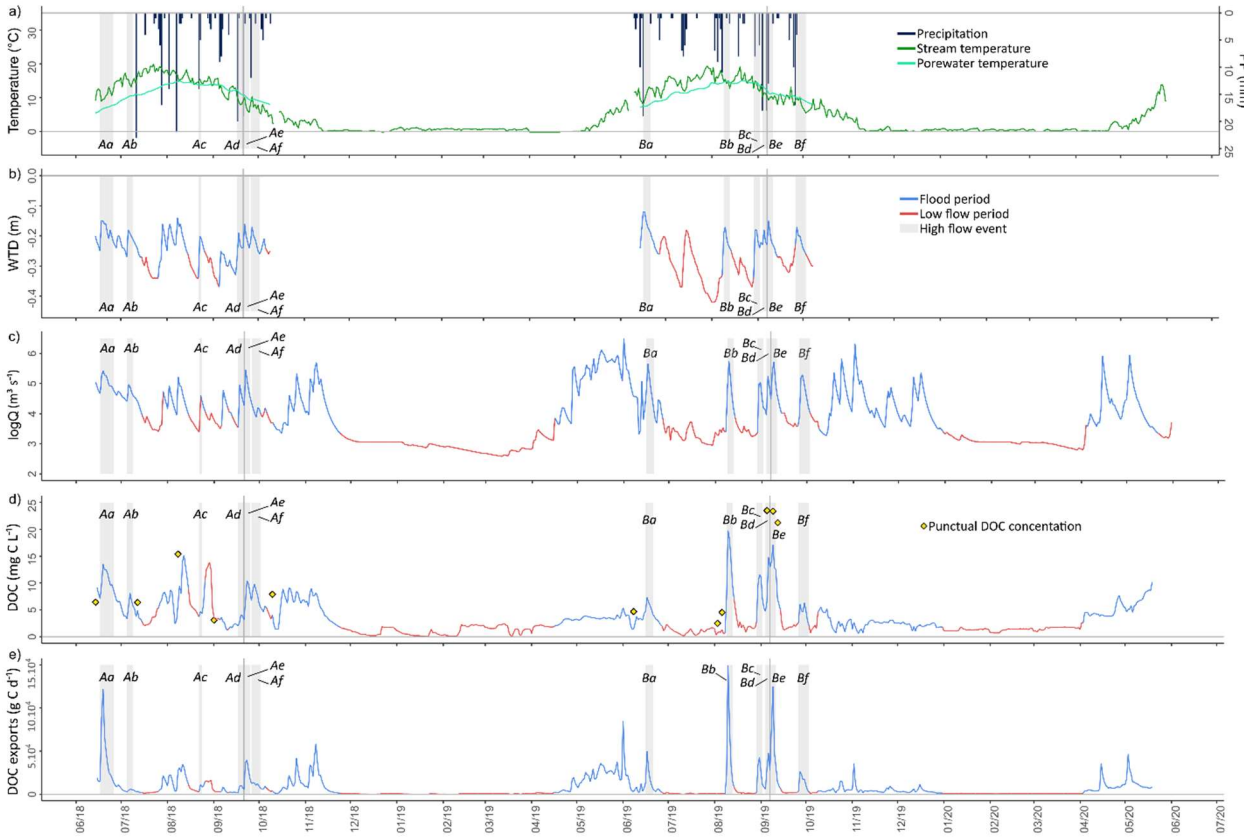

Figure 2.3 Times series of a) stream and porewater temperature and precipitation, b) water table depth (WTD), c) log-transformed stream discharge (log*Q*), d) the dissolved organic carbon (DOC) concentration in the stream and e) DOC exports, from June 2018 to May 2020. Colours in the b)–e) correspond to the periods of flood (in blue) and low flow (in red). Grey vertical bars represent individual storm events. Yellow diamonds represent DOC concentration analyses from punctual sampling at the stream outlet.

We calculated the specific DOC exports from the peatland by using an approach based on the distinction between the DOC sources during high flow and low flow. The assumption supporting this approach is that the peatland is the main contributor to DOC exports during high flow – because other sources are considered negligible – while during low flow, the most conservative approach is to consider the whole catchment as the potential DOC source. The surface considered in the specific DOC export calculation [*S* in equation (1)] is the catchment surface (2 219 574 m^2) during low flow and the peatland surface (1 702 353 m^2) during high flow.

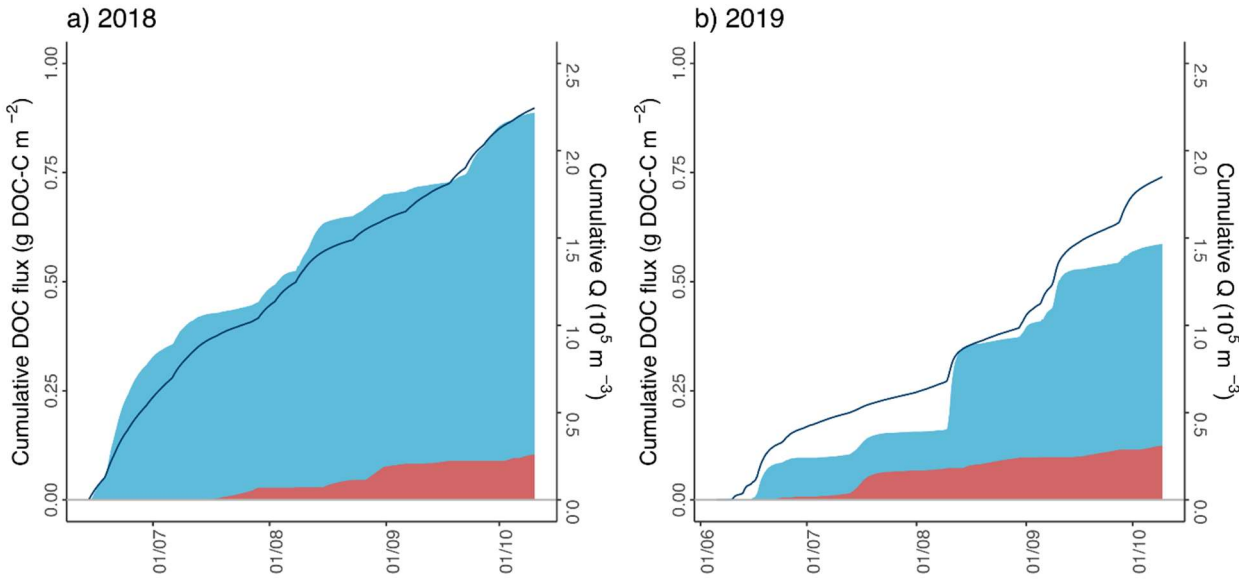

Figure 2.4 Cumulative dissolved organic carbon (DOC) exports (in g DOC-C m^{-2}) and the cumulative stream discharge (in m^3) during the a) 2018 and b) 2019 growing seasons. * The staircase trend observed in 2019 can be explained by long periods of drought with very low DOC concentration with discharge given the low DOC exports (Fig. 3e).

The specific annual DOC exports were 1.87 ± 0.75 g DOC-C m^{-2} y^{-1} for June 2018–May 2019 and 1.27 ± 0.35 g DOC-C m^{-2} y^{-1} for June 2019–May 2020 (Table 2.2 and Fig. 2.4). The strategy used to calculate the specific DOC exports by distinguishing high flow and low flow provides a better estimation of exports. If the most conservative surface (i.e., the catchment area) would have been used to calculate the specific exports, it would have been 1.46 ± 0.64 g DOC-C m^{-2} y^{-1} in 2018–2019 and 0.99 ± 0.31 g DOC-C m^{-2} y^{-1} in 2019–2020. Conversely, if the peatland surface area were used in the specific DOC export calculation, it would have been 1.91 ± 0.83 g DOC-C m^{-2} y^{-1} in 2018-2019 and 1.29 ± 0.41 g DOC-C m^{-2} y^{-1}. The proximity with these last values and the intermediate strategy we used (i.e., surface area considered in DOC exports calculation depending of hydrological conditions) is coherent given the dominance of DOC exports during high-flow periods of 92.6 % and 93.8 % for 2018-2019 and 2019-2020 respectively.

This approach provides a range for the plausible specific DOC exports from the peatland between 1.46 and 1.91 g DOC-C m^{-2} y^{-1} for 2018–2019 and between 0.99 and 1.29 g DOC-C m^{-2} y^{-1} for 2019–2020. During the period corresponding to the threshold of the 85th percentile of the *Q* measurements (i.e., 15% of the total time series with the highest measured *Q*), the DOC exports represented 63.6% of the total exports during the 2018–2019 period and 66% during the 2019–2020 period.

Table 2.2 a) Monthly specific dissolved organic carbon (DOC) flux (g C m^{-2} $month^{-1}$) at the outlet stream from June 2018 to May 2020 and distinguished fluxes during high flow when (1) the surface of the peatland is considered in the calculation and (2) the watershed is considered in the flux calculation. b) Summary of DOC fluxes during the two growing seasons, the total recorded and their proportion during high- and low-flow periods.

a)	2018-2019		2019-2020	
	DOC flux (g DOC-C m^{-2} $month^{-1}$)		DOC flux (g DOC-C m^{-2} $month^{-1}$)	
Month	High-flow	Low-flow	High-flow	Low-flow
June	0.452	0.000	0.102	0.008
July	0.130	0.022	0.000	0.009
August	0.167	0.053	0.229	0.016
September	0.144	0.011	0.327	0.012
October	0.208	0.003	0.080	0.005
November	0.208	0.003	0.099	0.000
December	0.000	0.010	0.060	0.001
January	0.000	0.003	0.000	0.010
February	0.000	0.004	0.000	0.008
March	0.000	0.006	0.000	0.010
April	0.052	0.008	0.136	0.001
May	0.418	0.000	0.157	0.000
Total per conditions	1.727 ± 0.72	0.138 ± 0.099	1.189 ± 0.551	0.079 ± 0.045
Specific flux	1.865 ± 0.746		1.268 ± 0.348	

b)	2018-2019			2019-2020		
	Proportion of measurements (%)	Flux (g DOC-C m^{-2} y^{-1})	Proportion of flux (%)	Proportion of measurements (%)	Flux (g DOC-C m^{-2} y^{-1})	Proportion of flux (%)
High-flow	59.1	1.727	92.6	44.1	1.189	93.8
Low-flow	40.9	0.138	7.4	55.9	0.079	6.2
Total	100.0	1.865	100.0	100.0	1.268	100.0

2.4.3 Analyses of the flood events

2.4.3.1 Description of the flood events

Twelve flood events were isolated over the two growing seasons, six in 2018 and six in 2019 (see the grey vertical bars in Fig. 2.3). The average flood event duration was 4.8 ± 2.1 days. Aa was the longest event (10 days) while Ac was the shortest event (2 days; Table annexe A.3).

The Bd event had the lowest rainfall (8 mm) while the Bb event had the highest rainfall (34 mm). The antecedent rainfall 14 days before the beginning of the event was between 10 mm during the Ac event and 71 mm before the Be event. The maximum discharge during flood events varied from 0.026 $m^3 s^{-1}$ (Ac) to 0.1 $m^3 s^{-1}$ (Be). The discharge increase (ΔQ) varied from 0.019 $m^3 s^{-1}$ (Ac) to 0.084 $m^3 s^{-1}$ (Bb). ΔWTD during an event was between 0.08 m during the Ba event and 0.25 m during the Bb event. The DOC peak concentration varied from 5.0 mg L^{-1} during the Ad event to 24.2 mg L^{-1} during the Bb event. Regarding ΔQ and ΔWTD, the Bb event also showed the highest DOC concentration increase (ΔDOC, 22.5 mg C L^{-1}). The Bb event also presented the highest hourly DOC exports (DOC_{load}), namely 3.14 kg DOC-C h^{-1}. The Bf event had the lowest DOC_{load} at 0.23 kg DOC-C h^{-1}.

The HI was always negative, associated with anticlockwise hysteresis, except for the Ba event that had an HI of 0.05, indicating the absence of a hysteretic relation between *Q* and DOC (Fig. 2.5). The HI varied from -0.16 for the Bf event to -0.56 for the Ae event. The β index was always positive, indicating a constant transport limitation of DOC during flood events. The Af event showed a FI of 0.02, reflecting the absence of change in the DOC concentration between the beginning of the event and the peak of *Q*. The positive FI for the other events indicated that the DOC concentration increased during the rising limb of the hydrograph and was between 0.25 for the Ae event and 0.98 for the Bb event.

The shortest lag time between the rainfall and the beginning of the *Q* increase (P–Q lag time) occurred during the Ba event (2 h). The longest P–Q lag time was during the Bc and Bd events (7 h). The *Q* lag time ranged from 15 h for the Ac event to 39 h between the beginning of the event and *Q* peak during the Bc event. The DOC lag time or the lag time between the peak of Q and the peak of DOC ranged from 7 h during the Ac event to 36 h during the Ad event. The shortest DOC_{90} occurred during the Ac event (2 h), while the longest DOC_{90} was 17 h during the Ae event.

2.4.3.2 Classification and typology of flood events

The hierarchical clustering performed on based PCA (presented in Fig. annexe A.3) classified the flood events into three groups (Fig. 2.6a). Cluster 1 included the Ab, Ac, Ad, Ae, Af, Bc and Bd events; cluster 2 comprised the Ba, Be and Bf events; and cluster 3 included the Aa and Bb events.

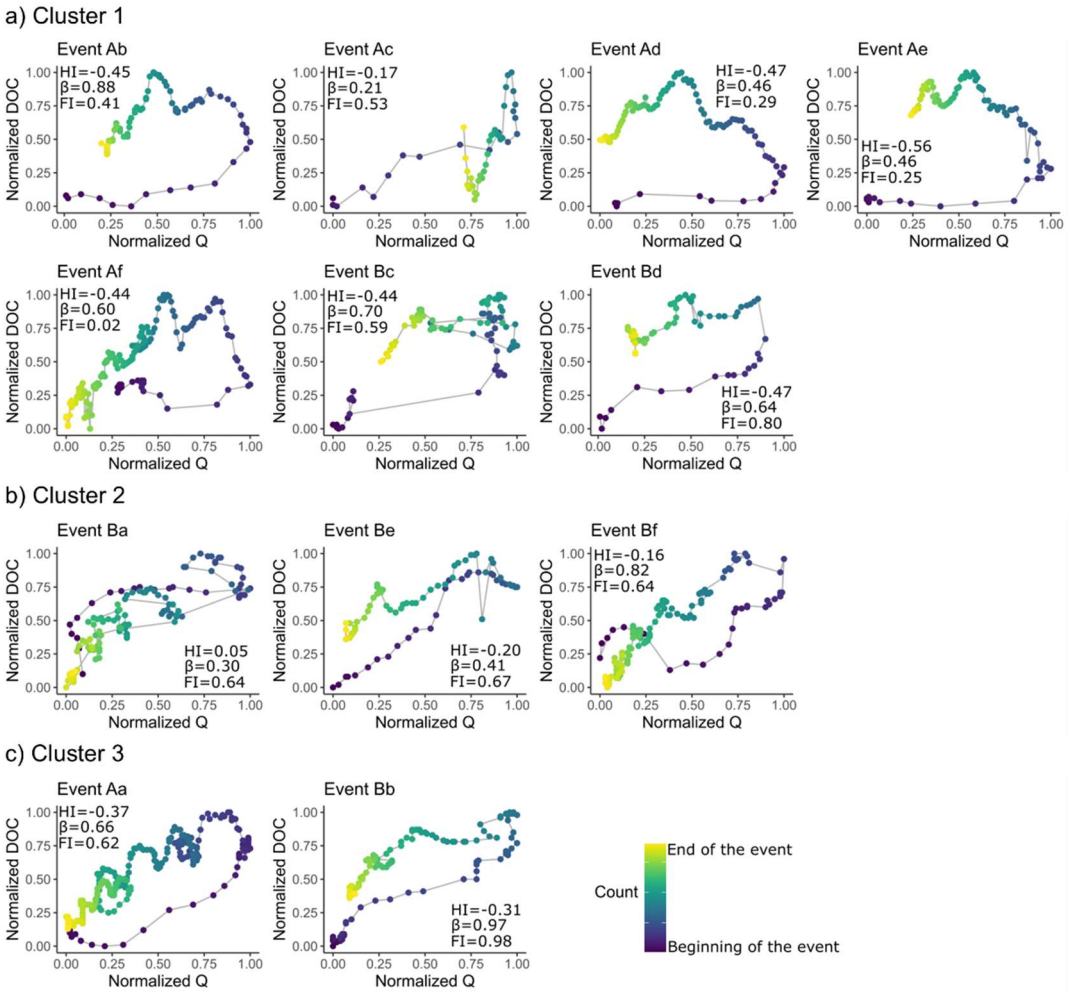

Figure 2.5 The hysteretic relations between the normalized stream discharge (*Q*) and the normalized dissolved organic carbon (DOC) for the events of a) cluster 1, b) cluster 2 and c) cluster 3. The colour represents the count of the measure, from 0 at the beginning of the event to the end. The hysteresis index (HI), the flushing index (FI) and the *β* index are presented for each event.

The average variable values by cluster are summarized in Table 2.3. The events of cluster 3 had greater DOC exports, namely 2.4 ± 0.1 kg C h^{-1}, compared with clusters 1 and 2 (0.6 ± 0.3 and 1 ± 2.1 kg DOC-C h^{-1}, respectively). The events of cluster 3 also had the highest DOC_{max} and ΔDOC of 19.4 ± 2.1 mg C L^{-1} and 15 ± 3.7 mg C L^{-1}, respectively. By contrast, the events of cluster 2 presented the lowest average DOC_{max} (8 ± 13.7 mg C L^{-1}), but the events of cluster 1 presented the lowest ΔDOC (6.4 ± 4.1 mg C L^{-1}).

Although the events of cluster 3 had the highest ΔDOC, the events of cluster 2 had the highest Q_{max} and Δ*Q*, namely 0.086 ± 0.018 and 0.065 ± 0.022 m^3 s^{-1}, respectively. Q_{max} and Δ*Q* for the events of cluster 3

were 0.081 ± 0.001 m^3 s^{-1} and 0.062 ± 0.010 m^3 s^{-1}, respectively. The events of cluster 1 had the lowest Q_{max} and ΔQ of 0.043 ± 0.012 and 0.029 ± 0.011 m^3 s^{-1}, respectively. The events of cluster 3 showed the lowest $WTD_{initial}$ (-0.31 ± 0.07 m) and the highest WTD_{max} (-0.11 ± 0.01 m) and thus the highest ΔWTD (0.19 ± 0.08 m). The events of cluster 2 presented the lowest ΔWTD (0.09 ± 0.11 m) and the highest $WTD_{initial}$ (-0.21 ± 0.09 m). Conversely, the events of cluster 1 showed a low $WTD_{initial}$ (-0.30 ± 0.06 m) and despite a relatively high ΔWTD of 0.15 ± 0.05, they reached the lowest average DOC_{max} (-0.15 ± 0.02 m).

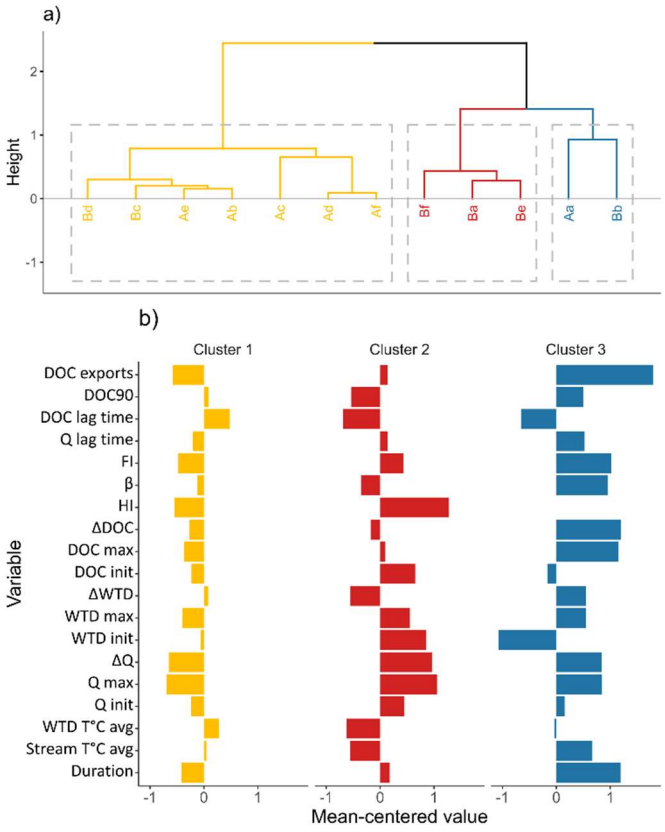

Figure 2.6 a) Representation of the hierarchical clustering performed on principal components discriminates the events into three clusters (Cluster 1 = yellow, Cluster 2 = red, Cluster 3 = blue). b) For each event, variables were mean centered and averaged by cluster. The representation of averaged mean centered values allow identifying the behavior of variables in each cluster.

Table 2.3 Summary of the variables and indexes (presented as mean ± standard deviation) for each cluster of flood events. The variables include the duration of events; the average stream temperature (T°C); the initial, maximum and change (Δ) in the stream discharge (*Q*); the water table depth (WTD); and the dissolved organic carbon (DOC) concentration. The hysteretic index (HI), flushing index (FI) and *β* index characterize the storm events. Precipitation variables comprise the total precipitation during events (PP event) and antecedent precipitation 2 days (AP2) and 14 days (AP14) prior to the beginning of an event. Total PP corresponds to the sum of AP14 and PP events. The P–Q lag time corresponds to the duration between a precipitation event and the beginning of the increase in *Q*. The *Q* lag time corresponds to the duration between the beginning of the discharge increase and the discharge peak. The DOC lag time corresponds to the duration between the discharge peak and the DOC peak. DOC_{90} corresponds to the period when 90% of the maximum DOC concentration was exceeded.

*As no precipitation data was available for the event Aa, it was not possible to calculate a standard deviation for the event of cluster 3. The values correspond of the results for the event Bb.

	Cluster 1	**Cluster 2**	**Cluster 3**
Duration (day)	3.9 ± 1.3	5.2 ± 1.5	7.3 ± 0.2
Stream T°C min (°C)	6.6 ± 3.6	5.6 ± 5.3	7.9 ± 1.3
Stream T°C max (°C)	15.6 ± 3.3	15.2 ± 5.2	19.5 ± 1
Stream T°C average (°C)	11.1 ± 3.1	9.5 ± 4.7	12.9 ± 0.6
Porewater T°C min (°C)	11.3 ± 1.9	9.1 ± 1.7	10.3 ± 5.7
Porewater T°C max (°C)	12.1 ± 1.8	10.2 ± 2.0	11.4 ± 4.9
Porewater T°C average (°C)	11.8 ± 1.9	9.5 ± 1.8	11.0 ± 5.2
Q initial (m^3 h^{-1})	55.9 ± 23.1	74.3 ± 12.5	66.3 ± 39.4
Q max (m^3 h^{-1})	153.8 ± 41.9	308.1 ± 65.9	289.8 ± 3.7
Δ*Q* (m^3 h^{-1})	98 ± 44.4	233.9 ± 78.5	223.5 ± 35.7
cumulative *Q* (m^3 h^{-1})	9562 ± 3036	19145 ± 790	29184 ± 835
WTD initial (m)	-0.30 ± 0.06	-0.21 ± 0.09	-0.31 ± 0.07
WTD max (m)	-0.15 ± 0.02	-0.12 ± 0.02	-0.11 ± 0.01
ΔWTD (m)	0.15 ± 0.05	0.09 ± 0.11	0.19 ± 0.08
DOC initial (mg C L^{-1})	3.5 ± 1.8	5.6 ± 2.9	3.7 ± 0.6
DOC max (mg C L^{-1})	10.3 ± 4.2	12.8 ± 8.8	18.7 ± 3.1
ΔDOC (mg C L^{-1})	6.8 ± 3.8	7.3 ± 11.8	15 ± 3.7
HI	-0.4 ± 0.1	-0.1 ± 0.1	-0.3 ± 0.1
β	0.6 ± 0.2	0.5 ± 0.1	0.8 ± 0.1
FI	0.4 ± 0.3	0.6 ± 0.2	0.8 ± 0.1
Ptot (mm)	19 ± 9	16 ± 12	34 ± NA
AP2 (mm)	6 ± 6	12 ± 1	20 ± NA
AP14 (mm)	34 ± 19	42 ± 11	42 ± NA
Total catchment wetness (mm)	53 ± 15	58 ± 24	76 ± NA
P-Q lagtime (h)	4.7 ± 2	3.3 ± 0	5 ± NA
Q lagtime (h)	23.7 ± 8.2	26 ± 1.4	28.5 ± 14.1
DOC lagtime (h)	24.1 ± 12.3	10.7 ± 3.5	11 ± 14.8
DOC_{90} (h)	9.7 ± 4.9	7 ± 4.2	11.5 ± 2.1
DOC load (kg DOC-C)	71.1 ± 36.4	161.4 ± 145.5	370.1 ± 23.2

DOC load_(kg DOC-C h^{-1})	0.8 ± 0.4	1.6 ± 1.3	2.1 ± 0.3

On average, the events of cluster 1 presented the lowest HI (-0.4 ± 01) while the events of cluster 2 showed the highest HI (-0.1 ± 0.1). The events of clusters 1 and 2 shared a similar β index of 0.5, while the events of cluster 3 had the highest β index (0.8 ± 0.1). The events of cluster 3 had the highest FI (0.8 ± 0.1), compared with 0.6 ± 0.2 for the events of cluster 2 and 0.3 ± 0.3 for the events of cluster 1.

For cluster 3, the rainfall data were only available for the Bb event. However, this event showed the highest total rainfall (76 mm), supported by the highest rainfall during the events and high rainfall before the event. The lowest rainfall before the events occurred for cluster 1 and the rainfall during the events of 19 mm on average led to the lowest total PP of 53 ± 15 mm, which was slightly lower than events of cluster 2 (58 ± 24 mm).

2.5 Discussion

2.5.1 Peatland hydrological connectivity controls DOC exports to the stream

Coupling high-frequency monitoring of DOC concentrations with hydrological measurements (*Q* and WTD) was important to better understand the relationships between DOC concentration dynamics at the outlet and the hydrological functioning of the peatland. In the studied peatland, we observed a control of hydrological variables (i.e., WTD and *Q*) on the DOC concentrations at the stream outlet (Table annexe A.2). The increase in WTD coincides to an increase in *Q* and DOC concentrations at the outlet and, consequently, to an increase in DOC exports (Fig. 2.2). DOC mobilization during high-flow periods exhibited anticlockwise hysteresis (Fig. 2.5), reflecting the pronounced connectivity between DOC-rich sources within the catchment and the stream (Tunaley et al., 2017). The positive FI and β index (Table 2.3 and Fig. 2.5) indicate accretion of DOC in the stream during flood episodes and reveal a transport limitation of DOC (Vaughan et al., 2017; Zarnetske et al., 2018).

The logarithmic relationship between WTD and *Q* (Fig. 2.2a) highlights the crucial contribution of peatland during high-flow periods. This mechanism has been described as the threshold of runoff and subsurface flow generation effect induced by a greater WTD (Frei et al., 2010) based on the transmissivity feedback mechanism (Bishop et al., 2004) and leading to *Q* increase. It also illustrates the coupling of WTD and DOC exports (Fig. 2.2b), which are favoured by subsurface flows of water into DOC-rich horizons and less

decomposed peat (Austnes et al., 2010) initiated by a rainfall event leading to the increase in WTD and confirmed by a significant positive correlation between DOC exports and WTD (cor = 0.75, $p < 0.0001$; Fig. 2.2b). An increase in the subsurface flows has been described as the dominant hydrological control on DOC mobilization and exports to peatland streams (Birkel et al., 2017; Bishop et al., 2004; Rosset et al., 2022). In addition, the fluctuating water table in the acrotelm enhances the DOC available to the lateral discharge during high-flow events (Kalbitz et al., 2000; Worrall et al., 2002; Grand-Clement et al., 2014). During the driest periods, the DOC diffuses through the peat and becomes available for further mobilization through lateral discharge during rewetting of the acrotelm (Worrall et al., 2008). This is consistent with the particularly important DOC exports measured during the summer of 2019 (the Bb event, Fig. 2.3), after July 2019, which was the driest month (27 mm of precipitation). As the increase in the DOC concentration and exports in the stream followed the WTD increase (Figs. 2.2 and 2.3), we assume that the DOC exported during high flow is mainly derived from leaching of the acrotelm.

The intermittence of DOC concentration peaks showed that DOC exports are constrained during flood episodes, which are characterized by rapid and significant increases in WTD and *Q* (Fig. 2.2). As DOC concentration variations and exports and hydrological variables are closely related, the shift from low- to high-flow periods can be viewed as the hydrological reconnection between peat – that is, the DOC reservoir – and the peatland drainage stream (Billett et al., 2006).

2.5.2 The succession of low- and high-flow determines specific peatland DOC exports

In contrast to the assumption that the peatland is the main source of exported DOC during high-flow periods, we found that the hydrological connection between the peat and the stream is less clear during the low-flow periods (Fig. 2.2a). Consequently, we used an alternative approach to calculate specific DOC exports by using two different catchment surface areas, depending on the discharge.

Based on the classification of the discharge in high- and low-flow periods, we calculated the specific exports of the peatland as the amount of DOC exported during the high-flow periods. During the low-flow periods, we used the more conservative approach; specifically, we used the total catchment area as the surface reference for the export calculation during those periods. This approach reposed on the hypothesis that DOC exported during high-flow mainly derived from the peat while during low-flow, the hydrological connectivity between the peat and the stream is not clear (Fig. 2.2a). Although the absence of DOC sources investigation within the catchment, the C-*Q* relationships might help to understand DOC sources through

hypothesis made on lateral flow pathways within the catchment. During the studied floods episodes, C-*Q* relationships exhibit homogeneous patterns characterized by anticlockwise hysteresis and increase of DOC concentrations during the rising limb of the flood (Fig. 2.5). We previously interpret them at the subsurface runoff in the DOC-rich acrotelm, cause by the rise of the water table (see section 5.1) and leading to the progressive reconnection between peat-derived DOC sources and the stream during flood events (Tunaley et al., 2016).

Understanding the DOC lateral transfer pathways is important to resolve the challenge of characterizing DOC sources and to estimate the contribution of forested soils which covered 17% of the studied site. In a mixed headwater catchment covered by only 22% of peatlands in riparian zones, Dick et al. (2015) estimated that 84% of exported DOC was derived from peat soils. In catchments dominated by mineral forested soils, Raymond and Saiers (2010) observed clockwise hysteretic loops, caused by the progressive depletion of available soil-derived DOC during the rising limb of the flood. Contrastingly, anticlockwise hysteretic loop combined with an increase of DOC concentrations during the rising limb was also observed from forested catchment. Despite the dominance of forested areas, authors attribute those relations to the contribution of riparian wetlands to DOC exports (Pellerin et al., 2012; Strohmeier et al., 2013). In our site, forested areas are concentrating on the west border of the catchment and some patches are in upstream sections of the stream, while riparian areas in the downstream section is composed of peat (Fig. 2.1). This tends to even more moderate the importance of forested areas in DOC exports contribution.

We argue that this pragmatic approach provides a more accurate estimation of the specific DOC exports from the peatland. The annual exports using this approach were 1.87 ± 0.75 g DOC-C m^{-2} y^{-1} in 2018–2019 and 1.27 ± 0.35 g DOC-C m^{-2} y^{-1} in 2019–2020. Approaches using the whole catchment area during the study period would have underestimated the exports by 21.6% in 2018–2019 and by 21.8% in 2019–2020. Conversely, using the peatland area within the catchment to calculate DOC exports would have overestimated the exports by only about 2% for 2018–2019 and 2019–2020, because the peatland covers 76.7% of the whole watershed and because of a disproportional larger amount of DOC was exported high flow. While the high-flow periods accounted for 59% and 44% of the complete time series in 2018–2019 and 2019–2020, respectively, the specific exports accounted for 92.6 % of the annual exports in 2018–2019 and 93.8% in 2019–2020 (Table 2.2b). This approach supports the dominance of the peatland contribution in annual DOC exports (Tipping et al., 2010) and the importance of high flow as key moments

of DOC exports (Rosset et al., 2019), particularly by the increase of the hydraulic connectivity between the peatland and the stream (Birkel et al., 2017; Tunaley et al., 2017).

In this study, DOC exports are lower than those previously measured in undisturbed boreal peatland drainage streams, which varied from 3.7 to 18.0 g DOC-C m^{-2} y^{-1} (Köhler et al., 2008, 2009; Juutinen et al., 2013; Leach et al., 2016). This low range of DOC exports might be related to the incertitude of the discharge during the spring freshet. The stream discharge during this period was derived from the PHIM model (Riahi, 2021) not by empirical measurements. Spring freshets is a key period for DOC exports as it can represent 30% to 55% of annual carbon exports (Leach et al., 2016). In our site, DOC exports during spring freshets (constrained during April and May, Fig. 2.3e) compose only 25% and 23% of the annual DOC exports for 2018-2019 and 2019-2020 respectively (Table 2.2a). However, even in a scenario of spring freshet contributing to 50% of DOC exports, estimated annual DOC exports would be about 2.2 and 1.6 g DOC-C m^{-2} y^{-1} for 2018-2019 and 2019-2020 respectively, remained in the lower range of those measured in the literature (3.7-18.0 g DOC-C m^{-2} y^{-1}).

The low DOC exports measured in our site can be explained by hydrometeorological conditions and particularly the low precipitation measured in the region at the Havre-Saint-Pierre airport meteorological station, located at 39 km south-west from the site during the studied years (Fig. annexe A.4). From May to October (the period including the ice-free season), precipitation was 530 mm in 2018 and 460 mm in 2019 while the average for the 1979-2019 period was 617 ± 104 mm. In addition, precipitation varied by a factor 1.15 between studied years and it could partially explain the interannual variability in DOC exports that was 1.5 times higher in 2018-2019 than 2019-2020. Those important interannual variations were previously observed in peatland drainage streams from a factor 1.6 to 3 and attributed to interannual variation of the discharge (Worrall et al., 2009; Dinsmore et al., 2013; Leach et al., 2016; Birkel et al., 2017; Rosset et al., 2019). The variability in the cumulative discharge at the stream outlet, 1.26 times higher in 2018–2019 compared with 2019–2020, also support interannual variations in DOC exports between the two years (Fig. 2.4).

In terms of total carbon flux in our studied peatland, Taillardat et al. (2022) estimated the stream carbon GHG (CO_2 and CH_4) aquatic exports as 1.08 g GHG-C m^{-2} y^{-1}. It gives a total aquatic carbon exports (GHG + DOC) ranged between 2.35 and 2.95 g C m^{-2} y^{-1} and a contribution of DOC exports accounting for 54-63% of the total aquatic carbon exports. This is in line with previous studies which observed a DOC contribution

to aquatic carbon flux ranged between 46 and 95% (Dinsmore et al., 2013; Dyson et al., 2011; Holden et al., 2012; Huotari et al., 2013; Leach et al., 2016; Nilsson et al., 2008; Roulet et al., 2007; Worrall et al., 2008). Despite low DOC exports measured in Bouleau peatland drainage stream, it seems that it not alter the expected proportion of DOC exports in comparison with GHG exports which mainly occurred during low-flow (Taillardat et al., 2022). Also, it seems unlikely that low DOC exports are due to in-stream processing as these are mainly observed during low-flow when the hydrological connectivity is limited (Casas-Ruiz et al., 2017; Raymond et al., 2016) and because Taillardat et al. (2022) estimates that only 17% of exported CO_2 results of in-stream processing against 81% from peat porewater drainage.

The low DOC exports need to be considered in the context of the ecosystem carbon budget. Our study and (Taillardat et al. (2022) are the first documenting aquatic carbon exports from an undisturbed peatland within the boreal biome in Eastern Canada. In order to better explain those low aquatic carbon exports, it would be pertinent to compare them with the net ecosystem exchange of the peatland and estimates which proportion of carbon accumulated yearly is offset by those outgoing fluxes.

2.5.3 Variability of DOC lateral transfer patterns and the implication in the annual DOC exports

The division of flood events between three clusters helped us understand the mechanisms leading to the different magnitudes of DOC exports (Table 2.3 and Fig. 2.6b). The events of cluster 1 seem to represent the most common type of flood events as it included 7 of the 12 events and accounted for 47.7% of the total event duration but with the lowest DOC_{load} of 0.6 ± 0.3 kg DOC h^{-1} (Table 2.3). While the cluster 1 was characterized by a ΔWTD slightly higher than the average (Fig. 2.6b) and despite precipitation event 2 days before the flood (AP2) which was twice lower cluster 2 and more than three times lower than cluster 3, it also presented the lowest $WTD_{initial}$ (-0.30 m; Table 2.3). Consequently, the lateral discharge did not lead to an important increase in Q compared with the other clusters (Table 2.3). In addition to the low ΔQ and Q_{max}, the low FI (Table 2.3) reflects the low accretion of DOC (Vaughan et al., 2017). While Tunaley et al. (2017) interpreted that a low HI reflects a DOC source distant from the stream, in our study site, it seems more related to progressive rewetting of the peat and slow lateral discharge leading to slow DOC mobilization to the stream (Bishop et al., 2004; Blaurock et al., 2021). Those conditions restricted the connectivity between DOC sources and the stream leading to low DOC loads (Fig. 2.7a).

a)

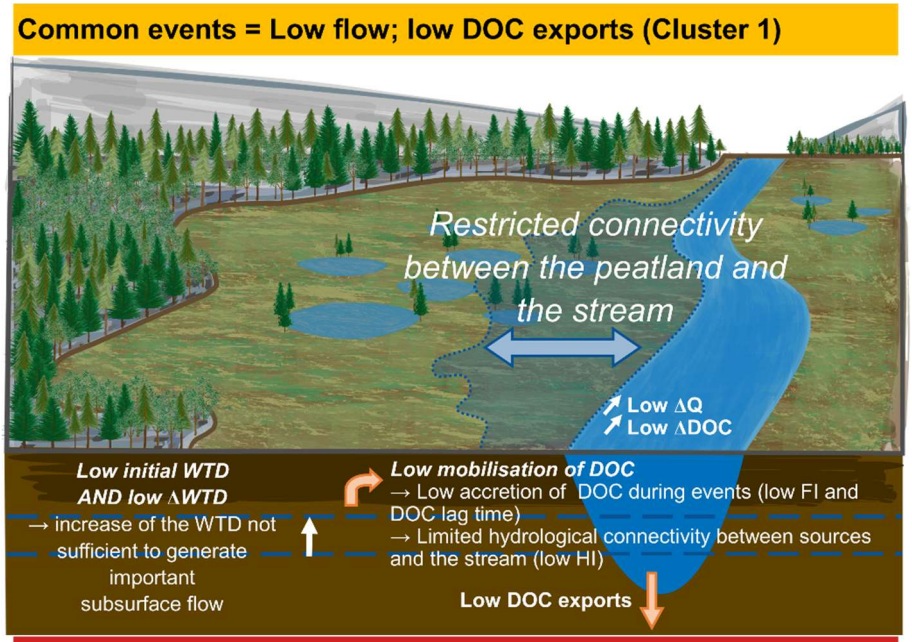
Common events = Low flow; low DOC exports (Cluster 1)
Restricted connectivity between the peatland and the stream
Low ΔQ
Low ΔDOC
Low initial WTD
AND low ΔWTD
→ increase of the WTD not sufficient to generate important subsurface flow
Low mobilisation of DOC
→ Low accretion of DOC during events (low FI and DOC lag time)
→ Limited hydrological connectivity between sources and the stream (low HI)
Low DOC exports

b)

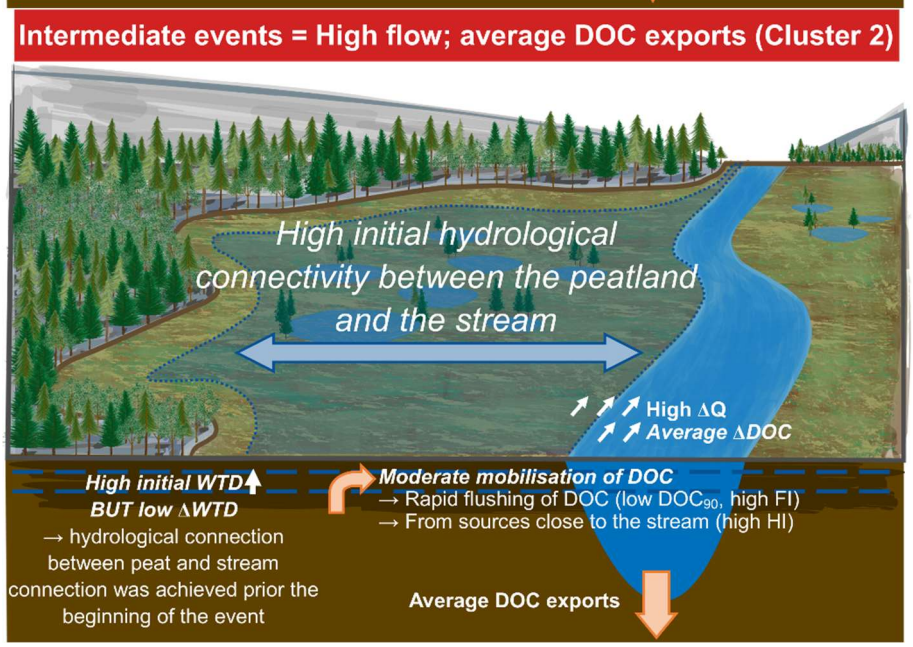
Intermediate events = High flow; average DOC exports (Cluster 2)
High initial hydrological connectivity between the peatland and the stream
High ΔQ
Average ΔDOC
High initial WTD
BUT low ΔWTD
→ hydrological connection between peat and stream connection was achieved prior the beginning of the event
Moderate mobilisation of DOC
→ Rapid flushing of DOC (low DOC90, high FI)
→ From sources close to the stream (high HI)
Average DOC exports

c)

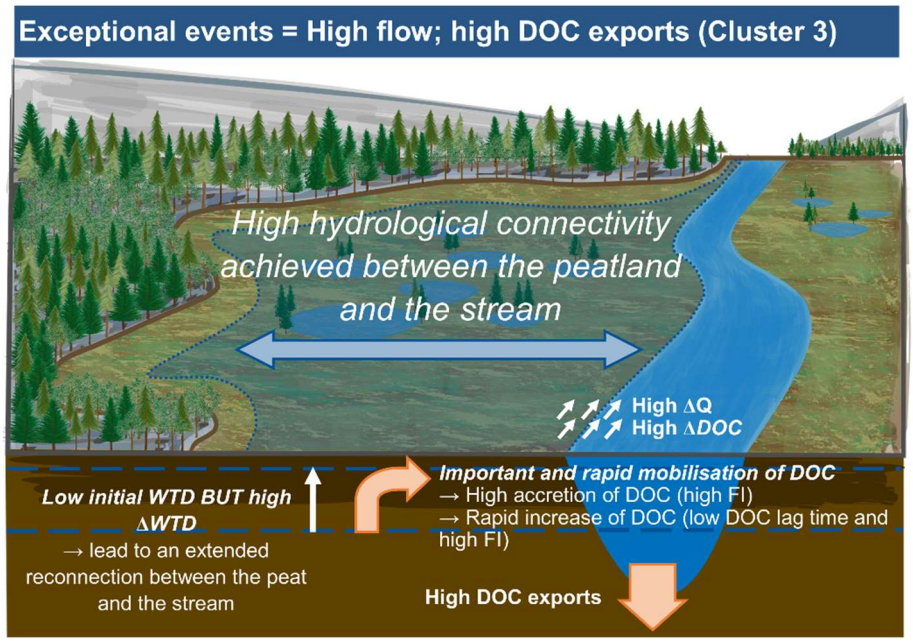

Figure 2.7 Theoretical models of flood events from a) events of low-flow and low dissolved organic carbon (DOC) loads (cluster 1), b) events of high-flow and average DOC loads (cluster 2) and c) events of high-flow and high DOC loads (cluster 3).

Cluster 2 comprised three events that occurred during the early and late growing season of 2019 (Fig. 2.6a). Those events had a comparable rainfall amount but a higher Δ*Q* compared with the events of cluster 1 (Table 2.3). The high $WTD_{initial}$ might indicate that these events succeeded a previously 'wet' period which was confirmed by higher precipitation 14 days before the event (AP14; Table 2.3) compared to cluster 1 and similar to cluster 3 but also by a P-Q lag time (i.e., the lag time between the precipitation event and the increase of discharge in the stream) lower than other clusters (Table 2.3). This can also be sustained by the higher FI than events of the cluster 1 and the highest HI (Fig. 2.5). It reflects rapid DOC mobilization, simultaneously to the *Q* increase, and from sources close to the stream (Blaurock et al., 2021; Tunaley et al., 2017). Those events might represent rapid flushing of DOC promoted by the high $WTD_{initial}$ and supported by the lowest DOC_{90} leading to moderate DOC loads of 1.0 kg DOC-C h^{-1} on average (Fig. 2.7b). Although the threshold of the lateral discharge generation was easily exceeded, the less negative HI suggests that DOC was mostly exported from sources close to the stream (Tunaley et al., 2017).

Cluster 3 comprised two events that occurred during early summer (Aa) and midsummer (Bb) where the highest ΔWTD and ΔDOC and high Δ*Q* led to the highest DOC_{max} (Fig. 2.6b). Event Bb, which is the only one with precipitation data, exhibit the highest precipitation during the flood event but also the highest AP2,

more than three times higher than cluster 3 and two times higher than cluster 2 (Table 2.3). Consequently, during those events DOC_{load} was 2.4–4 times higher than events of cluster 1 and cluster 2 respectively. Despite the low $WTD_{initial}$ of -0.31 m comparable to the events of cluster 1, those events presented greater DOC exports. These findings indicate that DOC_{load} is more constrained by the magnitude of the WTD increase rather than the initial WTD considering that WTD drawdown as well as the average porewater temperature and high stream temperature could stimulate the DOC production (Clark et al., 2009; Grand-Clement et al., 2014). During those events, the large WTD increase favoured the rapid circulation of water through the DOC-rich acrotelm (Inamdar et al., 2004) and supported by the high FI, indicating rapid flushing of DOC to the stream (Table 2.3). In addition, the anticlockwise hysteresis (HI of -0.3 in average, Table 2.3) highlights the extensive connectivity between DOC sources within the peatland and the stream (Pellerin et al., 2012; Tunaley et al., 2016), supporting the high DOC exports (Fig. 2.7c).

Cluster 3 events appear to be extreme and associated with events with a low probability of occurrence. DOC exported during those events contributed to 24.3% and 24.4% of the total exports while only representing 8.5% and 3.8% of the growing season 2018 and 2019, respectively (Table 2.2b). The event Bb presented highest AP2 and total precipitation (Table 2.3) leading to an important ΔWTD (Fig. 2.6b). These data suggest that the magnitude of a single event is at least as important as several events (Raymond & Saiers, 2010). Interestingly, those events did not happen during the same periods, revealing different export mechanisms.

The Aa event occurred at the end of the spring freshet, which is known as an important period of DOC exports (Tiwari et al., 2018). However, similar events were not observed during 2019 snowmelt and event Ba that occurred during this period was attributed to cluster 2 (Fig. 2.6a). However, similar amounts of DOC were exports during May 2019 compared to June 2018 that could reveal a delayed spring thaw in 2019 compared to 2018. Previous studies observed that variability in DOC exports can be influenced by interannual variation of meteorological conditions (Ågren et al., 2010; Dinsmore et al., 2013; Tiwari et al., 2018). The period covered by our study limits this type of interpretation but it is reinforcing the necessity of long-term DOC exports monitoring (Webb et al., 2019).

Conversely, the Bb event occurred during the warmest registered period, in August 2019, after 42 days of low flow and without a significant period of DOC exports between 26 June and 8 August 2019 (Figs. 2.3 and 2.4). A large amount of DOC was exported during high-flow events occurring throughout the warm

periods. This may coincide with conditions that have previously been described as favourable for DOC production which is accumulated within the peat during dry periods (Clark et al., 2007, 2009; Dinsmore et al., 2013). Then, the large rainfall events occurring before the event initiated an important WTD increase that leads to DOC mobilization (Table annexe A.3; Grand-Clement et al., 2014; Zhu et al., 2022).

2.6 Conclusion

Our study, measuring continuous DOC exports from a boreal peatland in north-eastern Canada, provides the very first insight concerning peatland DOC exports for this region. The use of high-frequency monitoring of hydrological variables and DOC concentrations has provided a comprehensive understanding of the temporal dynamics of DOC exports and the mobilization patterns of DOC in a boreal peatland. The relationship between WTD and *Q* highlights the major contribution of peat subsurface flows to *Q* during flood events. Our data suggest that during these events, the exported DOC is mainly leached from the peatland. While the determination of specific DOC exports from the peatland remains a challenge, here we have proposed a time series analysis split between low- and high-flow periods. During the flood periods, the surface considered in the export calculations is the peatland area within the catchment. By contrast, during the low-flow periods, the catchment area is considered the conservative surface reference in the calculation given the lack of a direct link between peat porewater discharge and DOC exports from the stream observed during the growing season. DOC exported during high flow represented 92.6% and 93.8% of the total DOC exports during 59% and 44% for the 2018–2019 and the 2019–2020 periods, respectively. In addition, the use of a simple catchment surface in the export calculation would underestimate the exports by 22% compared with the new approach we have proposed.

The study of DOC mobilization during flood events supports the idea that variations in WTD generate lateral discharge that controls the magnitude of DOC being exported from the stream. Based on hierarchical clustering, three types of events were characterized with contrasting wetness conditions. The most common events (cluster 1) had a low $WTD_{initial}$ and a small WTD increase that limited the extent of the connectivity between the DOC sources and the stream. Conversely, the events of cluster 3 showed an important WTD increase, easily exceeding the threshold of runoff generation to facilitate DOC mobilization and to increase its transfer through the stream. Those exceptional events can represent up to 24% of the total DOC exported during periods, accounting for 8% and 3% of the growing season in 2018 and 2019 respectively. The cluster 2 events represented intermediate conditions. While during those events the threshold of runoff generation was easily exceeded, previous events might have depleted DOC available

to be transferred to the stream. This event presented relatively low DOC loads despite the high peak WTD and *Q*.

The response of DOC mobilization to hydroclimatic conditions in peatland is a key element in the magnitude of DOC exports. With climate change, precipitation regimes, the ice-free season duration and the water balance of ecosystems will be affected. Consequently, an increase in drought followed by intensive rainfall in the context of climate change might increase the aquatic DOC exports in boreal peatlands.

Acknowledgments

The funding for this research was provided by the Natural Sciences and Engineering Research Council of Canada and Hydro-Quebec to Michelle Garneau (RDCPJ 514218-17). We thank Frederic Julien, Virginie Payre-Suc and Didier Lambrigot, from Laboratoire Ecologie Fonctionnelle et Environnement (UMR 5245 CNRS – UT3 – INPT, France), for performing DOC/TN and cation/anion analyses. Thanks to Dr Roman Teisserenc (ENSAT, Toulouse, France) and students Charles Bonneau, Charles-Élie Dubé-Poirier, Camille Girard, Pénélope Germain-Chartrand, Léonie Perrier, Guillaume Primeau, Khawla Riahi and Karelle Trottier for their assistance in the field.

CHAPITRE 3

Hydrological conditions control dissolved organic matter dynamics along a peatland drainage boreal headwater stream

Antonin Prijac[1,2,3], Laure Gandois[4], Pierre Taillardat[1,5], and Michelle Garneau[1,2,3,6]

[1]Centre de Recherche sur la Dynamique du Système Terre (GÉOTOP), Université du Québec à Montréal, Montréal, Canada
[2]Groupe de Recherche Inter-universitaire en limnologie (GRIL), Université du Québec à Montréal, Montréal, Canada
[3]Institut des Sciences de l'Environnement (ISE), Université du Québec à Montréal, Montréal, Canada
[4]Laboratoire Écologie Fonctionnelle et Environnement, UMR 5245, CNRS-UPS-INPT, Toulouse, France
[5]NUS Environmental Research Institute, National University of Singapore, Singapore
[6]Département de Géographie, Université du Québec à Montréal, Montréal, Canada

Article en préparation pour être prochainement soumise dans la revue Journal of Geophysical Research : Biogeosciences.

Résumé

Les conditions hydrologiques dans les ruisseaux de drainage des tourbières sont connues pour contraindre l'intensité des exports de carbone organique dissous (COD). L'influence des contrôles hydrologiques sur la composition de la matière organique dissoute (MOD) le long de ruisseaux traversant un bassin versant dominé par des tourbières est peu documentée. La MOD est une composante très réactive dans le bilan de carbone des tourbières, qui est sensible aux processus de dégradation qui peuvent soutenir localement les exports et les émissions de dioxyde de carbone (CO_2) une fois exportée dans les ruisseaux. L'étude explore les relations entre la composition de la MOD et l'hydrologie du bassin versant dans un ruisseau de 3 km traversant une tourbière boréale, de sa source à son exutoire. Les conditions hydrologiques influencent significativement la composition de la MOD. La MOD exportée pendant les périodes de hautes eaux a une composition similaire à celle de l'eau interstitielle de la tourbière en termes de ratio COD : NOD et d'aromaticité, mais un poids moléculaire moyen plus faible, soulignant l'export préférentiel de MOD de faible poids moléculaire récemment produite dans l'acrotelme. La composition de la MOD change faiblement le long du ruisseau pendant les hautes eaux et est rapidement transférée vers l'aval. En période de basses eaux, la MOD du ruisseau a une aromaticité et un poids moléculaire significativement plus élevé, mais un ratio COD : NOD plus faible. À la différence des périodes de hautes eaux, la composition de la MOD change le long du ruisseau pendant les basses eaux. Une importante augmentation de l'aromaticité et du poids moléculaire est observée. Ces changements de la composition de la MOD sont significativement corrélés au temps de résidence de l'eau dans le ruisseau et à la contribution de la minéralisation dans le flux de COD exporté à l'exutoire du ruisseau. Ces résultats montrent l'importance des processus de minéralisation du COD en période de basses eaux, qui peuvent soutenir les exports et les émissions de CO_2 du ruisseau.

Abstract

Hydrological conditions (i.e., high-flow versus low-flow) in peatland drainage streams influence both the quantity of exported dissolved organic carbon (DOC) and dissolved organic matter (DOM). Yet, our knowledge on DOM fate after export from the peatland remains limited. DOM is a highly reactive component within the peatland carbon cycle, sensitive to degradation processes that sustains emissions and exports of carbon dioxide (CO2) from streams. The present study demonstrates the relationships between DOM composition evolution and catchment hydrological conditions along a 3 km long headwater stream running through a boreal peatland, from its source to the outlet. Our results show that hydrological conditions significantly influenced DOM composition evolution along the stream. DOM exported during high-flow conditions presented a composition similar to peat porewater in terms of DOC:DON ratio and aromaticity, but a lower average molecular weight, indicating preferential exports of low molecular weight DOM recently produced in the acrotelm. The DOM composition changed little along the stream during high-flow as it was rapidly flushed downstream. During low-flow conditions, stream DOM presented significantly higher aromaticity, average molecular weight, but lower DOC:DON ratio compared to high-flow. Moreover, during low-flow conditions, DOM composition evolved along the stream in contrast to high-flow with a strong increase in DOM aromaticity and molecular weight along the stream. These changes in DOM composition were significantly correlated to the water residence time in the stream and to the estimated proportion of mineralized DOC to total DOC flux exported at the stream outlet. These results highlight the importance of hydrological conditions on DOM dynamics as DOM was locally mineralized during low-flow conditions while mineralization processes happened downstream under high-flow conditions.

3.1 Introduction

Among terrestrial ecosystems, peatlands play a crucial role in the carbon cycle as they represent an important carbon sink, as a result of accumulating organic carbon fixed by its vegetation under the form of peat (Charman, 2002; Z. Yu et al., 2010). It was also established that, at the catchment scale, the amount of carbon exported as dissolved organic carbon (DOC) is positively correlated to the proportion of the catchment area covered by peatlands (Billett et al., 2006a; Laudon et al., 2011; Olefeldt, Turetsky, et al., 2013; Rantakari et al., 2010). DOC is the main form of carbon being laterally exported from peatland ecosystems, accounting from 57 % to 97 % of aquatic carbon fluxes (Dinsmore et al., 2010, 2013; Holden et al., 2012; Leach et al., 2016; Roulet et al., 2007). The remaining part is constituted by particulate organic carbon (POC), dissolved carbon dioxide (CO_2) and methane (CH_4). Moreover, several studies have shown that DOC export from peatland can offset 14-132 % of its net ecosystem exchange (Dinsmore et al., 2010; Nilsson et al., 2008; Roulet et al., 2007; Worrall et al., 2008), even exceeding the net ecosystem exchange for some years (Koehler et al., 2011; Roulet et al., 2007).

The aquatic DOC export through peatland drainage streams is highly sensitive to hydrological conditions in catchments, and mainly in peatland areas. The rise of peatland water table depth (WTD) leads to the increase of hydrological connectivity between peatland and stream and facilitates DOC transfer through subsurface flow during flood periods (Birkel et al., 2017; Bishop et al., 2004; Frei et al., 2010; Laudon et al., 2011; Tunaley et al., 2016). Additionally to the importance of DOC in aquatic carbon exports, it is necessary to evaluate if this form of carbon is reactive and can be mineralized through biodegradation and photodegradation processes in streams (Lapierre & del Giorgio, 2014; Vonk et al., 2015), to fully understand its fate – either mineralized as CO_2 and sent back to the atmosphere or transported downstream. In headwater streams, dissolved organic matter (DOM) mineralization leads to CO_2 production (Hutchins et al., 2017; Rasilo et al., 2017) hence generating emissions of CO_2 from headwater streams (Taillardat et al., 2022; Wallin et al., 2013a).

Several studies previously explored the evolution of DOM composition along river transects (i.e., from its source to its outlet within a catchment) through the optical or molecular properties, or assessments of biodegradability. Those studies aimed at demonstrating the influence of land use change (Hope et al., 1997; Kamjunke et al., 2019; Miller, 2012; Yamashita et al., 2010), dams and reservoirs (Parks & Baker, 1997; Stackpoole et al., 2014; Zurbrügg et al., 2013) on DOM composition evolution in streams and rivers. The respective influence of multiple DOM sources and tributaries contributions within large river catchments

were also assessed using this approach (Cawley et al., 2012; del Giorgio & Pace, 2008; Frederick et al., 2012; Lambert et al., 2016; Mladenov et al., 2007; N. D. Ward et al., 2015). These studies focused on catchments with surface areas ranging from 5,500 km^2 (Yamashita et al., 2010) or larger (i.e., up to 1,353,000 km^2 in Stackpoole et al., 2014).

Consequently, Raymond et al. (2016) proposed the *pulse-shunt* concept to conceptualize the fate of DOC exported through streams and rivers networks. While Cole et al. (2007) described rivers as a reactor rather than the common acceptance of them as passive pipes, Raymond et al. (2016) hypothesized that streams can be one or the other depending on hydrological connectivity between terrestrial ecosystems (e.g., peatlands) and rivers. After precipitation or during snowmelt, important discharge and short residence times induce large mobilization of DOM through rivers leading to the passive transfer of DOM up to coastal ecosystems. Elsewhere, periods of low hydrological connectivity lead to lower DOM exports. The lower discharge and longer residence time during those periods enhance DOM mineralization in streams that sustains CO_2 exports and emissions.

Effects of hydrological connectivity on DOM mineralization at smaller scales and especially headwater stream catchments are less documented. Headwater streams are recognized to be molecularly more diversified compared to downstream rivers (Kamjunke et al., 2019; Lambert et al., 2016; Vannote et al., 1980; N. D. Ward et al., 2015; Zark & Dittmar, 2018), induced by the simultaneous contribution of allochthonous DOM derived terrestrial environments (e.g., peatlands) and autochthonous DOM production from biodegradation and photodegradation processes (Berggren et al., 2010; Mann et al., 2015; Vonk et al., 2015). Therefore, mineralization processes can be identified by using DOM composition evolution (Grand-Clement et al., 2014; Payandi-Rolland et al., 2020; Prijac et al., 2022). Low molecular weight compounds are preferentially degraded by microorganisms (Mann et al., 2015; Spencer et al., 2008, 2015a; Worrall et al., 2017), with a subsequent increase in aromaticity and molecular weight for the remaining DOM (Autio et al., 2016; Hulatt et al., 2014; Prijac et al., 2022). Conversely, photodegradation degrades aromatic compounds (Cory et al., 2007, 2013), and therefore decreases DOM molecular weight and aromaticity of stream DOM (Helms et al., 2008; Laurion & Mladenov, 2013; C. P. Ward & Cory, 2016). In addition to mineralization processes, stream DOM composition can vary according to its vertical stratification of DOM composition in contributing peat layers. This stratification is induced by WTD fluctuations, as well as impact on microbial and plant metabolism (Broder & Biester, 2015; Buzek et al.,

2019; Tfaily et al., 2013, 2018) leading to an increase of DOM aromaticity and molecular weight with depth (Tfaily et al., 2018).

In peatland-dominated headwater catchments, previous studies have explored changes in DOM composition by comparing different hydrological conditions (i.e., periods of low- and high-flow in the stream) or during different seasons (Austnes et al., 2010; Broder et al., 2017; Buzek et al., 2019; Grand-Clement et al., 2014). However, these studies only considered one sampling station in a stream and commonly selected the outlet of catchments (Austnes et al., 2010; Broder et al., 2017; Buzek et al., 2019) or compared distinct catchments according to their land cover (Grand-Clement et al., 2014). Despite those studies observed shift in DOM composition from recently produced DOM from the acrotelm during high-flow (Austnes et al., 2010) to more microbial-derived DOM during low-flow (Grand-Clement et al., 2014; Hutchins et al., 2017) they did not explore the change along a stream transect (i.e., from its source to its outlet).

The goal of this study is to understand the effect of hydrological conditions on DOM composition in a stream running through a boreal peatland-dominated catchment. While the *pulse-shunt* concept focused on variation of DOM exports under contrasted hydrological condition in the stream, here we hypothesized that for a peatland-dominated headwater catchment, DOM composition evolution is also influenced by hydrological conditions. While it commonly assumed that mineralization processes affect DOM composition, the contribution of the study would identify if and how residence time, under contrasted hydrological conditions, could affect mineralization process magnitude and consequently the DOM composition. More specifically, the study aims at i) comparing DOM composition in the stream and in the peat porewater under different hydroclimatic conditions and ii) describing the spatiotemporal variability of DOM composition under the different hydroclimatic conditions along a stream transect. The study combines investigations of DOM composition at different sampling stations along a 3 km long stream transect, and present punctual mass balance models under different hydrometeorological conditions (consisting of high-flow and low-flow conditions) to estimate peatland contribution of DOC exports.

3.2 Study site

The study site, within the Romaine River catchment (14 500 km^2) is located in north-eastern Canada, was previously described (Prijac et al., 2022, 2023; Taillardat et al., 2022). The site is in the eastern spruce-moss bioclimatic domain of the closed boreal forest (Payette, 2001) at the limit of the coastal plain and

the Highlands of the Laurentian Plateau of the Precambrian Shield (Dubois, 1980). The studied catchment is covered at 76% by the Bouleau peatland (50°31'N, 63°12'W; alt: 108 ± 5 m), an ombrotrophic slightly dome-shaped bog (Fig. 3.1). Peat accumulation was initiated at ca 9260 calibrated years before present and maximum peat depth reaches 440 cm (Primeau & Garneau, 2021). The peatland is positioned at the head of a catchment and the study focussed on the southern section of the peatland drained by a headwater stream of 3 km long, which is flowing from North to South predominantly on the western side of the peatland. The surface of the catchment drained by the stream is 2.22 km^2 and is covered at 76.7 % by peat, representing a surface area of 1.70 km^2.

As previously described (Prijac et al., 2022, 2023; Taillardat et al., 2022) the regional climate data give a mean annual temperature of 1.5°C and mean annual precipitation of 1011 mm of which 590 mm fall as snow. Average monthly positive temperature occurs from May to October with 1915 growing degree days above zero (Havre-Saint-Pierre meteorological station, mean 1990-2019, Environment of Canada). Over the growing seasons, average air temperature was 13.2 ± 6.9°C with a minimum temperature of -7.9°C in early October 2018 and a maximum of 30.8°C reached in late July 2018. Average precipitation events were 2 mm h^{-1} and maximum precipitation fallen in one hour was in July 2018 with a total of 22 mm. The wettest month was August 2018 with a total precipitation of 207 mm and the driest month of July 2018 with a total precipitation of 27 mm.

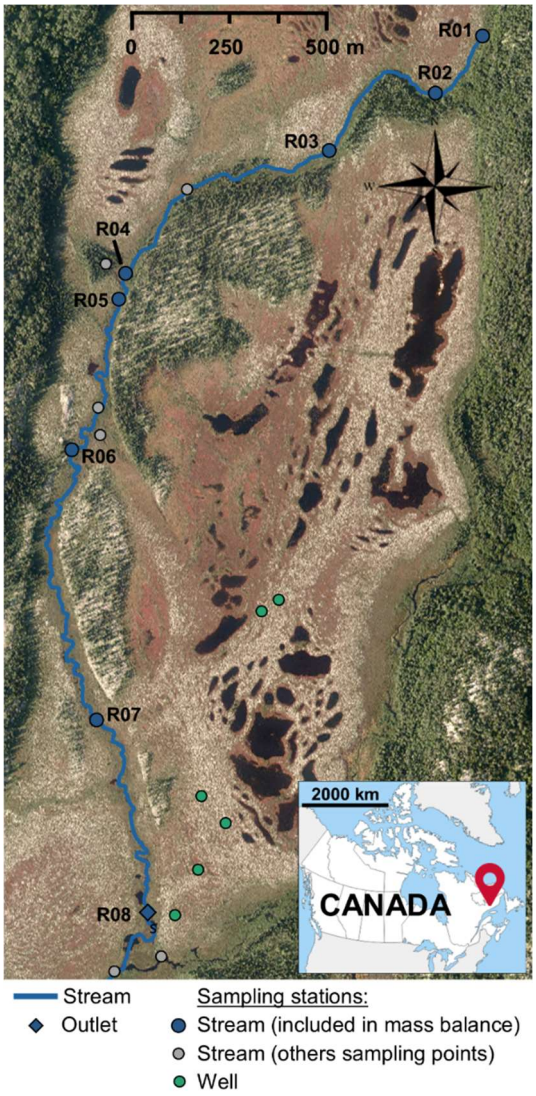

Figure 3.1 Bouleau peatland with the location of the sampling sites in wells (green dots), pools (yellow triangles) and in the stream (blue dots) and its tributaries (grey dots). The aerial photo was provided by Hydro-Québec.

3.3 Material and methods

3.3.1 Water sampling

The water sampling was performed four times during the growing season of 2019 (June, August, September, and October). Following the method described in Prijac et al. (2022, 2023), the water was sampled at the surface of eight stations along the headwater stream and peat porewater was sampled from six wells (P1 to P6, Fig. 3.1) located along a topographic gradient from the peatland dome (higher

elevation) to its southern edge, near the stream outlet (lower elevation). The peat porewater was collected into two meters long PVC wells, perforated, covered with a nylon sock to avoid infilling by peat and inserted in peat to collect water from the first two meters of the peat column.

Physicochemical parameters (temperature, pH, specific conductivity, and dissolved oxygen saturation) were measured at each sampling site using a multi-parameter portable meter (Multiline Multi-3620 IDS, WTW, Germany) calibrated before each field visit. Water samples were collected in clean polypropylene (PP) bottles (acid rinsed) and filtered on pre-combusted (4h at 450°C) GF/F filters (Whatman).

3.3.2 DOM analyses

3.3.2.1 DOC and DON concentrations

Following the method described in Prijac et al. (2022), the filtered water samples were prepared for DOC and total nitrogen (TN) analyses by acidification to pH 2 with 1M HCl and stored in 40 mL glass vials. The DOC and TN concentrations were analyzed using the catalytic oxidation method followed by non-dispersive infrared (NDIR) detection of CO_2 produced (TOC analyser TOC-L, Shimadzu, Japan) with limits of quantification of 0.1 mg C L^{-1} and 0.2 mg N L^{-1}. The samples were prepared for cation and anion analyses and stored in high-density polyethylene (HDPE) vials without acidification. These ions (chloride, ammonium, nitrites, and nitrates) were analyzed by high performance liquid chromatography (HPLC) coupled with a Dionex ICS-5000+ analyzer for anions (Thermo Fisher Scientific) and a Dionex DX-120 analyzer for cations (Thermo Fisher Scientific). The reference materials included ION-915 and ION 96.4 (Environment and Climate Change Canada, Canada). Analyses were performed at Laboratoire Ecologie fonctionnelle et environnement (UMR 5245 CNRS – UT3 – INPT, France). Dissolved organic nitrogen (DON) corresponds to the difference between the concentration of TN and the sum of concentration of inorganic nitrogen (ammonium, nitrites, and nitrates).

3.3.2.2 Stable isotopic analyses

Analyses of δ^{13}C-DOC were realized at the Jan Veizer stable isotope laboratory (University of Ottawa, Canada) following the method described in Prijac et al. (2022) and developed by Lalonde et al. (2014). The samples were acidified to pH 2 with 1M HCl and stored in 40 mL quality certified ultra-clean borosilicate glass vials. The first step involved catalytic oxidation of DOC followed by a solid-state non-dispersive infrared (SS-NDIR) detection of the CO_2 produced (OI Aurora 1030C, Xylem Analytics, USA). The CO_2 produced was passed through a chemical trap and a Nafion trap prior to ^{13}C isotopic analyses using

isotope-ratio mass spectroscopy (IRMS, Thermo Finnigan DeltaPlus XP, Thermo Electron Corporation, USA). The results were standardized with organic standards (KHP and sucrose) and $^{13}C/^{12}C$ ratios were expressed as per mil deviations from the international standard VPDB.

3.3.2.3 Optical analyses

As in Prijac et al. (2022), UV-visible analyses were performed on samples filtered on GF/F filters and absorbance was measured from 180 to 900 nm with a 5 nm resolution.

Absorbance analyses were performed on) Duetta (Horiba, Japan) over a wavelength range from 190 to 900 nm at 2 nm intervals. All analyses were realized at the Groupe de recherche interuniversitaire en limnologie (GRIL, UQAM, Canada).

The absorbance indices were calculated to provide information about DOM composition. These indices were $SUVA_{254}$ (L mg^{-1} m^{-1}) which is a proxy of the DOM's aromatic content, calculated and corrected to ferric iron interaction following the method described in Weishaar et al. (2003), *E*2 : *E*3 ratio, and spectral slope ratio (S_R) which are proxies of the average DOM molecular weight (Haan & Boer, 1987; Helms et al., 2008).

Spectrofluorometric analyses were also conducted on Duetta (Horiba, Japan) at the GRIL laboratory. Samples were excited at a range from 230 to 450 nm (at 2 nm resolution) and fluorescence was measured at a range from 240 to 600 nm (at a 5 nm resolution). Prior to the analyses, samples were diluted when necessary to maintain an absorbance intensity at 254 nm below 0.6 and avoid inner filter effect. A blank sample with MilliQ water (Merck-Millipore, Germany) was measured prior to sample analyses. Samples spectra were obtained by subtracting the blank spectra to eliminate the Raman scatter peak. The operation was conducted automatically by the analytical equipment.

3.3.3 Incubation experiments experiments for the determination of the proportion on mineralized DOC into the DOC exports

Incubation experiments were performed during three sampling periods in 2019, from 7 to 13 June, from 31 July to 7 August, and from 4 to 10 September. Samples were collected at the stream outlet where water temperature was monitored using an EXO2 probe (YSI, USA).

Incubation experiments followed the method described in Prijac et al. (2022) with samples filtered on GF/F filters (Whatman). Samples were placed on amber glass to test biodegradation (BIO) only and in transparent vials to test both bio and photodegradation (BIO+PHOTO). For *in situ* incubations (IS), the samples were placed 1-2 cm below the water surface at the outlet of the peatland (Fig. 3.1). For controlled conditions (CC), vials were placed in a dark room in a laboratory space near the study site (Havre-Saint-Pierre) where the temperature was maintained between 18 and 20°C and controlled twice each day. Both *in situ* and controlled conditions started the same day.

In the end, samples incubated under UF conditions (n = 27) and filtered on a GF/F filter (Whatman) to analyze only the dissolved fraction. All samples (n = 27) were prepared to DOC quantification before and after incubation. Calculation was made according to the method in Prijac et al. (2022). The apparent removal rate of dissolved organic carbon (RDOC), expressed in mg day^{-1}, corresponds to the amount of DOC removed during incubation and reported per day. Degradation rates correspond to the proportion of DOC lost per day of incubation and are expressed in %C d^{-1}.

3.3.4 In situ high frequency monitoring

According to the method described in Prijac et al. (2023) the fluorescence of DOM was measured at the drainage stream outlet at 1h intervals from June 2018 to May 2020 using an EXO2 multi-parameter probe (YSI, USA). At each sampling station, water samples were analyzed for the DOC concentration and fDOM measurements taken with the EXO2 multi-parameter probe along the stream. The relationship f(fDOM) = [DOC], where fDOM is the corrected signal fluorescence of DOM measured in quinine sulfate units (QSU) (de Oliveira et al., 2018) and [DOC] is the dissolved organic carbon concentration in mg C L^{-1}, was used for DOC concentration calibration.

In addition, the stream discharge was measured using a 'V-shaped' weir installed perpendicularly to the stream. The discharge was derived from the water level in the stream measured by an ultrasonic distance sensor (SR50, Campbell, USA) during the 2018 growing season and a water-level logger (U201-04, Hobo, Onset, USA) from June 2019, to replace the ultrasonic distance sensor, damaged during the spring freshet (Prijac et al., 2023). The calculation method was described by Taillardat et al. (2022).

The DOC concentration and the stream discharge measured hourly form June 2018 to May 2020 were used to calculate the DOC exports at the stream outlet, following the calculation method described in Prijac et al. (2023).

In addition, in the wells installed in the peat, WTD was recorded hourly at the six wells (Fig. 3.1) equipped with a water-level data logger (HOBO, Onset, USA) for 195 continuous measurement of WTD and temperature, from June 2018 to October 2020 as described in Prijac et al. (2022). The sensors were placed into wells, suspended with a measured metal wire and kept submerged (i.e., about -0.6 m below the peat surface). Another sensor 200 was installed next to a rain gauge to record atmospheric pressure variability and to correct piezometer pressure.

3.3.5 DOC mass balance along the stream

The stream was divided into 7 sections named *a* to *g* from upstream to the outlet according to Taillardat et al. (2022) and presented in Fig. 3.2.

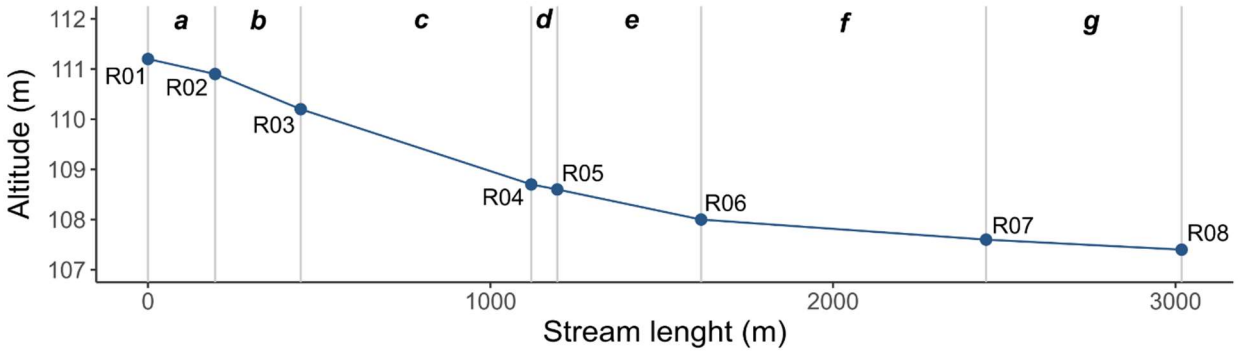

Figure 3.2 Altitudes of sampling stations along the stream from the upstream sampling station (R01) to the outlet (R08). Italic letters indicate the name of sections between two sampling points.

In 2019, stream discharge was measured at each water sampling locations (Figs. 3.1 and 3.2). At each section, water velocity was measured through a vertical cross-section using a portable flow velocity probe (Flow-mate model 2000, Marsh-McBirney Inc., USA) following the method described in Taillardat et al. (2022). The discharge at a station *i* (Q_i; $m^3 s^{-1}$) was calculated by multiplying velocity at the station (V_i; $m s^{-1}$) by the stream section (S_i; m^2) as described in equation (1):

$$Q_i = V_i \times S_i \quad (1)$$

As a deviation was observed at the stream outlet between stream discharge measured manually and high frequency measurements measured hourly at the outlet (station R08 on figures 3.1 and 3.2), a correction was applied to punctual discharge measurements, based on the linear relation between these two discharge measurement methods (R^2 = 0.97). The correction is presented in equation (2) :

$$Q_{cor\,i} = 1.163 \times Q_i - 1.5637 \quad (2)$$

DOC fluxes ($fDOC_i$; g h^{-1}) were calculated for a station *i* by multiplying DOC concentration at the station *i* (DOC_i; g m^{-3}) by discharge at the station *i* ($Q_{cor\,i}$) (Eq. 4).

$$fDOC_i = DOC_i \times Q_{cor\,i} \quad (3)$$

The quantity of DOC that could be mineralized in the stream section ($fDOC_{min\,i}$; g m^{-3}) was estimated based on degradation rates of DOC measured during incubation experiments. Then estimated $fDOC_{min\,i}$ (g m^{-3}) was multiplied by the concentration $[DOC]_i$ (g m^{-3}), the degradation rates (*m*; %C h^{-1}) and by the water volume of the section (V_i; m^3) as presented in equation (5).

$$fDOC_{min\,i} = [DOC]_i \times m \times V_i \quad (4)$$

Then, for a section *i*, a carbon mass balance was calculated (Eq. 6 and 7). The inputs included incoming DOC from the stream ($fDOC_{i-1}$), lateral inputs of DOC in section *i* ($fDOC_{lat.inp\,i}$), and inputs of DOC from tributaries ($fDOC_{trib\,i}$). The outputs included DOC exports measured at the outlet of section *i* ($fDOC_i$) and estimated mineralization flux of DOC ($fDOC_{min\,i}$) presented in equation (4).

$$\sum fDOC_{in} = \sum fDOC_{out}$$

$$fDOC_{i-1} + fDOC_{lat.inp\,i} + fDOC_{trib\,i} = fDOC_i + fDOC_{\min i} \quad (5)$$

Based on the equation (7), lateral inputs $fDOC_{lat.inp\,i}$ can be calculated:

$$fDOC_{lat.inp\,i} = fDOC_i + fDOC_{\min i} - fDOC_{i-1} - fDOC_{trib\,i} \quad (6)$$

The proportion of $fDOC_{min}$ along the stream to fDOC measured at the outlet of the section (%$fDOC_{min}$; %) was measured in order to evaluate the estimated contribution of DOC mineralization to the exported flux (Eq. 8).

$$\%fDOC_{min} = (\sum_{i=1}^{n} fDOC_{\min i})/fDOC_i \times 100 \qquad (7)$$

Residence time (r_j; h) per stream section was calculated by dividing the length of upstream section *j* (L_j; m) by velocity V_i (V_i; m s^{-1}) (Eq. 8):

$$r_j = L_j/V_i/3600 \qquad (9)$$

3.3.6 Statistical analyses

Statistical tests were performed on R (CRAN-Project) through the Rstudio interface (Rstudio inc., USA) and all figures were realized with the package ggplot2 (Wickham, 2016). Data curation and statistical analysis were performed on R studio (Rstudio inc., USA), an integrated development environment of the programming langage R (CRAN-Project). Figures were realized with the package ggplot2 (Wickham, 2016).

Comparisons of variance tests were performed using the method described in Prijac et al. (2022). The mention of 'significant differences' refers to statistical tests using the following method. First, normal distribution was tested using Shapiro and Wilk test, and normal distribution was considered true when p-value was >0.05. If distribution was not normal, a Kruskal and Wallis test was performed to compare the averages and significant differences were considered true when p-value was <0.05. Dunn tests were performed as post-hoc pairwise comparison tests to determine which group was significantly different (when p-value <0.05). Second, homogeneity of variance was tested using Levene test and was considered true when p-value was >0.05. If homogeneity of variance was not true, Welsh ANOVA was performed, and significant differences were admitted when p-value was <0.05. Estimated marginal means tests were performed as post-hoc tests to determine significantly different groups (p-value <0.05). In cases where normal distribution and homogeneity of variances were true, an ANOVA was performed, and significant differences were true when p-value was <0.05. When there were significant differences, Tukey tests were performed as post-hoc tests to determine which groups were significantly different (when p-value <0.05). The statistical tests were performed between hydrological conditions in the stream and between each hydrological conditions in the stream and peat porewater for variables including DOC concentration, DOC :

DON ratio, δ^{13}C-DOC, $SUVA_{254}$, $E2:E3$, S_R, FI and $\beta:\alpha$. The results are summarized in Table annexe B.1. In addition, correlation tests were performed between the variables previously mentioned and presented in correlograms for peat porewater (Fig. annexe B.1a), stream (Fig. annexe B.1b) and for high-flow (Fig. annexe B.1c) and low-flow conditions in the stream (Fig. annexe B.1d).

Linear models were performed at first between the variables including the discharge at the stream outlet (Q_{R08}), the proportion of $fDOC_{min}$ along the stream to the fDOC at the stream outlet ($\%fDOC_{min}$) and the total residence time in the stream (ΣRt). Linear models are summarized in Table annexe B.2. In a second time, linear regression was performed between the differences between the most upstream section and the outlet for the variables describing composition of DOM (Δ index) and Q_{R08} (summarized in the Table annexe B.3a), between Δ index and $\%fDOC_{min}$ (summarized in Table annexe B.3b) and between Δ index and ΣRt (summarized in Table annexe B.3c). The Δ index includes ΔDOC:DON, $\Delta SUVA_{254}$, $\Delta E2:E3$, ΔS_R, ΔFI and $\Delta\beta:\alpha$.

3.4 Results

3.4.1 Experimental degradability of stream DOM

As previously observed (Prijac et al., 2022), there was no significant difference between *in situ* and controlled conditions of incubation (stat = 2.66, p-value = 0.1, Kruskal-Wallis test) and between dark conditions and natural sunlight exposition (stat = 2.96, p-value = 0.09, Kruskal-Wallis test). This suggests a limited effect of temperature and sunlight on DOM degradation (Prijac et al., 2022). Only the conditions of filtered and unfiltered DOM presented significant differences (stat = 10.4, p-value = 0.001, Kruskal-Wallis test).

Table 3.1 Degradation rates (% day^{-1}) measured in the stream for *F* and UF conditions in June, August and September. *due to the low initial DOC concentration in August, no degradation rate was observable for *F* conditions.

		June	August	September
Degradation rate (% day^{-1})	*F*	3.5 ± 0.4	*	3.5 ± 0.4
	UF	4.4 ± 0.4	0.1 ± 0.04	4.6 ± 0.2

Degradation rates during June and September were similar for each filtered (*F*) and unfiltered (UF) conditions (Table 3.1). For *F* conditions, degradation rates were of 3.5 ± 0.4 % day^{-1} both months, and for

UF condition, 4.4 ± 0.4 % day^{-1} and 4.6 ± 0.2 % day^{-1} for June and September respectively. In August, no degradation rates were measured for *F* conditions and very low degradation rates for UF conditions (0.1 ± 0.04 % day^{-1}). This absence of sizeable degradation can be explained by a very low initial DOC concentration of 3.1 mg L^{-1}. In comparison with degradation rates in peat porewater and pools measured in Prijac et al. (2022), degradation was constantly higher in the stream for analogous incubation conditions.

3.4.2 Classification of the campaigns into low-flow and high flow conditions

The 2019 sampling periods were classified into low-flow and high-flow conditions previously defined by a Hidden Markov model as in Prijac et al. (2023). Three sampling periods occurred during high- flow. The campaign 19B1 occurred at the end of spring freshet in June 2019. The samples from campaigns 19B3a and 19B3b correspond to sampling periods in early autumn and occurred before and after an exceptional storm. Then, three sampling periods occurred during low-flow conditions in summer (campaigns 19B2a and 19B2b) and in mid-autumn (19B4).

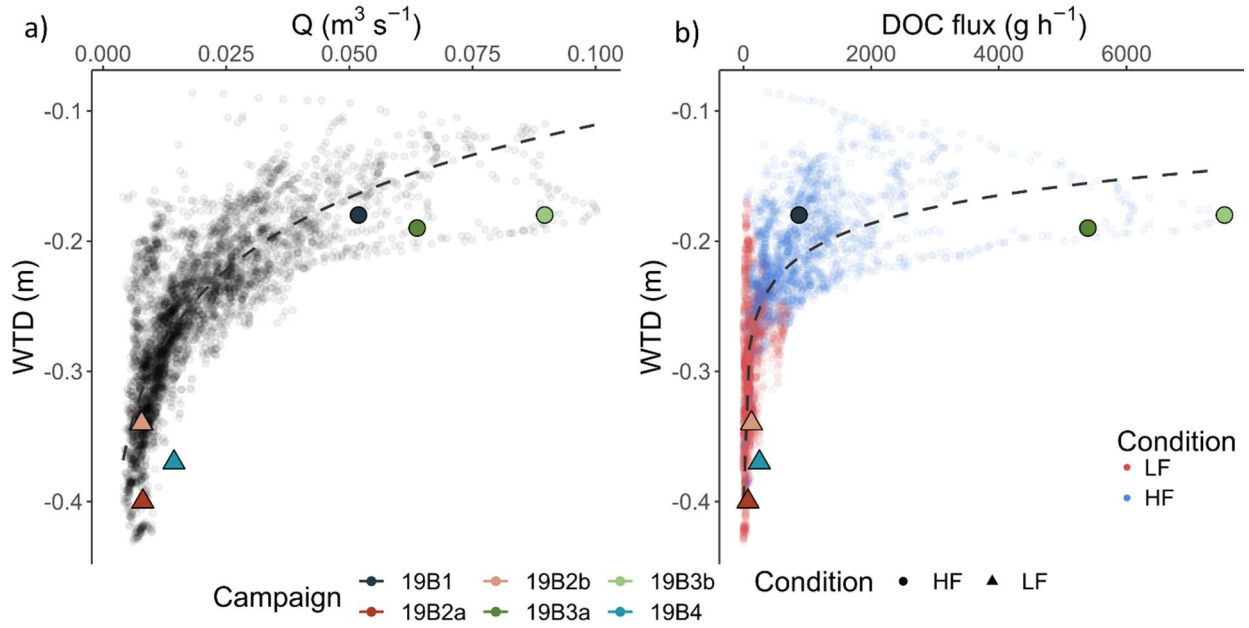

Figure 3.3 Representation of a) stream discharge at the outlet according to WTD and b) DOC flux at the outlet according to WTD measured during the six sampling periods of 2019 for WTD, Q at the stream outlet and DOC flux derived from high frequency data measurements at the study site (data from Prijac et al., 2023).

The classification into high and low-flow conditions allowed comparing hydrological conditions and DOC exports with the full-time series from Prijac et al. (2023; Fig. 3.3). During the campaign 19B1, DOC exports were low with 872 g h^{-1} for a Q of 0.0519 m^3 s^{-1} (Fig. 3.3a). During high-flow conditions, WTD varied in a

narrow range from -0.18 (19B1) to -0.19 m (19B3a). Campaigns 19B3a and 19B3b corresponded to the highest DOC exports recorded with values varying between 24.3×10^{-3} and 33.94×10^{-3} g DOC-C m^{-2} h^{-1} respectively with stream discharge at the outlet of 0.0638 m^3 s^{-1} during the campaign 19B3a and 0.0897 m^3 s^{-1} during campaign 19B3b (Fig 3.3b).

Table 3.2 Values for each sampling period for WTD, discharge at the stream outlet (QR08), water temperature at the stream outlet (W.T.), fDOC at the stream outlet (fDOCR08), proportion of fDOCmin along the stream to the fDOC measured at the outlet (%fDOCmin), total retention time in the stream (ΣRt) and WTD.

Campaign	Condition	Q_{R08} (m^3 s-1)	WT (°C)	$fDOC_{R08}$ ($\times10^{-3}$ g DOC-C m^{-2} h^{-1})	$\%fDOC_{min}$ (%)	ΣRt (h)	WTD (m)
19B1	High-flow	0.0519	14.3	3.93	2.21	34	-0.18
19B2a	Low-flow	0.0081	16.8	0.32	11.4	154	-0.40
19B2b	Low-flow	0.0078	17.2	0.58	9.88	80	-0.34
19B3a	High-flow	0.0638	13.8	24.3	0.98	13	-0.19
19B3b	High-flow	0.0897	12.8	33.94	0.93	18	-0.18
19B4	Low-flow	0.0144	8.6	1.14	5.08	42	-0.37

For low-flow conditions, discharge at the outlet ranged from 0.0078 m^3 s^{-1} (19B2b) to 0.0144 m^3 s^{-1} (19B4; Fig 3.3a). During low-flow, WTD varied between -0.40 m during the campaign 19B2a and -0.34 m during the campaign 19B2b and was -0.37 m during the campaign 19B4 (Fig. 3.3). The lowest DOC exports were measured during the campaign 19B2a with 72 g h^{-1} while it was 128 g h^{-1} during the campaign 19B2b and 252 g h^{-1} during the campaign 19B4 (Fig 3.3b).

Linear models between those indicators (*Q*, Rt and $\%fDOC_{min,}$) are summarized in the table annexe B.2. Negative correlations between *Q* and Rt (cor = -0.69, p-value < 0.0001) and between *Q* and $\%fDOC_{min}$ (cor = -0.59, p-value = 0.001) emerged while Rt and $\%fDOC_{min}$ were positively correlated (cor = 0.74, p-value < 0.0001). To summarize, high-flow conditions were characterized by high *Q* but shorter Rt and lower % $fDOC_{min}$, while the *Q* was lower during low-flow conditions, inducing longer Rt and higher $\%fDOC_{min}$.

3.4.3 DOM composition in peat porewater and in the stream under different hydrological conditions

DOC concentration and DOM composition differed significantly between high-flow and low-flow conditions in the stream. Contrastingly, no DOC concentration or DOM composition was significantly different in peat porewater between high-flow and low-flow conditions. Comparisons were then made

between peat porewater DOM (pooling all data) and stream DOM during high-flow conditions and low-flow conditions (Fig. 3.4). DOC concentration increased significantly in the stream during high-flow conditions, from 9.5 ± 7.1 mg L^{-1} on average during low-flow to 18.7 ± 9.6 mg L^{-1} during high-flow conditions (Table 3.3). Significant differences appeared between DOC concentration in the stream during low-flow and in peat porewater (18.0 ± 8.4 mg L^{-1}) but not during high-flow conditions (Fig. 3.4).

Table 3.3 Average (±SD) of physicochemical variables, DOC concentration, elemental ratio, isotopic ratio and optical indices in the stream (annual average and low-flow and high-flow averages) and in peat porewater (only annual average as no significant difference was found between low-flow and high-flow conditions in peat porewater).

	Stream			**Porewater**
	Annual	*Low flow*	*High flow*	
Water temperature (°C)	12.4 ± 4.3	11.5 ± 4.7	12.2 ± 3.8	13.4 ± 4.4
pH	4.8 ± 0.8	5.1 ± 0.8	4.5 ± 0.6	4.9 ± 0.7
Conductivity (µS cm^{-1})	27.0 ± 12.3	32.0 ± 14.5	23.1 ± 8.6	32.9 ± 19.3
Dissolved Oxygen (%sat)	68.2 ± 15.4	65.6 ± 16.4	70.2 ± 14.5	50.0 ± 17.1
DOC (mg C L^{-1})	14.6 ± 9.7	9.5 ± 7.1	18.7 ± 9.6	18.0 ± 8.4
DOC : DON ratio	41.5 ± 17.7	32.5 ± 17.8	48.8 ± 14.1	48.6 ± 18.8
δ^{13}C-DOC (‰)	-28.1 ± 0.5	-28.0 ± 0.6	-28.8 ± 0.4	-27.1 ± 0.8
$SUVA_{254}$ (L mg^{-1} m^{-1})	5.2 ± 1.2	5.8 ± 1.0	4.8 ± 1.1	5.0 ± 0.6
*E*2 : *E*3 ratio	3.7 ± 0.4	3.45 ± 0.46	3.88 ± 0.32	3.49 ± 0.17
S_R	0.69 ± 0.08	0.65 ± 0.09	0.72 ± 0.06	0.66 ± 0.04
β : α	0.62 ± 0.12	0.69 ± 0.15	0.57 ± 0.06	0.62 ± 0.07
FI	1.34 ± 0.09	1.39 ± 0.10	1.30 ± 0.06	1.36 ± 0.10

DOC:DON ratio was significantly higher during high-flow conditions, with 48.8 ± 14.1 on average, compared to 32.5 ± 17.8 during low-flow conditions (Fig. 3.4b). The average DOC:DON ratio during high-flow conditions in the stream was similar to the DOC:DON ratio in peat porewater (48.6 ± 18.8) while a significant difference was found between low-flow conditions in the stream and in peat porewater (Fig. 3.4b).

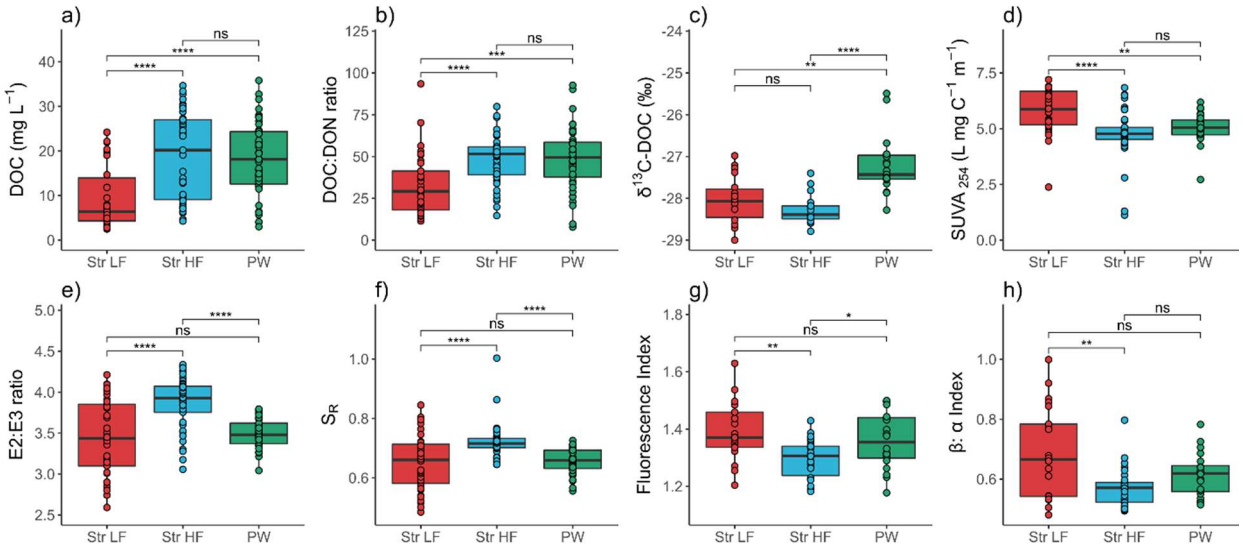

Figure 3.4 Box plots comparing values between sampling points during low-flow (Str LF) and high-flow periods in the stream (Str HF) and in peat porewater (PW) for a) DOC concentration, b) DOC:DON ratio, c) δ^{13}C-DOC, d) SUVA$_{254}$, e) *E*2 : *E*3 ratio, f) S_R, g) Fluorescence index and h) β : α index. No statistical difference was found between variables in peat porewater between high-flow and low-flow periods in the stream. The brackets indicate the significance of statistical differences between Str HF, Str LF and PW with ns: nonsignificant, * : p-values < 0.05, **: p-values < 0.01, ***: p-value < 0.001 and ****: p-value < 0.0001.

For δ^{13}C-DOC, no significant difference was observed between high (-28.8 ± 0.4 ‰) and low-flow (-28.0 ± 0.6 ‰; Fig. 3.4c) conditions. The δ^{13}C-DOC was slightly but significantly lower in the stream compared to the ratio of -27.1 ± 0.8 ‰ measured in peat porewater during both high- and low-flow conditions (Table 3.3).

During high-flow conditions in the stream, the SUVA$_{254}$ was significantly lower compared to low-flow conditions, with 4.8 ± 1.1 L mg^{-1} m^{-1} and 5.8 ± 1.0 L mg^{-1} m^{-1} respectively (Fig.3.4d). There was no significant difference between DOM aromaticity between stream during high-flow and peat porewater with a SUVA$_{254}$ of 5.5 ± 0.6 L mg^{-1} m^{-1}. The SUVA$_{254}$ in peat porewater was significantly lower compared to the stream in low-flow conditions (Table 3.3). During high-flow conditions, *E*2:*E*3 ratio was significantly higher with 3.88 ± 0.32 compared to low-flow (3.45 ± 0.46; Fig. 3.4e). The average *E*2:*E*3 ratio was significantly higher in the stream during high-flow compared to peat porewater (3.5 ± 0.2) while no significant difference was observed during low-flow between *E*2 : *E*3 in the stream and in peat porewater (Fig. 3.4e). As for *E*2 : *E*3 ratio, S_R was significantly higher during high-flow conditions (0.72 ± 0.06) compared to low-flow conditions (0.65 ± 0.09; Fig. 3.4f). Similarly to *E*2 : *E*3 ratio, S_R was slightly but significantly lower in

peat porewater (0.66 ± 0.04) compared to the stream during high-flow and not significantly different than S_R in the stream during low-flow (Table 3.3).

Fluorescence index (FI) was significantly lower during high-flow (1.30 ± 0.06) compared to low-flow conditions (1.39 ± 0.10; Fig. 3.4g). Also, FI was not significantly different between the stream during low-flow and peat porewater (1.36 ± 0.10) while it was significantly different between peat porewater and stream FI during high-flow (Fig. 3.4g). The β : α index in the stream during high-flow conditions was 0.57 ± 0.06 on average, and significantly lower than during high-flow conditions (0.69 ± 0.15; Fig. 3.4h). As for the β : α index, FI was not significantly different between peat porewater (1.36 ± 0.10) and the stream during low-flow but significantly different during high-flow conditions (Table 3.3).

3.4.4 Variations in stream discharge, DOC concentration and exports, and DOM composition along the stream transect

3.4.4.1 Variations in stream discharge and DOC fluxes

Along the stream transect, discharge ranged from 0.0129 $m^3 s^{-1}$ (19B1) to 0.437 $m^3 s^{-1}$ (19B3a) at the most upstream sampling station and from 0.0519 $m^3 s^{-1}$ (19B1) to 0.0897 $m^3 s^{-1}$ (19B3b) at the stream outlet (Fig. 3.5a). The most important discharge increase between the stream source to the outlet was by four times during the campaign 19B1 while it increased 1.5 times (19B3a) and 3 times (19B3b) during other campaigns.

DOC concentrations decreased during all campaigns along the stream, independently from hydrological conditions. However, during campaigns presenting the largest DOC export, the decrease was relatively limited, reaching 25.6 % during the campaign 19B3a and 13.5 % during campaing19B3b (Fig. 3.5b). In comparison, two thirds of DOC was lost from upstream to downstream during 19B1 campaign. The largest decrease in DOC concentration was observed during low-flow conditions, with a decrease from 76.2 % to 87% from the most upstream section to the outlet (Fig. 3.5b).

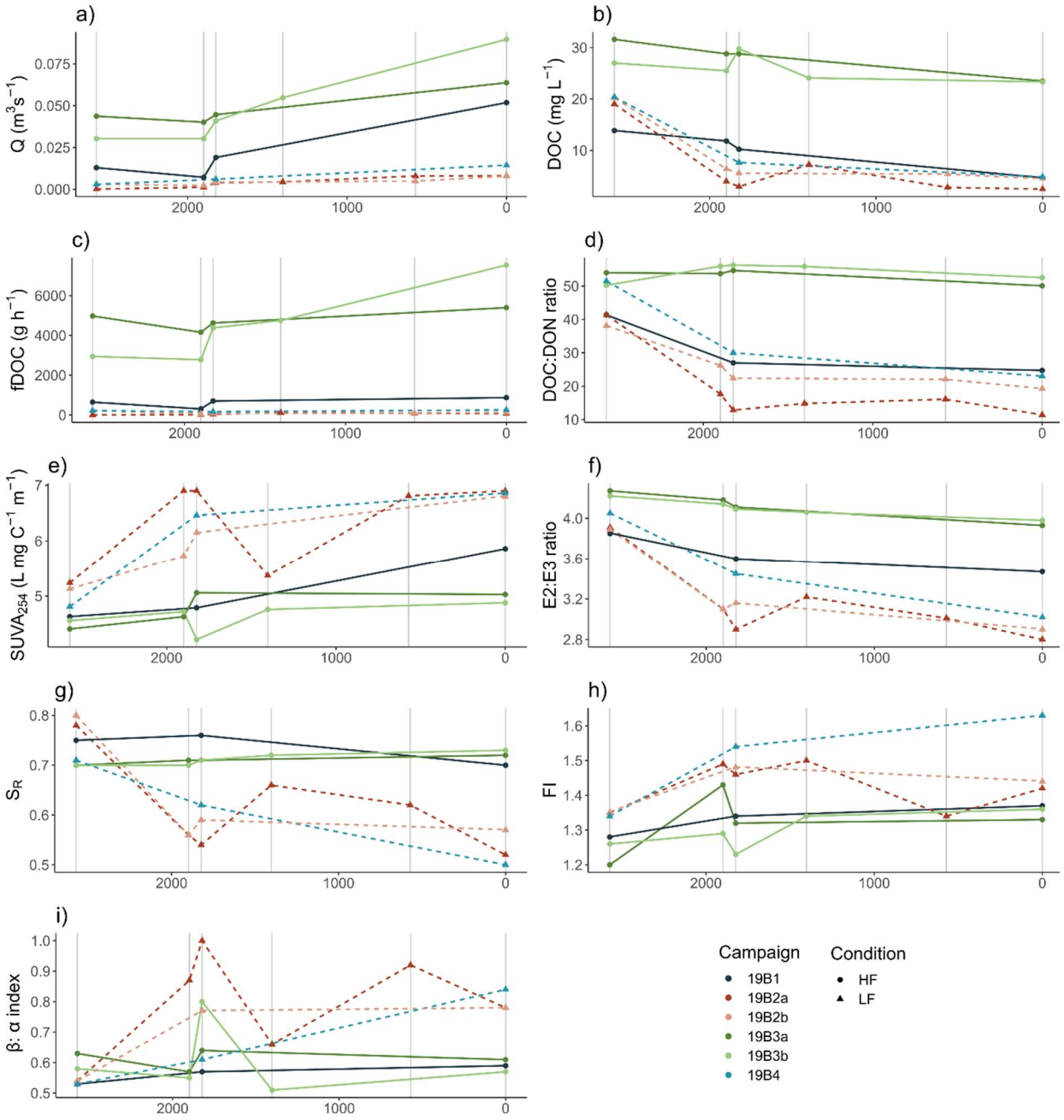

Figure 3.5 Dynamics of a) stream discharge (*Q*; in $m^3 s^{-1}$), b) DOC concentration (in mg L^{-1}), c) DOC flux (*f*DOC; in g h^{-1}), d) DOC : DON ratio, e) $SUVA_{254}$, f) *E*2 : *E*3 ratio, g) Spectral Slope Ratio (S_R), h) Fluorescence Index (FI) and i) *β* : *α* index according to the stream length, from the most upstream sampling station (2500 m) to the stream outlet (0 m). Points correspond to individual samples collected and grouped by fields campaigns in 2019.

DOC flux at the stream outlet ($fDOC_{R08}$) was highly variable between high- and low-flow conditions (Table 3.2). During most campaigns, a decrease in fDOC was observed for the most upstream section, and downstream, the fDOC constantly increased up to the stream outlet (Fig. 3.5c).

3.4.4.2 Spatiotemporal evolution of DOM composition

The DOC:DON ratio remained relatively steady along the transect during high-flow conditions, except during the campaign 19B1 when ratio decreased by 53.3 % in the most upstream section and then remained relatively steady. DOC:DON decreased rapidly and intensively along the transect during low-flow conditions, with ΔDOC:DON ranging from -18.8 to -29.9 (Fig. 3.5d).

The $SUVA_{254}$ constantly increased along the transect, with $\Delta SUVA_{254}$ ranging from 7% to 43% of increase. However, higher values $\Delta SUVA_{254}$ were observed during low-flow conditions (Fig. 3.5e).

As for DOC:DON ratio, the highest $E2 : E3$ ratios were measured during high-flow conditions (Fig. 3.5f). During all campaigns, $E2 : E3$ ratio decreased along the stream. Stronger decreases of $E2 : E3$ ratio was measured during low-flow ($\Delta E2 : E3$ ranged from -0.99 to -1.11), while $E2 : E3$ ratio decreased from -0.24 to -0.38 during high-flow conditions.

While S_R values were similar between high- and low-flow conditions for the most upstream sampling station, sharper decreases were observed during low-flow conditions, with ΔS_R ranging from -0.21 to -0.26 (from -29.6 to -33.3 %). During high-flow conditions, S_R fluctuated a little with ΔS_R ranging from -0.05 to 0.03. At the outlet, S_R was1.2 to 1.4 times higher for high-flow conditions compared to low-flow conditions (Fig. 3.5g).

The FI increased downstream during all campaigns (Fig. 3.5h). Despite the fact that FI was higher during low-flow conditions compared to high-flow conditions, the increase of FI seemed not to depend on hydrological conditions, with Δ FI ranging from 0.09 to 0.13 during high-flow and Δ FI ranging from 0.07 to 0.29 during low-flow conditions.

The $\beta : \alpha$ index followed a singular pattern among indices of DOM composition. During two of six campaigns (19B2a and 19B3b), an important increase was observed in section *c* but the index immediately decreased in the following section. Along the stream transect, $\beta : \alpha$ index increased during low-flow ($\Delta\beta : \alpha$ ranged from 0.24 to 0.31), while it remained steady during high-flow conditions (Fig. 3.5i).

3.4.5 Factors controlling change in DOM composition along the stream transect

In general, more intense changes were observed in the stream section for low-flow compared to high-flow (Fig. 3.6). During high-flow conditions, the DOC:DON barely did not change along the stream with an average ΔDOC:DON of -2.8 ± 12.5% while it decreased by -19.7 ± 20.5 % on average during low flow (Fig. 3.6a). The $SUVA_{254}$ presented lower changes during high-flow compared to low-flow with an average $\Delta SUVA_{254}$ of 4.2 ± 8.5% and 10.3 ± 16.1% for high-flow and low-flow respectively (Fig. 3.6b). Indices of DOM average molecular weight (*E*2:*E*3 ratio and S_R) showed a similar pattern with during high-flow low ($\Delta E2:E3$ = -2.5 ± 1.7%) to no changes (ΔS_R = 0.4 ± 3%) while an increase of DOM molecular weight was observed during low-flow ($\Delta E2:E3$ = -7.4 ± 9.7%, Fig. 3.6c, and ΔS_R = -8.1 ± 15.4%, Fig. 3.6d). For the florescence index, a more important increase was measured during low-flow (ΔFI = 4.2 ± 7.5%) compared to high-flow conditions (ΔFI = 2 ± 8%, Fig. 3.6e). The $\beta:\alpha$ index also showed a greater increase during low-flow conditions ($\Delta\beta:\alpha$ = 17.1 ± 28.9%) compared to high-flow conditions ($\Delta\ \beta:\alpha$ = 3.4 ± 19.7%, Fig. 3.6f).

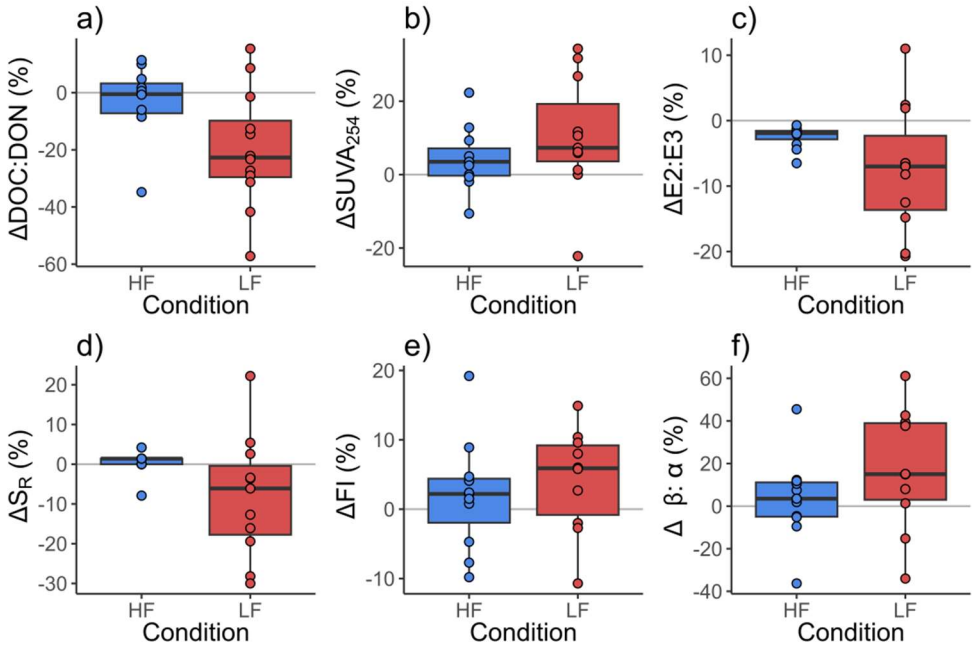

Figure 3.6 Box plots of relative change in DOM composition (in %) along the stream (from the source to the outlet) according to hydrological conditions (HF = high-flow, LF = low-flow) for a) DOC:DON ratio, b) $SUVA_{254}$, c) *E*2:*E*3 ratio, d) S_R, e) FI and f) $\beta:\alpha$ index.

3.5 Discussion

3.5.1 Rapid export of peat-derived DOM during high-flow conditions

During high-flow conditions, the higher average DOC concentration of 18.7 mg C L^{-1} , compared to an average DOC concentration of 9.5 mg C L^{-1} during low-flow conditions, suggested flushing of DOC associated with a discharge increase (Fig. 3.4a; Prijac et al., 2023). The high discharge and short residence time (Rt) during those periods (Table 3.2) induced only little change in DOM composition from the stream source to its outletDuring these periods, the rise of the WTD in the peat increased the hydrological connectivity between the source of DOM and the stream and led to an important mobilization of DOC within the catchment and specifically from the peatland. The composition of exported DOM presented similarities with peat porewater DOM (Fig. 3.4). During high-flow, high DOC : DON ratio, jointly with low $SUVA_{254}$ and high *E*2 : *E*3 ratio was previously observed by Austnes et al. (2010) and suggested the mobilization of recently produced and less biodegraded DOM.

Differences in composition of exported DOM and peat porewater DOM were also observed through differences in average DOM molecular weight. Indices *E*2 : *E*3 and S_R showed that DOM exported through the stream during high-flow presented significantly lower molecular weight compared to peat porewater (Fig. 3.4e-f and Table 3.3). This is consistent with the significant differences found between δ^{13}C-DOC during high-flow conditions and in peat porewater. DOM with lower molecular weight was found to be depleted in δ^{13}C (Guo & Macdonald, 2006), consistently with the weak but significant negative correlation found in the stream between *E*2 : *E*3 ratio and δ^{13}C-DOC (cor = -0.53; p = 0.035; Fig. annexe B.1b). The lowest δ^{13}C-DOC and *E*2 : *E*3 ratio supports the hypothesis that DOM exported during high-flow conditions corresponds to low molecular weight molecules recently produced in the acrotelm (Austnes et al., 2010) and potentially more labile (Hutchins et al., 2017).

3.5.2 During low-flow conditions, long residence time drives DOM processing

During low-flow conditions, DOM composition was characterized by a high DOM aromaticity (Fig. 3.5e) and average molecular weight (Fig. 3.5f-g) that increased along the stream transect due to mineralization processes influenced by longer residence time. During low-flow conditions, DOM composition presented characteristics of more processed DOM, reflected by $SUVA_{254}$ 1.2 times higher during low-flow compared to low-flow conditions (Fig. 3.4d), which is known to increase with biodegradation (Autio et al., 2016; Hulatt et al., 2014; Prijac et al., 2022; Saadi et al., 2006). In addition, the DOM exported during low-flow

presented higher DOM average molecular weight, reflected by higher $E2 : E3$ ratio and S_R compared to the ones measured in the stream during high-flow (Table 3.3) but with a similar molecular weight compared to the peat porewater (Fig. 3.4e-f). Higher FI and $\beta : \alpha$ index measured during low-flow conditions (Fig. 3.4g-h) reflected a higher proportion of microbial derived DOM (Cory et al., 2010b; McKnight et al., 2001; Parlanti, 2000; Wilson & Xenopoulos, 2009).

Similarity between isotopic ratios during low-flow and high-flow conditions (δ^{13}C-DOC = -28.8 ± 0.4; Table 3.3), suggests that the main source of DOM in the stream is the peatland as low isotopic ratio is expected for peat-derived DOM (≈-28 ‰; Elder et al., 2000; Buzek et al., 2019). Hence, even during low-flow conditions, peatlands are the main contributors to stream DOM in the context of peatland dominated catchment surface (Prijac et al., 2023). This is consistent with previous studies stating that wetlands and more specifically peatlands are the main source of DOM to surface water in complex catchments (Billett et al., 2006a; Dick et al., 2015; Freeman et al., 2001; Rosset et al., 2019).

Contrastingly to high-flow conditions, more intense changes in DOM composition during low-flow were measured along the stream transect (Fig. 3.6 and Table 3.2). We hypothesize that unlike high-flow conditions, longer residence promote a shift in DOM composition along the stream. This is coherent with higher contributions of potential bio-mineralization (%fDOC$_{min}$) measured in the stream during low-flow conditions (Table 3.2). The low-flow conditions, characterized by longer residence time and higher bio-mineralization, induced a high decrease in DOC:DON ratio (Fig. 3.6a) and an increase in average DOM molecular weight and aromaticity, through higher average ΔSUVA$_{254}$ (Fig. 3.6b) and lower average Δ$E2$:$E3$ (Fig. 3.6c) and ΔS_R (Fig. 3.6d). This is also in line with Austnes et al. (2010) who measured higher DOM aromaticity and molecular weight under low-flow conditions. Increase of DOM molecular weight during low-flow conditions is also consistent with preferential removal of low molecular weight molecules once DOM is transferred into streams (Berggren et al., 2010; Hutchins et al., 2017). This is also in accordance with the increase of DOM aromaticity observed during low-flow conditions (Fig. 3.5b) that could reduce the potential biodegradability of DOM (Payandi-Rolland et al., 2020). The rapid change in DOM composition observed at our site might reflect the importance of rapid processing of allochthonous DOM in headwater streams during low-flow conditions (Hutchins et al., 2017).

3.5.3 Understanding changes in DOM composition into the pulse-shunt concept

No major changes in DOM composition were observed along the stream during high-flow conditions, associated with shorter residence times (from 13 to 34h; Table 3.2) contrastingly to low flow conditions (Fig. 3.6). Based on incubation experiments, we could estimate the amount of bio-mineralized DOC in the stream (%$fDOC_{min}$) and a positive correlation emerged between the %$fDOC_{min}$ and ΣRt (Table annexe B.2) and a negative correlation between the %$fDOC_{min}$ and the discharge at the outlet (Q_{R08}; Table annexe B.2). Those relationships and differences in DOM composition between hydrological conditions give a molecular perspective to the flux based *pulse-shunt* concept (Raymond et al., 2016). During high-flow, the strong hydrological connectivity between the peatland and the stream favoured DOC flux but the shorter residence time reduced the contribution of DOC mineralization, down to less than 1% of fDOC at the stream outlet for the highest Q_{R08} measured (Table 3.2). During those high-flow conditions, DOC was rapidly transferred downstream and mainly acted as a passive pipe as DOM composition was poorly impacted by bio-mineralization which was limited by shorter residence time (Casas-Ruiz et al., 2017). Contrastingly to high-flow condition, observation of important changes in DOM composition during low-flow conditions, induced by longer residence time which favored DOC mineralization in the stream, also give a new contribution to the *pulse-shunt* concept (Raymond et al., 2016). During low-flow conditions, which accounted for 44 % to 59 % of the year in the study site (Prijac et al., 2023), the headwater stream represented an active environment for DOC mineralization (Casas-Ruiz et al., 2020; Raymond et al., 2016).

DOC exports at the outlet of the stream ($fDOC_{R08}$) measured during low-flow conditions were between 3.5 and 104.6 times lower compared to fDOC at the outlet measured during high-flow conditions (Table 3.2). In addition, we previously observed that between 64 and 66 % of the total annual exports at the study site occurred during the top 25 % of the highest Q (Prijac et al., 2023) which tends to minor the contribution of mineralization during low-flow. Despite those low fDOC, the most important %$fDOC_{min}$ coincided with the highest CO_2 exports and emissions measured at our study site during low-flow (Taillardat et al., 2022). It suggests that during low-flow, mineralization processes of exported DOM contribute, at least partially given the low fDOC, to aquatic CO_2 flux (Hutchins et al., 2017). Conversely, as exported DOM is rapidly transferred downstream during high-flow, aquatic CO_2 flux are mainly sustained by lateral transfer from the peat and emissions are stimulated by stream turbulence (Taillardat et al., 2022) rather than in-stream processing.

3.6 Conclusion

We demonstrated that DOM exported through the stream is mostly derived from the peatland but undergo important degradation processes during low-flow conditions. It supports the hypothesis that the DOC exported during high-flow conditions could specifically correspond to the recently produced DOM leached from the acrotelm which is potentially labile once exported in downstream to the catchment.

This study is the first that explores changes in DOM composition evolution along a stream running through a peatland catchment and under contrasted high-flow and low-flow hydrological conditions. Results reveal contrasted DOM composition dynamics between high- and low-flow conditions and higher DOC concentrations during high-flow conditions. During these high-flow conditions, DOM presented higher DOC:DON ratio, lower DOM aromaticity and molecular weight, higher contributions of terrestrial-derived DOM and lower contribution of microbial-derived DOM when compared to low-flow conditions.

In addition, greater changes in DOM composition were observed in the stream during low-flow conditions while DOM composition remained almost unchanged during high-flow. It is expressed by an increase of DOM aromaticity and molecular weight with an increase of the contribution of microbial-derived DOM, suggesting that those changes are induced by DOM degradation. The longer residence we observed during low-flow favored DOM microbial processing given the positive correlation between retention time (Rt) and the proportion of DOC mineralization to the outlet DOC exports (%$fDOC_{min}$) which supports the hypothesis that changes in DOM composition is induced by instream microbial processing.

Those results are the first to document drivers of DOM composition changes along the headwater stream of a peatland dominated catchment and under different hydroclimatic conditions. Our results support the important role of DOC mineralization on DOM composition within the ecosystem boundaries, predominantly during low-flow, when the stream retention time is longer. In the perspective of climate change, the periods of drought are expected to be longer as the intensity of flood events could increase with more frequent intense rainfall events. This could potentially change the balance between the exports of recently produced DOM during high-flow conditions and the higher contribution of mineralization to DOM exported under low-flow conditions.

Acknowledgements

This research has been supported by the Natural Sciences and Engineering Research Council of Canada and Hydro-Québec funding to Michelle Garneau (Grant RDCPJ-51421817). We thank Katherine Velghe and Alice Parks from GRIL for their laboratory training and assistance in absorbance and fluorescence analyses, as well as Professor Paul del Giorgio for access to his laboratory. Frederic Julien, Virginie Payre-Suc, and Didier Lambrigot, from Laboratoire Ecologie Fonctionnelle et Environnement, are acknowledged for performing DOC/TN and cations/anions analyses. We thank Roman Teisserenc (Ensat, Toulouse) and Charles Bonneau, Charles-Élie Dubé-Poirier, Camille Girard, Pénélope Germain-Chartrand, Éloïse Le Stum-Boivin, Léonie Perrier, Louis-Martin Pilote, Guillaume Primeau, Khawla Riahi, and Karelle Trottier for their assistance in the field.

CHAPITRE 4

Dissolved organic matter concentration and composition discontinuity at the peat–pool interface in a boreal peatland

Antonin Prijac[1,2,3], Laure Gandois[4], Laurent Jeanneau[6], Pierre Taillardat[1,7], and Michelle Garneau[1,2,3,5]

[1]Centre de Recherche sur la Dynamique du Système Terre (GÉOTOP), Université du Québec à Montréal, Montréal, Canada
[2]Groupe de Recherche Inter-universitaire en limnologie (GRIL), Université du Québec à Montréal, Montréal, Canada
[3]Institut des Sciences de l'Environnement (ISE), Université du Québec à Montréal, Montréal, Canada
[4]Laboratoire Écologie Fonctionnelle et Environnement, UMR 5245, CNRS-UPS-INPT, Toulouse, France
[5]Département de Géographie, Université du Québec à Montréal, Montréal, Canada
[6]Laboratoire Géosciences Rennes, UMR 6118, CNRS-Université de Rennes, Rennes, France
[7]Integrated Tropical Peatlands Research Program (INTPREP), National University of Singapore, Singapore

Article publié en septembre 2022 dans la revue Biogeosciences.

Résumé

Les mares sont des microformes fréquentes dans les tourbières et peuvent représenter entre 5 et 50% de la surface de l'écosystème. Les mares jouent un rôle important dans le cycle du carbone en libérant du dioxyde de carbone et du méthane dans l'atmosphère. Cependant, l'origine de ce carbone n'est pas bien identifiée. Une hypothèse est que la majorité du carbone émis depuis les mares provient majoritairement de la minéralisation de la matière organique dissoute (MOD) allochtone (i.e., provenant des plantes) de la tourbière, plutôt que de la production primaire *in situ*. Afin de tester cette hypothèse, cette étude a examiné l'origine, la composition et la dégradabilité de la MOD dans l'eau interstitielle et les mares d'une tourbière boréale ombrotrophe du nord-est du Québec (Canada) durant deux années au cours de la saison de croissance. L'évolution temporelle de la concentration en carbone organique dissous (COD), des propriétés optiques, de la composition moléculaire (THM-GC-MS), de la signature des isotopes stables (δ^{13}C-COD), et de la dégradabilité de la MOD ont été déterminées. Cette étude a démontré que la MOD, à la fois dans l'eau interstitielle et les mares, présente une composition variée et représente un élément hautement dynamique de l'écosystème. Les analyses isotopiques et moléculaires ont montré que la MOD des mares était dérivée des végétaux. Cependant, la composition de la MOD dans les deux environnements est nettement différente. La MOD de l'eau interstitielle était plus aromatique, avec un plus haut poids moléculaire et un ratio COD : NOD (azote organique dissous) comparable à celles des mares. La dynamique temporelle de la concentration en COD et de la composition de la MOD diffère également. Dans l'eau interstitielle, la concentration en COD montre une forte augmentation saisonnière, depuis 9 mg L^{-1} et pour atteindre un plateau au-dessus de 20 mg L^{-1} en été et en automne. Ceci est expliqué par la productivité saisonnière de la végétation de la tourbière, qui est plus importante que la dégradation microbienne. Dans les mares, la concentration de COD augmente également, mais reste deux fois plus faible que dans l'eau interstitielle à la fin de la saison de croissance ($\approx$ 10 mg L^{-1}). Ces différences peuvent être expliquées par une combinaison de processus physiques, chimiques et biologiques. La conductivité hydraulique limitée dans les horizons de tourbe les plus profonds et les temps de résidence de la MOD plus longs peuvent favoriser à la fois la transformation microbienne de la MOD dans la tourbe et l'interaction entre les composés aromatiques de la MOD et la matrice tourbeuse, expliquent en partie le changement de composition entre la composition de la MOD dans l'eau interstitielle et dans les mares. Cette étude ne rapporte pas de photolabilité de la MOD et seulement une faible dégradabilité microbienne. Ainsi, il est probable que la MOD ait été dégradée à l'interface entre la tourbe et les mares. La combinaison d'analyses quantitatives et qualitatives présentées dans cette étude démontre que la majorité du carbone présent et libéré par les mares provient de la végétation de la tourbière. Ces résultats montrent que les mares représentent des éléments clés du fonctionnement écologique et biogéochimique des tourbières.

Abstract

Pools are common features of peatlands and can represent from 5 to 50% of the peatland ecosystem's surface area. Pools play an important role in the peatland carbon cycle by releasing carbon dioxide and methane to the atmosphere. However, the origin of this carbon is not well constrained. A hypothesis is that the majority of the carbon emitted from pools predominantly originates from mineralised allochthonous (i.e., plant-derived) dissolved organic matter (DOM) from peat, rather than in situ primary production. To test this hypothesis, this study examined the origin, composition, and degradability of DOM in peat porewater and pools of an ombrotrophic boreal peatland in northeastern Quebec (Canada) for two years over the growing season. The temporal evolution of dissolved organic carbon (DOC) concentration, the optical properties, molecular composition (THM-GC-MS), stable isotopic signature (δ^{13}C-DOC), and degradability of DOM were determined. This study demonstrates that DOM, in both peat porewater and pools, presents a diverse composition, and constitutes highly dynamic components of peatland ecosystems. The molecular and isotopic analyses showed that DOM in pools was derived from plants. However, DOM compositions in the two environments were markedly different. Peat porewater DOM was more aromatic, with a higher molecular weight and DOC : DON ratio compared to pools. The temporal dynamics of DOC concentration and DOM composition also differed. In peat porewater, the DOC concentration followed a strong seasonal increase, starting from 9 mg L^{-1} and reaching a plateau above 20 mg L^{-1} in summer and autumn. This was explained by seasonal peatland vegetation productivity, which is greater than microbial DOM degradation. In pools, DOC concentration also increased but remained two times lower than in the peat porewaters at the end of the growing season (~10 mg L^{-1}). Those differences might be explained by a combination of physical, chemical, and biological factors. The limited hydraulic conductivity in deeper peat horizons and associated DOM residence time and might have favoured both DOM microbial transformation within the peat and the interaction of DOM aromatic compounds with the peat matrix, explaining part of the shift of DOM compositions between peat porewater and pools. This study did not report any photolability of DOM and only limited microbial degradability. Thus, it is likely that the DOM might have been microbially transformed at the interface between peat and pools. The combination of DOM quantitative and qualitative analysis presented in this study demonstrate that most of the carbon present within and released from the pools originates from peat vegetation. These results demonstrate that pools represent a key component of the peatland ecosystem ecological and biogeochemical functioning.

4.1 Introduction

Northern peatlands constitute one of the most important terrestrial reservoirs of organic carbon (C) containing about 530 ± 160 Pg C while only covering ~ 3 % of the global terrestrial land surface (Z. C. Yu, 2012). The ecosystem carbon accumulation rates of peatlands are typically greater than the losses to the atmosphere through peat degradation and lateral transfer (Billett et al., 2006, 2012; Blodau et al., 2007; Tunaley et al., 2017). Peatlands are characterised by a mosaic of surface microforms, such as hummocks, lawns, hollows, and pools (Charman, 2002). Considering peatlands as a patchwork of microforms rather than a homogeneous ecosystem is critical to accurately quantify their carbon balance and the role they play in the modern global carbon cycle. Carbon dynamics between microforms are closely related to the vegetation type and water table depth which influence the carbon dioxide (CO_2) and methane (CH_4) exchange with the atmosphere (Chaudhary et al., 2018; Nungesser, 2003). Among the different microforms, pools can constitute an important proportion of peatland ecosystem surface areas, ranging from 5 to 50 % (White, 2011; Pelletier et al., 2014, 2015) and represent a net carbon source to the atmosphere (Pelletier et al., 2014). While most studies of peatland carbon dynamics have focused on terrestrial microforms (Nungesser, 2003; Pelletier et al., 2011; Shi et al., 2015; Chaudhary et al., 2018; Graham et al., 2020), the composition and processes of production and degradation of organic carbon in pools remain poorly documented.

The composition of dissolved organic matter (DOM) has previously been documented in peatland porewater. A complex mixture of compounds with a diversity of composition, functional groups, and ages seem to co-exist (Tipping et al., 2010; Kaplan & Cory, 2016; Raymond & Spencer, 2015; Tiwari et al., 2018; Dean et al., 2019; Tfaily et al., 2018). The production of DOM in peat porewater is controlled by vegetation productivity, peat temperature (Rydin et al., 2013; Kane et al., 2014), and microbial activity (Worrall et al., 2008).

It has also been shown that pools can represent active compartments of peatland ecosystems for DOM (Deshpande et al., 2016; Folhas et al., 2020; Laurion et al., 2021; Laurion & Mladenov, 2013; Payandi-Rolland et al., 2020) – a topic that has been less studied. The DOM of pools may derive from surrounding terrestrial peat (i.e., allochthonous) or be the result of their internal primary production through phytoplankton and microbial production (i.e., autochthonous). In both peat porewater and pools, DOM is affected by biodegradation processes and by photodegradation in pools (Lapierre & del Giorgio, 2014; Vonk et al., 2015). Changes in DOC concentrations and DOM composition are commonly observed and

associated with a wide range of degradation rates (Frey et al., 2016; Payandi-Rolland et al., 2020; Moody & Worrall, 2021). The composition and reactivity of DOM transferred from the terrestrial to aquatic compartments of peatlands highly depend on the hydrology and hydroclimatic context, and the biological and chemical processes occurring during their transfer (Jaffé et al., 2012; Kaplan & Cory, 2016). The DOM transfers between peatlands and aquatic ecosystems are well documented for streams (Elder et al., 2000; Billett et al., 2006, 2012; Austnes et al., 2010; Knorr, 2013; Frey et al., 2016; Buzek et al., 2019; Dean et al., 2019; Rosset et al., 2019) but more rarely for pools (Arsenault et al., 2019; Banaś, 2013; Payandi-Rolland et al., 2020).

Differences in DOM composition and concentration between peat porewater and pools have been observed, but the processes involved remain unclear (Payandi-Rolland et al., 2020; Schindler et al., 1997). Studies conducted in temperate peatlands have highlighted that the morphology (e.g., size, shape, depth, slope of banks) and surrounding vegetation influence the carbon content and hydrochemistry in the pools (Banaś, 2013; Arsenault et al., 2018, 2019). Others have explained the changes in DOM composition in pools as the result of photodegradation and biodegradation (Arsenault et al., 2019; Laurion et al., 2021; Laurion & Mladenov, 2013). Studies investigating the changes in DOM composition in peatland porewater and pools have mostly been focused on temperate (Arsenault et al., 2019; Banaś, 2013), subarctic, and Arctic regions (Laurion & Mladenov, 2013; Deshpande et al., 2016; Burd et al., 2020; Payandi-Rolland et al., 2020; Laurion et al., 2021; Moody & Worrall, 2021), but there is no insight about changes in DOM compositions in boreal peatlands non affected by permafrost.

Because DOM may derive from different sources and be subjected to various processes of transformation and degradation, apprehending the complexity of the origin, composition, and properties of the molecules that compose the DOM is challenging. The use of complementary analytical methods is a good approach to characterise DOM and attempt to understand its origin and composition (Folhas et al., 2020; Tfaily et al., 2013). The DOC : DON elementary ratio is used to estimate the extent of microbial processing of DOM (Autio et al., 2016; McKnight et al., 1994). The absorbance and fluorescence are recognised tools to estimate the average DOM molecular weight and aromaticity (Haan & Boer, 1987; Weishaar et al., 2003; Helms et al., 2008), discriminate the origin of DOM between microbial and plant sources (McKnight et al., 2001; Cory et al., 2010), and highlight microbial degradation (Parlanti, 2000; Wilson & Xenopoulos, 2009). The stable carbon isotopic signature of DOC (δ^{13}C-DOC) can be used to discriminate between terrestrial and aquatic plant-derived DOM and also the extend of microbial processing of DOM (Elder et al., 2000;

Billett et al., 2012; Buzek et al., 2019). Finally, the analysis of target molecules using TMH-GC-MS allows the definition of indicators of DOM sources and processing degradation stage (Jeanneau et al., 2014, 2015; Kaal et al., 2017, 2020).

The aim of this study is to clarify the role that pools play in the production, transfer, and transformation of organic carbon within peatland ecosystems. We identified three possible scenarios. First, pools are mineralisation hotspots that can decompose the laterally exported fresh organic matter from adjacent peat porewater. Second, pools represent passive pipes that only collect the remaining refractory DOM laterally exported from peat porewater. Third, pools represent a sub-ecosystem within the peatland where both primary productivity and heterotrophic respiration exist. To determine which scenario is the most accurate, we studied the spatiotemporal variability of DOM over two growing seasons in a boreal ombrotrophic peatland. The objectives of this study were to: i) identify the differences in the origin, quantity, composition, and degradability of DOM between peat porewater and pools; ii) understand which factors induce those differences; and iii) clarify the contribution of DOM in pools to the peatland carbon cycle.

4.2 Study site

The study site is located in northeastern Quebec, Canada, within the Romaine River watershed (14,500 km^2), adjacent to the Labrador border. It is located in the eastern spruce-moss bioclimatic domain of the closed boreal forest (Payette, 2001) at the limit of the coastal plain and the Highlands of the Laurentian Plateau of the Precambrian Shield (Dubois, 1980). The Bouleau peatland (unofficial name; 50°31'N, 63°12'W; alt: 108 ± 5 m) is an ombrotrophic, slightly dome-shaped bog with a total surface area of 1.18 km^2 (Taillardat et al., 2022). Peat accumulation was initiated at ca. 9260 cal BP and the maximum peat depth reaches 440 cm (Primeau & Garneau, 2021). The mean annual temperature is 1.5°C and the mean annual precipitation is 1011 mm, of which 590 mm falls as snow. The average monthly positive temperatures occur from May to October with 1915 growing degree days above 0°C (Havre-Saint-Pierre Meteorological Station, mean 1990-2019; Environment of Canada, 2019).

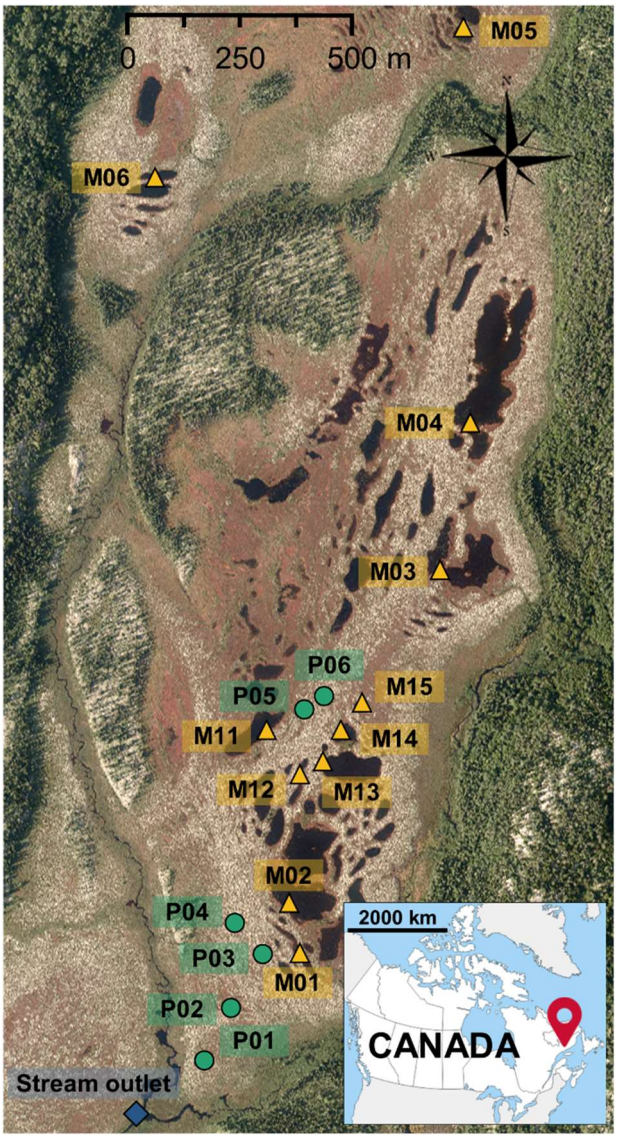

Figure 4.1 Bouleau peatland with the location of the sampling sites (green dots: wells for peat porewater; yellow triangles: pools; blue diamond: stream outlet). The aerial photo was provided by Hydro-Québec.

The surface microforms of the Bouleau peatland show a clear patterned surface of alternating dry hummocks, lawns, hollows, and pools. The surface vegetation varies according to the microtopography with *Sphagnum fuscum*, *S. capillifolium*, and *Cladonia rangiferina* on hummocks, *S. magellanicum*, *S. rubellum*, *S. cuspidatum*, and *Trichophorum cespitosum* on lawns, and *S. majus* and *S. pulchrum* on hollows (Primeau & Garneau, 2021). Pools cover 9 % of the peatland surface area and are characterised by their elliptical morphology, steep banks, and slightly concave bottoms. Because of the steep banks, no aquatic vegetation is observed along the edges of the pools.

4.3 Material and methods

4.3.1 Water sampling

Sampling was performed five times during the 2018 growing season (June, July, August, September, and October) and four times in 2019 (June, August, September, and October).

The peat porewater was sampled from six wells (P1 to P6, Fig. 4.1) located along a topographic transect from the dome to the southern edge of the peatland. Two meters long PVC wells were perforated and covered with a nylon sock to avoid infilling by peat. They were inserted in peat to collect water in the first two meters of the peat column. This method allows collecting the fluctuating water table which moves through the peat. In 2018, six pools were chosen along a north-south axe giving a distance gradient to the stream outlet (M01 to M06, Fig. 4.1). In 2019, the pools were divided into five class sizes, and one pool was chosen into each class (M11 to M15, Fig. 4.1). The pool sizes varied from 30 to 2065 m^2 with a mean depth between 70 and 120 cm. Pools were sampled from their banks and from the surface of the water column.

The physicochemical parameters (temperature, pH, specific conductivity, and dissolved oxygen saturation) of peat porewater and pool water were measured using a multi-parameter portable meter (Multiline Multi 3620 IDS, WTW, Germany) at each sampling site and calibrated before each field visit. All water samples were collected in clean polypropylene (PP) bottles and filtered on pre-combusted (4h at 450°C) GF/F filters (Whatman). Samples collected during each field campaign and analyses performed are synthesized in Table annexe C.1.

4.3.2 Water level and temperature monitoring

4.3.2.1 Instrumentation

The six wells were equipped with a water-level data logger U20-001-04 in 2018 and replaced with a U20l-04 in 2019 (HOBO, Onset, USA) for continuous measurements of the water table depth (WTD) and temperature from June 2018 to October 2020. Water temperature was recorded hourly in pools M11 to M15 using HOBO TMC50 probes coupled with a HOBO U12-008 data logger (Onset, USA) from June 2019 to August 2020. A water-level data logger was installed in pool M11 (Fig. 4.1), and water-level variations were measured from May 20th to August 28th 2020. Height variations (in cm) between the peatland surface at wells P5 and P6 and adjacent pool M11 was measured using a Zip Level Pro-2000 (Technidea, USA).

Those measurements allowed the water levels in the pool to be compared with those in the two wells (Fig. annexe C.2). An EXO2 multiparameter probe (YSI, USA) was installed at the outlet of the peatland stream to record water temperature hourly, from June 2018 to August 2020.

4.3.2.2 Season definition

Samples from the two studied years were pooled according to seasons. In this study, seasons were defined based on air and water temperatures measured at the site (Fig. annexe C.3). Spring was defined by the end of the seasonal thaw that occurred in May to the end of June. Summer included the months of July and August when air and water temperatures were at their warmest. Finally, the autumn season corresponded to the months of September and October when air and water temperature decreased to zero.

4.3.3 Quantitative analyses

The filtered water samples (through GF/F filters) were prepared for DOC and total nitrogen (TN) analyses by acidification to pH 2 with 1 M HCl and stored in 40 mL glass vials. The DOC and TN concentrations were analysed using the catalytic oxidation method followed by the non-dispersive infrared (NDIR) detection of the CO_2 produced (TOC analyser TOC-L, Shimadzu, Japan) with limits of quantification of 0.1 mg C L^{-1} and 0.2 mg N L^{-1}.

The samples were prepared for cation and anion analyses and stored in high-density polyethylene (HDPE) vials without acidification. Those ions (chloride, ammonium, nitrites, and nitrates) were analysed by high-performance liquid chromatography (HPLC) coupled with a Dionex ICS-5000+ analyser for anions (Thermo Fisher Scientific) and a Dionex DX-120 analyser for cations (Thermo Fisher Scientific).

The reference materials included ION-915 and ION 96.4 (Environment and Climate Change Canada, Canada). The analyses were performed at EcoLab (UMR 5245 CNRS – UT3 – INPT, France).

Dissolved organic nitrogen (DON) corresponds to the difference between the concentration of TN and the sum of concentration of inorganic nitrogen (ammonium, nitrites, and nitrates).

4.3.4 Qualitative analyses

4.3.4.1 Stable isotopic analyses

Analyses of δ^{13}C-DOC were realised on 41 samples selected from peat porewater (n = 20) and pools (n = 21; Table annexe C.1) at the Jan Veizer stable isotope laboratory (University of Ottawa, Canada) following the method developed by Lalonde et al. (2014). The samples were acidified to pH 2 with 1M HCl and stored in 40 mL quality certified ultra-clean borosilicate glass vials. The first step involved the catalytic oxidation of DOC followed by a solid-state non-dispersive infrared (SS-NDIR) detection of the CO_2 produced (OI Aurora 1030C, Xylem Analytics, USA). The produced CO_2 was passed through a chemical trap and a Nafion trap prior to ^{13}C isotopic analyses using isotope-ratio mass spectroscopy (IRMS, Thermo Finnigan DeltaPlus XP, Thermo Electron Corporation, USA). The results were standardised with organic standards (KHP and sucrose) and the $^{13}C/^{12}C$ ratios were expressed as per mil deviations from the international standard VPDB.

4.3.4.2 Optical analyses

The samples for UV-visible spectroscopy analyses were stored at 4°C in glass vials following filtration on GF/F filters. The absorbance was measured from 180 to 900 nm with a 5 nm resolution. The absorbance analyses were performed on Ultrospec 3100 (Biochrom, United Kingdom) for 2018 samples and on Duetta (Horiba, Japan) for 2019 samples, over a wavelength range from 190 to 900 nm at 2 nm intervals. All analyses were performed at the GRIL laboratory (GRIL, UQAM, Canada). For comparison, ten samples from the 2019 campaign were randomly selected and analysed on both equipment, Duetta and Ultrospec 3100. A pairwise t-test revealed slight but significant differences between absorbance at 254 nm from the two series (t = -3.9013, df = 9, p-value = 0.0036). As no significant effect was observed between years on absorbance indices, no correction was performed on absorbance spectra.

The absorbance indices were calculated to provide information about DOM composition. Those indices were $SUVA_{254}$ (L mg^{-1} m^{-1}) which is a proxy of the of DOM's aromatic content (Weishaar et al., 2003), $E2$: $E3$ ratio, and spectral slope ratio (S_R) which are proxies of the average DOM molecular weight (Haan & Boer, 1987; Helms et al., 2008).

In 2019, spectrofluorometric analyses were also conducted on Duetta (Horiba, Japan) at the GRIL laboratory. Samples were excited at a range from 230 to 450 nm (at 2 nm resolution) and fluorescence were measured at a range from 240 nm to 600 nm (at a 5 nm resolution). Prior to the analyses, the samples were diluted when necessary to maintain an absorbance intensity at 254 nm below 0.6. A blank sample

with MilliQ water (Merck-Millipore, Germany) was measured prior to the sample analyses. The sample spectra were obtained by subtracting the blank spectra to eliminate the Raman scatter peak. The operation was conducted automatically by the analytical equipment.

Two indices were calculated to provide qualitative information on the fluorescent fraction of the DOM. The fluorescence index (FI), lower values (FI ≈ 1.4) of which indicate a plant origin while higher values (FI ≈ 1.9) indicate a microbial origin of DOM (Cory et al., 2010; McKnight et al., 2001). The β : α index, which is known as a proxy of biological activity, and an increase in the ratio of which corresponds to an increasing proportion of the recently produced DOM derived from microbial activity (Parlanti, 2000; Wilson & Xenopoulos, 2009).

4.3.4.3 Molecular analyses

Thermally assisted hydrolysis methylation-gas chromatography-mass spectrometry (THM-GC-MS) was performed on 37 samples from peat porewater (n = 18) and pools (n = 19; Table annexe C.1). Those samples were selected to include summer and autumn 2018 and spring, summer, and autumn 2019. The THM-GC-MS analyses were conducted on freeze-dried samples from 100 mL of water previously filtered on GF/F filters (Whatman) and followed the procedure described by Jeanneau et al. (2015). One milligram of the sample was introduced into an 80 µL stainless steel reactor with an excess of tetramethylammonium hydroxide (6 mg). The THM reaction was performed at 400°C using a vertical microfurnace pyroliser PZ-2020D (Frontier Laboratories, Japan). The reaction products were injected into a gas chromatograph GC-2010 (Shimadzu, Japan) equipped with a SLB 5MS capillary column in split mode (60 m × 0.25 mm ID, 0.25 µm film thickness). The compounds were detected with a mass spectrometer QP2010+ (Shimadzu, Japan) operating in full scan mode. Analyses were realised at the Geosciences Rennes laboratory (UMR 6118 – Univ. Rennes – CNRS, France).

For each chromatogram, the compounds were identified based on known *m/z* ratios (Table annexe C.1) through comparison with the NIST library. The area of each compound was integrated for each *m/z* and corrected by a mass spectra factor (MSF). The MSF corresponds to the reciprocal of the integrated fragment proportion and the entire related fragmentogram in the NIST library. The relative proportion of each compound was calculated by dividing the compound area (for all cumulated peaks) by the sum of total integrated compound areas and expressed as a percentage.

All compounds were classified into five groups and their relative proportions were calculated: %CAR of carbohydrates compounds (derived from both plant and microbial metabolism), %LMW_FA for low molecular weight fatty acids (derived from microbial metabolism), %HMW_FA for high molecular weight fatty acids, %SOA for small organic acids, and %PHENOLS for phenol markers (derived from plant metabolism). The indices were calculated for each sample, derived from molecular analyses, and presented as in Jeanneau et al. (2015). The *C* / *V* ratio corresponds to the sum of coumaric and ferulic acids divided by the sum of vanillic acid, vanillaldehyde, and acetovanillone. The deoxyC6:C5 ratio is a mixing model based on the proportion of deoxyC6 carbohydrates (derived mainly from microorganisms) and the proportion of C5 carbohydrates (derived mainly from plants). Values close to 0.5 suggested a dominant contribution of plant-derived DOM while values close to 2 corresponded to the contribution of microbial-derived DOM (Rumpel & Dignac, 2006). The last index corresponds to the proportion of plant-derived markers, *f*VEG, which is the difference between the total markers and the microbial-derived markers, *f*MIC. The *f*MIC corresponds to the proportion of microbial carbohydrates multiplied by the total proportion of carbohydrates, summed up by the proportion of microbial fatty acids, and multiplied by the total proportion of fatty acids. The MIC : VEG index corresponds to the ratio of microbial-derived markers divided by the proportion of plant-derived markers.

4.3.5 Incubation of dissolved organic matter

4.3.5.1 Experimental design

The objective of DOM incubation experiments was to test the sensitivity of DOM to biodegradation and photodegradation and how it could affect its composition. The incubation experiments were designed to test the effects of temperature (in situ versus controlled) and total organic carbon versus dissolved organic carbon on DOM degradation rates.

DOM from peat porewater and pools was incubated during three sampling periods in 2019, from 7 to 13 June, 31 July to 7 August, and 4 to 10 September. An incubation time of six days had to be adjusted to seven days during the last campaign due to logistical constraints. Pool M11 was used to monitor the water level using a barometric pressure sensor and was also sampled for incubations. The peat porewater samples consisted of a mix of equal water volumes between five different wells. This strategy was used because the water quantity in piezometers was limited and not sufficient to perform all incubation conditions.

The incubation experiments were performed on 100 ml of water filtered on GF/F filters (F) and in unfiltered (UF) conditions. Amber borosilicate glass vials of 125 mL were used to test biodegradation (BIO) only and transparent borosilicate vials of 125 mL were used for bio and photodegradation (BIO+PHOTO). Each condition was incubated in triplicates with a headspace of 25 mL and bottles were tightly closed. Considering the absence of standardised incubation media between porewater and pools (Vonk et al., 2015), measured biodegradation rates could be dependent on the abundance and the activity of microorganisms in the samples from each environment.

For *in situ* incubations (IS), the peat porewater samples were placed 1-2 cm below the water surface at the outlet of the peatland (Fig. 4.1), where water temperature was recorded hourly with the EXO2 probe. The pool samples were placed 1-2 cm below the water surface of pool M11 (Fig. 4.1). For controlled conditions (CC), the vials were placed in a dark room in a laboratory space at Havre-Saint-Pierre where the temperature was maintained between 18 and 20°C and controlled twice each day. Both *in situ* and controlled conditions started the same day. There is no value available for F conditions in pools in August due to variability between the incubated water volume suggesting that vial caps were loose.

4.3.5.2 Post-incubation analyses

In the end, samples incubated under UF conditions (n = 18) were filtered on a GF/F filter to analyse only the dissolved fraction. All samples (n = 36) were prepared for DOC, TN and inorganic N quantification, and absorbance analyses, before and after the incubation experiments. The apparent removal rate of dissolved organic carbon (RDOC), expressed in mg day^{-1}, corresponds to the amount of DOC removed during incubation, reported per day, and calculated following Equation (1).

$$RDOC\ (mg\ day^{-1}) = \left([DOC]_{pre-incubation} - [DOC]_{post-incuba}\right) / incubation\ time \quad (1)$$

$[DOC]_{pre\text{-}incubation}$ (mg L^{-1}): DOC concentration at the beginning of incubation

$[DOC]_{post\text{-}incubation}$ (mg L^{-1}): DOC concentration at the end of incubation

The degradation rates correspond to the proportion of DOC lost per day of incubation and are expressed in %C day^{-1} according to Equation (2).

$$Degradation\ rate\ (\%\ C.day^{-1}) = \frac{\left([DOC]_{pre-incubation} - [DOC]_{post-incu}\right)}{[DOC]_{pre-incubati}} \times 100 \Big/ incubation\ time \quad (2)$$

Changes in the DOC : DON ratio and absorbance indices were determined in proportion to the initial values per day for the variable *i* following Equation (3).

$$\Delta i\ (day^{-1}) = \frac{i_{post-incubation} - i_{pre-incubatio}}{i_{pre-incubatio}} / incubation\ time \qquad (3)$$

Δ*i* is the change of the variable *i* during the imcubation. $i_{\text{pre-incubation}}$ is the initial value of the variable *i* at the beginning of incubation and $i_{\text{post-incubation}}$ is the value of the variable *i* at the end of incubation.

4.3.6 Statistical analyses

All statistical tests were performed on R (CRAN-Project) through the RStudio interface (RStudio inc., USA) and all figures were realised with the package ggplot2 (Wickham, 2016).

Comparisons of variance tests were performed and in the following sections, the mention of significant differences refers to statistical tests using the following method. First, normal distribution was tested using the Shapiro and Wilk test, and normal distribution was considered true when the p-value was >0.05. If the distribution was not normal, a Kruskal and Wallis test was performed to compare the averages and significant differences were considered true when the p-value was <0.05. Dunn tests were performed as *post-hoc* pairwise comparison tests to determine which group was significantly different (when the p-value <0.05). Second, the homogeneity of variance was tested using the Levene test and was considered true when the p-value was >0.05. If the homogeneity of variance was not true, Welsh ANOVA was performed, and significant differences were admitted when the p-value was <0.05. Estimated marginal means tests were performed as *post-hoc* tests to determine significantly different groups (p-value <0.05). In cases where the normal distribution and homogeneity of variances were true, an ANOVA was performed, and significant differences were true when the p-value was <0.05. When there were significant differences, the Tukey tests were performed as *post-hoc* tests to determine which groups were significantly different (when the p-value < 0.05). The results of the statistical tests are summarised in Table annexe C.2.

Principal component analyses (PCA) were used to explore relationships between DOM qualitative variables in peat porewater and pools. The selected variables were quantitative variables as DOC concentrations and qualitative variables as the DOC : DON ratio, optical indices ($SUVA_{254}$, *E*2 : *E*3 ratio, and S_R), and molecular indices (deoxyC6 : *C*5, *f*VEG, *f*MIC, MIC : VEG ratio, *C* / *V* ratio, and Ac:Al(V) ratio), as well as molecular compound proportions (%SOA, %CAR, and %CAR_MIC, %LMW_FA, %HMW_FA, and %Phenols).

Environmental and seasonal variables were used as supplementary qualitative variables. Prior to PCA, a correlation matrix was performed to identify strong correlations between the variables (Fig. annexe C.1). One of the correlated variables was excluded from PCA when the correlation was >0.90 or <-0.90, with p-values <0.05. Therefore, the DOC : DON ratio (DOC : DON ~ DOC, cor = 0.90, p-value <0.0001), %CAR_MIC (%CAR-MIC ~ deoxyC6 : *C*5 ratio, cor = 0.99, p-value <0.0001), and *f*MIC (*f*MIC ~ MIC:VEG ratio, cor = 0.98, p-value <0.0001) were excluded from the PCA data set. The PCA was performed with the package FactoMineR (Lê et al., 2008). The ellipses in the representation of the first two axes of the PCA correspond to the function *addEllipses* from the R package FactoMineR used to add concentration ellipses to the plot.

4.4 Results

4.4.1 Hydrodynamics and physicochemical characteristics

Pool and peat water levels followed the same seasonal trend, although the water level in the pools was always lower than in peat. Thus, the preferential water flow goes from peat porewater to pools. The response of the water level to precipitation was slower and buffered in pools compared to peat (Fig. annexe C.2) and an average time lag of 13 hours was measured between the WTD peak of peat and pools.

Peat porewater temperatures were constantly lower compared to pools, with 13.4 ± 4.4°C in peat porewater against 17.1 ± 5.5°C in pools when averaged over the two growing seasons. In both environments, the pH was acidic with an average of 4.9 ± 0.7 in peat porewater and 4.4 ± 0.3 in pools. Specific conductivity was on average almost two times higher in peat porewater than in pools, with 33.0 ± 19.3 µS cm^{-1} and 14.0 ± 6.1 µS cm^{-1} in peat porewaters and pools, respectively. Pool waters were characterised by their constant saturation in dissolved oxygen, with 99.9 ± 5.2%sat on average, while dissolved oxygen saturation was 50.04 ± 17.1%sat in peat porewater (Table 4.1).

4.4.2 Evolution of DOC concentrations and DOC:DON ratio

The DOC concentrations in peat porewater were significantly higher than in pools (Fig.4.2a). In both environments, the DOC concentrations showed the same seasonal trends with a significant increase from spring to summer. The DOC concentrations increased significantly in peat porewater from 9.2 ± 4.2 mg L^{-1} in spring, reaching a plateau above 20 mg L^{-1} during summer and autumn. In pools, the DOC concentrations also increased significantly from 7.5 ± 3.2 mg L^{-1} in spring to a plateau above 10 mg L^{-1} in summer and autumn.

Table 4.1 Peat porewater and pool seasonal average (±SD) of physicochemical variables (water temperature, pH, specific conductivity, and dissolved oxygen saturation), dissolved organic carbon (DOC) concentrations, and DOC to dissolved organic nitrogen (DON) ratio (DOC : DON), isotopic signature of DOC (δ^{13}C-DOC), optical indices ($SUVA_{254}$, *E*2 : *E*3 ratio, and spectral slope ratio), fluorescence indices (fluorescence index and β : α index), and molecular indices (*f*VEG, *f*MIC, deoxyC6 : *C*5, and *C* / *V* ratio, as well as %Phenols, %CAR, %CAR_MIC, %SOA, %LMW_FA, and %HMW_FA).

	Peat porewater			Pools		
	Spring	Summer	Autumn	Spring	Summer	Autumn
Physicochemical parameters						
Water temperature (°C)	12.3±5.2	16.5 ±2.3	11.8±4.2	14.8±1.7	22.8±2.9	13.7±4.9
pH	4.4±0.6	5.2±0.3	4.9±0.7	4.4±0.2	4.5±0.2	4.3±0.2
Conductivity (µS cm^{-1})	41.7±23.9	26.1±7.4	33.5±21.7	8.39±1.7	12.1±3.5	19.1±5.5
Dissolved oxygen (%sat)	56.0±16.2	45.3±16.8	50.4±17.5	101.0±2.9	102.0±5.8	97.5±4.9
Organic matter quantitative proxies						
DOC (mg L^{-1})	9.2±4.2	20.2±8.5	22.5±5.4	7.5±3.2	10.4±3.7	12.4±4.0
DOC : DON	32.3±12.4	52.8±22.5	56.6±8.2	26.2±7.7	32.0±7.5	31.7±6.6
DON (mg L^{-1})	0.29±0.1	0.39±0.08	0.39±0.06	0.29±0.1	0.39±0.11	0.39±0.09
Isotopic and optical indices						
δ^{13}C-DOC (‰)	-26.0±0.9	-27.3±0.3	-27.5±0.5	-27.5±0.3	-27.1±0.4	-26.8±0.8
$SUVA_{254}$ (L mg^{-1} m^{-1})	6.0±1.5	5.13±0.5	5.55±1.0	2.88±1.5	3.13±0.5	3.86±0.6
*E*2 : *E*3 ratio	3.4±0.2	3.5±0.2	3.6±0.2	4.0±0.1	4.2±0.2	4.4±0.2
S_R	0.67±0.04	0.64±0.05	0.67±0.03	0.77±0.06	0.81±0.05	0.72±0.05
Fluorescence index	1.39±0.09	1.40±0.13	1.33±0.07	1.27±0.04	1.26±0.03	1.27±0.04
β : α index	0.63±0.10	0.65±0.08	0.59±0.05	0.62±0.03	0.69±0.07	0.61±0.07
Molecular indices and family compound proportions						
fVEG (%)	68.6±1.1	69.8±3.6	62.7±3.2	64.3±10.6	60.8±6.7	62.8±3.5
fMIC (%)	5.8±1.4	7.2±3.4	5.8±2.3	8.0±5.2	11.7±6.0	7.2±2.0
MIC : VEG ratio	0.09±0.02	0.10±0.05	0.09±0.4	0.14±0.13	0.20±0.12	0.12±0.04
deoxyC6 : *C*5	0.67±0.11	0.64±0.25	0.50±0.17	0.73±0.10	1.10±0.19	0.91±0.33
C / *V*	0.37±0.11	0.37±0.13	0.22±0.07	0.18±0.04	0.22±0.08	0.19±0.04
%Phenols (%)	57.6±6.3	54.1±9.2	53.6±4.6	59.0±10.1	53.3±8.5	54.6±7.9
%SOA (%)	19.9±0.4	18.1±5.8	26.6±6.3	21.5±3.9	20.4±4.7	24.5±3.5
%CAR (%)	7.3±1.6	5.7±3.2	6.7±5.2	4.6±2.2	8.8±9.4	7.8±6.6
%MIC_CAR (%)	0.11±0.08	0.11±0.15	0.05±0.07	0.15±0.07	0.40±0.13	0.28±0.22
%LMW_FA (%)	5.0±0.7	6.7±3.0	5.2±1.9	7.2±5.9	7.6±3.8	5.6±1.6
%HMW_FA (%)	4.6±4.4	10.6±8.6	3.00±3.3	1.4±0.1	2.9±1.3	2.1±1.0

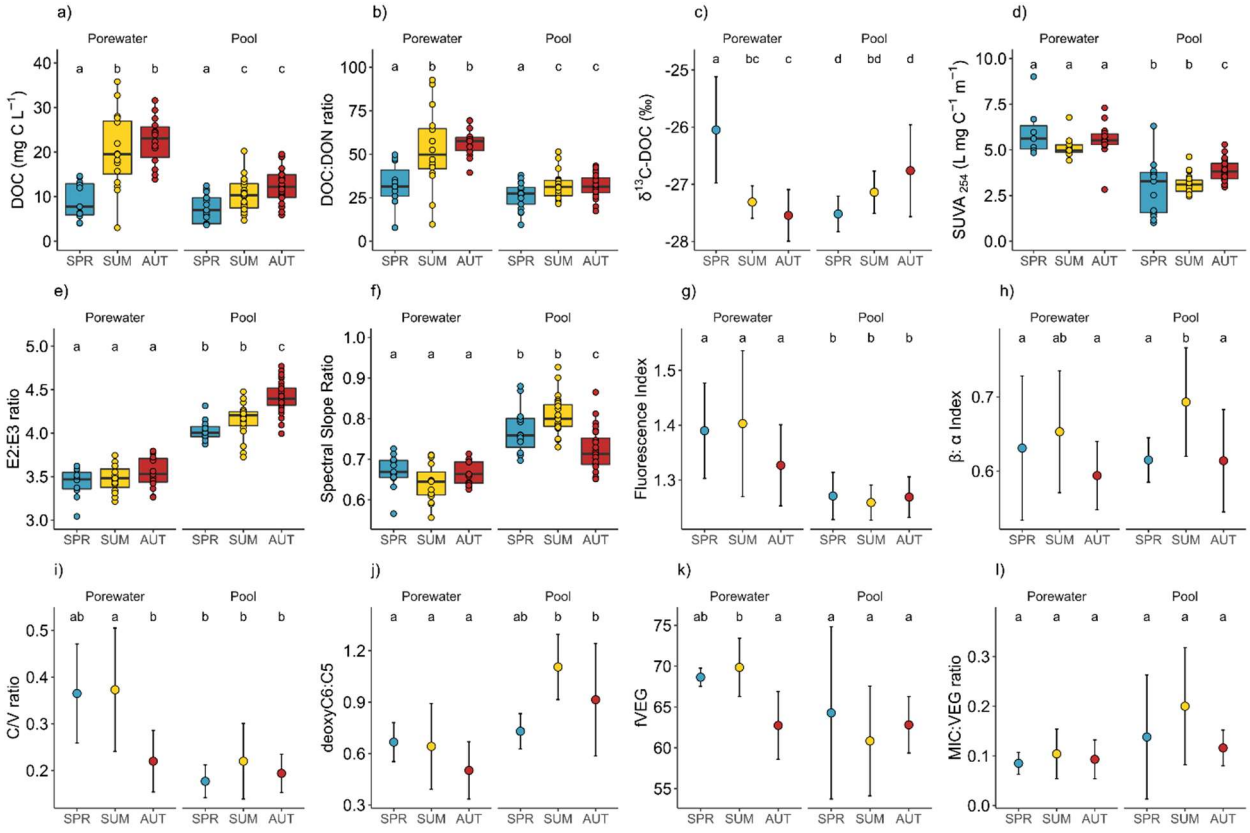

Figure 4.2 Box plots (a to b and d to f) and dot plots (c and g to i): a) DOC concentrations, b) DOC : DON ratio, c) δ^{13}C-DOC, d) SUVA$_{254}$, e) *E*2 : *E*3 ratio, f) spectral slope ratio, g) fluorescence index, h) *β* : *α* index, i) *C* / *V* ratio, j) deoxy*C*6 : *C*5, k) *f*VEG, and l) MIC : VEG ratio. Each plot represents the evolution of variables during the growing season (SPR: spring; SUM: summer; AUT: autumn) in peat porewater and pools. Dot plots were used when n < 5 for at least one season. Error bars represent standard deviations. Box plots were used when n > 5 for each season. The dots represent each individual measurement, and boxes represent the lower (25th percentile) and the upper quartile (75th percentile); the median (50th percentile) is represented by the bold black horizontal bar in the boxes. Whiskers represent the interquartile range. Letters represent the significant differences between seasons. For each individual plot, conditions which share a letter do not present statistical differences.

Peat porewater presented a significantly higher DOC : DON ratio than pools. In both environments, the DOC : DON ratio increased significantly from spring to a plateau in summer and autumn (Fig. 4.2.b). In peat porewater, the DOC : DON ratio increased from 32.3 ± 12.4 in spring to 52.8 ± 22.5 and 56.6 ± 8.2 in summer and autumn, respectively (Fig. 4.2.b). In pools, the DOC : DON ratio increased from 26.2 ± 7.7 in spring to a plateau of 32.0 ± 7.5 in summer and 31.7 ± 6.6 in autumn.

4.4.3 Evolution of isotopic composition of DOM

Different trends for δ^{13}C-DOC were identified between peat porewater and pools (Fig. 4.2.c). In peat porewater, δ^{13}C-DOC decreased significantly from spring, when the ratio was -26.0 ± 0.9 ‰, to autumn when the ratio dropped to -27.5 ± 0.5 ‰. In pools, δ^{13}C-DOC showed a nonsignificant increase from -27.5 ± 0.3 ‰ in spring to -26.8 ± 0.8 ‰ in autumn. In summer, δ^{13}C-DOC was significantly different between peat porewater and pools.

4.4.4 Evolution of the optical and fluorescent properties of DOM

The DOM presented different optical properties between peat porewater and pools. Among those, $SUVA_{254}$ was significantly higher in porewater than in pools during the whole growing season, indicating a higher aromaticity of peat porewater DOM (Table 4.1). During the growing season, there were no major changes of $SUVA_{254}$ in peat porewater, but a slight increase was observed in pools during the autumn (Fig. 4.2.d).

The $E2 : E3$ ratio was significantly higher in pools than in peat porewater, indicative of a lower average molecular weight. Compared to $SUVA_{254}$, the $E2 : E3$ ratio showed no significant trends in peat porewater, but it slightly increased in pools from 4.02 ± 0.11 in spring to 4.41 ± 0.18 in autumn, suggesting a decrease in the average molecular weight during the growing season (Fig. 4.2.e).

The lower spectral slope ratio (S_R) of peat porewater DOM also suggested a higher molecular weight than in pool DOM. During the growing season, the S_R was steady in peat porewater with no significant changes between seasons, suggesting a homogeneity of the molecular weight of DOM (Fig. 4.2.f). In pools, S_R values increased from spring to summer and decreased in autumn. Thus, according to the S_R, the lowest average molecular weight was reached during the summer in pools.

The fluorescence index (FI) was significantly higher in peat porewater than in pools but varied within a narrow range, close to typical terrestrial-derived organic matter (Fig. 4.2.g). During the growing season, the index remained steady in both environments with an average of 1.36 ± 0.10 in peat porewater against 1.27 ± 0.04 in pools.

The $\beta : \alpha$ index did not differ significantly between peat porewater and pools, where it was on average 0.62 ± 0.07 and 0.64 ± 0.07, respectively (Fig. 4.2.h). During the growing season, the index remained steady

in peat porewater. In pools, the β : α index increased significantly from spring to summer: from 0.62 ± 0.03 to reaching a peak at 0.69 ± 0.07. As the changes observed for the FI, variations of the β : α index were limited to a small range.

4.4.5 Evolution of the molecular composition of DOM

Phenol markers dominated (54 %) the molecular markers of DOM for both peat porewater and pools (Table 4.1). A similar proportion of small organic acids (22 % on average) was measured in both environments. Carbohydrates represented 6 % of the total markers in peat porewater and up to 8% in pools. The distribution of fatty acids differed between the two environments. While low molecular weight fatty acids showed similar proportions in peat porewater (5.8 %) and pools (6.7 %), high molecular weight fatty acids, which are associated with plant inputs, were almost three times higher in peat porewater (6.1 %) than in pools (2.3 %).

In addition, three modifications of the molecular composition of DOM between the two environments must be highlighted. First, the *C* / *V* ratio (Fig. 4.2.i), a lignin compositional proxy, was significantly higher in peat porewater than in pools ($p < 0.01$). While it remained almost stable in pools, it decreased in peat porewater from 0.37 ± 0.12 during spring and summer to 0.22 ± 0.07 during autumn. Secondly, the deoxyC6 : *C*5 ratio (Fig. 4.2j), a carbohydrate ratio, was significantly higher in pools (0.97 ± 0.28) than in peat porewater (0.57 ± 0.20) ($p < 0.0001$). While it remained almost stable in peat porewater, it was maximal in summer (1.10 ± 0.19) compared to spring (0.73 ± 0.10) and autumn (0.91 ± 0.33). In pools, this evolution emphasised an increase in the contribution of microbial exudates among the carbohydrate compounds in pools. Finally, the fraction of plant-derived compounds among the identified markers, *f*VEG (Fig. 4.2.l), was always higher than 50 % in both environments, highlighting the dominance of plant-derived DOM. However, *f*VEG was significantly higher in peat porewater than in pools ($p = 0.02$). Comparatively to the variations observed for the *C* / *V* ratio, *f*VEG remained almost stable in pools, while it decreased in peat porewater in autumn.

4.4.6 Global assessment of DOM quality in peat porewater and pools

The PCA analyses of the peat porewater and pool samples indicate that the first two components, represented by the two axes of Figure 4.3, accounted for 56.3 % of the total variance. Individuals represented in the first two dimensions, showed a clear separation of both environments along the first dimension (Fig. 4.3). The major contributors of the first axis were S_R (19.8 %), *E*2 : *E*3 ratio (14.4 %),

deoxyC6 : *C*5 (12.8 %), DOC concentration (12.7 %), and finally MIC : VEG ratio (11.8 %). For the second axis, the major contributors were the proportion of phenols (%Phenols; 20.8 %), *C* / *V* ratio (18.5 %), and high molecular weight fatty acids (%HMW_FA; 17.3 %). Other variables contributed less than 10 % to the first two axes.

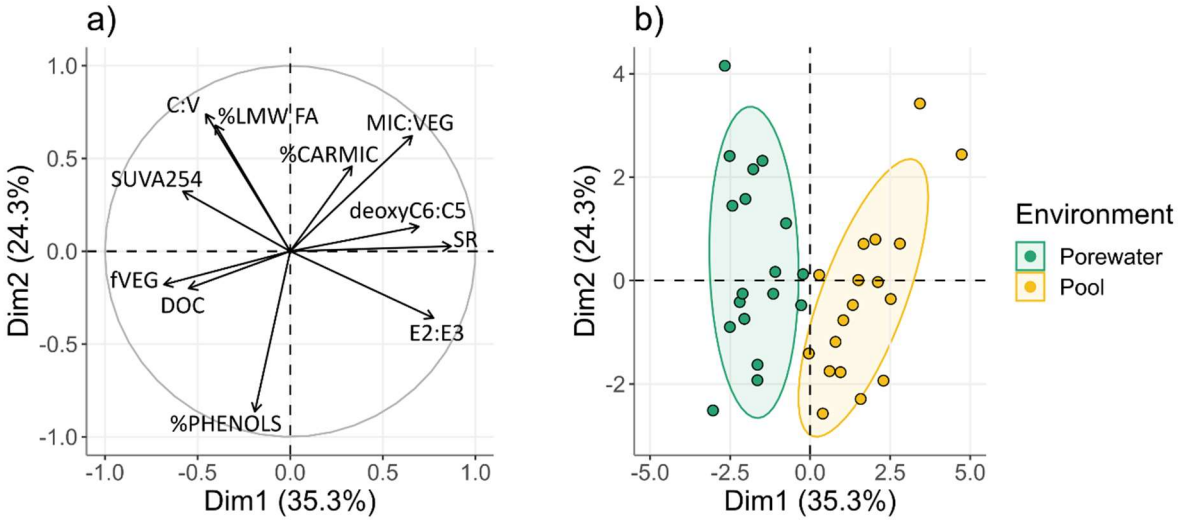

Figure 4.3 Representation of the first two dimensions of principal component analysis (PCA) of a) physicochemical, quantitative, and qualitative parameters as variables and b) individuals.

In pools, the DOM was characterised by a lower average molecular weight and aromaticity and a higher contribution of microbial-derived DOM compared to peat porewater. Inversely, in peat porewater, the DOC concentrations were higher, and DOM presented higher aromaticity, and a higher contribution of plant-derived DOM, characterised by a higher *f*VEG. There was no effect of the sampling season on the variances.

4.4.7 Experimental degradability of peat porewater and peat DOM

Statistical tests revealed no significant differences in the average degradation rate between *in situ* and controlled conditions of biodegradation (section 4.3.5.1). In addition, no significant differences appeared between the average degradation rate where biodegradation only was tested and those where biodegradation and photodegradation were both tested. This suggests that temperature and sunlight had a limited effect on the DOM degradation. As a consequence, all experimental conditions (both *in situ* and controlled) were pooled in the following section. The DOM degradation rates were significantly higher for

peat porewater than pools. The degradation rates were significantly higher for the incubation conditions of unfiltered samples (UF) compared to filtered sample (*F*) conditions (Fig. 4.4).

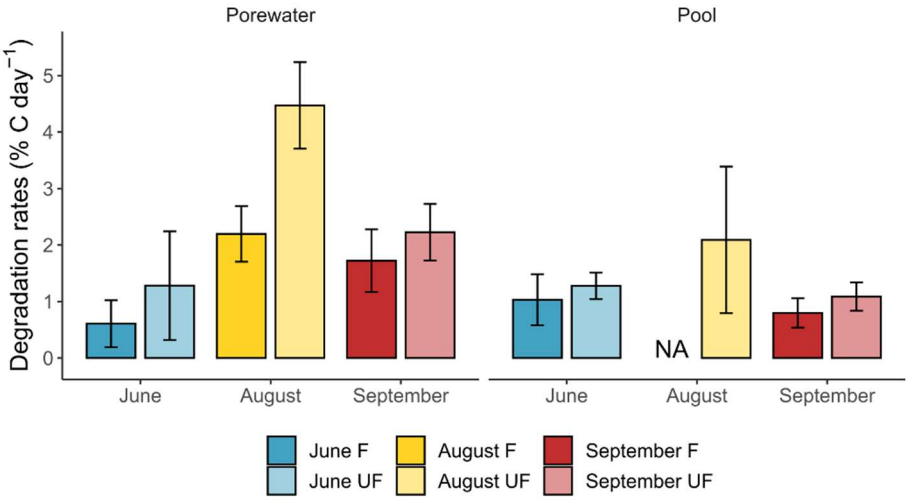

Figure 4.4 Seasonal degradation rates (in % C d^{-1}) for DOC and TOC incubation conditions in peat porewater and pools.

On average, the DOC degradation rates were 1.6 times higher for incubation under unfiltered conditions (2.5 ± 1.5 %C day^{-1}) compared to filtered conditions (1.5 ± 0.8 %C day^{-1}) in peat porewater. In pools, degradation rates were twice as high for UF (1.1 ± 1.1 %C day^{-1}) than for *F* conditions (0.5 ± 0.6 %C day^{-1}).

In peat porewater, the DOC degradation rates for *F* and UF conditions followed similar seasonal trends. The DOC degradation rates were low in June (0.6 ± 0.4 %C day^{-1}) and twice as high for UF conditions (1.3 ± 1.0 %C day^{-1}). The degradation rates reached a peak in August, with 2.2 ± 0.5 %C day^{-1} for *F* and 4.5 ± 0.8 %C day^{-1} for UF conditions. Then, the DOC degradation rates decreased in autumn to 1.7 ± 0.6 %C day^{-1} and 2.2 ± 0.5 %C day^{-1} for *F* and UF incubation conditions, respectively.

After excluding the UF condition of August, there was no persistent significant difference between *F* and UF conditions. In June, the DOC degradation rates were similar between the *F* and UF conditions with rates of 1.0 ± 0.5 %C day^{-1} and 1.3 ± 0.2 %C day^{-1}, respectively. Then, an increase to 2.1 ± 1.3 %C day^{-1} was observed in August for UF conditions which were two times lower than the rate measured in peat porewater under the same conditions. Finally, the DOC degradation rates diminished in September, with

0.8 ± 0.3 %C day^{-1} for *F* and 1.1 ± 0.3 %C day^{-1} for UF incubation conditions. Those degradation rates were 2 times lower than those observed in peat porewater in autumn.

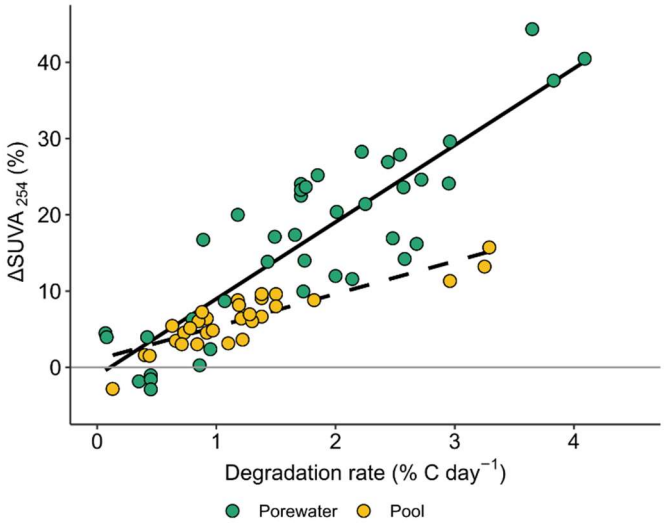

Figure 4.5 Relations between changes in $SUVA_{254}$ ($\Delta SUVA_{254}$) during incubation experiments and linear regression in peat porewater (solid line) and pools (dashed line).

As observed in Figure 4.5, $\Delta SUVA_{254}$ was strongly and positively correlated with degradation rates, with specific dependence in pools (n = 29, cor = 0.82; p <0.0001) and peat porewaters (n = 33, cor = 0.65; p <0.0001).

4.5 Discussion

4.5.1 Differences in DOM concentration and composition between peat porewater and pools despite a similar source

The DOM concentration and composition strongly differed between peat porewater and pools, despite a clear common plant origin. Peat porewater DOM was characterized by high DOC concentrations and a DOM composed by both recently produced and biodegraded DOM. In pools, DOC concentrations were 2 times lower compared to the peat porewater (Fig. 4.2.a). Pool DOM was characterized by a dominant contribution of allochthonous DOM (i.e., plant-derived) but also presented characteristics of microbial degraded DOM.

At our site located in the boreal ecozone, the average DOC concentration in peat porewater increased from 9.2 to 22.5 mg L^{-1} from spring to autumn. During the growing season, DOC concentrations are in general below 20 mg L^{-1} in boreal and subarctic regions which are lower than in temperate regions (Table annexe C.4). This latitudinal trend suggests that the balance between DOM production and processing in peat porewater is controlled by climate and most likely by temperature (Kane et al., 2014). At our site, both DOM production and consumption followed a strong seasonal trend in peat porewater, with DOM production being more intense, as DOC concentrations were multiplied by 2.5 during the growing season (Table 4.1).

DOM production by plants within peat porewater followed a strong seasonal trend. This is revealed by three observations. First, peat porewater showed a greater proportion of plant-derived DOM towards the end of the growing season as indicated by the lowest δ^{13}C-DOC measured in the autumn. Second, the high DOC : DON ratios measured in peat porewater at our study site - up to six times higher than those in Austnes et al. (2010), and the increase of DOC : DON ratio during the growing season (Fig. 4.2.b), - indicated a high contribution of recently produced DOM. Third, the slight decrease of δ^{13}C-DOC (Fig. 4.2.c) as well as the contribution of high molecular weight fatty acids from spring to summer confirm the high contribution of plant-derived DOM. However, peat porewater DOM composition also suggested a contribution from microbial processing. First, the molecular analysis revealed the presence of microbial markers, as high as 6.4 ± 2.7%, as expressed by *f*MIC (Table 4.1). Second, the incubation experiments highlighted that the labile fraction of DOM, represented 2.0 ± 1.3% of peat porewater DOC (Fig. 4.4). Third, the high $SUVA_{254}$ values (Fig. 4.2.d) we observed might reflect the importance of biodegradation processes of DOM in peat porewater as $SUVA_{254}$ increase with biodegradation (Hulatt et al., 2014; Autio et al., 2016, Fig. 4.5). The average $SUVA_{254}$ of 5.5 L mg^{-1} m^{-1} measured in the Bouleau peatland porewater was, in general, higher than those previously measured in peatlands from temperate regions i.e. <3.6 L mg^{-1} m^{-1} (Arsenault et al., 2019; Heinz & Zak, 2018; Tfaily et al., 2015), except for Austnes et al. (2010) who reported a similar aromaticity and average DOM molecular weight in a Welsh ombrotrophic peatland. These indicators of microbial degradation within the peat also showed a seasonal trend, with higher DOM biodegradability measured in summer (Fig. 4.4), and the lowering of the *f*VEG at the end of the growing season. Then, most of the DOM present in peat porewater is derived from the active vegetation at the surface of the peatland but has been partially decomposed through microbial degradation.

In pools, the DOM composition also presented specific features, with lower DOC concentrations, aromaticity, and average molecular weight compared to peat porewater (Fig. 4.2). Our results highlighted a dominant contribution of allochthonous DOM in pools despite the presence of microbial-derived DOM. The DOC concentrations in pools (10.5 mg L^{-1} in average) were similar to those previously reported in the literature (Table annexe C.4) which, unlike peat porewater, do not follow any latitudinal trend. The DOC concentration remained relatively steady during the growing season, only multiplied by 1.6 compared to an increase by a factor of 2.5 in peat porewater (Table 4.1). The $SUVA_{254}$ values measured in the Bouleau peatland pools (3.4 ± 0.9 L mg^{-1} m^{-1} on average; Fig. 4.2.d) were similar to those reported from Arctic regions with values of about 4 L mg^{-1} m^{-1} (Laurion & Mladenov, 2013; Peura et al., 2016; Gandois et al., 2019; Laurion et al., 2021) suggesting a contribution of plant-derived DOM from peat at our site and supported by the high DOC:DON ratio, ranging from 9.4 to 51.4 (Fig. 4.2.b).

Yet, the slightly higher deoxyC6 : *C*5 and the higher %LMW_FA in pools indicate the presence of microbial markers. Microbial processing follows a seasonal trend in pools (the highest microbial activity occurred in summer), which appear to be stronger compared to peat porewater. This is revealed by the evolution of δ^{13}C-DOC, increasing during the growing season (Fig. 4.2.c) and revealing an increasing proportion of processed DOM. The increase of aromaticity, from 2.9 to 3.9 L cm^{-1}, might also reflect this microbial processing and its increasing contribution during the growing season. This is supported by indices as the S_R, deoxyC6 : *C*5, MIC : VEG ratio and β : α index following a pronounced seasonal trend with a peak reached in summer (Fig. 4.2). This suggests that pool DOM is mostly derived from active vegetation in the peat but undergoes more intense microbial degradation.

4.5.2 The DOM compositional differences between peat porewater and pools are explained by hydrological, chemical, and biological processes

The observed differences in DOM composition between peat porewater and pools were persistent during the growing season and under different hydroclimatic conditions. We propose that those differences were driven by a combination of hydrological, chemical, and biological factors. Along a peatland to pool transect, both DOM concentrations and compositions remained stable within the peatland and changed sharply at the interface between the peatland and an adjacent pool (Fig. annexe C.4).

Hydrological flow paths in the peatland and at the transitional zone between peat and pools might play a role in the shift of DOC concentrations and DOM composition between porewater and pools. The two

environments appear to be hydrologically connected, based on synchronous variations of the water levels in adjacent environments with a strong buffering of water levels in pools (Fig. annexe C.2). This buffering can be explained by the decrease of hydraulic conductivity with depth in peat which limits water exchanges (Holden et al., 2018). This suggests that the preferential flow path for lateral advection occurs at shallower depths when WTD is high (Birkel et al., 2017). Alternatively, it has been shown that deep flow paths (below 2 m depth) could supply surface flow (Levy et al., 2014; Peralta-Tapia et al., 2015) and might transport deeper DOM to the surface water (Campeau et al., 2017), and could contribute to water supply in pools. The DOM composition in deep peat porewater has been reported to be relatively similar to shallow layers with high aromaticity and average molecular weight (Tfaily et al., 2018). If this process could provide DOM to pools, it could not explain the shift in DOM composition between environments.

At our studied peatland, a decrease in the water storage coefficient (Riahi et al., submitted) and an increase in peat density with depth has been documented (Primeau & Garneau, 2021), and should inhibit water flow movements. In addition to slower water circulation, peat pore structure stimulates interactions between DOM and partially degraded peat which can adsorb both hydrophilic and hydrophobic compounds (Kalbitz et al., 2000; Rezanezhad et al., 2016). Changes in composition between peat porewater and pools might be induced by the selective interaction between DOM aromatic compounds and peat during their slow transfer. As we observed $SUVA_{254}$ values 1.6 times higher in peat porewater compared to pools (Fig. 4.2), those aromatic products might selectively interact with peat or at least reduced its mobility and explained the lower DOC concentration and DOM aromaticity measured in pools (Table 4.1), since aromatic compounds are known to constitute the hydrophobic fraction of DOM (Dilling & Kaiser, 2002).

Then, DOM microbial processing, occurring at different rates within peat, at the interface between peat and pools and within the pool, might greatly contribute to the observed differences in DOM composition. Peat porewater DOM composition reflects microbial degradation occurring within the peat (*f*MIC, Table 4.1), and shows a greater degradation potential compared to pool DOM (Fig. 4.4). The slow water circulation and long residence time of DOM within peat might promote interactions with microorganisms, allowing microbial degradation of DOM (Catalán et al., 2016; Kalbitz et al., 2000). Yet, a significantly higher contribution of microbial-derived DOM was observed in pools, as expressed by a higher deoxyC6 : *C*5 and higher %LMW_FA and lower *f*VEG indices, and the decrease in the average DOM molecular weight as shown by the higher S_R and *E*2 : *E*3 ratio. The significantly lower *C* / *V* ratio measured in pools also support

the higher DOM microbial processing in pools. The coumaric and ferulic acids, composing the *C* fraction, are preferentially biodegraded compared the vanillic acid, vanillaldehyde, and acetovanillone, composing the *V* fraction (Goñi and Hedges, 1992), resulting in a decrease of the *C* / *V* ratio, as observed from peat porewater to pools.

The signature of microbial-derived DOM in pools supports the hypothesis that DOM degradation processes occur at the interface between peat porewater and pools (Fig. annexe C.4) and within the pools. A shift gradual sharp changes in physicochemical parameters between the two environments, such as the slight increase in pH and temperature, and the rise of dissolved oxygen concentrations, may favour the microbial turnover of the fraction of labile peat porewater DOM (higher than in pool, Fig. 4.4; Schindler et al., 1997; Kalbitz et al., 2000; Worrall et al., 2008; Peura et al., 2016) Additionally, our data did not evidence any photodegradation during DOM incubation in peat porewater and pools, suggesting that the DOM photodegradation was not sizeable by our experimental design. This contrasts with previous studies which observed DOM photodegradation and changes in DOM composition in boreal and temperate aquatic ecosystems of Eastern Canada (Lapierre & del Giorgio, 2014; C. P. Ward & Cory, 2016) and the United Kingdom (Jones et al., 2016). The absence of sizeable photodegradation suggests that this process did not drive the DOM composition in pools, compared to biodegradation. The clear pattern of the $SUVA_{254}$ increase observed during the incubation experiments was independent to the exposition of DOM with the solar radiation. This is consistent with the biodegradation of non-aromatic molecules (Spencer et al., 2008, 2015; Mann et al., 2015; Worrall et al., 2017) leading to an increase of $SUVA_{254}$ (Hulatt et al., 2014; Autio et al., 2016) while photooxidation has been shown to induce a decrease of DOM aromaticity (Laurion & Mladenov, 2013; C. P. Ward & Cory, 2016). This is supporting the hypothesis that the peat-derived DOM biodegradation is an important driver of DOM composition in the pools.

4.5.3 Implication of the DOM exchange from peat to pools for the peatland carbon cycle

Boreal peatland pools were previously identified as a continuous source of carbon dioxide (CO_2) to the atmosphere during ice-free seasons, offsetting some of the carbon uptake by the vegetation (Pelletier et al., 2014, 2015). This release of CO_2 was assumed to be the product of DOM mineralization through microbial productivity in pools (Billett et al., 2004; Payandi-Rolland et al., 2020; Striegl et al., 2012). Since our results showed low degradation rates in pools, we suggest that DOM could have been partially biodegraded within the peat and at the interface zone between peat porewater and pools, limiting further its degradation within pools (Payandi-Rolland et al., 2020). This reactive interface could be comparable

with the hyporheic zone (riparian water-saturated zone between the peat and the stream) which can be an active component of the carbon cycle through the active DOM mineralisation and CH_4 oxidation at this interface (Rasilo et al., 2017).

The long-term apparent rate of carbon accumulation (LORCA) measured in the Bouleau peatland has been estimated to be 35.5 g C m^{-2} y^{-1} and the recent apparent rate of carbon accumulation (RERCA) 85.1 g C m^{-2} y^{-1} (Primeau & Garneau, 2021). Based on a total pool volume of approximately 136 350 m^3, an average DOC concentration of 10.1 mg L^{-1} (Table 4.1), and an average potential degradation rate between 1.9 % day^{-1} in peat porewater and 0.9 %C day^{-1} in pools (Fig. 4.4), the degradation of pool DOM could average between 1.5 g C m^{-2} y^{-1} and 3.1 g C m^{-2} y^{-1} for our site. This is equivalent to 5.4 % to 11.1 % of the LORCA and 2.2 % to 4.6 % of the RERCA. Those proportions suggest that the processing of DOM in pools might have a substantial impact on the peatland carbon budget. The integration of carbon exchange at the pool-atmosphere interface would tend to ultimately minimize the carbon sink capacity of peatlands often reported from studies focusing on vegetation to atmosphere exchange. It is also important to note that DOM in pools is mainly derived from the recently produced DOM in peat, and unlikely from deeper (and older) peat layers. However, DOM degradation is not the only source of carbon emissions from pools which can also be supplied by the lateral transfer of CO_2 and CH_4 (Rasilo et al., 2017) and by CH_4 ebullition (Repo et al., 2007). However, the importance of the pools as a potential carbon source to the atmosphere needs to be moderate in comparison with the CO_2 and the CH_4 exported and emitted in the headwater stream of the peatland. This flux of 8.8 g C m^{-2} y^{-1} (Taillardat et al., 2022), accounted for 22.8 % of the LORCA which is between 2 and 4 times higher to the carbon potentially emitted by pools.

Results presented in this study are from a boreal peatland, without permafrost or anthropogenic disturbances that could influence the carbon production and transformation processes through the peat-pool complex. The morphology of pool banks and vegetation surrounding the pools may play an important role in the DOM dynamics and DOC concentrations of pools, as suggested by Arsenault et al. (2018, 2019), who studied 156 pools with a range of surface and depth comparable to our study site. A study conducted on ten peatland pools showed that the size of the contact surface between water and peat (influenced by pool size, depth, and the slope of the banks) influenced the concentrations and composition of DOM (Banaś, 2013). However, the pools studied by Banaś (2013) were up to ten times larger and deeper than in our studied peatland pools. At our site, there was no significant difference between the pools in their range of size (from 30 to 2065 m^2) and depth (from 70 to 120 cm) except for $SUVA_{254}$ (Table annexe C.5).

Despite the slight effect observed on $SUVA_{254}$, the DOM dynamics do not seem related to the pools morphology and depth. It supports the hypothesis that DOM transfer and biodegradation from peat porewater to pools are the main driver on its dynamic and implication to the peatland carbon cycle rather than pools morphological features.

Our study suggests that peat-derived DOM degradation and release through pools could play a substantial role on the net carbon budget of our studied peatland (<10 % of the LORCA). Moreover, the influence of pools in the peatland carbon cycle should be considered from the perspective of climate change. DOM production and biodegradation rates seem to be controlled by temperature (Fig. 4.2 and 4.4) during the growing season and longer ice-free seasons and higher temperatures might impact the importance of pools in the peatland carbon cycle.

4.6 Conclusion

This study demonstrated that DOM is a highly dynamic component of the carbon cycle in peatland, with important differences identified in its concentration and composition in both peat porewater and pools. Those differences being persistent throughout the growing season and different hydroclimatic conditions.

The strong increase of DOC concentrations in peat porewater over the growing season highlighted the intense production of DOM in this environment. DOC concentrations increased by 2.5 during the growing season (against a DOC concentration increase by a factor of 1.7 of in pools), despite microbial processing of DOM occurring within the peat.

The molecular analysis of DOM in pools revealed the dominant contribution of allochthonous DOM derived from the peatland vegetation, supported by the dominance of plant makers (*f*VEG and %Phenols) and high DOC : DON ratio. Despite this similar plant origin, peat porewater and pools DOM had very different concentrations, composition, and dynamics over the growing season. The DOM in pools was less aromatic and showed lower molecular weight compared to peat porewater.

Based on our investigations, we suggest that a combination of hydrological, chemical, and biological processes explain those differences. The low hydraulic conductivity in peat might favour DOM microbial processing before its transfer to the aquatic compartments. Low hydraulic conductivity could also lead to the selective adsorption of aromatic compounds with degraded peat supporting the decrease of

concentration and the lower aromaticity of DOM observed in pools. We observed abrupt changes in DOM concentration and composition at the interface between peat and pools which were persistent during the growing season. The rapid modification of physicochemical conditions (e.g., temperature and oxygen availability) between those two environments might influence the biodegradation of DOM at the interface between the peat and the pools and within the pools. This is confirmed by the higher proportion of microbial molecular markers identified in the pool.

Although DOM is microbially degraded both at the interface and within the pool, the carbon emissions generated by those processes could be substantial (between 5.5 and 11 % of the LORCA). The importance of pools in the carbon cycle needs to be still studied in a context of temperatures increasing, that could stimulate DOM production in peat porewater and its microbial processing in peat pore water, and in pools after its transfer.

Acknowledgments

We thank Katherine Velghe and Alice Parks from GRIL for their laboratory training and assistance in absorbance and fluorescence analyses, as well as Paul Del Giorgio for access to his laboratory. Marine Liotaud, from Géosciences Rennes, is acknowledged for performing THM-GC-MS analyses, and Frederic Julien, Virginie Payre-Suc, and Didier Lambrigot, from Laboratoire Ecologie Fonctionnelle et Environnement, are acknowledged for performing DOC/TN and cations/anions analyses. We thank Roman Teisserenc (Ensat, Toulouse) and Charles Bonneau, Charles-Élie Dubé-Poirier, Camille Girard, Pénélope Germain-Chartrand, Léonie Perrier, Guillaume Primeau, Khawla Riahi, and Karelle Trottier for their assistance in the field.

CONCLUSION GÉNÉRALE

Les travaux présentés dans cette thèse ont permis de décrire pour la première fois les flux et la dynamique spatio-temporelle du carbone organique dissous (COD) dans une tourbière ombrotrophe de l'est du Canada. Les efforts placés sur la mesure à haute fréquence des exports de COD, des variations du niveau de la nappe de la tourbière, ainsi que du débit du ruisseau, ont souligné l'importance des évènements de crue sur la contribution des exports de COD. Par ailleurs, l'étude de l'évolution de la composition de la matière organique dissoute (MOD) au sein du complexe tourbière-mare-ruisseau a mis en évidence la dynamique temporelle au sein de ces milieux au cours de la saison de croissance. L'étude de la MOD de l'eau interstitielle et des mares montre un changement brusque de sa composition entre les deux milieux, principalement contrôlé par des processus de production et de biodégradation. Cette étude est également la première à présenter le changement de la composition de la MOD dans le continuum tourbière-ruisseau en fonction des conditions hydrologiques. Bien que la MOD exportée présente une composition semblable à celle de l'eau interstitielle, des variations de la composition de la MOD sont décelées en fonction des conditions hydrologiques. On observera alors une MOD similaire à celle de l'eau interstitielle (à l'exception du poids moléculaire) et transférée rapidement vers l'exutoire de la tourbière en période de hautes eaux, sans que sa composition soit altérée. En revanche, les processus de biodégradation au sein du ruisseau en période de basses eaux changent significativement la composition de la MOD exportée.

La tourbière au centre du cycle du carbone d'un bassin versant boréal

Les mesures à haute fréquence du niveau de la nappe dans la tourbière et du débit dans le ruisseau ont permis de mettre en évidence le contrôle de l'hydrologie de la tourbière sur le débit à l'exutoire. L'atteinte d'un seuil au niveau de la nappe dans la tourbière (situé entre -0.33 et -0.18 m), appelé seuil de génération de l'écoulement (*threshold of runoff generation* ; Frei et al., 2010), entraine une augmentation du débit dans le ruisseau (Fig. 2.2.a). Cette relation, appelée mécanisme de rétroaction de la transmissivité (*transmissivity feedback mechanism*; Bishop et al., 2004), illustre également le synchronisme entre les variations hydrologiques au sein de la tourbière et les exports de COD, soutenu par la corrélation significativement positive entre le niveau de la nappe et la quantité de COD exportée (Fig. 2.2.b). Cette observation met en évidence le contrôle de la tourbière sur les exports de COD. Cela est renforcé par l'étude individuelle des évènements de crues dont l'interprétation des indices (indice β >0, indice de circulation >0 et l'indice hystérétique indiquant des hystérèses antihoraires) confirme le contrôle et la

limite du transport au sein du bassin versant et notamment de la tourbière (Fig. 2.6). De ce fait, les périodes de crues sont cruciales dans le cycle du carbone des tourbières en favorisant les exports de COD.

L'identification de ce seuil de génération de l'écoulement confirme que la majorité des exports de COD ont lieu durant les périodes de crues (Raymond et al., 2016; Tipping et al., 2010). Ce mécanisme supporte l'hypothèse que les exports de COD durant les épisodes de crues proviennent majoritairement de la tourbière et que les autres sources sont négligeables. Par opposition, durant les basses eaux, la connectivité hydrologique entre la tourbière et le ruisseau apparaissant plus faible, la source du COD exportée ne peut pas être clairement établie. Ces hypothèses ont servi à proposer une nouvelle approche pour calculer les exports de COD spécifiques provenant de la tourbière. Dans un premier temps, une approche statistique, utilisant un modèle de Markov caché, a permis de décomposer l'hydrogramme de crue entre les périodes de hautes eaux et les périodes de basses eaux. Dans un second temps, le calcul du flux spécifique a été effectué selon cette décomposition de la série temporelle. Durant les périodes de basses eaux, la surface du bassin versant a été prise en compte dans le calcul du flux normalisé alors que pendant les périodes de hautes eaux, la surface du bassin versant couverte par la tourbière a été utilisée dans le calcul du flux spécifique. Cette approche a permis de montrer d'une part que la majorité du flux avait lieu durant les périodes de crues puisque 63.6 à 66 % des exports de COD ont eu lieu pendant les 15% des débits les plus élevés. D'autre part, cette approche a mis en évidence que la méthode de calcul communément utilisée et la plus conservatrice, qui tient compte de la surface totale du bassin versant comme surface de référence pour le calcul des exports spécifiques (Birkel et al., 2017; Dick et al., 2015; Dinsmore et al., 2013; Koehler et al., 2009; Köhler et al., 2008; Worrall et al., 2009), les exports spécifiques seraient sous-estimés d'environ 22 % comparativement à la méthode de calcul que nous avons utilisé. À l'inverse, du fait que la tourbière couvre 76.7 % de la surface du bassin versant, l'utilisation de cette surface ne surestimerait que de 1.9 à 2.2 % les exports de COD. Bien que la tourbière soit un élément central du cycle du carbone dans le bassin versant, les flux d'export de carbone organique calculés à l'exutoire du ruisseau soient entre 1.31 à 1.92 g C m^{-2} an^{-1}, sont faibles comparativement aux flux mesurés dans des travaux antérieurs soient entre 3.7 et 18.0 g C m^{-2} an^{-1} (Dinsmore et al., 2013; Juutinen et al., 2013; Koehler et al., 2009; Köhler et al., 2008; Leach et al., 2016).

Évolution spatio-temporelle de la matière organique dissoute

L'influence des conditions hydrologiques dans le continuum tourbière-ruisseau sur la composition de la MOD

L'étude de la composition de la MOD le long du continuum tourbière-ruisseau et durant des conditions hydrologiques contrastées a mis de l' avant un changement de composition marqué entre les périodes de hautes eaux et de basses eaux. En période de hautes eaux, la composition de la MOD était semblable à celle de l'eau interstitielle en termes de ratio COD : NOD et d'aromaticité. En revanche, la MOD exportée dans le ruisseau pendant les hautes eaux avait un poids moléculaire moyen ainsi qu'une signature isotopique plus faible que la MOD de l'eau interstitielle. Cela peut s'expliquer par la méthode d'échantillonnage de l'eau interstitielle qui n'a pas permis d'identifier la stratification de la composition de la MOD dans la tourbe (Buzek et al., 2019; Tfaily et al., 2018). Ainsi, les différences de poids moléculaire et de signature isotopique pourraient s'expliquer par les exports de MOD récemment produite dans l'acrotelme, aux profondeurs où se produisent les écoulements de subsurface (Austnes et al., 2010). Au cours de son transfert, la composition de la MOD est restée relativement stable (Fig. 3.5). Du fait des débits importants et du faible temps de résidence dans le ruisseau (Table 3.1), la MOD a rapidement été transférée en aval sans que sa composition ne soit altérée.

Pendant les périodes de basses eaux, la MOD a été caractérisée par une aromaticité et un poids moléculaire moyen plus élevé et qui augmentaient le long du ruisseau, en comparaison avec les périodes de hautes eaux (Fig. 3.4). Ces constatations, similaires à celles faites par Austnes et al. (2010), indiquent que la composition de la MOD en période de basses eaux présente les caractéristiques de MOD biodégradée (Autio et al., 2016; Hulatt et al., 2014). La composition de la MOD a effectivement varié significativement le long du transect lors des épisodes de basses eaux. On a retracé une augmentation de l'aromaticité (augmentation du $SUVA_{254}$) et du poids moléculaire (diminution du ratio $E2 : E3$ et du S_R) ainsi qu'une diminution du ratio COD : NOD et une augmentation de l'indice $\beta : \alpha$. Ces changements de composition de la MOD étaient significativement corrélés à la contribution de la minéralisation de la MOD au bilan de masse (Fig. 3.8) mettant ainsi en évidence l'influence des processus de minéralisation sur les changements rapides de composition de la MOD en période de basses eaux lorsque les débits sont plus faibles et les temps de résidence plus longs.

L'observation de la stabilité de la composition de la MOD en période de hautes eaux, en contraste avec les changements rapides de composition lorsque les temps de résidence sont plus longs en période de basses

eaux, illustre parfaitement le concept de *pulse-shunt* décrit par Raymond et al. (2016). En effet, le ruisseau de tête de bassin est passé d'un état de « tuyau passif » en périodes de hautes eaux à un état de compartiment actif en périodes de basses eaux. Cet état de compartiment réactif entrainera la transformation de la composition de la MOD sous l'influence des processus de dégradation, favorisés par des temps de résidence plus longs (Casas-Ruiz et al., 2017). Durant les périodes de hautes eaux, la MOD est rapidement transférée vers les écosystèmes aquatiques en aval et sans altération de sa composition (Raymond et al., 2016). De plus, cette MOD provenant de la production récente dans l'acrotelme a un potentiel de minéralisation important une fois transférée vers l'aval.

Comment les processus de production et de biodégradation structurent la composition de la MOD dans le complexe tourbe-mare

L'étude de la composition de la MOD dans l'eau interstitielle a mis de l'avant des différences de composition entre les deux compartiments, bien que la MOD des mares soit issue de la production de MOD dans l'eau interstitielle. Dans l'eau interstitielle, une augmentation de la production de MOD au cours de la saison de croissance, illustrée par la diminution du δ^{13}C-COD, l'augmentation du rapport COD : NOD et l'augmentation de la contribution d'acides gras de haut poids moléculaire a été enregistrée (Fig. 4.2). Cette augmentation de la contribution de MOD fraichement produite dans l'eau interstitielle au cours de la saison de croissance a mis en évidence le contrôle de la température et de la phénologie (activité de la végétation) sur la production de MOD (Kane et al., 2014). Cependant, conjointement à la production de MOD dans l'eau interstitielle, les valeurs de $SUVA_{254}$, la proportion de *f*MIC et la diminution du *f*VEG au cours de la saison de croissance ont révélé également une production de MOD dérivée des processus de biodégradation au sein de l'eau interstitielle. Les valeurs de $SUVA_{254}$, les rapports COD : NOD élevés, et les marqueurs moléculaires (%Phenols et *f*VEG) ont témoigné de la contribution de MOD allochtone dans les mares et donc dérivée de la production de MOD dans la tourbière. Cependant, l'évolution de la composition de la MOD dans les mares au cours de la saison de croissance a montré un pic d'activité microbienne en été (Fig. 4.2.i). Cela démontre le contrôle des apports progressifs de MOD allochtone au cours de la saison de croissance ainsi que de l'activité microbienne lorsque les températures sont les plus favorables. Cette étude est la première à documenter la dynamique temporelle de la MOD au cours de la saison de croissance dans l'eau interstitielle et les mares d'une tourbière boréale. Elle montre que, malgré la faible superficie couverte par les mares (7.4 % de la surface de la tourbière), la dégradation de la MOD transférée depuis l'eau interstitielle de la tourbière vers les mares pourrait soutenir les émissions de CO_2

mesurées à leur surface en représentant une source de carbone à l'échelle de la tourbière (Pelletier et al., 2011, 2014).

Les résultats d'incubation n'ont pas permis de mesurer des processus de photodégradation de la MOD. Une hypothèse serait que la composition de la MOD dans ces milieux ne serait pas sensible aux processus de photodégradation. Bien qu'il ait déjà été observé que la MOD pouvait être résistante aux processus de photodégradation (Shirokova et al., 2019), Laurion et al. (2021) ont montré que l'exposition à des processus de biodégradation ou de photodégradation pouvait induire des changements de la composition de la MOD spécifique à chacun des processus. Or, les expériences d'incubations réalisées sur les échantillons d'eau interstitielle et de mares révèlent une augmentation de l'aromaticité de la MOD (Fig. 4.5). L'augmentation de l'aromaticité de la MOD lors d'incubation est considérée comme étant propre aux processus de biodégradation (Autio et al., 2016; Hulatt et al., 2014). Par ailleurs, l'absence de photodégradation pourrait aussi s'expliquer par le design expérimental de notre étude où les conditions expérimentales ont été limitées à six jours. Or, des études ont montré que, bien que la biodégradation du COD interviendrait durant les premières heures d'incubation (Moody & Worrall, 2021), les processus de photodégradation pouvaient intervenir lors de périodes de temps plus longs soient plusieurs jours (Shirokova et al., 2019). Ces éléments tendent à souligner que, du fait de l'absence de photodégradation mesurable sur une période de six jours ni de changement de la composition de la MOD propre à ces processus, la biodégradation est un processus plus déterminant que la photodégradation dans l'interprétation de changements de composition entre l'eau interstitielle des tourbières et des mares. Cette étude est la première cependant qui présente des résultats d'expériences de biodégradation et de photodégradation *in situ* dans des mares de tourbières.

Impact du changement climatique sur les flux de carbone fluviaux

Les résultats de la présente recherche ont mis en évidence qu'à la fois les flux de COD et la composition de la MOD étaient variables selon les conditions météorologiques et hydrologiques. Dans un contexte où les changements du climat se sont particulièrement accentués dans le nord du Canada (Bush & Lemmen, 2019), il semble important de s'interroger sur les conséquences que cela pourrait engendrer sur le bilan de carbone des tourbières et sur les flux de carbone fluvial supportés par la dynamique du COD. Les projections climatiques dans la région d'étude prévoient une augmentation des températures moyennes et des précipitations annuelles, ainsi qu'une diminution des précipitations sous forme neigeuse (Bush & Lemmen, 2019).

Alors que le débit est communément utilisé comme étant un prédicteur des flux de COD (Clark et al., 2007; Dawson et al., 2008) et la température comme un indicateur de la production de COD dans la tourbière (Clark et al., 2009) et donc de la quantité de COD disponible à l'export (Grand-Clement et al., 2014), les résultats ont également mis en avant le rôle du niveau de la nappe sur les exports de COD. Ce rôle du niveau de la nappe a été observé à la fois sur l'ensemble de la série temporelle (Fig. 2.2.b), mais également lors d'épisodes de crues isolés (Fig. 2.5.b). Ainsi, la diminution de la nappe et l'augmentation des températures ne favoriseraient pas la production de COD (Clark et al., 2007; Grand-Clement et al., 2014; Worrall et al., 2008) qui est par la suite transporté vers les ruisseaux par les écoulements latéraux. Inversement, Laudon et al. (2012) ont mentionné que l'augmentation des températures pourrait avoir un effet négatif sur la quantité de COD disponible pour les exports latéraux. En effet, cela pourrait avoir comme conséquence d'augmenter la minéralisation de la matière organique dans la tourbe, limitant par conséquent la quantité de COD disponible pour les flux aquatiques.

Les résultats ont montré également que les conditions hydrologiques dans le ruisseau ont eu des effets sur les processus de minéralisation du COD, mis en évidence par les changements de composition de la MOD (Fig. 3.8). Ainsi, les processus de minéralisation pendant les périodes de basses eaux ont entrainé une modification plus importante de la composition de la MOD, comparativement aux périodes de crues où la composition est restée relativement stable (Fig. 3.5). Comme ces processus de minéralisation induisent des exports et des émissions de CO_2 dans les ruisseaux de tête de bassin versant (Rasilo et al., 2017), il est important de questionner comment ils pourraient affecter le cycle du carbone dans un contexte de changements climatiques. En effet, le changement de régime des crues et donc de l'alternance entre les périodes de basses eaux et de hautes eaux pourrait engendrer des conséquences sur la quantité de COD exportée, mais également sur la quantité de COD disponible pour la minéralisation dans les ruisseaux. Des périodes de sécheresse plus longues et plus intenses, entrainant une baisse simultanée du niveau de la nappe et du débit, auraient pour conséquence d'augmenter les périodes de faible flux, tel qu'observé dans les séries temporelles (Fig. 2.3). Bien que le flux de minéralisation durant ces périodes ait contribué en plus grande proportion aux exports de COD, ces derniers n'ont constitué qu'entre 6.2 et 7.4 % des exports annuels de COD (Tableau 2.2b). Par ailleurs, l'augmentation d'évènements exceptionnels de crues pourrait entrainer l'export d'une proportion importante du flux annuel de COD, comme ce fut le cas pour l'évènement *Bb* (Tableau 2.2b et tableau annexe A.3), contribuant pour 26.9 % du flux de COD de la saison de croissance en seulement 4.5 jours. Ce COD rapidement exporté au-delà des limites du bassin versant sans subir de processus de minéralisation pouvant entrainer l'émission de CO_2 à la surface du

ruisseau favoriserait des émissions en aval. Ainsi, les bilans futurs de carbone , notamment la proportion de COD exporté et son exposition à des processus de minéralisation, semblent particulièrement sensibles aux changements dans le régime de précipitation et son incidence sur l'hydrologie des tourbières, ainsi qu'à l'augmentation des températures et son influence sur les périodes de sécheresse et la production de COD.

ANNEXE A

Supplementary information : Hydrological connectivity controls dissolved organic carbon exports in a peatland-dominated boreal catchment stream

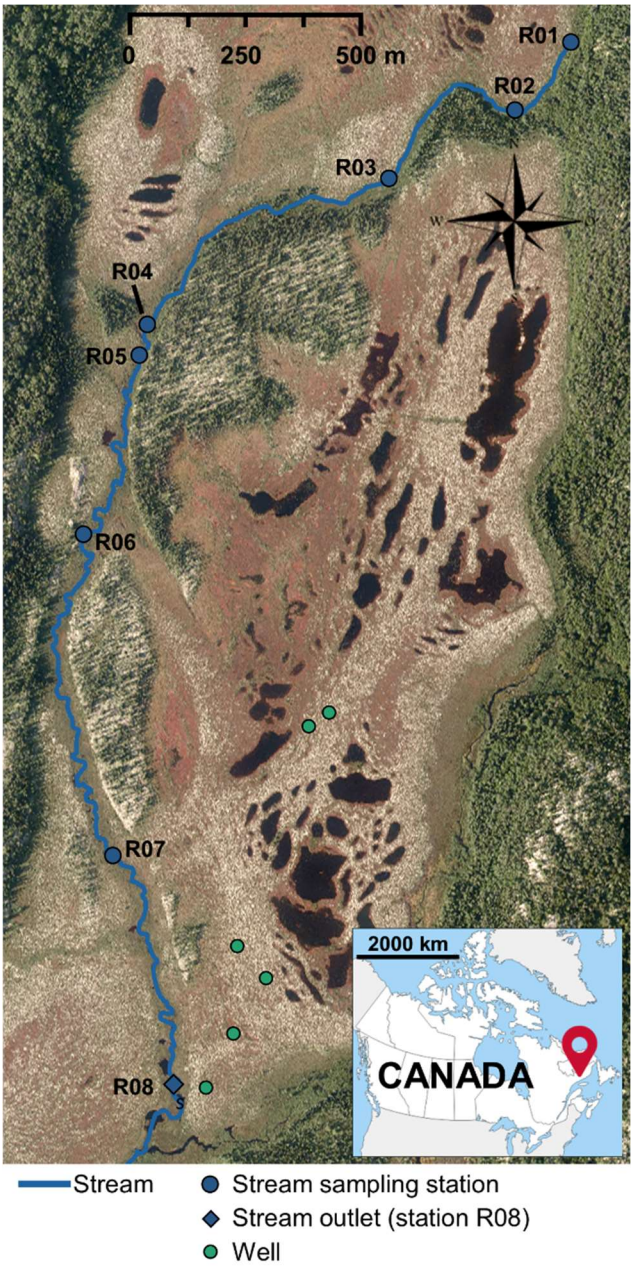

Figure annexe A.1 Aerial photo of the Bouleau peatland with the location of wells were water-level data loggers have been installed (green dots), sampling sites along the stream (blue dots) and the outlet of the peatland drainage stream (the aerial photo was provided by Hydro-Quebec).

Table annexe A.1 Models of fDOM captor calibration for DOC concentrations.

Model reference	Sonde	Covered period	Model	*n*	R^2	p-value
Calibration Model I	EXO2-A	June 2018-August 2018	[DOC] = 0.2489 * fDOMcor - 1.2088	20	0.94	< 0.0001
Calibration Model II.1	EXO2-B	August 2018-July 2019	[DOC] = 0.4074 *fDOMcor – 0.8373	29	0.82	< 0.0001
Calibration Model II.2	EXO2-A	July 2019-August 2019	[DOC] = 4.3114 * fDOMcor + 0.9833	10	0.98	< 0.0001
Calibration Model II.3	EXO2-B	August 2019-May 2020	[DOC] = 8.3384 * fDOMcor + 3.1014	10	0.80	< 0.0001

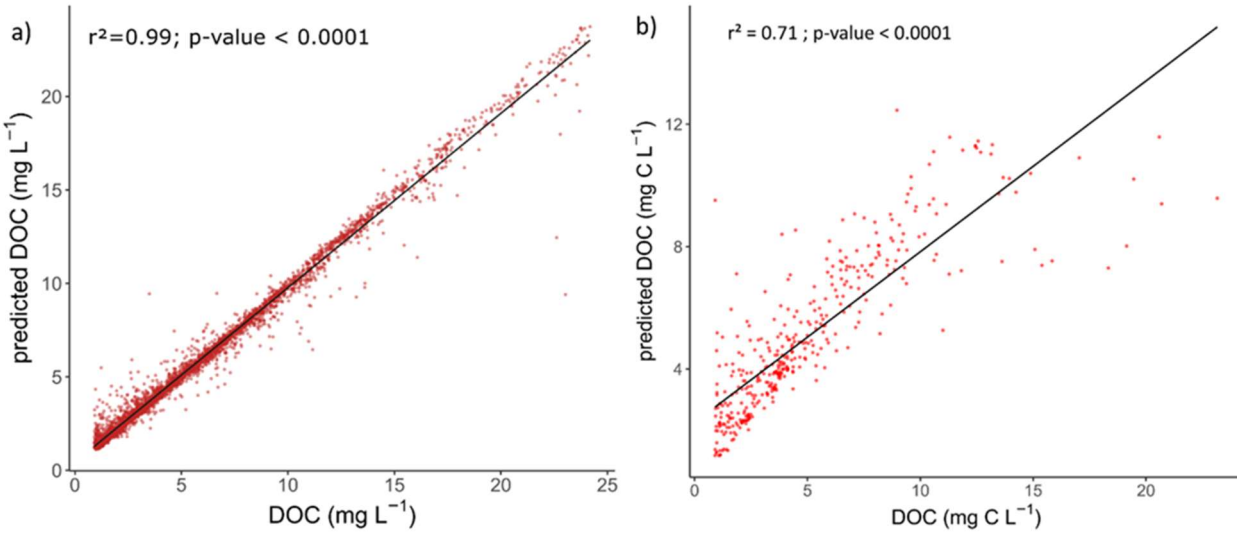

Figure annexe A.2 Relation between observed DOC concentrations and DOC predicted by random forest model on the training dataset for a) the growing season data set and b) the daily-interval data set.

Table annexe A.2 Importance of variables in the random forest model of DOC concentrations (%MeanDecreaseAccuracy) and correlation between DOC concentrations and hydrological and physicochemical variables for the data set from the growing season.

DOC ~	Variable importance (%MeanDecreaseAccuracy)	Correlations					
		Complete Time Serie		Growing season		High flow Events	
		Rho	p-value	Rho	p-value	Rho	p-value
WTD	24.47	0.43	<0.0001	0.43	<0.0001	0.22	<0.0001
Porewater T°	16.52	n.a.	n.a.	-0.06	0.0007	-0.23	<0.0001
Q	16.33	0.41	<0.0001	0.39	<0.0001	0.42	<0.0001
SPC	12.04	-0.12	<0.0001	-0.26	<0.0001	-0.23	<0.0001
pH	7.97	-0.05	<0.0001	-0.10	<0.0001	-0.19	<0.0001
DO (%sat)	5.94	0.19	<0.0001	-0.06	0.0003	0.00	0.9271
Water T°	3.25	0.30	<0.0001	-0.05	0.0039	0.09	0.0013
Air T°	2.75	n.a.	n.a.	-0.01	0.7322	0.12	<0.0001
DO (mg L^{-1})	NA	-0.02	0.085	-0.02	0.3245	-0.05	0.06

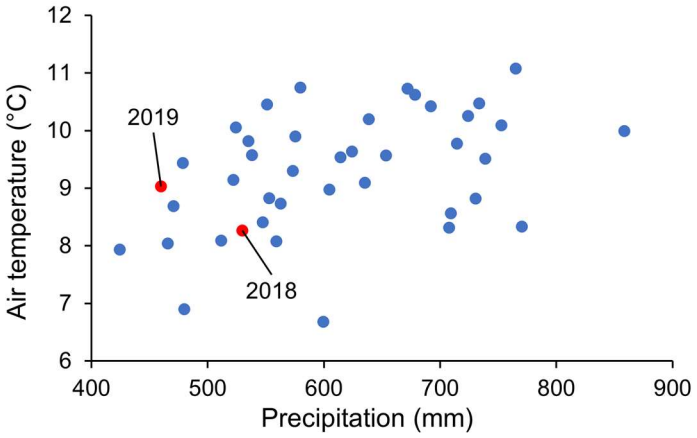

Figure annexe A.3 Precipitation (mm) and air temperature (°C) from May to October at Havre-Saint-Pierre airport (Havre-Saint-Pierre meteorological station, mean 1979–2019, Environment of Canada). Each point represents an individual year from 1979 to 2019. Studied years (i.e., 2018 and 2019) are represented in red.

ANNEXE B

Supplementary information : Hydrological conditions control dissolved organic matter dynamics along a peatland drainage boreal headwater stream

Table annexe B.1 Results of statistical test for DOC concentrations, DOC : DON ratio, δ^{13}C-DOC, absorbance indices ($SUVA_{254}$, $E2 : E3$ ratio and S_R) and fluorescence indices (FI and $\beta : \alpha$ Index). Statistical tests were based on models for comparison between the average values for the peat porewater, the stream during low flow and the stream during high flow. Significant differences were represented in bold. In the table, statistical test was abbreviating as K-W for Kusrall and Wallis test, WAOV for Welsh analyses of variances and AOV for analyses of variances and environments were abbreviated as PW for peat porewater, Str LF for stream during low flow condition and Str HF for stream during high flow conditions.

Variable	TEST	STAT		Conditions		
				PW ~ Str HF	PW ~ Str LW	Str HF ~ Str LF
DOC	K-W	27.1	stat	0.446	**-4.24**	**-4.82**
			p-value	1	**< 0.0001**	**< 0.0001**
DOC : DON	AoV	12.203	stat	0.173	**-16.1**	**-16.2**
			p-value	0.999	**0.0001**	**< 0.0001**
δ^{13}C-DOC	K-W	22.9	stat	**-4.59**	**-3.36**	1.27
			p-value	**< 0.0001**	**0.0023**	0.617
$SUVA_{254}$	K-W	28.2	stat	-2.06	**3.08**	**5.29**
			p-value	0.118	**0.0061**	**< 0.0001**
$E2 : E3$	WAoV	66.7	stat	**0.392**	-0.0405	**-0.433**
			p-value	**< 0.0001**	0.87	**< 0.0001**
S_R	K-W	30	stat	**5.02**	0.587	**-4.25**
			p-value	**< 0.0001**	1	**< 0.0001**
Fluorescence Index	AoV	7.689	stat	**-0.0628**	0.0293	**0.0921**
			p-value	**0.036**	0.524	**0.001**
$\beta : \alpha$	K-W	9.65	stat	-1.96	0.914	**3**
			p-value	0.149	1	**0.0082**

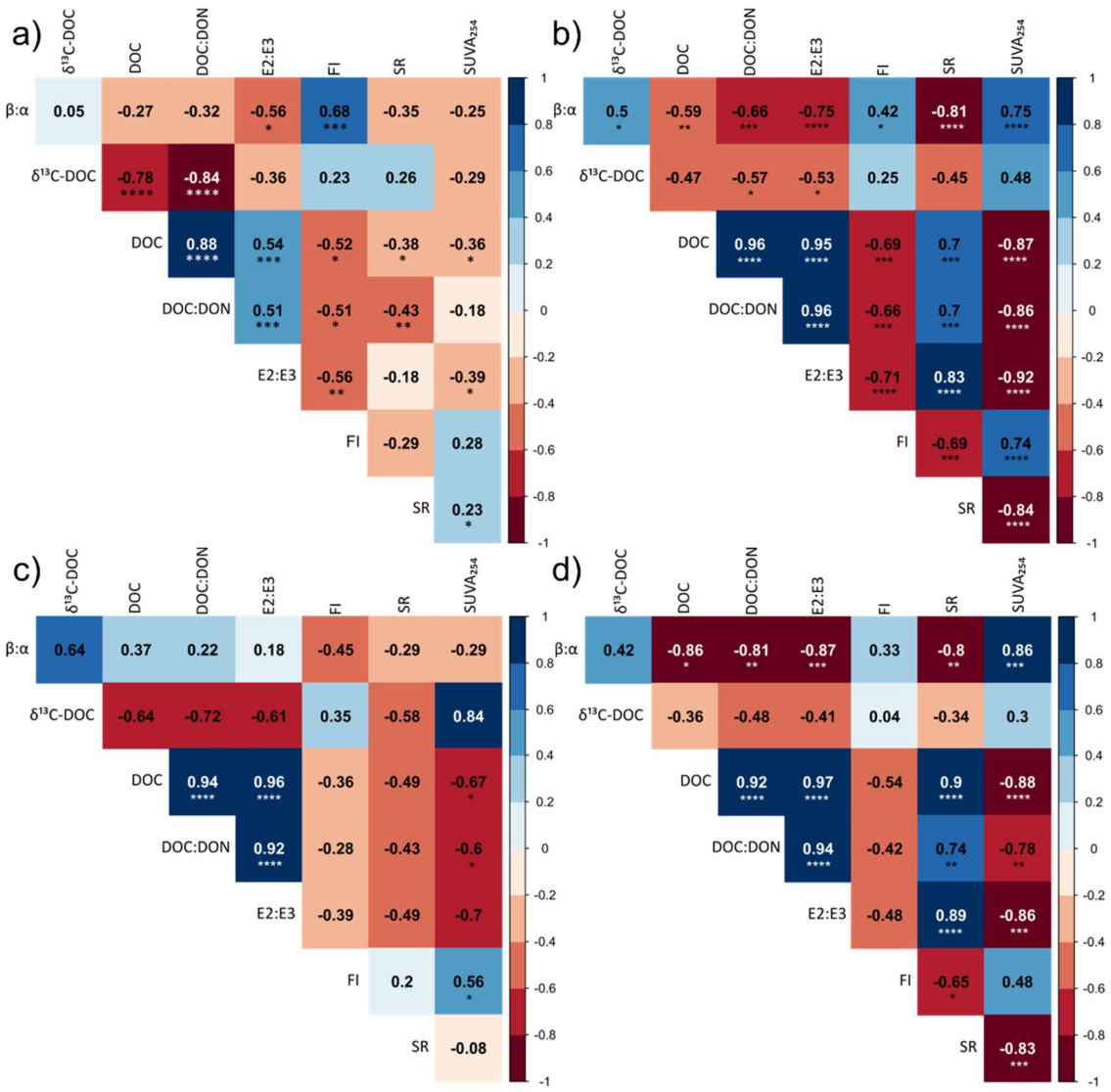

Figure annexe B.1 Correlograms for DOC concentration and DOM composition index including DOC : DON ratio, δ^{13}C-DOC, SUVA$_{254}$, *E*2 : *E*3, S$_R$, FI and *β* : *α* for a) the porewater, b) the stream, c) the stream during high flow conditions and d) the stream during low flow conditions. The significance of correlations was indicated as follows : * : p-value < 0.05, ** : p-value < 0.01, *** : p-value < 0.001, **** : p-value < 0.0001.

Table annexe B.2 Synthesis of the linear regressions and correlations between the Q_{R08} and the %fDOC$_{min}$ and the ΣRt, and between the %fDOC$_{min}$ and the ΣRt.

	Linear regression	R^2	Cor	p-value
%fDOC$_{min}$ ~ Q_{R08}	y = -118x + 9.715	0.722	-0.88	0.0201
ΣRt ~ Q_{R08}	y = -1145x + 101.7	0.429	-0.74	0.0947
ΣRt ~ %fDOC$_{min}$	y = 10.78x + 1.996	0.826	0.93	0.0076

Table annexe B.3 Synthesis of the linear regressions and correlations of the differences in DOM composition index from the most upstream section to the outlet according to a) the discharge at the stream outlet (Q_{R08}), b) the proportion of fDOC$_{min}$ to the fDOC at the stream outlet (%fDOC$_{min}$), and c) the residence time in the stream (ΣRt).

a)

Model	Linear regression	R^2	Cor	p-value
ΔDOC : DON ~ Q_{R08}	y = 347.6x - 29.57	0.809	0.92	0.0093
ΔSUVA$_{254}$ ~ Q_{R08}	y = -18.45x + 1.982	0.863	-0.94	0.0047
Δ$E2$: $E3$ ~ Q_{R08}	y = 11.25x - 1.124	0.909	0.96	0.0020
ΔS_R ~ Q_{R08}	y = 3.732x - 0.2632	0.930	0.97	0.0012
ΔFI ~ Q_{R08}	y = -0.4875x + 0.1475	-0.198	-0.20	0.6970
Δβ : α ~ Q_{R08}	y = -3.909x + 0.2902	0.837	-0.93	0.0067

b)

Model	Linear regression	R^2	Cor	p-value
ΔDOC : DON ~ %fDOC$_{min}$	y = -2.138x - 5.063	0.468	-0.76	0.0810
ΔSUVA$_{254}$ ~ %fDOC$_{min}$	y = 0.1055x + 0.7223	0.402	0.72	0.1049
Δ$E2$: $E3$ ~ %fDOC$_{min}$	y = -0.0787x - 0.2817	0.766	-0.90	0.0141
ΔS_R ~ %fDOC$_{min}$	y = -0.0267x + 0.019	0.831	-0.93	0.0072
ΔFI ~ %fDOC$_{min}$	y = -0.0031x + 0.1444	-0.211	-0.18	0.7368
Δβ : α ~ %fDOC$_{min}$	y = 0.0249x + 0.0102	0.539	0.79	0.0590

c)

Model	Linear regression	R^2	Cor	p-value
ΔDOC : DON ~ ΣRt	y = -0.1737x - 6.069	0.389	-0.71	0.1105
ΔSUVA$_{254}$ ~ ΣRt	y = 0.0072x + 0.849	0.161	0.57	0.2341
Δ$E2$: $E3$ ~ ΣRt	y = -0.0058x - 0.3502	0.504	-0.78	0.0692
ΔS_R ~ ΣRt	y = -0.0020x - 0.0028	0.573	-0.81	0.0499
ΔFI ~ ΣRt	y = -0.0005x + 0.1564	-0.120	-0.32	0.5331
Δβ : α ~ ΣRt	y = 0.0017x + 0.0395	0.253	0.63	0.1759

ANNEXE C

Supplementary information : Dissolved organic matter concentration and composition discontinuity at the peat–pool interface in a boreal peatland

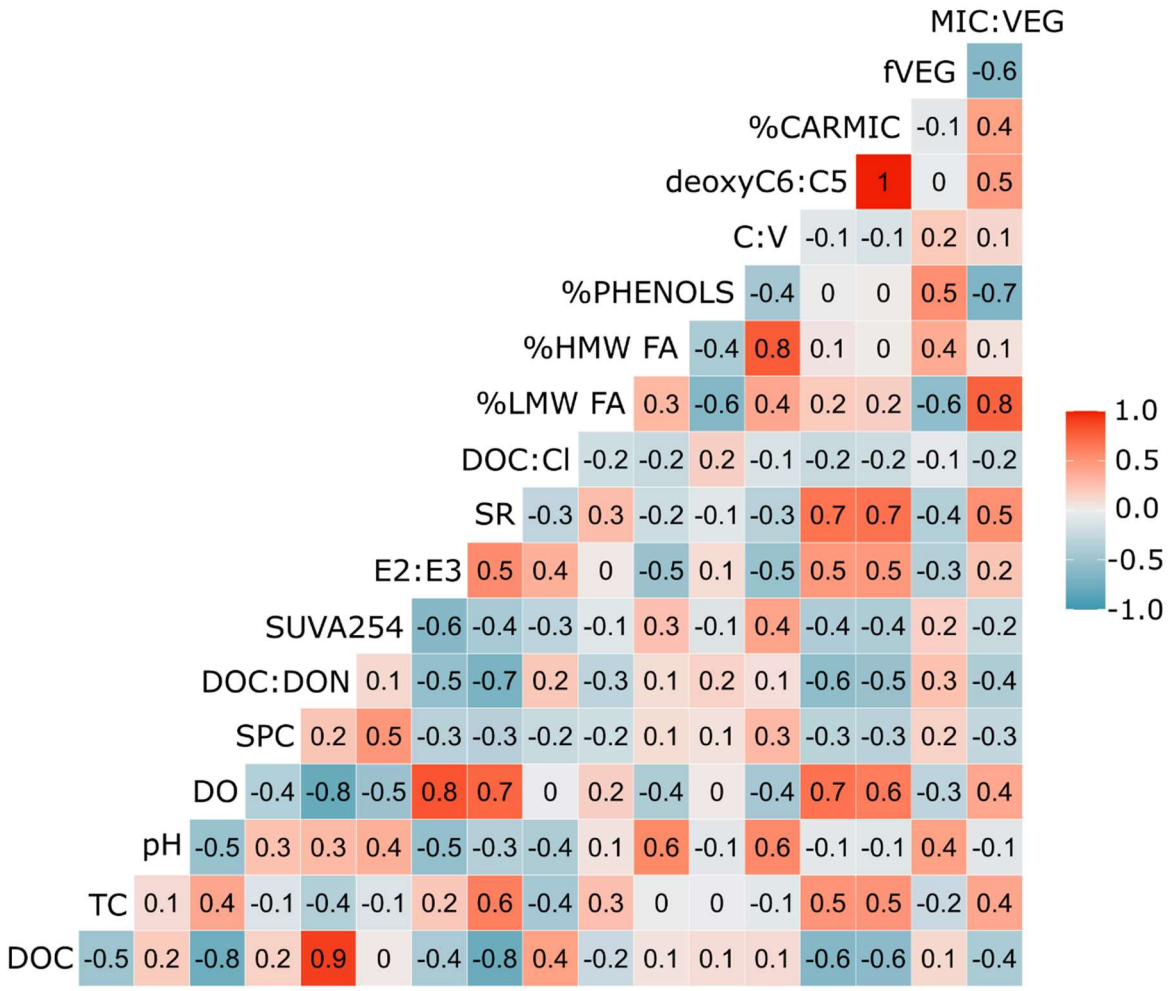

Figure annexe C.1 Correlogram of punctual variables as physico-chemical parameters (water temperature, pH, dissolved oxygen, and specific conductivity), DOC concentrations, DOC : DON ratio. DOC : Cl ratio, absorbance indices ($SUVA_{254}$, *E*2 : *E*3 ratio and S_R), and molecular index (deoxyC6 : *C*5 ratio, *f*VEG, *C* / *V* ratio), molecular family proportions (%Phenols, %SOA, %CAR_MIC, %LMW_FA, %HMW_FA)

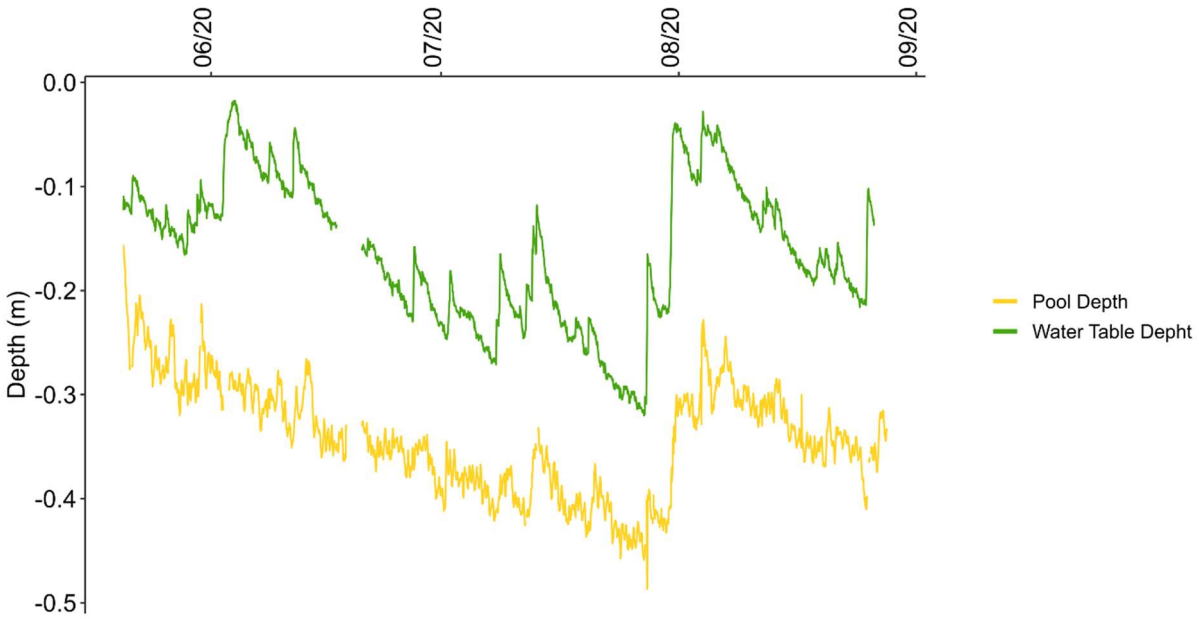

Figure annexe C.2 Variation of pool depth as the difference between peat surface at a reference point and water surface and water table depth at the reference point.

Table annexe C.1 Synthesis of number of samples number per analysis per field campaigns.

Year	Campaign	Environment	Analyses					
			DOC; DOC:DON	Isotopic	Absorbance	Fluorescence	Molecular	Incubation
2018	June	Porewater	5	1	5			
		Pools	6	2	4			
	July	Porewater	4	2	4		3	
		Pools	6	3	6		3	
	August	Porewater	6		6		3	
		Pools	6		6		3	
	September	Porewater	4	2	4		3	
		Pools	6	3	6		3	
	October	Porewater						
		Pools	6	2	6			
2019	June	Porewater	6	3	6	6	2	x
		Pools	11	3	11	11	2	x
	August	Porewater	6	3	5	5	1	x
		Pools	11	3	11	11	3	x
	September	Porewater	5	5	5	4	3	x
		Pools	11	3	11		2	x
	October	Porewater	5	3	5	5	3	
		Pools	5	3	5	5	3	

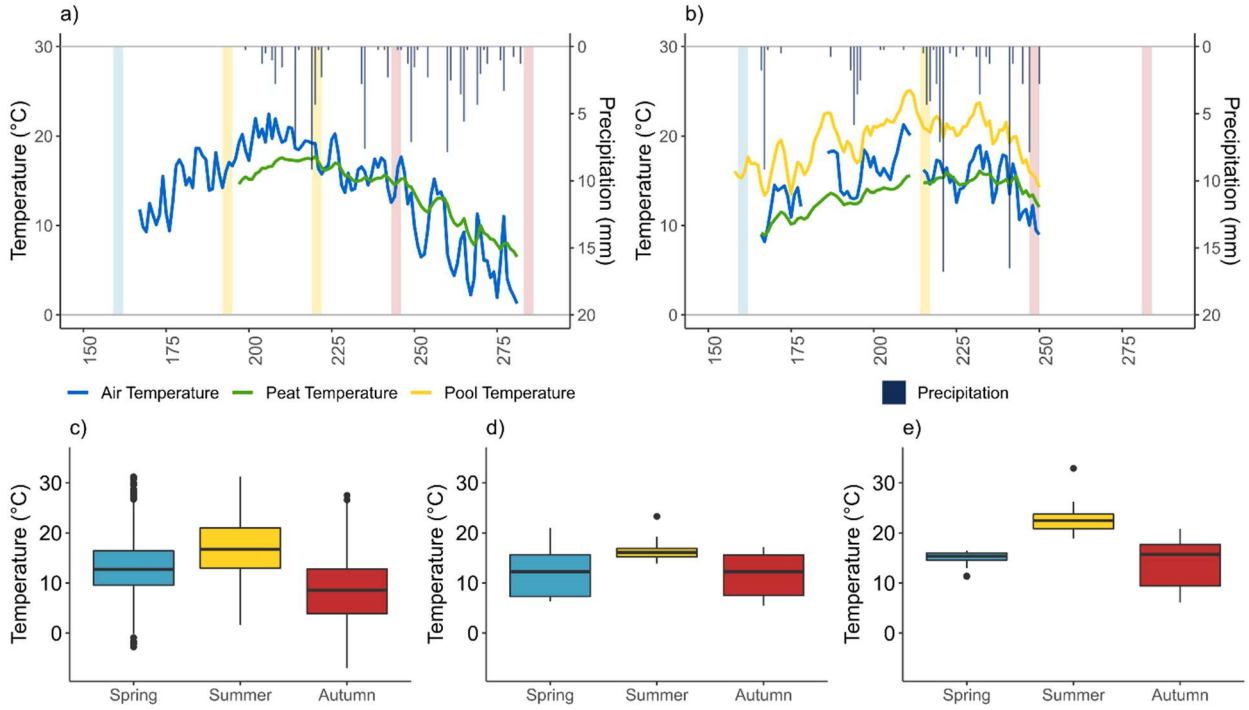

Figure annexe C.3 Daily average air, peat and pool temperature (for 2019 exclusively) and precipitation in a) 2018 and b) 2019. Vertical bands represent the sampling period and colours represent the seasons (blue = spring, yellow = summer, red = autumn). Box plot of seasonal c) air temperature, punctual measurements of d) peat porewater and e) pool water temperatures. For boxplots, boxes represent the lower (25th percentile) and the upper quartile (75th percentile) and median (50th percentile), whiskers represent the interquartile range.

a)

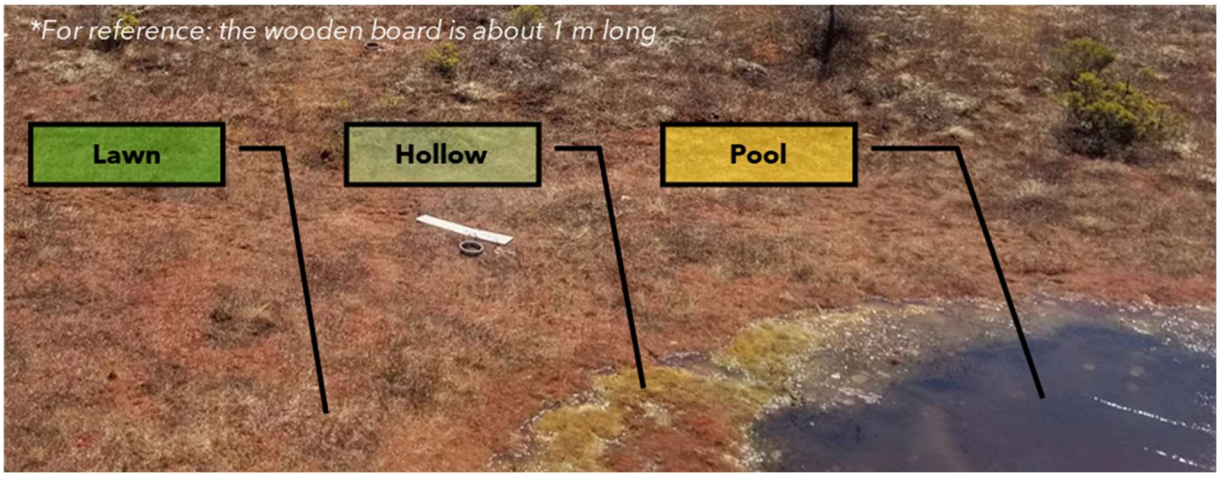

b)

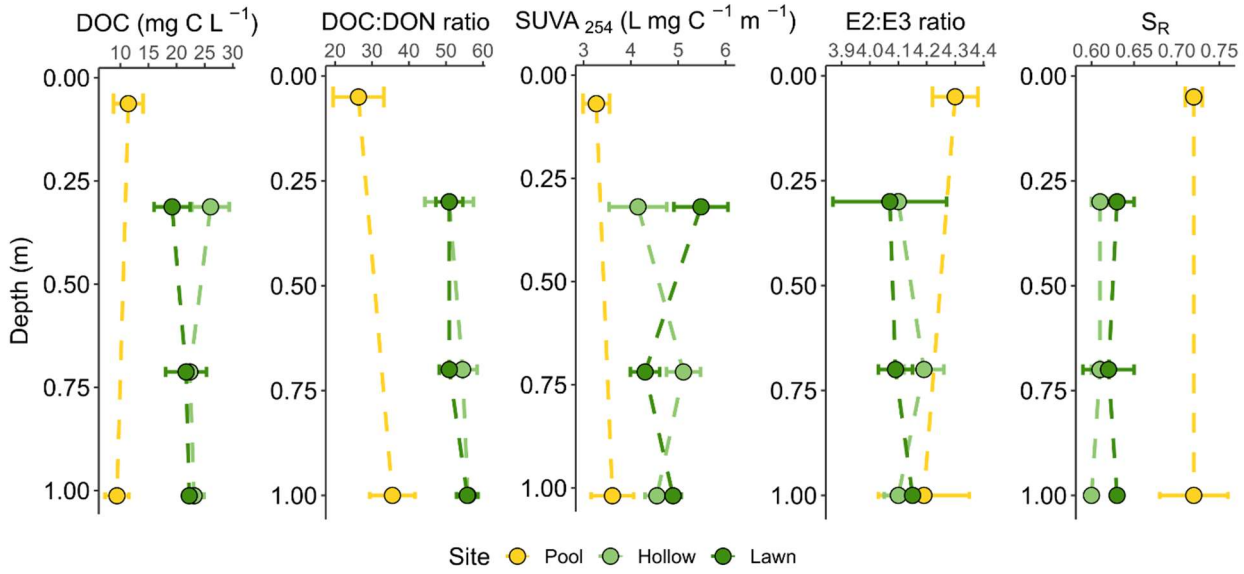

Figure annexe C.4 a) Photo of the sampled pool, hollow and lawn. b) Variations of DOC concentrations (in mg C L^{-1}), DOC : DON ratio, $SUVA_{254}$ (in L mg C^{-1} cm^{-1}), *E*2 : *E*3 ratio and spectral slope ratio in two contiguous microforms (one lawn and one hollow) and their adjacent pool (M11 on Fig. 1) at 3 depths in peat porewater (-0.3 m, -0.75 m and -1 m) and at the surface and in depth of the pool. Samples were taken in June, August, and September 2019. Points represents the average of each variable and error bars the standard deviation. Variables were always significantly different between pool and lawn and pool and hollow, except for *E*2 : *E*3 ratio, but never significantly different between lawn and hollow.

Table annexe C.2 List of compounds analysed by THM-GC-MS and their related *m/z* and mass specra factor (msf) used for their integration and molecular groups associated with them.

Compounds	m/z	msf	Groups
2-butenedioic acid dimethyl ester (fumaric acid)	113	3.3	SOA
Butanedioic acid dimethyl ester (succinic acid)	115	4.5	SOA
heptadienoic acid methyl ester	111	3.9	SOA
2-methylbutanedioic acid dimethyl ester (methylsuccinic acid)	59	2.4	SOA
Pentanedioic acid dimethyl ester (glutaric acid)	59	5.6	SOA
Pentose	129	4	CAR
Desoxyhexose	129	4	CAR
Hexose	129	4	CAR
$C_{8:0}$	74	3	FA
$C_{9:0}$	74	3.6	FA
$C_{10:0}$	74	3	FA
$C_{12:0}$	74	3	LMW FA
$\alpha,\omega C_{9:0}$	74	10.2	FA
$C_{13:0}$	74	4.1	LMW FA
$brC_{14:0}$	74	3.1	LMW FA
$C_{14:0}$	74	3.1	LMW FA
$iC_{15:0}$	74	3.3	LMW FA
$\alpha C_{15:0}$	74	3.3	LMW FA
$C_{15:0}$	74	3.3	LMW FA
$brC_{16:0}$	74	4.9	LMW FA
$C_{16:1}$	74	14.5	LMW FA
$C_{16:1}$	74	14.5	LMW FA
$C_{16:0}$	74	4.9	FA
$iC_{17:0}$	74	3.9	LMW FA
$\alpha C_{17:0}$	74	3.9	LMW FA
$C_{17:1}$	74		LMW FA
$C_{17:0}$	74	3.9	LMW FA
$C_{18:1}$	74	14.6	LMW FA
$C_{18:0}$	74	4.5	FA
$\omega OHC_{16:0}$	74	11.3	HMW FA
$C_{20:0}$	74	4.9	HMW FA
$\omega OHC_{18:0}$	74	17.3	HMW FA
$C_{21:0}$	74	7.5	HMW FA
$\alpha,\omega C_{18:0}$	74	17.7	HMW FA
$C_{22:0}$	74	4.9	HMW FA
$\omega OHC_{20:0}$	74	12.9	HMW FA
$C_{23:0}$	74	8.4	HMW FA
$\alpha,\omega C_{20:0}$	74	10.8	HMW FA
$C_{24:0}$	74	4.4	HMW FA
$\omega OHC_{22:0}$	74	13.5	HMW FA
$C_{25:0}$	74	7.7	HMW FA
$\alpha,\omega C_{22:0}$	74	10.8	HMW FA
$C_{26:0}$	74	4.5	HMW FA
$\omega OHC_{24:0}$	74	13.5	HMW FA
$C_{27:0}$	74	5.1	HMW FA
$\alpha,\omega C_{24:0}$	74	9.7	HMW FA
$C_{28:0}$	74	4.9	HMW FA
benzoic acid methyl ester	105	2.9	PHE
1,2-dimethoxybenzene	138	4.7	PHE
1,4-dimethoxybenzene	138	6	PHE

1,3-dimethoxybenzene	138	3.8	PHE
dimethoxytoluene	152	5.7	PHE
3-methoxybenzaldehyde	136	4.3	PHE
4-methoxybenzaldehyde	136	3.8	PHE
methoxyacetophenone	135	3.5	PHE
3-methoxybenzoic acid methyl ester	135	3.9	PHE
4-methoxybenzoic acid methyl ester	135	2.8	PHE
1,2,3-trimethoxybenzene	168	3.8	PHE
1,2,4-trimethoxybenzene	168	4.3	PHE
1,3,5-trimethoxybenzene	168	3	PHE
trimethoxytoluene	167	7	PHE
1,2,3,4-tetramethoxybenzene	198	3.5	PHE
1,2,3,5-tetramethoxybenzene	198	13.5	PHE
3,4-dimethoxybenzaldehyde (vanilaldehyde)	166	4.2	PHE
3,4-dimethoxyacetophenone (acetovanilone)	165	2.8	PHE
3,5-dimethoxybenzoic acid methyl ester	196	5.1	PHE
3,4-dimethoxybenzoic acid methyl ester (vaniclic acid)	196	5.6	PHE
3,4,5-trimethoxybenzaldehyde (syringealdehyde)	196	6.7	PHE
3-(4-methoxyphenyl)prop-2-enoic acid methyl ester	192	6.7	PHE
3,4,5-trimethoxyacetophenone (acetosyringeone)	195	4.8	PHE
cis-1,2-Dimethoxy-4-(2-methoxyethenyl)benzene	194	5.1	PHE
trans-1,2-Dimethoxy-4-(2-methoxyethenyl)benzene	194	5.1	PHE
3,4,5-trimethoxybenzoic acid emthyl ester (syringic acid)	226	5.3	PHE
3-(4-methoxyphenyl)but-2-enoic methyl ester	206	8.8	PHE
4-Methoxycarbonylmethoxybenzoic acid methyl ester	193	5.1	PHE
cis-1,2,3-Trimethoxy-5-(2-methoxyethenyl)benzene	224	7.0	PHE
trans-1,2,3-Trimethoxy-5-(2-methoxyethenyl)benzene	224	7.0	PHE
3-(3,4-dimethoxyphenyl)prop-2-enoic acid methyl ester	222	3.7	PHE

RÉFÉRENCES

Ågren, A., Haei, M., Köhler, S. J., Bishop, K., & Laudon, H. (2010). Regulation of stream water dissolved organic carbon (DOC) concentrations during snowmelt; the role of discharge, winter climate and memory effects. Biogeosciences, 7(9), 2901-2913. https://doi.org/10.5194/bg-7-2901-2010

Aho, K. S., & Raymond, P. A. (2019). Differential response of greenhouse gas evasion to storms in forested and wetland streams. *Journal of Geophysical Research: Biogeosciences*, *124*(3), 649-662. https://doi.org/10.1029/2018JG004750

Aiken, G., Kaplan, L. A., & Weishaar, J. (2002). Assessment of relative accuracy in the determination of organic matter concentrations in aquatic systemsThis is the work of U.S Government employees engaged in their official duties. As such it is in the public domain and exempt from copyright. U.S. Government. *Journal of Environmental Monitoring*, *4*(1), 70-74. https://doi.org/10.1039/b107322m

Aitkenhead, J. A., Hope, D., & Billett, M. F. (1999). The relationship between dissolved organic carbon in stream water and soil organic carbon pools at different spatial scales. *Hydrological Processes*, *13*(8), 1289-1302. https://doi.org/10.1002/(SICI)1099-1085

Aitkenhead, J. A., McDowell, W. H., & Neff, J. C. (2003). Sources, production, and regulation of allochthonous dissolved organic matter inputs to surface waters. In *Aquatic Ecosystems : Interactivity of Dissolved Organic Matter* (Academic Press, p. 26-59). Elsevier.

Arsenault, J., Talbot, J., & Moore, T. R. (2018). Environmental controls of C, N and P biogeochemistry in peatland pools. *Science of The Total Environment*, *631-632*, 714-722. https://doi.org/10.1016/j.scitotenv.2018.03.064

Arsenault, J., Talbot, J., Moore, T. R., Beauvais, M., Franssen, J., & Roulet, N. T. (2019). The spatial heterogeneity of vegetation, hydrology and water chemistry in a peatland with open-water pools. *Ecosystems*, *22*(6), 1352-1367. https://doi.org/10.1007/s10021-019-00342-4

Aufdenkampe, A. K., Mayorga, E., Raymond, P. A., Melack, J. M., Doney, S. C., Alin, S. R., Aalto, R. E., & Yoo, K. (2011). Riverine coupling of biogeochemical cycles between land, oceans, and atmosphere. *Frontiers in Ecology and the Environment*, *9*(1), 53-60. https://doi.org/10.1890/100014

Austnes, K., Evans, C. D., Eliot-Laize, C., Naden, P. S., & Old, G. H. (2010). Effects of storm events on mobilisation and in-stream processing of dissolved organic matter (DOM) in a Welsh peatland catchment. *Biogeochemistry*, *99*, 157-173. https://doi.org/10.1007/s10533-009-9399-4

Autio, I., Soinne, H., Helin, J., Asmala, E., & Hoikkala, L. (2016). Effect of catchment land use and soil type on the concentration, quality, and bacterial degradation of riverine dissolved organic matter. *Ambio*, *45*(3), 331-349. https://doi.org/10.1007/s13280-015-0724-y

Banaś, K. (2013). The hydrochemistry of peatland lakes as a result of the morphological characteristics of their basins. *Oceanological and Hydrobiological Studies*, *42*(1), 28-39. https://doi.org/10.2478/s13545-013-0057-z

Berggren, M., Laudon, H., Haei, M., Ström, L., & Jansson, M. (2010). Efficient aquatic bacterial metabolism of dissolved low-molecular-weight compounds from terrestrial sources. *The ISME Journal*, *4*(3), 408-416. https://doi.org/10.1038/ismej.2009.120

Bertilsson, S., & Jones, J. B. (2003). Supply of dissolved organic matter to aquatic ecosystems : autochthonous sources. In *Aquatic Ecosystems Interactivity of Dissolved Organic Matter* (Academic Press, p. 512). Elsevier.

Billett, M. F., Deacon, C. M., Palmer, S. M., Dawson, J. J. C., & Hope, D. (2006a). Connecting organic carbon in stream water and soils in a peatland catchment. *Journal of Geophysical Research: Biogeosciences*, *111*(G2), n/a-n/a. https://doi.org/10.1029/2005JG000065

Billett, M. F., Deacon, C. M., Palmer, S. M., Dawson, J. J. C., & Hope, D. (2006b). Connecting organic carbon in stream water and soils in a peatland catchment. *Journal of Geophysical Research: Biogeosciences*, *111*(G2), n/a-n/a. https://doi.org/10.1029/2005JG000065

Billett, M. F., Dinsmore, K. J., Smart, R. P., Garnett, M. H., Holden, J., Chapman, P., Baird, A. J., Grayson, R., & Stott, A. W. (2012). Variable source and age of different forms of carbon released from natural peatland pipes. *Journal of Geophysical Research: Biogeosciences*, *117*(G2), n/a-n/a. https://doi.org/10.1029/2011JG001807

Billett, M. F., Palmer, S. M., Hope, D., Deacon, C., Storeton-West, R., Hargreaves, K. J., Flechard, C., & Fowler, D. (2004). Linking land-atmosphere-stream carbon fluxes in a lowland peatland system. *Global Biogeochemical Cycles*, *18*(1), n/a-n/a. https://doi.org/10.1029/2003GB002058

Birkel, C., Broder, T., & Biester, H. (2017). Nonlinear and threshold-dominated runoff generation controls DOC export in a small peat catchment. *Journal of Geophysical Research: Biogeosciences*, *122*(3), 498-513. https://doi.org/10.1002/2016JG003621

Bishop, K., Seibert, J., Köhler, S., & Laudon, H. (2004). Resolving the Double Paradox of rapidly mobilized old water with highly variable responses in runoff chemistry. *Hydrological Processes*, *18*(1), 185-189. https://doi.org/10.1002/hyp.5209

Blaurock, K., Beudert, B., Gilfedder, B. S., Fleckenstein, J. H., Peiffer, S., & Hopp, L. (2021). Low hydrological connectivity after summer drought inhibits DOC export in a forested headwater catchment. *Hydrology and Earth System Sciences*, *25*(9), 5133-5151. https://doi.org/10.5194/hess-25-5133-2021

Blodau, C., Roulet, N. T., Heitmann, T., Stewart, H., Beer, J., Lafleur, P., & Moore, T. R. (2007). Belowground carbon turnover in a temperate ombrotrophic bog. *Global Biogeochemical Cycles*, *21*(GB1021). https://doi.org/10.1029/2005GB002659

Bradshaw, C. J. A., & Warkentin, I. G. (2015). Global estimates of boreal forest carbon stocks and flux. *Global and Planetary Change*, *128*, 24-30. https://doi.org/10.1016/j.gloplacha.2015.02.004

Broder, T., & Biester, H. (2015). Hydrologic controls on DOC, As and Pb export from a polluted peatland – the importance of heavy rain events, antecedent moisture conditions and hydrological connectivity. *Biogeosciences*, *12*(15), 4651-4664. https://doi.org/10.5194/bg-12-4651-2015

Broder, T., Knorr, K.-H., & Biester, H. (2017). Changes in dissolved organic matter quality in a peatland and forest headwater stream as a function of seasonality and hydrologic conditions. *Hydrology and Earth System Sciences*, *21*(4), 2035-2051. https://doi.org/10.5194/hess-21-2035-2017

Burd, K., Estop-Aragonés, C., Tank, S. E., & Olefeldt, D. (2020). Lability of dissolved organic carbon from boreal peatlands : Interactions between permafrost thaw, wildfire, and season. *Canadian Journal of Soil Science*, *100*(4), 503-515. https://doi.org/10.1139/cjss-2019-0154

Bush, E., & Lemmen, D. S. (2019). *Canada's Climate Change Report*. Natural Ressources Canada, Government of Canada.

Buzek, F., Novak, M., Cejkova, B., Jackova, I., Curik, J., Veselovsky, F., Stepanova, M., Prechova, E., & Bohdalkova, L. (2019). Assessing DOC export from a *Sphagnum* -dominated peatland using $\delta^{13}C$ and $\delta^{18}O$–H_2O stable isotopes. *Hydrological Processes*, hyp.13528. https://doi.org/10.1002/hyp.13528

Campeau, A., Bishop, K. H., Billett, M. F., Garnett, M. H., Laudon, H., Leach, J. A., Nilsson, M. B., Öquist, M. G., & Wallin, M. B. (2017). Aquatic export of young dissolved and gaseous carbon from a pristine boreal fen : Implications for peat carbon stock stability. *Global Change Biology*, *23*(12), 5523-5536. https://doi.org/10.1111/gcb.13815

Casas-Ruiz, J. P., Catalán, N., Gómez-Gener, L., von Schiller, D., Obrador, B., Kothawala, D. N., López, P., Sabater, S., & Marcé, R. (2017). A tale of pipes and reactors : Controls on the in-stream dynamics of dissolved organic matter in rivers: Controls on in-stream DOM dynamics. *Limnology and Oceanography*, *62*(S1), S85-S94. https://doi.org/10.1002/lno.10471

Casas-Ruiz, J. P., Spencer, R. G. M., Guillemette, F., Schiller, D., Obrador, B., Podgorski, D. C., Kellerman, A. M., Hartmann, J., Gómez-Gener, L., Sabater, S., & Marcé, R. (2020). Delineating the continuum of dissolved organic matter in temperate river networks. *Global Biogeochemical Cycles*, *34*(8). https://doi.org/10.1029/2019GB006495

Catalán, N., Marcé, R., Kothawala, D. N., & Tranvik, Lars. J. (2016). Organic carbon decomposition rates controlled by water retention time across inland waters. *Nature Geoscience*, *9*(7), 501-504. https://doi.org/10.1038/ngeo2720

Cawley, K. M., Wolski, P., Mladenov, N., & Jaffé, R. (2012). Dissolved organic matter biogeochemistry along a transect of the Okavango delta, Botswana. *Wetlands*, *32*(3), 475-486. https://doi.org/10.1007/s13157-012-0281-0

Chapin, F. S., Woodwell, G. M., Randerson, J. T., Rastetter, E. B., Lovett, G. M., Baldocchi, D. D., Clark, D. A., Harmon, M. E., Schimel, D. S., Valentini, R., Wirth, C., Aber, J. D., Cole, J. J., Goulden, M. L., Harden, J. W., Heimann, M., Howarth, R. W., Matson, P. A., McGuire, A. D., … Schulze, E.-D. (2006). Reconciling carbon-cycle concepts, terminology, and methods. *Ecosystems*, *9*(7), 1041-1050. https://doi.org/10.1007/s10021-005-0105-7

Charman, D. (2002). *Peatlands and Environment Change* (1st Edition). Willey.

Chasar, L. S., Chanton, J. P., Glaser, P. H., Siegel, D. I., & Rivers, J. S. (2000). Radiocarbon and stable carbon isotopic evidence for transport and transformation of dissolved organic carbon, dissolved

inorganic carbon, and CH_4 in a northern Minnesota peatland. *Global Biogeochemical Cycles*, *14*(4), 1095-1108. https://doi.org/10.1029/1999GB001221

Chaudhary, N., Miller, P. A., & Smith, B. (2018). Biotic and abiotic drivers of peatland growth and microtopography : A model demonstration. *Ecosystems*, *21*(6), 1196-1214. https://doi.org/10.1007/s10021-017-0213-1

Chi, J., Nilsson, M. B., Laudon, H., Lindroth, A., Wallerman, J., Fransson, J. E. S., Kljun, N., Lundmark, T., Ottosson Löfvenius, M., & Peichl, M. (2020). The net landscape carbon balance—integrating terrestrial and aquatic carbon fluxes in a managed boreal forest landscape in Sweden. *Global Change Biology*, *26*(4), 2353-2367. https://doi.org/10.1111/gcb.14983

Clark, J. M., Ashley, D., Wagner, M., Chapman, P. J., Lane, S. N., Evans, C. D., & Heathwaite, A. L. (2009). Increased temperature sensitivity of net DOC production from ombrotrophic peat due to water table draw-down. *Global Change Biology*, *15*(4), 794-807. https://doi.org/10.1111/j.1365-2486.2008.01683.x

Clark, J. M., Lane, S. N., Chapman, P. J., & Adamson, J. K. (2007). Export of dissolved organic carbon from an upland peatland during storm events : Implications for flux estimates. *Journal of Hydrology*, *347*(3-4), 438-447. https://doi.org/10.1016/j.jhydrol.2007.09.030

Clark, J. M., Lane, S. N., Chapman, P. J., & Adamson, J. K. (2008). Link between DOC in near surface peat and stream water in an upland catchment. *Science of The Total Environment*, *404*(2-3), 308-315. https://doi.org/10.1016/j.scitotenv.2007.11.002

Clymo, R. S., & Bryant, C. L. (2008). Diffusion and mass flow of dissolved carbon dioxide, methane, and dissolved organic carbon in a 7-m deep raised peat bog. *Geochimica et Cosmochimica Acta*, *72*(8), 2048-2066. https://doi.org/10.1016/j.gca.2008.01.032

Cole, J. J., Prairie, Y. T., Caraco, N. F., McDowell, W. H., Tranvik, L. J., Striegl, R. G., Duarte, C. M., Kortelainen, P., Downing, J. A., Middelburg, J. J., & Melack, J. (2007). Plumbing the global carbon cycle : Integrating inland waters into the terrestrial carbon budget. *Ecosystems*, *10*(1), 172-185. https://doi.org/10.1007/s10021-006-9013-8

Cook, S., Whelan, M. J., Evans, C. D., Gauci, V., Peacock, M., Garnett, M. H., Kho, L. K., Teh, Y. A., & Page, S. E. (2018). Fluvial organic carbon fluxes from oil palm plantations on tropical peatland. *Biogeosciences*, *15*(24), 7435-7450. https://doi.org/10.5194/bg-15-7435-2018

Cory, R. M., Boyer, E. W., & McKnight, D. M. (2011). Spectral methods to advance understanding of dissolved organic carbon dynamics in forested catchments. In D. F. Levia, D. Carlyle-Moses, & T. Tanaka (Éds.), *Forest Hydrology and Biogeochemistry* (Vol. 216, p. 117-135). Springer Netherlands. https://doi.org/10.1007/978-94-007-1363-5_6

Cory, R. M., Crump, B. C., Dobkowski, J. A., & Kling, G. W. (2013). Surface exposure to sunlight stimulates CO_2 release from permafrost soil carbon in the Arctic. *Proceedings of the National Academy of Sciences*, *110*(9), 3429-3434. https://doi.org/10.1073/pnas.1214104110

Cory, R. M., McKnight, D. M., Chin, Y.-P., Miller, P., & Jaros, C. L. (2007). Chemical characteristics of fulvic acids from Arctic surface waters : Microbial contributions and photochemical transformations.

Journal of Geophysical Research: Biogeosciences, *112*(G4), n/a-n/a. https://doi.org/10.1029/2006JG000343

Cory, R. M., Miller, M. P., McKnight, D. M., Guerard, J. J., & Miller, P. L. (2010a). Effect of instrument-specific response on the analysis of fulvic acid fluorescence spectra : Evaluating instrument-specific response. *Limnology and Oceanography: Methods*, *8*(2), 67-78. https://doi.org/10.4319/lom.2010.8.67

Dawson, J. J. C., Soulsby, C., Tetzlaff, D., Hrachowitz, M., Dunn, S. M., & Malcolm, I. A. (2008). Influence of hydrology and seasonality on DOC exports from three contrasting upland catchments. *Biogeochemistry*, *90*(1), 93-113. https://doi.org/10.1007/s10533-008-9234-3

Dean, J. F., Garnett, M. H., Spyrakos, E., & Billett, M. F. (2019). The potential hidden age of dissolved organic carbon exported by peatland streams. *Journal of Geophysical Research*, *124*, 328-341. https://doi.org/10.1029/ 2018JG004650

del Giorgio, P. A., & Pace, M. L. (2008). Relative independence of organic carbon transport and processing in a large temperate river : The Hudson River as both pipe and reactor. *Limnology and Oceanography*, *53*(1), 185-197. https://doi.org/10.4319/lo.2008.53.1.0185

Denis, M., Jeanneau, L., Pierson-Wickman, A.-C., Humbert, G., Petitjean, P., Jaffrézic, A., & Gruau, G. (2017). A comparative study on the pore-size and filter type effect on the molecular composition of soil and stream dissolved organic matter. *Organic Geochemistry*, *110*, 36-44. https://doi.org/10.1016/j.orggeochem.2017.05.002

de Oliveira, G., Bertone, E., Stewart, R., Awad, J., Holland, A., O'Halloran, K., & Bird, S. (2018). Multi-parameter compensation method for accurate in situ fluorescent dissolved organic matter monitoring and properties characterization. *Water*, *10*(9), 1146. https://doi.org/10.3390/w10091146

Deshpande, B. N., Crevecoeur, S., Matveev, A., & Vincent, W. F. (2016). Bacterial production in subarctic peatland lakes enriched by thawingpermafrost. *Biogeosciences*, *13*(15), 4411-4427. https://doi.org/10.5194/bg-13-4411-2016

de Wit, H. A., Austnes, K., Hylen, G., & Dalsgaard, L. (2015). A carbon balance of Norway : Terrestrial and aquatic carbon fluxes. *Biogeochemistry*, *123*(1-2), 147-173. https://doi.org/10.1007/s10533-014-0060-5

Dick, J. J., Tetzlaff, D., Birkel, C., & Soulsby, C. (2015). Modelling landscape controls on dissolved organic carbon sources and fluxes to streams. *Biogeochemistry*, *122*(2-3), 361-374. https://doi.org/10.1007/s10533-014-0046-3

Dilling, J., & Kaiser, K. (2002). Estimation of the hydrophobic fraction of dissolved organic matter in water samples using UV photometry. *Water Research*, *36*(20), 5037-5044. https://doi.org/10.1016/S0043-1354(02)00365-2

Dinerstein, E., Olson, D., Joshi, A., Vynne, C., Burgess, N. D., Wikramanayake, E., Hahn, N., Palminteri, S., Hedao, P., Noss, R., Hansen, M., Locke, H., Ellis, E. C., Jones, B., Barber, C. V., Hayes, R., Kormos, C.,

Martin, V., Crist, E., … Saleem, M. (2017). An ecoregion-based approach to protecting half the terrestrial realm. *BioScience*, *67*(6), 534-545. https://doi.org/10.1093/biosci/bix014

Dinsmore, K. J., Billett, M. F., & Dyson, K. E. (2013). Temperature and precipitation drive temporal variability in aquatic carbon and GHG concentrations and fluxes in a peatland catchment. *Global Change Biology*, *19*(7), 2133-2148. https://doi.org/10.1111/gcb.12209

Dinsmore, K. J., Billett, M. F., Skiba, U. M., Rees, R. M., Drewer, J., & Helfter, C. (2010). Role of the aquatic pathway in the carbon and greenhouse gas budgets of a peatland catchment. *Global Change Biology*, *16*(10), 2750-2762. https://doi.org/10.1111/j.1365-2486.2009.02119.x

Downing, B. D., Boss, E., Bergamaschi, B. A., Fleck, J. A., Lionberger, M. A., Ganju, N. K., Schoellhamer, D. H., & Fujii, R. (2009). Quantifying fluxes and characterizing compositional changes of dissolved organic matter in aquatic systems in situ using combined acoustic and optical measurements : In situ measurements for DOC fluxes and characterization. *Limnology and Oceanography: Methods*, *7*(1), 119-131. https://doi.org/10.4319/lom.2009.7.119

Dubois, J. M. M. (1980). *Environments quaternaires et évolution postglaciaire d'une zone côtière en émersion en bordure sud du bouclier canadien : La moyennne Côte Nord du Saint-Laurent, Québec* [University of Ottawa]. http://dx.doi.org/10.20381/ruor-15610

Dyson, K. E., Billett, M. F., Dinsmore, K. J., Harvey, F., Thomson, A. M., Piirainen, S., & Kortelainen, P. (2011). Release of aquatic carbon from two peatland catchments in E. Finland during the spring snowmelt period. *Biogeochemistry*, *103*(1-3), 125-142. https://doi.org/10.1007/s10533-010-9452-3

Elder, J. F., Rybicki, N. B., Carter, V., & Weintraub, V. (2000). Sources and yields of dissolved carbon in northern Wisconsin stream catchments with differing amounts of peatland. *Wetlands*, *20*(1), 113-125. https://doi.org/10.1672/0277-5212(2000)020[0113:SAYODC]2.0.CO;2

Evans, C. D., Renou-Wilson, F., & Strack, M. (2016). The role of waterborne carbon in the greenhouse gas balance of drained and re-wetted peatlands. *Aquatic Sciences*, *78*(3), 573-590. https://doi.org/10.1007/s00027-015-0447-y

Evans, M. G., Burt, T. P., Holden, J., & Adamson, J. K. (1999). Runoff generation and water table fluctuations in blanket peat : Evidence from UK data spanning the dry summer of 1995. *Journal of Hydrology*, *221*(3-4), 141-160. https://doi.org/10.1016/S0022-1694(99)00085-2

Fenner, N., Freeman, C., & Reynolds, B. (2005). Observations of a seasonally shifting thermal optimum in peatland carbon-cycling processes; implications for the global carbon cycle and soil enzyme methodologies. *Soil Biology and Biochemistry*, *37*(10), 1814-1821. https://doi.org/10.1016/j.soilbio.2005.02.032

Folhas, D., Duarte, A. C., Pilote, M., Vincent, W. F., Freitas, P., Vieira, G., Silva, A. M. S., Duarte, R. M. B. O., & Canário, J. (2020). Structural characterization of dissolved organic matter in permafrost peatland lakes. *Water*, *12*(11), 3059. https://doi.org/10.3390/w12113059

Frederick, Z. A., Anderson, S. P., & Striegl, R. G. (2012). Annual estimates of water and solute export from 42 tributaries to the Yukon River. *Hydrological Processes*, *26*(13), 1949-1961. https://doi.org/10.1002/hyp.8255

Freeman, C., Evans, C. D., Monteith, D. T., Reynolds, B., & Fenner, N. (2001). Export of organic carbon from peat soils. *Nature*, *412*(6849), 785-785. https://doi.org/10.1038/35090628

Frei, S., Lischeid, G., & Fleckenstein, J. H. (2010). Effects of micro-topography on surface–subsurface exchange and runoff generation in a virtual riparian wetland—A modeling study. *Advances in Water Resources*, *33*(11), 1388-1401. https://doi.org/10.1016/j.advwatres.2010.07.006

Frey, K. E., Sobczak, W. V., Mann, P. J., & Holmes, R. M. (2016). Optical properties and bioavailability of dissolved organic matter along a flow-path continuum from soil pore waters to the Kolyma River mainstem, East Siberia. *Biogeosciences*, *13*(8), 2279-2290. https://doi.org/10.5194/bg-13-2279-2016

Gandois, L., Hoyt, A. M., Hatté, C., Jeanneau, L., Teisserenc, R., Liotaud, M., & Tananaev, N. (2019). Contribution of peatland permafrost to dissolved organic matter along a thaw gradient in north Siberia. *Environmental Science & Technology*, *53*(24), 14165-14174. https://doi.org/10.1021/acs.est.9b03735

Glatzel, S., Lemke, S., & Gerold, G. (2006). Short-term effects of an exceptionally hot and dry summer on decomposition of surface peat in a restored temperate bog. *European Journal of Soil Biology*, *42*(4), 219-229. https://doi.org/10.1016/j.ejsobi.2006.03.003

Godsey, S. E., Hartmann, J., & Kirchner, J. W. (2019). Catchment chemostasis revisited : Water quality responds differently to variations in weather and climate. *Hydrological Processes*, *33*(24), 3056-3069. https://doi.org/10.1002/hyp.13554

Godsey, S. E., Kirchner, J. W., & Clow, D. W. (2009). Concentration-discharge relationships reflect chemostatic characteristics of US catchments. *Hydrological Processes*, *23*(13), 1844-1864. https://doi.org/10.1002/hyp.7315

Gómez-Gener, L., Hotchkiss, E. R., Laudon, H., & Sponseller, R. A. (2021). Integrating discharge-concentration dynamics across carbon forms in a boreal landscape. *Water Resources Research*, *57*(8). https://doi.org/10.1029/2020WR028806

Goñi, M. A., & Hedges, J. I. (1992). Lignin dimers : Structures, distribution, and potential geochemical applications. *Geochimica et Cosmochimica Acta*, *56*(11), 4025-4043. https://doi.org/10.1016/0016-7037(92)90014-A

Graham, J. D., Glenn, N. F., Spaete, L. P., & Hanson, P. J. (2020). Characterizing peatland microtopography using gradient and microform-based approaches. *Ecosystems*, *23*(7), 1464-1480. https://doi.org/10.1007/s10021-020-00481-z

Grand-Clement, E., Luscombe, D. J., Anderson, K., Gatis, N., Benaud, P., & Brazier, R. E. (2014). Antecedent conditions control carbon loss and downstream water quality from shallow, damaged peatlands. *Science of The Total Environment*, *493*, 961-973. https://doi.org/10.1016/j.scitotenv.2014.06.091

Guilpart, E., Espanmanesh, V., Tilmant, A., & Anctil, F. (2021). Combining split-sample testing and hidden Markov modelling to assess the robustness of hydrological models. *Hydrology and Earth System Sciences*, *25*(8), 4611-4629. https://doi.org/10.5194/hess-25-4611-2021

Guo, L., & Macdonald, R. W. (2006). Source and transport of terrigenous organic matter in the upper Yukon River : Evidence from isotope ($\delta^{13}C$, $\Delta^{14}C$, and $\delta^{15}N$) composition of dissolved, colloidal, and particulate phases. *Global Biogeochemical Cycles*, *20*(2), n/a-n/a. https://doi.org/10.1029/2005GB002593

Haan, H. D., & Boer, T. D. (1987). Applicability of light absorbance and fluorescence as measures of concentration and molecular size of dissolved organic carbon in humic Lake Tjeukemeer. *Water Research*, *21*(6), 731-734. https://doi.org/10.1016/0043-1354(87)90086-8

Hansen, A. M., Kraus, T. E. C., Pellerin, B. A., Fleck, J. A., Downing, B. D., & Bergamaschi, B. A. (2016). Optical properties of dissolved organic matter (DOM) : Effects of biological and photolytic degradation. *Limnology and Oceanography*, *61*(3), 1015-1032. https://doi.org/10.1002/lno.10270

Harte, D. (2021). *Hidden Markov Models* [CRAN].

Heinz, M., & Zak, D. (2018). Storage effects on quantity and composition of dissolved organic carbon and nitrogen of lake water, leaf leachate and peat soil water. *Water Research*, *130*, 98-104. https://doi.org/10.1016/j.watres.2017.11.053

Helms, J. R., Stubbins, A., Ritchie, J. D., Minor, E. C., Kieber, D. J., & Mopper, K. (2008). Absorption spectral slopes and slope ratios as indicators of molecular weight, source, and photobleaching of chromophoric dissolved organic matter. *Limnology and Oceanography*, *53*(3), 955-969. https://doi.org/10.4319/lo.2008.53.3.0955

Hoag, R. S., & Price, J. S. (1995). A field-scale, natural gradient solute transport experiment in peat at a Newfoundland blanket bog. *Journal of Hydrology*, *172*(1-4), 171-184. https://doi.org/10.1016/0022-1694(95)02696-M

Holden, J., & Burt, T. P. (2003). Runoff production in blanket peat covered catchments : BLANKET PEAT RUNOFF. *Water Resources Research*, *39*(7). https://doi.org/10.1029/2002WR001956

Holden, J., Moody, C. S., Edward Turner, T., McKenzie, R., Baird, A. J., Billett, M. F., Chapman, P. J., Dinsmore, K. J., Grayson, R. P., Andersen, R., Gee, C., & Dooling, G. (2018). Water-level dynamics in natural and artificial pools in blanket peatlands. *Hydrological Processes*, *32*(4), 550-561. https://doi.org/10.1002/hyp.11438

Holden, J., Smart, R. P., Dinsmore, K. J., Baird, A. J., Billett, M. F., & Chapman, P. J. (2012). Natural pipes in blanket peatlands : Major point sources for the release of carbon to the aquatic system. *Global Change Biology*, *18*(12), 3568-3580. https://doi.org/10.1111/gcb.12004

Hope, D., Billett, M. F., & Cresser, M. S. (1997). Exports of organic carbon in two river systems in NE Scotland. *Journal of Hydrology*, *193*(1-4), 61-82. https://doi.org/10.1016/S0022-1694(96)03150-2

Hugelius, G., Loisel, J., Chadburn, S., Jackson, R. B., Jones, M., MacDonald, G., Marushchak, M., Olefeldt, D., Packalen, M., Siewert, M. B., Treat, C., Turetsky, M., Voigt, C., & Yu, Z. (2020). Large stocks of peatland carbon and nitrogen are vulnerable to permafrost thaw. *Proceedings of the National Academy of Sciences*, *117*(34), 20438-20446. https://doi.org/10.1073/pnas.1916387117

Hulatt, C. J., Kaartokallio, H., Asmala, E., Autio, R., Stedmon, C. A., Sonninen, E., Oinonen, M., & Thomas, D. N. (2014). Bioavailability and radiocarbon age of fluvial dissolved organic matter (DOM) from a northern peatland-dominated catchment : Effect of land-use change. *Aquatic Sciences*, *76*(3), 393-404. https://doi.org/10.1007/s00027-014-0342-y

Huotari, J., Nykänen, H., Forsius, M., & Arvola, L. (2013). Effect of catchment characteristics on aquatic carbon export from a boreal catchment and its importance in regional carbon cycling. *Global Change Biology*, *19*(12), 3607-3620. https://doi.org/10.1111/gcb.12333

Hutchins, R. H. S., Aukes, P., Schiff, S. L., Dittmar, T., Prairie, Y. T., & del Giorgio, P. A. (2017). The optical, chemical, and molecular dissolved organic matter succession along a boreal soil-stream-river continuum. *Journal of Geophysical Research: Biogeosciences*, *122*(11), 2892-2908. https://doi.org/10.1002/2017JG004094

Hyvönen, R., Ågren, G. I., Linder, S., Persson, T., Cotrufo, M. F., Ekblad, A., Freeman, M., Grelle, A., Janssens, I. A., Jarvis, P. G., Kellomäki, S., Lindroth, A., Loustau, D., Lundmark, T., Norby, R. J., Oren, R., Pilegaard, K., Ryan, M. G., Sigurdsson, B. D., … Wallin, G. (2007). The likely impact of elevated [CO_2], nitrogen deposition, increased temperature and management on carbon sequestration in temperate and boreal forest ecosystems : A literature review. *New Phytologist*, *173*(3), 463-480. https://doi.org/10.1111/j.1469-8137.2007.01967.x

Inamdar, S. P., Christopher, S. F., & Mitchell, M. J. (2004). Export mechanisms for dissolved organic carbon and nitrate during summer storm events in a glaciated forested catchment in New York, USA. *Hydrological Processes*, *18*(14), 2651-2661. https://doi.org/10.1002/hyp.5572

Ingram, H. A. P. (1983). Mires : Swamp, bog, fen and moor. General studies. In *Hydrology* (A. J. P. Gore, p. 67-158). Elsevier.

Ivanov, K. E. (1981). *Water movement in Mirelands*. Academic Press.

Jaffé, R., Yamashita, Y., Maie, N., Cooper, W. T., Dittmar, T., Dodds, W. K., Jones, J. B., Myoshi, T., Ortiz-Zayas, J. R., Podgorski, D. C., & Watanabe, A. (2012). Dissolved organic matter in headwater streams : Compositional variability across climatic regions of North America. *Geochimica et Cosmochimica Acta*, *94*, 95-108. https://doi.org/10.1016/j.gca.2012.06.031

Järveoja, J., Nilsson, M. B., Gažovič, M., Crill, P. M., & Peichl, M. (2018). Partitioning of the net CO_2 exchange using an automated chamber system reveals plant phenology as key control of production and respiration fluxes in a boreal peatland. *Global Change Biology*, *24*(8), 3436-3451. https://doi.org/10.1111/gcb.14292

Jeanneau, L., Denis, M., Pierson-Wickmann, A.-C., Gruau, G., Lambert, T., & Petitjean, P. (2015). Sources of dissolved organic matter during storm and inter-storm conditions in a lowland headwater catchment : Constraints from high-frequency molecular data. *Biogeosciences*, *12*(14), 4333-4343. https://doi.org/10.5194/bg-12-4333-2015

Jeanneau, L., Jaffrezic, A., Pierson-Wickmann, A.-C., Gruau, G., Lambert, T., & Petitjean, P. (2014). Constraints on the sources and production mechanisms of dissolved organic matter in soils from molecular biomarkers. *Vadose Zone Journal*, *13*(7), vzj2014.02.0015. https://doi.org/10.2136/vzj2014.02.0015

Jones, T. G., Evans, C. D., Jones, D. L., Hill, P. W., & Freeman, C. (2016). Transformations in DOC along a source to sea continuum; impacts of photo-degradation, biological processes and mixing. *Aquatic Sciences*, *78*(3), 433-446. https://doi.org/10.1007/s00027-015-0461-0

Jonsson, A., Algesten, G., Bergström, A.-K., Bishop, K., Sobek, S., Tranvik, L. J., & Jansson, M. (2007). Integrating aquatic carbon fluxes in a boreal catchment carbon budget. *Journal of Hydrology*, *334*(1-2), 141-150. https://doi.org/10.1016/j.jhydrol.2006.10.003

Jutebring Sterte, E., Lidman, F., Sjöberg, Y., Ploum, S. W., & Laudon, H. (2022). Groundwater travel times predict DOC in streams and riparian soils across a heterogeneous boreal landscape. *Science of The Total Environment*, *849*, 157398. https://doi.org/10.1016/j.scitotenv.2022.157398

Juutinen, S., Väliranta, M., Kuutti, V., Laine, A. M., Virtanen, T., Seppä, H., Weckström, J., & Tuittila, E.-S. (2013). Short-term and long-term carbon dynamics in a northern peatland-stream-lake continuum : A catchment approach. *Journal of Geophysical Research: Biogeosciences*, *118*(1), 171-183. https://doi.org/10.1002/jgrg.20028

Kaal, J., Cortizas, A. M., & Biester, H. (2017). Downstream changes in molecular composition of DOM along a headwater stream in the Harz mountains (Central Germany) as determined by FTIR, Pyrolysis-GC–MS and THM-GC–MS. *Journal of Analytical and Applied Pyrolysis*, *126*, 50-61. https://doi.org/10.1016/j.jaap.2017.06.025

Kaal, J., Plaza, C., Nierop, K. G. J., Pérez-Rodríguez, M., & Biester, H. (2020). Origin of dissolved organic matter in the Harz Mountains (Germany) : A thermally assisted hydrolysis and methylation (THM-GC–MS) study. *Geoderma*, *378*, 114635. https://doi.org/10.1016/j.geoderma.2020.114635

Kalbitz, K., Solinger, S., Park, J.-H., Michalzik, B., & Matzner, E. (2000). Controls on the dynamics of dissolved organic matter in soils : A review. *Soil Science*, *165*(4), 277-304. https://doi.org/10.1097/00010694-200004000-00001

Kamjunke, N., Hertkorn, N., Harir, M., Schmitt-Kopplin, P., Griebler, C., Brauns, M., von Tümpling, W., Weitere, M., & Herzsprung, P. (2019). Molecular change of dissolved organic matter and patterns of bacterial activity in a stream along a land-use gradient. *Water Research*, *164*, 114919. https://doi.org/10.1016/j.watres.2019.114919

Kane, E. S., Mazzoleni, L. R., Kratz, C. J., Hribljan, J. A., Johnson, C. P., Pypker, T. G., & Chimner, R. (2014). Peat porewater dissolved organic carbon concentration and lability increase with warming : A field temperature manipulation experiment in a poor-fen. *Biogeochemistry*, *119*(1-3), 161-178. https://doi.org/10.1007/s10533-014-9955-4

Kaplan, L. A. (1992). Comparison of high-temperature and persulfate oxidation methods for determination of dissolved organic carbon in freshwaters. *Limnology and Oceanography*, *37*(5), 1119-1125. https://doi.org/10.4319/lo.1992.37.5.1119

Kaplan, L. A., & Cory, R. M. (2016). Dissolved organic matter in stream ecosystems. In *Stream Ecosystems in a Changing Environment* (p. 241-320). Elsevier. https://doi.org/10.1016/B978-0-12-405890-3.00006-3

Kehagias, Ath. (2004). A hidden Markov model segmentation procedure for hydrological and environmental time series. *Stochastic Environmental Research and Risk Assessment (SERRA)*, *18*(2), 117-130. https://doi.org/10.1007/s00477-003-0145-5

Kim, S., Kramer, R. W., & Hatcher, P. G. (2003). Graphical method for analysis of ultrahigh-resolution broadband mass spectra of natural organic matter, the van Krevelen diagram. *Analytical Chemistry*, *75*(20), 5336-5344. https://doi.org/10.1021/ac034415p

Knorr, K.-H. (2013). DOC-dynamics in a small headwater catchment as driven by redox fluctuations and hydrological flow paths – are DOC exports mediated by iron reduction/oxidation cycles? *Biogeosciences*, *10*(2), 891-904. https://doi.org/10.5194/bg-10-891-2013

Koehler, A.-K., Buffam, I., Laudon, H., & Bishop, K. H. (2008). Climate's control of intra-annual and interannual variability of total organic carbon concentration and flux in two contrasting boreal landscape elements. *Journal of Geophysical Research*, *113*(G3), G03012. https://doi.org/10.1029/2007JG000629

Koehler, A.-K., Murphy, K., Kiely, G., & Sottocornola, M. (2009). Seasonal variation of DOC concentration and annual loss of DOC from an Atlantic blanket bog in South Western Ireland. *Biogeochemistry*, *95*(2-3), 231-242. https://doi.org/10.1007/s10533-009-9333-9

Koehler, A.-K., Sottocornola, M., & Kiely, G. (2011). How strong is the current carbon sequestration of an Atlantic blanket bog? *Global Change Biology*, *17*(1), 309-319. https://doi.org/10.1111/j.1365-2486.2010.02180.x

Köhler, S. J., Buffam, I., Laudon, H., & Bishop, K. H. (2008). Climate's control of intra-annual and interannual variability of total organic carbon concentration and flux in two contrasting boreal landscape elements. *Journal of Geophysical Research*, *113*(G3), G03012. https://doi.org/10.1029/2007JG000629

Kortelainen, P., Mattsson, T., Finér, L., Ahtiainen, M., Saukkonen, S., & Sallantaus, T. (2006). Controls on the export of C, N, P and Fe from undisturbed boreal catchments, Finland. *Aquatic Sciences*, *68*(4), 453-468. https://doi.org/10.1007/s00027-006-0833-6

Laganière, J., Cavard, X., Brassard, B. W., Paré, D., Bergeron, Y., & Chen, H. Y. H. (2015). The influence of boreal tree species mixtures on ecosystem carbon storage and fluxes. *Forest Ecology and Management*, *354*, 119-129. https://doi.org/10.1016/j.foreco.2015.06.029

Lalonde, K., Middlestead, P., & Gélinas, Y. (2014). Automation of 13C 12C ratio measurement for freshwater and seawater DOC using high temperature combustion. *Limnology and Oceanography: Methods*, *12*(12), 816-829. https://doi.org/10.4319/lom.2014.12.816

Lamb, A. L., Wilson, G. P., & Leng, M. J. (2006). A review of coastal palaeoclimate and relative sea-level reconstructions using δ13C and C/N ratios in organic material. *Earth-Science Reviews*, *75*(1-4), 29-57. https://doi.org/10.1016/j.earscirev.2005.10.003

Lambert, T., Teodoru, C. R., Nyoni, F. C., Bouillon, S., Darchambeau, F., Massicotte, P., & Borges, A. V. (2016). Along-stream transport and transformation of dissolved organic matter in a large tropical river. *Biogeosciences*, *13*(9), 2727-2741. https://doi.org/10.5194/bg-13-2727-2016

Langlois, J. L., Johnson, D. W., & Mehuys, G. R. (2005). Suspended sediment dynamics associated with snowmelt runoff in a small mountain stream of Lake Tahoe (Nevada). *Hydrological Processes*, *19*(18), 3569-3580. https://doi.org/10.1002/hyp.5844

Lapierre, J.-F., & del Giorgio, P. A. (2014). Partial coupling and differential regulation of biologically and photochemically labile dissolved organic carbon across boreal aquatic networks. *Biogeosciences*, *11*(20), 5969-5985. https://doi.org/10.5194/bg-11-5969-2014

Laudon, H., Berggren, M., Ågren, A., Buffam, I., Bishop, K., Grabs, T., Jansson, M., & Köhler, S. (2011). Patterns and dynamics of dissolved organic carbon (DOC) in boreal streams : The role of processes, connectivity, and scaling. *Ecosystems*, *14*(6), 880-893. https://doi.org/10.1007/s10021-011-9452-8

Laudon, H., Buttle, J., Carey, S. K., McDonnell, J., McGuire, K., Seibert, J., Shanley, J., Soulsby, C., & Tetzlaff, D. (2012). Cross-regional prediction of long-term trajectory of stream water DOC response to climate change. *Geophysical Research Letters*, *39*(18). https://doi.org/10.1029/2012GL053033

Laudon, H., Köhler, S., & Buffam, I. (2004). Seasonal TOC export from seven boreal catchments in northern Sweden. *Aquatic Sciences - Research Across Boundaries*, *66*(2), 223-230. https://doi.org/10.1007/s00027-004-0700-2

Laurion, I., Massicotte, P., Mazoyer, F., Negandhi, K., & Mladenov, N. (2021). Weak mineralization despite strong processing of dissolved organic matter in Eastern Arctic tundra ponds. *Limnology and Oceanography*, *66*(S1), 1-17. https://doi.org/10.1002/lno.11634

Laurion, I., & Mladenov, N. (2013). Dissolved organic matter photolysis in Canadian arctic thaw ponds. *Environmental Research Letters*, *8*(3), 035026. https://doi.org/10.1088/1748-9326/8/3/035026

Lawler, D. M., Petts, G. E., Foster, I. D. L., & Harper, S. (2006). Turbidity dynamics during spring storm events in an urban headwater river system : The Upper Tame, West Midlands, UK. *Science of The Total Environment*, *360*(1-3), 109-126. https://doi.org/10.1016/j.scitotenv.2005.08.032

Lê, S., Josse, J., & Husson, F. (2008). FactoMineR : An R Package for Multivariate Analysis. *Journal of Statistical Software*, *25*(1), 1-18. https://doi.org/10.18637/jss.v025.i01

Leach, J. A., Larsson, A., Wallin, M. B., Nilsson, M. B., & Laudon, H. (2016). Twelve year interannual and seasonal variability of stream carbon export from a boreal peatland catchment. *Journal of Geophysical Research: Biogeosciences*, *121*(7), 1851-1866. https://doi.org/10.1002/2016JG003357

Leenheer, J. A. (2009). *Systematic Approaches to Comprehensive Analyses of Natural Organic Matter*. *3*, 138.

Levy, Z. F., Siegel, D. I., Dasgupta, S. S., Glaser, P. H., & Welker, J. M. (2014). Stable isotopes of water show deep seasonal recharge in northern bogs and fens. *Hydrological Processes*, *28*(18), 4938-4952. https://doi.org/10.1002/hyp.9983

Lloyd, C. E. M., Freer, J. E., Johnes, P. J., & Collins, A. L. (2016). Technical note : Testing an improved index for analysing storm discharge–concentration hysteresis. *Hydrology and Earth System Sciences*, *20*(2), 625-632. https://doi.org/10.5194/hess-20-625-2016

Lund, M., Christensen, T. R., Mastepanov, M., Lindroth, A., & Ström, L. (2009). Effects of N and P fertilization on the greenhouse gas exchange in two northern peatlands with contrasting N deposition rates. *Biogeosciences*, *6*(10), 2135-2144. https://doi.org/10.5194/bg-6-2135-2009

Lund, M., Lafleur, P. M., Roulet, N. T., Lindroth, A., Christensen, T. R., Aurela, M., Chojnicki, B. H., Flanagan, L. B., Humphreys, E. R., Laurila, T., Oechel, W. C., Olejnik, J., Rinne, J., Schubert, P., & Nilsson, M. B. (2009). Variability in exchange of CO2 across 12 northern peatland and tundra sites. *Global Change Biology*, no-no. https://doi.org/10.1111/j.1365-2486.2009.02104.x

Mann, P. J., Davydova, A., Zimov, N., Spencer, R. G. M., Davydov, S., Bulygina, E., Zimov, S., & Holmes, R. M. (2012). Controls on the composition and lability of dissolved organic matter in Siberia's Kolyma River basin. *Journal of Geophysical Research: Biogeosciences*, *117*(G1). https://doi.org/10.1029/2011JG001798

Mann, P. J., Eglinton, T. I., McIntyre, C. P., Zimov, N., Davydova, A., Vonk, J. E., Holmes, R. M., & Spencer, R. G. M. (2015). Utilization of ancient permafrost carbon in headwaters of Arctic fluvial networks. *Nature Communications*, *6*(1), 7856. https://doi.org/10.1038/ncomms8856

McKnight, D. M., Andrews, E. D., Spaulding, S. A., & Aiken, G. R. (1994). Aquatic fulvic acids in algal-rich antarctic ponds. *Limnology and Oceanography*, *39*(8), 1972-1979. https://doi.org/10.4319/lo.1994.39.8.1972

McKnight, D. M., Boyer, E. W., Westerhoff, P. K., Doran, P. T., Kulbe, T., & Andersen, D. T. (2001). Spectrofluorometric characterization of dissolved organic matter for indication of precursor organic material and aromaticity. *Limnology and Oceanography*, *46*(1), 38-48. https://doi.org/10.4319/lo.2001.46.1.0038

Miller, M. P. (2012). The influence of reservoirs, climate, land use and hydrologic conditions on loads and chemical quality of dissolved organic carbon in the Colorado River. *Water Resources Research*, *48*(12). https://doi.org/10.1029/2012WR012312

Mladenov, N., McKnight, D. M., Macko, S. A., Norris, M., Cory, R. M., & Ramberg, L. (2007). Chemical characterization of DOM in channels of a seasonal wetland. *Aquatic Sciences*, *69*(4), 456-471. https://doi.org/10.1007/s00027-007-0905-2

Moody, C. S., & Worrall, F. (2021). Towards understanding organic matter fluxes and reactivity in surface waters : Filtering impact on DOC/POC degradation. *Hydrological Processes*, *35*(3). https://doi.org/10.1002/hyp.14067

Moore, T. R., Paré, D., & Boutin, R. (2008). Production of dissolved organic carbon in Canadian forest soils. *Ecosystems*, *11*(5), 740-751. https://doi.org/10.1007/s10021-008-9156-x

Nilsson, M., Sagerfors, J., Buffam, I., Laudon, H., Eriksson, T., Grelle, A., Klemedtsson, L., Weslien, P., & Lindroth, A. (2008). Contemporary carbon accumulation in a boreal oligotrophic minerogenic

mire—A significant sink after accounting for all C-fluxes. *Global Change Biology*, *14*(10), 2317-2332. https://doi.org/10.1111/j.1365-2486.2008.01654.x

Nobrega, S., & Grogan, P. (2008). Landscape and ecosystem-level controls on net carbon dioxide exchange along a natural moisture gradient in Canadian low Arctic tundra. *Ecosystems*, *11*(3), 377-396. https://doi.org/10.1007/s10021-008-9128-1

Nungesser, M. K. (2003). Modelling microtopography in boreal peatlands : Hummocks and hollows. *Ecological Modelling*, *165*(2-3), 175-207. https://doi.org/10.1016/S0304-3800(03)00067-X

Olefeldt, D., Roulet, N., Giesler, R., & Persson, A. (2013). Total waterborne carbon export and DOC composition from ten nested subarctic peatland catchments-importance of peatland cover, groundwater influence, and inter-annual variability of precipitation patterns. *Hydrological Processes*, *27*(16), 2280-2294. https://doi.org/10.1002/hyp.9358

Olefeldt, D., Turetsky, M. R., & Blodau, C. (2013). Altered composition and microbial versus UV-mediated degradation of dissolved organic matter in boreal soils following wildfire. *Ecosystems*, *16*(8), 1396-1412. https://doi.org/10.1007/s10021-013-9691-y

Page, D. W., van Leeuwen, J. A., Spark, K. M., & Mulcahy, D. E. (2002). Pyrolysis characterisation of plant, humus and soil extracts from Australian catchments. *Journal of Analytical and Applied Pyrolysis*, *65*(2), 269-285. https://doi.org/10.1016/S0165-2370(02)00005-0

Palmroth, S., Oren, R., McCarthy, H. R., Johnsen, K. H., Finzi, A. C., Butnor, J. R., Ryan, M. G., & Schlesinger, W. H. (2006). Aboveground sink strength in forests controls the allocation of carbon below ground and its [CO_2]-induced enhancement. *Proceedings of the National Academy of Sciences*, *103*(51), 19362-19367. https://doi.org/10.1073/pnas.0609492103

Parks, S. J., & Baker, L. A. (1997). Sources and transport of organic carbon in an Arizona river-reservoir system. *Water Research*, *31*(7), 1751-1759. https://doi.org/10.1016/S0043-1354(96)00404-6

Parlanti, E. (2000). Dissolved organic matter fuorescence spectroscopy as a tool to estimate biological activity in a coastal zone submitted to anthropogenic inputs. *Organic Geochemistry*, *31*, 1765-1781.

Payandi-Rolland, D., Shirokova, L. S., Tesfa, M., Bénézeth, P., Lim, A. G., Kuzmina, D., Karlsson, J., Giesler, R., & Pokrovsky, O. S. (2020). Dissolved organic matter biodegradation along a hydrological continuum in permafrost peatlands. *Science of The Total Environment*, *749*, 141463. https://doi.org/10.1016/j.scitotenv.2020.141463

Payette, S. (2001). Le contexte physique et biogéographique. In *Écologie des tourbières du Québec-Labrador* (p. 9-37). Presses de l'Université Laval.

Pellerin, B. A., Saraceno, J. F., Shanley, J. B., Sebestyen, S. D., Aiken, G. R., Wollheim, W. M., & Bergamaschi, B. A. (2012). Taking the pulse of snowmelt : In situ sensors reveal seasonal, event and diurnal patterns of nitrate and dissolved organic matter variability in an upland forest stream. *Biogeochemistry*, *108*(1-3), 183-198. https://doi.org/10.1007/s10533-011-9589-8

Pelletier, L., Garneau, M., & Moore, T. R. (2011). Variation in CO2 exchange over three summers at microform scale in a boreal bog, Eastmain region, Québec, Canada. *Journal of Geophysical Research*, *116*(G3), G03019. https://doi.org/10.1029/2011JG001657

Pelletier, L., Strachan, I. B., Garneau, M., & Roulet, N. T. (2014). Carbon release from boreal peatland open water pools : Implication for the contemporary C exchange: Carbon release from peatland pools. *Journal of Geophysical Research: Biogeosciences*, *119*(3), 207-222. https://doi.org/10.1002/2013JG002423

Pelletier, L., Strachan, I. B., Roulet, N. T., & Garneau, M. (2015). Can boreal peatlands with pools be net sinks for CO2 ? *Environmental Research Letters*, *10*(3), 035002. https://doi.org/10.1088/1748-9326/10/3/035002

Peralta-Tapia, A., Sponseller, R. A., Tetzlaff, D., Soulsby, C., & Laudon, H. (2015). Connecting precipitation inputs and soil flow pathways to stream water in contrasting boreal catchments. *Hydrological Processes*, *29*(16), 3546-3555. https://doi.org/10.1002/hyp.10300

Peura, S., Wauthy, M., Simone, D., Eiler, A., Einarsdóttir, K., Rautio, M., & Bertilsson, S. (2016). Ontogenic succession of thermokarst thaw ponds is linked to dissolved organic matter quality and microbial degradation potential. *Limnology and Oceanography*, *65*, S248-S263. https://doi.org/10.1002/lno.11349

Phillips, J. D. (2003). Sources of nonlinearity and complexity in geomorphic systems. *Progress in Physical Geography: Earth and Environment*, *27*(1), 1-23. https://doi.org/10.1191/0309133303pp340ra

Prijac, A., Gandois, L., Jeanneau, L., Taillardat, P., & Garneau, M. (2022). Dissolved organic matter concentration and composition discontinuity at the peat–pool interface in a boreal peatland. *Biogeosciences*, *19*(18), 4571-4588. https://doi.org/10.5194/bg-19-4571-2022

Prijac, A., Gandois, L., Taillardat, P., Bourgault, M.-A., Riahi, K., Ponçot, A., Tremblay, A., & Garneau, M. (2023). Hydrological connectivity controls dissolved organic carbon exports in a peatland-dominated boreal catchment stream. Hydrology and Earth System Sciences, Discussions [preprint], 1-33. https://doi.org/10.5194/hess-2022-426

Primeau, G., & Garneau, M. (2021). Carbon accumulation in peatlands along a boreal to subarctic transect in eastern Canada. *The Holocene*, *31*(5), 858-869. https://doi.org/10.1177/0959683620988031

Prowse, C. W. (1984). Some Thoughts on Lag and Hysteresis. *Area*, *16*(1), 8.

Quinton, W. L., Hayashi, M., & Carey, S. K. (2008). Peat hydraulic conductivity in cold regions and its relation to pore size and geometry. *Hydrological Processes*, *22*(15), 2829-2837. https://doi.org/10.1002/hyp.7027

Randerson, J. T., Chapin, F. S., Harden, J. W., Neff, J. C., & Harmon, M. E. (2002). Net ecosystem production: A comprehensive measure of net carbon accumulation by cosystems. *Ecological Applications*, *12*(4), 937-947. https://doi.org/10.1890/1051-0761(2002)012[0937:NEPACM]2.0.CO;2

Rantakari, M., Mattsson, T., Kortelainen, P., Piirainen, S., Finér, L., & Ahtiainen, M. (2010). Organic and inorganic carbon concentrations and fluxes from managed and unmanaged boreal first-order

catchments. *Science of The Total Environment*, *408*(7), 1649-1658. https://doi.org/10.1016/j.scitotenv.2009.12.025

Rasilo, T., Hutchins, R. H. S., Ruiz-González, C., & del Giorgio, P. A. (2017). Transport and transformation of soil-derived CO2, CH4 and DOC sustain CO2 supersaturation in small boreal streams. *Science of The Total Environment*, *579*, 902-912. https://doi.org/10.1016/j.scitotenv.2016.10.187

Raymond, P. A., & Saiers, J. E. (2010). Event controlled DOC export from forested watersheds. *Biogeochemistry*, *100*(1-3), 197-209. https://doi.org/10.1007/s10533-010-9416-7

Raymond, P. A., Saiers, J. E., & Sobczak, W. V. (2016). Hydrological and biogeochemical controls on watershed dissolved organic matter transport : Pulse-shunt concept. *Ecology*, *97*(1), 5-16. https://doi.org/10.1890/14-1684.1

Raymond, P. A., & Spencer, R. G. M. (2015). Riverine DOM. In *Biogeochemistry of Marine Dissolved Organic Matter* (p. 509-533). Elsevier. https://doi.org/10.1016/B978-0-12-405940-5.00011-X

Repo, E., Huttunen, J. T., Naumov, A. V., Chichulin, A. V., Lapshina, E. D., Bleuten, W., & Martikainen, P. J. (2007). Release of CO2 and CH4 from small wetland lakes in western Siberia. *Tellus B: Chemical and Physical Meteorology*, *59*(5), 788-796. https://doi.org/10.1111/j.1600-0889.2007.00301.x

Rezanezhad, F., Price, J. S., Quinton, W. L., Lennartz, B., Milojevic, T., & Cappellen, P. V. (2016). Structure of peat soils and implications for water storage, flow and solute transport : A review update for geochemists. *Chemical Geology*, 75-84. http://dx.doi.org/10.1016/j.chemgeo.2016.03.010

Riahi, K. (2021). *Analyse du bilan hydrologique d'une tourbière ombrotrophe située dans le bassin versant de la rivière Romaine, Côte-Nord, Québec* [Maîtrise en Sciences de la Terre]. Université du Québec, Institut National de la Recherche Scientifique.

Rosset, T., Binet, S., Antoine, J.-M., Lerigoleur, E., Rigal, F., & Gandois, L. (2020). Drivers of seasonal- and event-scale DOC dynamics at the outlet of mountainous peatlands revealed by high-frequency monitoring. *Biogeosciences*, *17*(13), 3705-3722. https://doi.org/10.5194/bg-17-3705-2020

Rosset, T., Binet, S., Rigal, F., & Gandois, L. (2022). Peatland dissolved organic carbon export to surface waters : Global significance and effects of anthropogenic disturbance. *Geophysical Research Letters*, *49*(5). https://doi.org/10.1029/2021GL096616

Rosset, T., Gandois, L., Le Roux, G., Teisserenc, R., Durantez Jimenez, P., Camboulive, T., & Binet, S. (2019). Peatland contribution to stream organic carbon exports from a montane watershed. *Journal of Geophysical Research: Biogeosciences*, *124*(11), 3448-3464. https://doi.org/10.1029/2019JG005142

Roulet, N. T., Lafleur, P. M., Richard, P. J. H., Moore, T. R., Humphreys, E. R., & Bubier, J. (2007). Contemporary carbon balance and late Holocene carbon accumulation in a northern peatland. *Global Change Biology*, *13*(2), 397-411. https://doi.org/10.1111/j.1365-2486.2006.01292.x

Rumpel, C., & Dignac, M.-F. (2006). Gas chromatographic analysis of monosaccharides in a forest soil profile : Analysis by gas chromatography after trifluoroacetic acid hydrolysis and reduction–

acetylation. *Soil Biology and Biochemistry*, *38*(6), 1478-1481. https://doi.org/10.1016/j.soilbio.2005.09.017

Rydin, H., Jeglum, J. K., & Bennett, K. D. (2013). *The biology of peatlands* (2nd ed). Oxford University Press.

Saadi, I., Borisover, M., Armon, R., & Laor, Y. (2006). Monitoring of effluent DOM biodegradation using fluorescence, UV and DOC measurements. *Chemosphere*, *63*(3), 530-539. https://doi.org/10.1016/j.chemosphere.2005.07.075

Sarkkola, S., Koivusalo, H., Laurén, A., Kortelainen, P., Mattsson, T., Palviainen, M., Piirainen, S., Starr, M., & Finér, L. (2009). Trends in hydrometeorological conditions and stream water organic carbon in boreal forested catchments. *Science of The Total Environment*, *408*(1), 92-101. https://doi.org/10.1016/j.scitotenv.2009.09.008

Schindler, D. W., Curtis, P. J., Bayley, S. E., Parker, B. R., Beaty, K. G., & Stainton, M. P. (1997). Climate-induced changes in the dissolved organic carbon budgets of boreal lakes. *Biogeochemistry*, *36*, 9-28.

Schulze, E. -D., Lloyd, J., Kelliher, F. M., Wirth, C., Rebmann, C., Lühker, B., Mund, M., Knohl, A., Milyukova, I. M., Schulze, W., Ziegler, W., Varlagin, A. β., Sogachev, A. F., Valentini, R., Dore, S., Grigoriev, S., Kolle, O., Panfyorov, M. I., Tchebakova, N., & Vygodskaya, Nn. (1999). Productivity of forests in the Eurosiberian boreal region and their potential to act as a carbon sink –- a synthesis. *Global Change Biology*, *5*(6), 703-722. https://doi.org/10.1046/j.1365-2486.1999.00266.x

Sharma, S., Futter, M. N., Spence, C., Venkiteswaran, J. J., & Whitfield, C. J. (2022). Modelling subarctic watershed dissolved organic carbon response to hydroclimatic regime. *Science of The Total Environment*, 159382. https://doi.org/10.1016/j.scitotenv.2022.159382

Shein, J. (1979). *Discharge characteristics of triangular-notch thin-plate weirs* (Report N^{o} 79-1476; Open-File Report, p. 1-62). U.S. Geological Survey.

Shi, X., Thornton, P. E., Ricciuto, D. M., Hanson, P. J., Mao, J., Sebestyen, S. D., Griffiths, N. A., & Bisht, G. (2015). Representing northern peatland microtopography and hydrology within the Community Land Model. *Biogeosciences*, *12*(21), 6463-6477. https://doi.org/10.5194/bg-12-6463-2015

Shirokova, L. S., Chupakov, A. V., Zabelina, S. A., Neverova, N. V., Payandi-Rolland, D., Causserand, C., Karlsson, J., & Pokrovsky, O. S. (2019). Humic surface waters of frozen peat bogs (permafrost zone) are highly resistant to bio- and photodegradation. *Biogeosciences*, *16*(12), 2511-2526. https://doi.org/10.5194/bg-16-2511-2019

Spencer, R. G. M., Aiken, G. R., Wickland, K. P., Striegl, R. G., & Hernes, P. J. (2008). Seasonal and spatial variability in dissolved organic matter quantity and composition from the Yukon River basin, Alaska. *Global Biogeochemical Cycles*, *22*(4), n/a-n/a. https://doi.org/10.1029/2008GB003231

Spencer, R. G. M., Mann, P. J., Dittmar, T., Eglinton, T. I., McIntyre, C., Holmes, R. M., Zimov, N., & Stubbins, A. (2015a). Detecting the signature of permafrost thaw in Arctic rivers. *Geophysical Research Letters*, *42*(8), 2830-2835. https://doi.org/10.1002/2015GL063498

Spencer, R. G. M., Mann, P. J., Dittmar, T., Eglinton, T. I., McIntyre, C., Holmes, R. M., Zimov, N., & Stubbins, A. (2015b). Detecting the signature of permafrost thaw in Arctic rivers. *Geophysical Research Letters*, *42*(8), 2830-2835. https://doi.org/10.1002/2015GL063498

Stackpoole, S. M., Stets, E. G., & Striegl, R. G. (2014). The impact of climate and reservoirs on longitudinal riverine carbon fluxes from two major watersheds in the Central and Intermontane West. *Journal of Geophysical Research: Biogeosciences*, *119*(5), 848-863. https://doi.org/10.1002/2013JG002496

Striegl, R. G., Dornblaser, M. M., McDonald, C. P., Rover, J. A., & Stets, E. G. (2012). Carbon dioxide and methane emissions from the Yukon River system. *Global Biogeochemical Cycles*, *26*(4), 2012GB004306. https://doi.org/10.1029/2012GB004306

Strohmeier, S., Knorr, K.-H., Reichert, M., Frei, S., Fleckenstein, J. H., Peiffer, S., & Matzner, E. (2013). Concentrations and fluxes of dissolved organic carbon in runoff from a forested catchment : Insights from high frequency measurements. *Biogeosciences*, *10*(2), 905-916. https://doi.org/10.5194/bg-10-905-2013

Surridge, B. W. J., Baird, A. J., & Heathwaite, A. L. (2005). Evaluating the quality of hydraulic conductivity estimates from piezometer slug tests in peat. *Hydrological Processes*, *19*(6), 1227-1244. https://doi.org/10.1002/hyp.5653

Taillardat, P., Bodmer, P., Deblois, C. P., Ponçot, A., Prijac, A., Riahi, K., Gandois, L., del Giorgio, P. A., Bourgault, M. A., Tremblay, A., & Garneau, M. (2022). Carbon Dioxide and Methane Dynamics in a Peatland Headwater Stream : Origins, Processes and Implications. *Journal of Geophysical Research: Biogeosciences*, *127*(7). https://doi.org/10.1029/2022JG006855

Tank, S. E., Fellman, J. B., Hood, E., & Kritzberg, E. S. (2018). Beyond respiration : Controls on lateral carbon fluxes across the terrestrial-aquatic interface. *Limnology and Oceanography Letters*, *3*(3), 76-88. https://doi.org/10.1002/lol2.10065

Tfaily, M. M., Cooper, W. T., Kostka, J. E., Chanton, P. R., Schadt, C. W., Hanson, P. J., Iversen, C. M., & Chanton, J. P. (2014). Organic matter transformation in the peat column at Marcell Experimental Forest : Humification and vertical stratification: Organic matter dynamics. *Journal of Geophysical Research: Biogeosciences*, *119*(4), 661-675. https://doi.org/10.1002/2013JG002492

Tfaily, M. M., Corbett, J. E., Wilson, R., Chanton, J. P., Glaser, P. H., Cawley, K. M., Jaffé, R., & Cooper, W. T. (2015). Utilization of PARAFAC-modeled excitation-emission matrix (EEM) fluorescence spectroscopy to identify biogeochemical processing of dissolved organic matter in a northern peatland. *Photochemistry and Photobiology*, *91*(3), 684-695. https://doi.org/10.1111/php.12448

Tfaily, M. M., Hamdan, R., Corbett, J. E., Chanton, J. P., Glaser, P. H., & Cooper, W. T. (2013). Investigating dissolved organic matter decomposition in northern peatlands using complimentary analytical techniques. *Geochimica et Cosmochimica Acta*, *112*, 116-129. https://doi.org/10.1016/j.gca.2013.03.002

Tfaily, M. M., Wilson, R. M., Cooper, W. T., Kostka, J. E., Hanson, P., & Chanton, J. P. (2018). Vertical Stratification of peat pore water dissolved organic matter composition in a peat bog in northern

Minnesota : Pore water DOM composition in a peat bog. *Journal of Geophysical Research: Biogeosciences*, *123*(2), 479-494. https://doi.org/10.1002/2017JG004007

Tipping, E., Billett, M. F., Bryant, C. L., Buckingham, S., & Thacker, S. A. (2010). Sources and ages of dissolved organic matter in peatland streams : Evidence from chemistry mixture modelling and radiocarbon data. *Biogeochemistry*, *100*(1-3), 121-137. https://doi.org/10.1007/s10533-010-9409-6

Tiwari, T., Sponseller, R. A., & Laudon, H. (2018). Extreme climate effects on dissolved organic carbon concentrations during snowmelt. *Journal of Geophysical Research: Biogeosciences*, *123*(4), 1277-1288. https://doi.org/10.1002/2017JG004272

Tunaley, C., Tetzlaff, D., Lessels, J., & Soulsby, C. (2016). Linking high-frequency DOC dynamics to the age of connected water sources. *Water Resources Research*, *52*(7), 5232-5247. https://doi.org/10.1002/2015WR018419

Tunaley, C., Tetzlaff, D., & Soulsby, C. (2017). Scaling effects of riparian peatlands on stable isotopes in runoff and DOC mobilisation. *Journal of Hydrology*, *549*, 220-235. https://doi.org/10.1016/j.jhydrol.2017.03.056

van Heemst, J. D. H., del Rio, J. C., Hatcher, P. G., & de Leeuw, J. W. (2000). Characterization of estuarine and fluvial dissolved organic matter by thermochemolysis using tetramethylammonium hydroxide. *Acta Hydrochimica et Hydrobiologica*, *28*(2), 69-76. https://doi.org/10.1002/(SICI)1521-401X(20002)28:2<69::AID-AHEH69>3.0.CO;2-L

Vannote, R. L., Minshall, W. G., Cummins, K. W., Sedell, J. R., & Cushing, C. E. (1980). The River Continuum Concept. *Can. J. Fish. Aquat. Sci.*, *37*(1), 130-137. https://doi.org/10.1139/f80-017

van Verseveld, W. J., McDonnell, J. J., & Lajtha, K. (2009). The role of hillslope hydrology in controlling nutrient loss. *Journal of Hydrology*, *367*(3-4), 177-187. https://doi.org/10.1016/j.jhydrol.2008.11.002

Vaughan, M. C. H., Bowden, W. B., Shanley, J. B., Vermilyea, A., Sleeper, R., Gold, A. J., Pradhanang, S. M., Inamdar, S. P., Levia, D. F., Andres, A. S., Birgand, F., & Schroth, A. W. (2017). High-frequency dissolved organic carbon and nitrate measurements reveal differences in storm hysteresis and loading in relation to land cover and seasonality. *Water Resources Research*, *53*(7), 5345-5363. https://doi.org/10.1002/2017WR020491

Virkkala, A., Aalto, J., Rogers, B. M., Tagesson, T., Treat, C. C., Natali, S. M., Watts, J. D., Potter, S., Lehtonen, A., Mauritz, M., Schuur, E. A. G., Kochendorfer, J., Zona, D., Oechel, W., Kobayashi, H., Humphreys, E., Goeckede, M., Iwata, H., Lafleur, P. M., … Luoto, M. (2021). Statistical upscaling of ecosystem CO_2 fluxes across the terrestrial tundra and boreal domain : Regional patterns and uncertainties. *Global Change Biology*, *27*(17), 4040-4059. https://doi.org/10.1111/gcb.15659

Visser, I., & Speekenbrink, M. (2010). **depmixS4** : An *R* Package for Hidden Markov Models. *Journal of Statistical Software*, *36*(7). https://doi.org/10.18637/jss.v036.i07

Vonk, J. E., Tank, S. E., Mann, P. J., Spencer, R. G. M., Treat, C. C., Striegl, R. G., Abbott, B. W., & Wickland, K. P. (2015). Biodegradability of dissolved organic carbon in permafrost soils and aquatic systems : A meta-analysis. *Biogeosciences*, *12*(23), 6915-6930. https://doi.org/10.5194/bg-12-6915-2015

Wallin, M. B., Grabs, T., Buffam, I., Laudon, H., Ågren, A., Öquist, M. G., & Bishop, K. (2013a). Evasion of CO_2 from streams—The dominant component of the carbon export through the aquatic conduit in a boreal landscape. *Global Change Biology*, *19*(3), 785-797. https://doi.org/10.1111/gcb.12083

Wallin, M. B., Grabs, T., Buffam, I., Laudon, H., Ågren, A., Öquist, M. G., & Bishop, K. (2013b). Evasion of CO2 from streams—The dominant component of the carbon export through the aquatic conduit in a boreal landscape. *Global Change Biology*, *19*(3), 785-797. https://doi.org/10.1111/gcb.12083

Ward, C. P., & Cory, R. M. (2016). Complete and partial photo-oxidation of dissolved organic matter draining permafrost soils. *Environmental Science & Technology*, *50*(7), 3545-3553. https://doi.org/10.1021/acs.est.5b05354

Ward, N. D., Krusche, A. V., Sawakuchi, H. O., Brito, D. C., Cunha, A. C., Moura, J. M. S., da Silva, R., Yager, P. L., Keil, R. G., & Richey, J. E. (2015). The compositional evolution of dissolved and particulate organic matter along the lower Amazon River—Óbidos to the ocean. *Marine Chemistry*, *177*, 244-256. https://doi.org/10.1016/j.marchem.2015.06.013

Webb, J. R., Santos, I. R., Maher, D. T., & Finlay, K. (2019). The importance of aquatic carbon fluxes in net ecosystem carbon budgets : A catchment-scale review. *Ecosystems*, *22*(3), 508-527. https://doi.org/10.1007/s10021-018-0284-7

Weishaar, J. L., Aiken, G. R., Bergamaschi, B. A., Fram, M. S., Fujii, R., & Mopper, K. (2003). Evaluation of specific ultraviolet absorbance as an indicator of the chemical composition and reactivity of dissolved organic carbon. *Environmental Science & Technology*, *37*(20), 4702-4708. https://doi.org/10.1021/es030360x

White, M. (2011). *Modèle de développement des tourbières minérotrophes aqualysées du Haut-Boréal québécois*. Université Laval.

Wickham, H. (2016). *Ggplot2 elegant graphics for data analysis*. Springer International Publishing. https://doi.org/10.1007/978-3-319-24277-4

Wilson, H. F., & Xenopoulos, M. A. (2009). Effects of agricultural land use on the composition of fluvial dissolved organic matter. *Nature Geoscience*, *2*(1), 37-41. https://doi.org/10.1038/ngeo391

Woodwell, G. M., & Whittaker, R. H. (1968). Primary production in terrestrial ecosystems. *American Zoologist*, *8*(1), 19-30. https://doi.org/10.1093/icb/8.1.19

Worrall, F., Burt, T. P., Rowson, J. G., Warburton, J., & Adamson, J. K. (2009). The multi-annual carbon budget of a peat-covered catchment. *Science of The Total Environment*, *407*(13), 4084-4094. https://doi.org/10.1016/j.scitotenv.2009.03.008

Worrall, F., Gibson, H. S., & Burt, T. P. (2008). Production vs. solubility in controlling runoff of DOC from peat soils – The use of an event analysis. *Journal of Hydrology*, *358*(1-2), 84-95. https://doi.org/10.1016/j.jhydrol.2008.05.037

Worrall, F., Moody, C. S., Clay, G. D., Burt, T. P., & Rose, R. (2017). The flux of organic matter through a peatland ecosystem : The role of cellulose, lignin, and their control of the ecosystem oxidation

state: Flux of Organic Matter Through a Peat. *Journal of Geophysical Research: Biogeosciences*, *122*(7), 1655-1671. https://doi.org/10.1002/2016JG003697

Yamashita, Y., Scinto, L. J., Maie, N., & Jaffé, R. (2010). Dissolved organic matter characteristics across a subtropical wetland's landscape : Application of optical properties in the assessment of environmental dynamics. *Ecosystems*, *13*(7), 1006-1019. https://doi.org/10.1007/s10021-010-9370-1

Yu, Z. C. (2012). Northern peatland carbon stocks and dynamics : A review. *Biogeosciences*, *9*(10), 4071-4085. https://doi.org/10.5194/bg-9-4071-2012

Yu, Z., Loisel, J., Brosseau, D. P., Beilman, D. W., & Hunt, S. J. (2010). Global peatland dynamics since the Last Glacial Maximum. *Geophysical Research Letters*, *37*(13), n/a-n/a. https://doi.org/10.1029/2010GL043584

Zarnetske, J. P., Bouda, M., Abbott, B. W., Saiers, J., & Raymond, P. A. (2018). Generality of hydrologic transport limitation of watershed organic carbon flux across ecoregions of the United States. *Geophysical Research Letters*, *45*(21). https://doi.org/10.1029/2018GL080005

Zhu, X., Chen, L., Pumpanen, J., Ojala, A., Zobitz, J., Zhou, X., Laudon, H., Palviainen, M., Neitola, K., & Berninger, F. (2022). The role of terrestrial productivity and hydrology in regulating aquatic dissolved organic carbon concentrations in boreal catchments. *Global Change Biology*, gcb.16094. https://doi.org/10.1111/gcb.16094

Zuecco, G., Penna, D., Borga, M., & van Meerveld, H. J. (2016). A versatile index to characterize hysteresis between hydrological variables at the runoff event timescale : A Hysteresis Index for Variables at the Runoff Event Timescale. *Hydrological Processes*, *30*(9), 1449-1466. https://doi.org/10.1002/hyp.10681

Zurbrügg, R., Suter, S., Lehmann, M. F., Wehrli, B., & Senn, D. B. (2013). Organic carbon and nitrogen export from a tropical dam-impacted floodplain system. *Biogeosciences*, *10*(1), 23-38. https://doi.org/10.5194/bg-10-23-2013